Technische Universität Dortmund
Fakultät für Chemie

Dissertation
zur Erlangung des akademischen Grades eines
Doktors der Naturwissenschaften

Development of a FRET-Based Fluorescent Biosensor for ERK2 Activity

vorgelegt von
Thies Klüßendorf

May 2011

Dekan: Prof. Dr. Heinz Rehage
1. Gutachter: Prof. Dr. Philippe I.H. Bastiaens
2. Gutachter: Prof. Dr. Frank Wehner

Contents

Abstract

The dynamic properties of biological systems are the result of the underlying dynamic interactions of their individual components. The mitogen-activated protein kinase (MAPK) network is a conserved signalling module that regulates cellular fate such as growth and differentiation. The activity of extracellular signal-regulated kinase 2 (ERK2) is regulated by complex spatio-temporal dynamics that play an important role for specific downstream signalling effects. One of the main challenges to understand MAPK signalling and the mechanisms enabling signal propagation inside cells is the lack of means to detect kinase activity with high spatio-temporal resolution in living cells. While traditional biochemical techniques are limited to population averages with poor temporal and practically no spatial resolution, previously published FRET-based biosensors for ERK2 activity suffer from several serious disadvantages, including the indirect detection of ERK2 activity via substrate phosphorylation or conformational change, a low dynamic range and insufficient spatial resolution (Fujioka *et al.*, 2006; Sato *et al.*, 2007; Harvey *et al.*, 2008a). Therefore, a method to visualise and quantify ERK2 activity on a single cell level with high spatio-temporal resolution and a wide dynamic range was developed.

The most direct approach to measure kinase activity in living cells is the visualisation of transient enzyme-substrate (ES) interactions. The formation of ES complexes can be detected by measuring Förster resonance energy transfer/fluorescent donor lifetimes (FRET/FLIM) between a donor-tagged kinase and an acceptor-labeled substrate peptide (Yudushkin *et al.*, 2007). However, FLIM approaches rely on a high fraction of donor molecules undergoing FRET (i.e. a high fraction of enzyme in complex with its substrate) and K_{M}-values for short peptides of known ERK2 substrates are in a range of 100 μM - 1 mM. It is thus difficult to get sufficiently high substrate concentrations inside cells.

In an attempt to increase local substrate concentrations the substrate peptide was fused to ERK2 via a flexible peptide linker. This sensor design of ERK2 Activity Sensor 4 (EAS4) is generic and should in principle be applicable to all kinases. It is based on the reversible binding and phosphorylation of a short substrate peptide by the kinase of interest. Binding of the substrate peptide to the active site of the kinase induces a global conformational change of EAS4 that can be measured by a change in the FRET signal obtained from an attached FRET pair of fluorescent proteins. Thus, this newly developed FRET-based fluorescent ERK2 biosensor approach is the first that directly reports spatio-temporal kinase activity by visualising transient ES interactions and displays a dynamic range and spatial resolution superior to previously published ERK2

biosensors. In addition, EAS4 revealed that heregulin (HRG)-induced sustained ERK activity in MCF-7 cells is primarily cytosolic, while HRG-induced nuclear and epidermal growth factor (EGF)-induced ERK activity is transient, demonstrating the potential of EAS4.

Die dynamischen Eigenschaften von biologischen Systemen sind das Ergebnis der zugrundliegenden dynamischen Wechselbeziehungen der individuellen Komponenten. Die Mitogen-activated Protein Kinase (MAPK)-Kaskade ist ein evolutionär konserviertes Signalweiterleitungsmodul, das das Schicksal von Zellen wie Wachstum oder Differenzierung reguliert. Die Aktivierung von Extracellular Signal-regulated Kinase 2 (ERK2) folgt einer komplexen zeitlichen und räumlichen Dynamik, die eine wichtige Rolle für bestimmte nachgeordnete Signaleffekte spielt. Eine der Hauptherausforderungen für das Verständnis von MAPK Signalweiterleitung und der Mechanismen, die Signalweiterleitung innerhalb der Zelle ermöglichen, ist der Mangel an Methoden um Kinase-Aktivität mit hoher zeitlicher und räumlicher Auflösung in lebenden Zellen zu erfassen. Während traditionelle, biochemische Methoden auf Messungen von Durchschnittswerten aus einer Vielzahl von Zellen begrenzt sind, haben bereits veröffentlichte, auf FRET basierende Biosensoren für ERK2-Aktivität mehrere schwere Nachteile wie die nur indirekte Ermittlung von ERK2-Aktivität über die Phosphorylierung eines Substrats oder über eine Konformationsänderung, einen niedrigen, dynamischen Messbereich und ungenügende räumliche Auflösung (Fujioka et al.*, 2006; Sato* et al.*, 2007; Harvey* et al.*, 2008a). Deshalb wurde in der vorliegenden Arbeit eine Methode entwickelt, um ERK2-Aktivität in einzelnen Zellen mit hoher zeitlicher und räumlicher Auflösung und einem grossen dynamischen Messbereich sichtbar zu machen und zu quantifizieren.*

Der direkteste Ansatz um Kinase-Aktivität in lebenden Zellen zu messen ist die Sichtbarmachung von kurzlebigen Enzym-Substrat (ES) Wechselwirkungen. Die Bildung eines ES-Komplexes kann über die Messung von Förster Resonanzenergietransfer/Fluoreszenzlebenszeiten (FRET/FLIM) zwischen einer Donor-markierten Kinase und einem Akzeptor-markierten Substratpeptid nachgewiesen werden (Yudushkin et al.*, 2007). Allerdings sind FLIM-Methoden auf ein grossen Anteil an Donormolekülen angewiesen, die FRET eingehen (d.h. einen hohen Anteil an Enzym im Komplex mit seinem Substrat) und kurze Peptide aus bekannten ERK2-Substraten haben K_M-Werte in einem Bereich von 100 μM - 1 mM. Es ist deshalb schwierig, ausreichend hohe Substratkonzentration innerhalb von Zellen zu erreichen.*

In einem Versuch, die lokale Substratkonzentration zu erhöhen, wurde das Substratpeptid über einen flexiblen Peptidlinker mit ERK2 verbunden. Der Aufbau von ERK2 Activity Sensor 4 (EAS4) sollte prinzipiell auf alle Kinasen anwendbar sein. Er basiert auf der reversiblen Bindung und Phosphorylierung eines kurzen Substratpeptids durch die untersuchte Kinase. Die Bindung des Substratpeptids im aktiven Zentrum der Kinase verursacht eine umfassende Konformationsänderung von EAS4, die über eine Änderung des FRET-Signals erfasst werden kann, das durch Anhängen eines FRET-Paares fluoreszierender Protein erzielt wird. Deshalb ist dieser neu entwickelte, auf FRET basierende, flu-

oreszierende ERK2-Biosensor der Erste, der direkte Kinase-Aktivität in Raum und Zeit anzeigt, indem kurzlebige ES-Wechselwirkungen sichtbar gemacht werden. EAS4 zeichnet sich ausserdem durch einen dynamischen Messbereich und eine räumliche Auflösung aus, die zuvor veröffentlichten ERK2 Biosensoren überlegen ist. Zusätzlich konnte mit Hilfe von EAS4 gezeigt werden, dass Heregulin (HRG)-vermittelte, anhaltende ERK Aktivität in MCF-7 Zellen vornehmlich im Zytosol zu finden ist, während HRG-vermittelte ERK2-Aktivität im Zellkern sowie EGF-vermittelte ERK2-Aktivität transient ist. Dies zeigt das Potential von EAS4 für die weitere Untersuchung von biologischen Fragestellungen.

1 Introduction

Complex systems like whole organisms or even living cells cannot be fully described by counting the involved molecules (assuming that all of these are known). Further information about the location, mobility and time frame of appearance of each molecule would be required (Schultz, 2007).

Dynamic networks of interacting proteins are the core machinery of living cells. Protein interacting networks build and degrade the cell's DNA, RNA, lipids, carbohydrates and proteins, form the cell's structure and allow its movement, provide energy and convert chemicals as well as sense, integrate and process information (Grünberg and Serrano, 2010). Essentially, the dynamic properties of biological systems are a result of the underlying dynamic interactions of their individual components (Schultz, 2007; Verveer and Bastiaens, 2008; Dehmelt and Bastiaens, 2010; Grecco and Verveer, 2011).

One example for protein interaction networks are signalling networks. Signal propagation events are tightly controlled in both space and time. One challenge, however, is that a limited number of signalling components, capable of a relatively small repertoire of biochemical reactions, is used in a combinatorial fashion to generate different, specific biological fates (Kolch, 2005). This raises the question as to how signalling specificity is achieved. A complete understanding of signal transduction systems requires information about the spatio-temporal dynamics of intracellular signalling (Miyawaki, 2003; Schultz, 2007; Verveer and Bastiaens, 2008; Grecco and Verveer, 2011).

Traditional, biochemical methods to analyse protein networks and activities in general or signalling networks in particular using immunoblots and radioactive labeling, DNA microarrays, and mass spectrometry are restricted to population averages and therefore provide very little or no spatio-temporal information. Immunofluorescence provides only poor temporal information about protein activities due to the fixation process. Modern fluorescence microscopy techniques, such as Förster resonance energy transfer (FRET), fluorescence recovery after photobleaching (FRAP) or fluorescence correlation spectroscopy (FCS) now provide sufficient spatial and temporal resolution to study quantitative protein interactions (Miyawaki, 2003; Yasuda, 2006; Schultz, 2007; Grecco and Verveer, 2011).

Fluorescence imaging of biosensors enables direct visualisation of biological functions, e.g. signalling activities and measurements of molecular activity patterns in cells. In addition, information from different biosensors can help to gain information about causal connectivities and offers the possibility to determine cell-to-cell variability (Wouters

et al., 2001; Miyawaki, 2003; Dehmelt and Bastiaens, 2010).

To understand the organising principles of protein-protein interactions that underlie spatio-temporal dynamics of cell biology in general or signal transduction in particular, information from quantitative imaging has to be integrated with computational models of signal transduction networks (such as described in Schoeberl *et al.*, 2002). These models can then serve to formulate new hypotheses that can be tested experimentally (Dehmelt and Bastiaens, 2010).

1.1 Signalling by Extracellular Signal-Regulated Kinase (ERK)

A fundamental property of living cells is the ability to sense and respond appropriately to changing environmental conditions and various other stimuli. Transmission of extracellular signals to their intracellular targets is mediated by a network of interacting proteins that regulate a large number of cellular processes (Seger and Krebs, 1995). Intracellular events following growth factor stimulation are of particular interest because malfunctioning/defective regulation of growth factor regulated processes often leads to altered proliferation or cellular transformation (Seger and Krebs, 1995; Wolf and Seger, 2002; Dhillon *et al.*, 2007).

Growth factor signalling is mediated by membrane-bound growth factor receptors. These ususally contain a protein tyrosine kinase either as an integral part or as an associated protein in or at their intracellular domain. In response to growth factor stimulation receptor tyrosine kinase are activated and tyrosyl phosphorylation is rapidly translated into changes of the phosphorylation levels of cytosolic and nuclear proteins on serine and threonine residues, which in turn leads to a change in the properties of the target protein (reviewed in Seger and Krebs, 1995.

1.1.1 Signalling via the Mitogen-Activated Protein Kinase (MAPK) Network

Many of these phosphorylation signals are propagated by activation of evolutionary conserved mitogen-activated protein kinases (MAPKs) within the cell. MAPK-mediated signalling is critical for the regulation of proliferation, differentiation and survival in mammalian cells (Chang and Karin, 2001).

Six distinct MAPK modules are currently distinguished in mammalian cells and are usually named after the last kinase of the series (Fig. 1.1) (reviewed in Chen *et al.*, 2001; Chang and Karin, 2001; Dhillon *et al.*, 2007):

1. the extracellular signal-regulated kinase (ERK1/2).
2. the ERK3/4 module, activated by serum and stress.

3. the Jun N-terminal kinase (JNK) module, also known as stress-activated protein kinases (SAPK1). It is activated in reponse to various types of stress, e.g. inflammatory cytokines, tumor necrosis factor-alpha, interleukin-1, and osmolar stress, but also by hormones and growth factors.
4. the p38 MAPK module, also known as SAPK2-4.
5. the ERK5 module, activated by oxidative stress, hyperosmolarity and mitogens, such as serum or certain growth factors.
6. the ERK7/8 module.

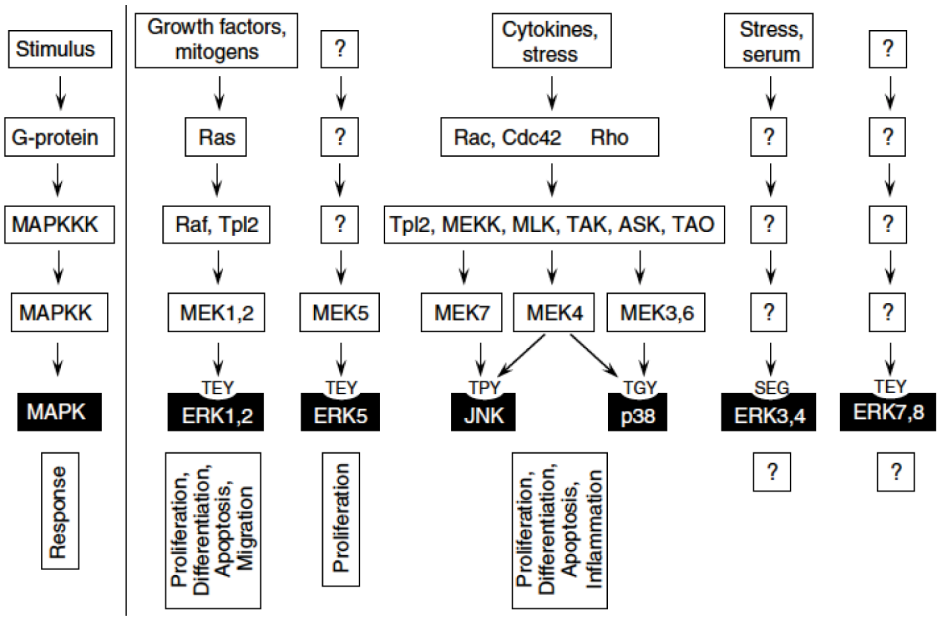

Figure 1.1: Schematic overview of MAPK pathways (adapted from Chen *et al.*, 2001).

The Raf/MEK/ERK module can be activated by a large number of different growth factors, hormones or neurotransmitters (e.g. epidermal growth factor (EGF), platelet-derived growth factor, fibroblast growth factor, neurite growth factor, angiotensin II, endothelin, thrombin, or norepinephrine). While hormones and cytokines activate the ERK1/2 module via G-protein-coupled receptors, growth factors usually activate the ERK1/2 module through receptor tyrosine kinases (Wolf and Seger, 2002).

The Raf/MEK/ERK module is activated by Ras-family GTPases (Fig. 1.2) that couple signals from the activated receptor to Raf-family serine/threonine kinases by a yet not fully understood mechanism. Raf kinases in turn phosphorylate and activate the dual-specificity kinases MEK1 and MEK2 (Seger *et al.*, 1992; Pagès *et al.*, 1994), the only known substrate of which are ERK1/2. Phosphorylated MEK1/2 subsequently activate ERK1/2 by phosphorylation of Thr183 and Tyr185 in their activation loop (Ahn *et al.*, 1991; Payne *et al.*, 1991; Robbins *et al.*, 1993). In resting cells, ERK1/2 are pri-

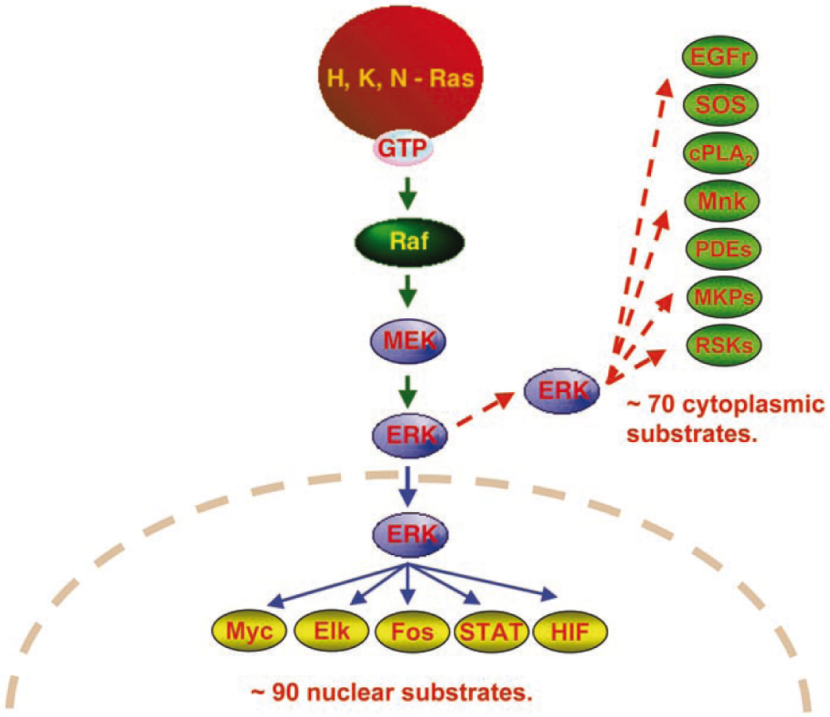

Figure 1.2: The Raf-MEK-ERK cascade. In the classical model, the Raf/MEK/ERK cascade is activated via Ras and consecutively each kinase layer phosphorylates and activates the downstream layer. Phosphorylated ERK1/2 then either translocates to the nucleus to activate its targets or phosphorylates its targets in the cytosol (adapted from Casar *et al.*, 2009).

marily located in the cytosol, mediated by interactions with cytosolic anchors (Chen *et al.*, 2001; Yoon and Seger, 2006; Yao and Seger, 2009). Phosphorylation of ERK1/2 leads to its dissociation from these anchors and rapid translocation to the nucleus (Chen *et al.*, 1992; Gonzalez *et al.*, 1993; Lenormand *et al.*, 1993; Fukuda *et al.*, 1997; Adachi *et al.*, 1999).

Computational analysis of MAPK signalling has proposed a number of theoretical mechanisms that are involved in signal propagation from membrane receptors to the site of action by MAPK, including spatial gradients of phospho-proteins (Brown and Kholodenko, 1999; Kholodenko, 2006), travelling waves of phospho-proteins (Markevich *et al.*, 2006), oscillations in the MAPK cascade (Kholodenko, 2000, 2006) or the signalling endosome hypothesis (Howe and Mobley, 2004; Howe, 2005; Kholodenko, 2006).

The formation of spatial gradients of phospho-proteins in living cells is based on a membrane bound kinase that phosphorylates (signalling) proteins, which then diffuse into the cytosol, where they become dephosphorylated by evenly distributed, opposing

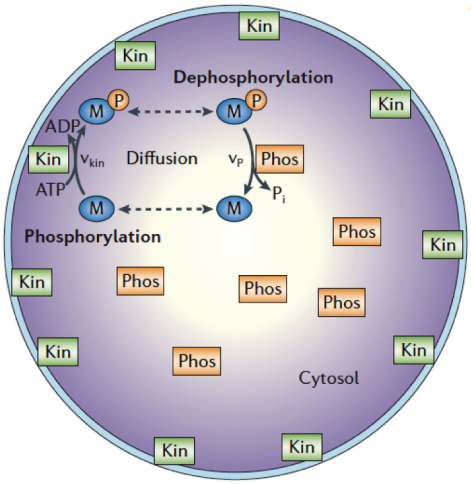

Figure 1.3: Spatial gradients of phospho-proteins inside living cells. Spatial segregation of a kinase and the opposing phosphatase in a protein-phosphorylation-dephosphorylation cycle generates intracellular gradients of phospho-proteins. The kinase (Kin) is localised to the cell membrane, whereas the phosphatase (Phos) is homogeneously distributed in the cytoplasm. The concentration gradient is shown by colour intensity. v_{kin} = kinase rate; v_p = phosphatase rate (adapted from Kholodenko, 2006).

phosphatases (Fig. 1.3). System analysis of the MAPK cascade considering measured values for kinase and phosphatase activities as well as protein diffusion proposes the existence of steep phospho-/signalling protein gradients inside cells that could even lead to subthreshold levels at their site of action (e.g. the nucleus). Indeed, such phospho-protein gradients have been observed (Niethammer *et al.*, 2004; Maeder *et al.*, 2007; Yudushkin *et al.*, 2007).

Several mechanisms to overcome the proposed gradients have been suggested. These include spatio-temporal regulation of protein phosphatase activity and travelling waves of phosphoproteins (Markevich *et al.*, 2006; Kholodenko, 2006). Regulating phosphatases in a spatial and signal-dependent manner (e.g. inhibiting phosphatase activity upon incoming signals, subsequently resulting in less steep phospho-protein gradients) might be one way to enable signal propagation. Travelling waves of phospho-proteins arise from bistability in the two-step phosphorylation and dephosphorylation cycle of ERK and may extend the phospho-protein signal from the membrane to the cell interior (Fig. 1.4). For a kinase cascade in which a kinase at each level subsequently activates the downstream kinase, phospho-protein gradients become shallower down the cascade and may spread even further upon signalling (Fig. 1.4). Introduction of an additional positive feedback by which a downstream kinase also phosphorylates its upstream activator, allows the propagation of phosphorylation waves with high velocities over potentially very large distances, e.g. during retrograde survival signalling in neurons (Markevich *et al.*, 2006).

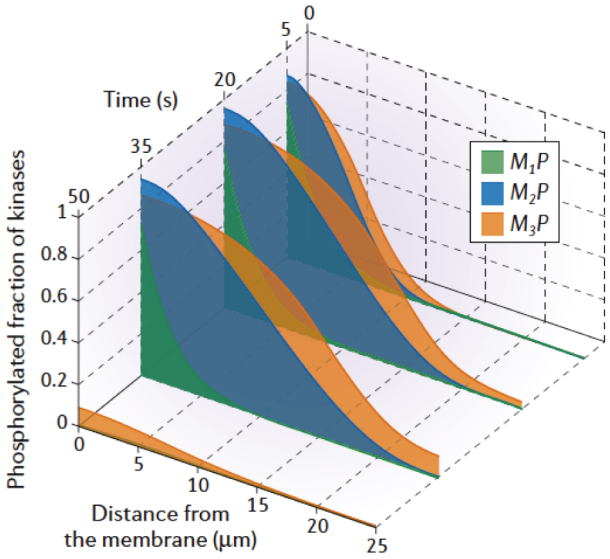

Figure 1.4: Travelling waves of phospho-proteins. Propagation of a travelling wave of phospho-proteins through a three-tiered kinase cascade in response to a transient, 30-second pulse of activity by the input = membrane bound kinase. Additional positive feedback in the cytosol may enable phosphorylation waves to propagate with high velocity over exceedingly long distances, potentially aiding in retrograde survival signalling in neurons. M_1P = phosphorylated kinase of the first level level, activated by the membrane-bound kinase; M_2P = phosphorylated second level kinase, activated by M_1P; M_3P = M_2P-activated kinase (adapted from Kholodenko, 2006).

Another mechanism to overcome spatial gradients of phospho-proteins inside living cells has been proposed with the signalling endosome hypothesis (Howe and Mobley, 2004; Howe, 2005). The signalling endosome hypothesis suggests that signalling complexes associated with endosomal membranes can be specifically transported in direction of the nucleus rather than randomly spread their signal into the cell by diffusion (Fig. 1.5). Association with endosomal membranes may also protect signalling proteins from deactivation.

Although spatial gradients of phospho-MAPKs have been shown to occur in yeasts (Maeder *et al.*, 2007), these data only provide poor temporal resolution. Moreover, no proof of phospho-MAPK gradients in mammalian cells exists until today. In addition, while spatio-temporal regulation of protein phosphatase activity has been shown to occur (Yudushkin *et al.*, 2007), the travelling waves of phospho-proteins and the signalling endosome hypothesis as mechanisms to overcome phospho-proteins gradients remain unproven. Traditional biochemical techniques do not allow the exploration of these features and previously published ERK biosensors suffer from serious disadvantages, such as a low dynamic range, indirect measurements of ERK activity and the requirement to fuse them to subcellular localisation sequences to obtain spatial information. Thus, a new

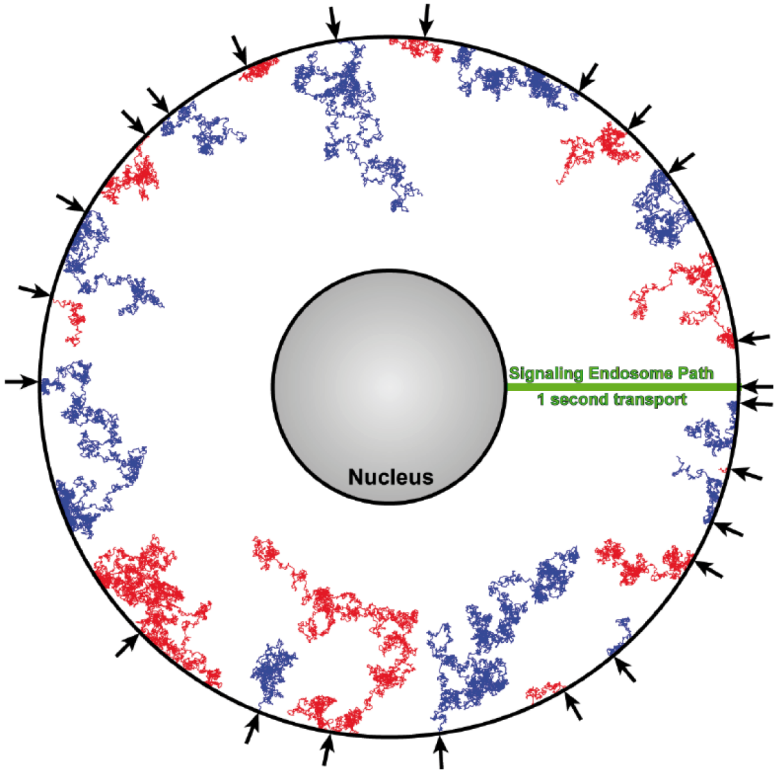

Figure 1.5: The signalling endosome hypothesis. Only "directed" transport of signalling molecules with endosomes allows signals to reach the nucleus. Representative trajectories of simulated diffusion and dephopshorylation of STAT-3 in response to Interleukin-6 signalling in 22 single events (red and blue), compared to the movement of a signalling endosome. Time frame in both cases was 1 second at 37 °C (adapted from Howe, 2005).

fluorescent ERK biosensor directly reporting MAPK activity may prove useful in the elucidation of the MAPK signalling features.

There is a plethora of data showing the importance of endosomal trafficking for MAPK signalling (Di Guglielmo *et al.*, 1994; Vieira *et al.*, 1996; Kranenburg *et al.*, 1999; Pierce *et al.*, 2000; Jiang and Sorkin, 2002; Taub *et al.*, 2007; Uhles *et al.*, 2007). For example, ERK could not be fully activated in response to EGF when receptor-mediated endocytosis was blocked by dominant negative dynamin (Vieira *et al.*, 1996). Also, appropriate trafficking of the activated EGF receptor is a prerequisite for correct spatio-temporal regulation of MAPK signalling (Taub *et al.*, 2007). A functional ERK2 biosensor may also provide new insights into the relationship of endocytosis and MAPK signalling.

1.1.2 The Extracellular Signal-Regulated Kinase (ERK)

ERK1 and ERK2 are two 44 and 42 kDa serine/threonine kinases, respectively. Like other protein kinases, ERK 1/2 are composed of a small and a big lobe (Fig. 1.6) (Chen *et al.*, 2001; Yao and Seger, 2009). The active site is formed at the interface of N- and C-terminal domains and in unphosphorylated ERK2, it is masked by the activation loop. The conformational change of the activation loop is induced by Thr183 and Tyr185 phosphorylation and coordinated by the amino acids between Asp173 and His176 of the activation loop and by the amino acids of the so-called L16 lip (Canagarajah *et al.*, 1997).

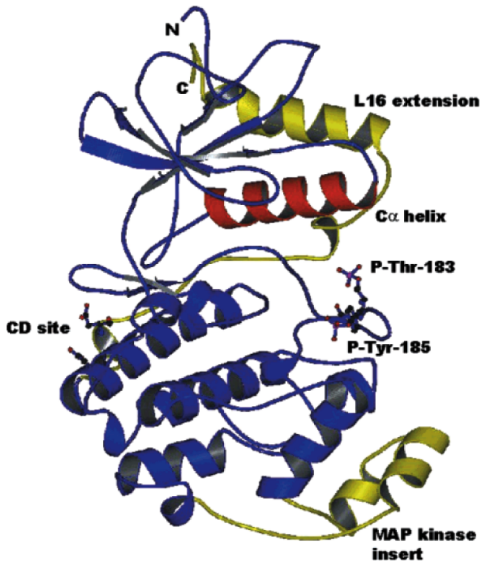

Figure 1.6: The three-dimensional structure of ERK2. The active site of ERK2 is formed at the interface of two folding domains. Phosphorylation sites (Thr183 and Tyr185) in the activation loop, the MAP kinase insert, the common docking (CD) motif, α helix C, and the C-terminal extension L16 are shown (adapted from Chen *et al.*, 2001).

ERK1/2 execute their functions through a large number of downstream target proteins, depending on the condition, cell type and cellular compartment (reviewed in Yoon and Seger, 2006). To be fully active, ERK2 has to be phosphorylated on a conserved Thr-Xxx-Tyr motif in the activation loop (Ahn *et al.*, 1991; Payne *et al.*, 1991; Robbins *et al.*, 1993). Phosphorylation is non-processive (it requires two separate phosphorylation events) (Ferrell and Bhatt, 1997) and induces a global conformational change (Canagarajah *et al.*, 1997) of the kinase that exposes the substrate-binding pocket in order to position the Ser/Thr to be phosphorylated in close proximity towards the γ-phosphate of prebound ATP. These changes induce full activity of ERK1/2, which is approximately five orders of magnitude higher than their basal activity.

The consensus phosphorylation site of ERK is Pro-Xxx-Ser/Thr-Pro, with the first proline residue being not as conserved (Gonzalez *et al.*, 1991) and Xxx as any amino

acid except proline. However, the interaction between the phospho-acceptor motif of the ERK substrate and the active site of ERK does not provide sufficient affinity and specificity (Yoon and Seger, 2006). Two additional docking motifs are being used for improved substrate recognition. One motif found in many ERK interaction partners is the D domain, a basic and hydrophobic region that interacts with ERK1/2's cytosolic retention sequence (CRS), also called common docking (CD) motif (Tanoue *et al.*, 2000). Binding of the D domain to the CRS/CD motif is independent of ERK's activity/phosphorylation state and thus can be responsible for a pre-existing ERK-substrate association. That would facilitate the phosphorylation reaction as described for scaffold proteins (see Section 5.3) (Chen *et al.*, 2001; Yoon and Seger, 2006).

The other docking motif is called the DEF (docking site for ERK) domain, which usually occurs in the form Phe-Xxx-Phe-Pro (Jacobs *et al.*, 1999; Fantz *et al.*, 2001). This motif cannot be found in all ERK substrates and is therefore believed to increase target specificity of some ERK substrates. The hydrophobic pocket that is the DEF-binding site is located in close proximity of ERK's active site (Lee *et al.*, 2004) and is only accessible for ERK substrates when the activation loop is phosphorylated. Thus, only active ERK molecules can bind to the DEF domain (Yoon and Seger, 2006).

Signalling of the Raf/MEK/ERK module is regulated by dynamic subcellular localisation (Yao and Seger, 2009). This spatial and temporal regulation is achieved by translocation of some components between subcellular compartments, the association with anchoring of scaffold proteins and a distinct set of MAPK phosphatases in each compartment (Fig. 1.7). ERK1/2 activation and localisation is dynamically controlled by continuous phosphorylation and dephosphorylation which can be differentially regulated upon stimulation (Costa *et al.*, 2006).

MEK functions as the cytoplasmic anchor of ERK1/2 in resting cells. Co-expression of MEK1 with ERK1/2 is able to retain ERK in the cytosol of unstimulated cells (Fukuda *et al.*, 1997; Rubinfeld *et al.*, 1999; Adachi *et al.*, 2000; Burack and Shaw, 2005) and this cytoplasmic retention of ERK is mediated by direct interaction with the nuclear export sequence (NES) of MEK (Fukuda *et al.*, 1997) and its D domain. Since only dephosphorylated, inactive ERK1/2 binds to MEK1/2 (Canagarajah *et al.*, 1997; Adachi *et al.*, 1999), this mechanism is thought to restore an activatable cytoplasmic pool of ERK1/2 probably ensuring and enabling sustained, continuous or oscillating ERK1/2 activation (Adachi *et al.*, 2000). In resting cells, ERK1/2 are primarily located in the cytosol, mediated by interactions with cytosolic anchors such as the MEK1/2, certain phosphatases, KSR, β-arrestin, MP1, PEA15 and some cytoskeletal proteins (Reszka *et al.*, 1995; Fukuda *et al.*, 1997; Adachi *et al.*, 1999; Blanco-Aparicio *et al.*, 1999; Morrison, 2001; Formstecher *et al.*, 2001; Gaumont-Leclerc *et al.*, 2004; Casar *et al.*, 2009; Yao and Seger, 2009). In addition, ERK dimerisation (Khokhlatchev *et al.*, 1998) is involved in binding to scaffold proteins and activation of cytosolic substrates (Casar *et al.*, 2008).

Activation of MEK leads to the dissociation of the ERK1/2 from their cytosolic anchors and is required for translocation of ERK1/2 to the nucleus (Fukuda *et al.*, 1997;

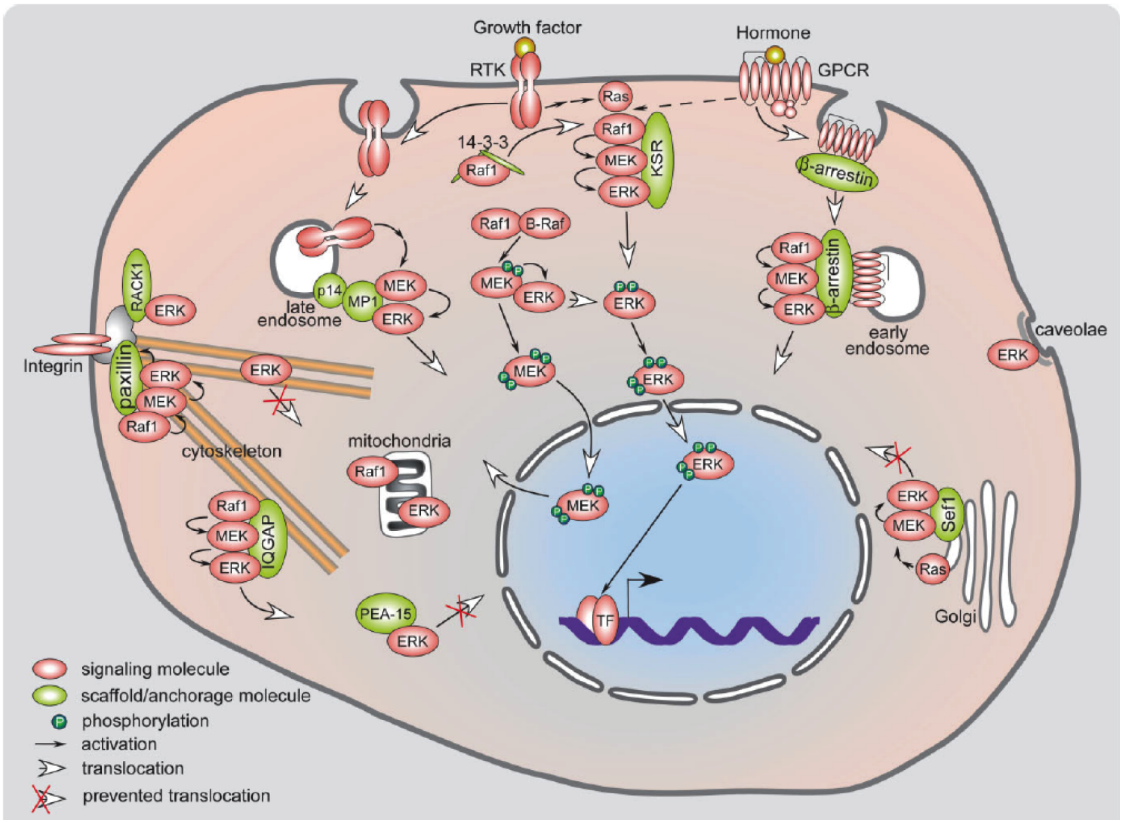

Figure 1.7: Intracellular localisation of different components of Raf/MEK/ERK signalling. Dynamic subcellular localisation of ERK is achieved by shuttling to subcellular compartments and controlled by various anchoring and scaffold proteins as well as a distinct set of MKPs in each compartment (adapted from Yao and Seger, 2009).

Adachi *et al.*, 1999). Translocation of ERK1/2 is phosphorylation-dependent and kinase activity is not required as e.g. kinase-dead mutants of ERK2 accumulate in the nucleus as well (Khokhlatchev *et al.*, 1998). Nuclear accumulation is rapid with a peak at around 5 - 15 min (Chen *et al.*, 1992; Lenormand *et al.*, 1993; Fukuda *et al.*, 1997; Adachi *et al.*, 1999; Ando *et al.*, 2004; Burack and Shaw, 2005; Costa *et al.*, 2006; Cohen-Saidon *et al.*, 2009), but is also reported to persist for hours (Volmat *et al.*, 2001). Phosphorylated ERK1/2 (ppERK1/2) translocates via passive and active transport mechanisms (Adachi *et al.*, 1999; Ando *et al.*, 2004; Burack and Shaw, 2005). A novel nuclear translocation signal (NTS) seems to mediate nuclear translocation of ERK1/2 (Chuderland *et al.*, 2008).

Nuclear export of ERK1/2 is mediated by the interaction of ERK with MEK1/2 via MEK's NES and the MEK-ERK complex is actively transported into the cytosol (Adachi *et al.*, 2000).

Since the activation of ERK requires phosphorylation on both threonine and tyrosine residues, it can be inactivated by serine/threonine phosphatases, tyrosine phosphatases or dual specificity phosphatases. A certain subgroup of dual specificity phosphatases known as MAP kinase phosphatases (MKPs) specifically dephosphorylates members of the MAPK family (extensively reviewed in Camps *et al.*, 2000). Stimulation of MAPK induces rapid MKP transcription. MKPs then translocate to specific subcellular compartments to inactivate MAPKs and prevent their anew activation by direct interactions.

More than 180 distinct substrates of ERK1/2 have been identified so far (Yoon and Seger, 2006; Yao and Seger, 2009). Despite the vast interest of the research community in nuclear ERK signalling and the resulting negligence for cytosolic ERK targets, approximately 50 % of the ERK substrates can be found in the cytosol (Fig. 1.2). ERK substrates can be classified into several functional groups including: a) transcription factors, b) protein kinases and phosphatases, c) cytoskeletal and scaffold proteins, d) receptors and signalling molecules, e) apoptosis-related proteins and f) others.

1.2 Visualisation of Spatio-Temporal Dynamics of Intracellular MAPK Signalling

Protein-protein interactions, as e.g. in MAPK signalling, have traditionally been analysed by biochemical and biophysical methods including affinity chromatography, co-immunoprecipitation, yeast two-hybrid screens, immunoblots and radioactive labeling (Chen *et al.*, 2003). However, while - without doubt - these techniques have generated invaluable information for the elucidation of e.g. the components of signalling pathways, they are restricted to measurements of the average activation status of a given MAPK in a population of cells (Pertz, 2010) and therefore provide very little or no spatio-temporal information. Immunofluorescence in principle offers good spatial resolution but provides only poor temporal information about protein activities due to the fixation process and is therefore unsuitable to study fast dynamic processes. As far as known, only dynamic, live cell imaging approaches using fluorescent biosensors offer sufficient spatio-temporal resolution to probe enzyme or specifically MAPK activity (Bastiaens and Pepperkok, 2000; Wouters *et al.*, 2001; Miyawaki, 2003; Yasuda, 2006; Schultz, 2007; Grecco and Verveer, 2011).

In a simple version of a fluorescent biosensor, the protein of interest is fused to a fluorescent protein (FP) and its translocation followed upon stimulation and/or activation (Wouters *et al.*, 2001). Indeed, fluorescently labeled ERK1/2 has been widely used to study dynamics of ERK activation (Ando *et al.*, 2004; Costa *et al.*, 2006; Cohen-Saidon *et al.*, 2009; Shankaran *et al.*, 2009) as its phosphorylation and thus activation induces nuclear translocation (Lenormand *et al.*, 1993; Khokhlatchev *et al.*, 1998; Lenormand *et al.*, 1998; Adachi *et al.*, 1999). Nuclear translocation of ERK2 has also been used in this study to assess growth factor stimulation in living cells (e.g. see Section 3.1). However, the phosphorylation state of ERK1/2 does not necessarily reflect its activity

as demonstrated by the finding that total ERK1/2 phosphorylation levels are unaltered when disruption of ERK dimerisation blocks cytoplasmic ERK signaling (Casar *et al.*, 2008). Here, total ERK1/2 phosphorylation levels suggest that ERK is fully active, completely ignoring that the cytoplasmic pool is blocked (Casar *et al.*, 2009). Analogously, overexpression of PEA15 prevents nuclear entry of ppERK1/2, inhibiting nuclear while concurrently enhancing cytoplasmic ERK signalling (Formstecher *et al.*, 2001; Casar *et al.*, 2009). Furthermore, ERK1/2 expressed on endogenous levels has been found to reside in the nucleus for hours after stimulation while being quickly dephosphorylated (Volmat *et al.*, 2001). And even more convincing, while nuclear translocation of ERK1/2 is phosphorylation dependent, kinase activity is not required as e.g. kinase-dead mutants of ERK2 also accumulate in the nucleus (Khokhlatchev *et al.*, 1998). Thus, the prominent nuclear translocation of ERK1/2 has caused a striking negligence for cytoplasmic ERK1/2 signalling (Casar *et al.*, 2009) for obvious reasons - it does not provide any information of cytoplasmic ERK1/2 activity.

ERK2 activation has been analysed by intermolecular FRET studies proving the direct cytoplasmic interaction of MEK1 and ERK2 in resting cells. Stimulation with EGF led to the loss of FRET and its slow recovery when ERK returned to the cytoplasm (Burack and Shaw, 2005; Fujioka *et al.*, 2006) in agreement with biochemical evidence for the MEK-ERK interaction (Fukuda *et al.*, 1997; Adachi *et al.*, 1999, 2000). But this assay also only resolves known dynamics for ERK activation since the dissociation and reassociation of the MEK-ERK complex is simply another approach to probe for ERK phosphorylation. Therefore, it does not provide information about spatio-temporal activity of ERK2. To date, as far as known, only one study reports FRET between ERK2 and a downstream substrate but it does not present time-resolved information (Debata *et al.*, 2010).

Genetically encoded, intramolecular FRET-based biosensor that report protein activities have been developed for many signalling kinases (as reviewed in Zhang *et al.*, 2002; Miyawaki, 2003; Giepmans *et al.*, 2006; Li *et al.*, 2006; Aoki *et al.*, 2008). Advantages of those FRET sensors are: they can be modularly constructed by simple genetic manipulations (Li *et al.*, 2006) according to in-principle generic design strategies (Sato *et al.*, 2002; Sato and Umezawa, 2004; Aoki *et al.*, 2008). They can be easily delivered into cells by transient or stable transfection and expression. They can be targeted to specific organelles, cells or tissues, allowing imaging of kinase activities from subcellular levels to whole organisms (Li *et al.*, 2006). There is a relatively low chance of interaction of individual parts of the sensor molecule with endogenous proteins. Additionally, due to their fixed donor-acceptor stoichiometry, they are in principle suitable for ratiometric FRET imaging, reducing instrumental costs and increasing signal-to-noise ratio, and simplifying data acquisition and analysis (Miyawaki, 2003; Yasuda, 2006; Aoki *et al.*, 2008; Grecco and Verveer, 2011).

Drawbacks of those type of FRET probes is the relatively large size of the two FPs that have to be introduced increasing sensor protein size by at least 50 kDa. Problems may also arise from sensor protein overexpression as binding of endogenous proteins

to the biosensor required for sensor action may perturb normal signalling. Differential susceptibility to photobleaching of the two fluorophores may cause artifacts in the analysis when not handled properly. Maturation of FPs is relatively slow and it should be kept in mind that efficiency of the sensor protein folding, maturation and degradation or proteolysis may effect the measurements (Miyawaki, 2003; Li *et al.*, 2006). Additional problems with data analysis or interpretation (e.g. imprecise spatial or temporal resolution) may arise due to the specific design of the FRET sensor being used.

A number of FRET-based intramolecular fluorescent biosensors for ERK2 have been described in the literature. However, they all suffer from several serious disadvantages.

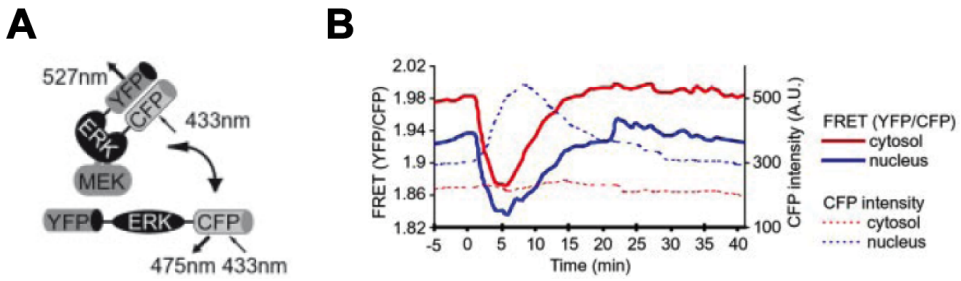

Figure 1.8: Miu2 - a FRET-based probe for monitoring ERK2 activation in living cells. A) Schematic representation of the Miu2 design. ERK2 is sandwiched by CFP and YFP. Dissociation of ERK2 from the MEK-ERK complex upon phosphorylation results in a decrease of FRET. B) ERK2 activation dynamics as measured with Miu2 in HeLa cells (adapted from Fujioka *et al.*, 2006).

Miu2 comprises of ERK2 and the FRET pair CFP-YFP fused to ERK2's N- and C-terminus (Fujioka *et al.*, 2006). The N- and C-termini of ERK2 are in close proximity. Phosphorylation of the kinase by MEK1 induces a global conformational change that alters the distance and orientation between the fluorophore pair, thereby changing the FRET signal (Fig. 1.8A). Miu2 therefore only reports the dynamics of a phosphorylation-induced conformational change of ERK2 (or the presence of phosphorylated versus non-phorphorylated ERK2) rather than localised ERK2 activity. In addition, the dynamic range of Miu2 with an approximately 6 % change is rather low (Fujioka *et al.*, 2006).

However, while confirming earlier findings about ERK activation and MEK-ERK interactions, Miu2 has not yet been proven to contribute to new findings of spatio-temporal ERK dynamics.

Another fluorescent reporter for ERK2 activity, termed ERK Activity Sensor 3 (EAS-3) is based on the conformational change of a substrate peptide for ERK2 (Green and Alberola-Ila, 2005). Amino acids 375-404 of the human transcription factor Elk1, including two minimal consensus ERK1/2 phosphorylation sites, were used as a peptide linker to fuse ECFP and EYFP. Phosphorylation of the hElk1(375-404) sequence results

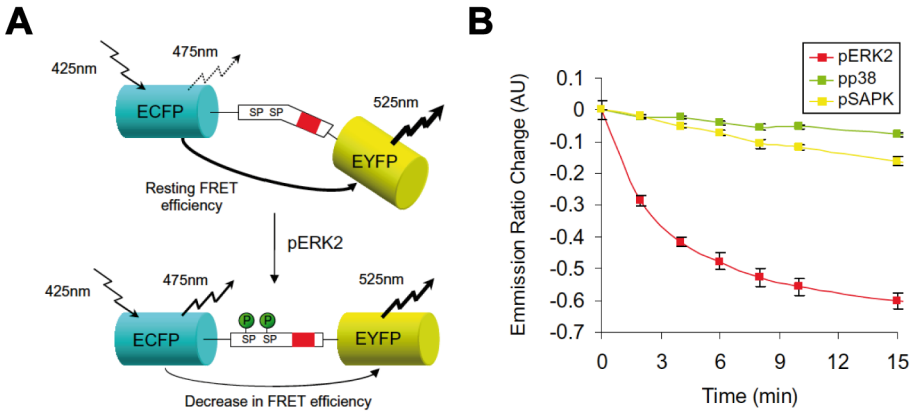

Figure 1.9: EAS-3 - a substrate-based FRET sensor for ERK2 activity. A) Schematic representation of the EAS-3 probe. A short substrate peptide of ERK2 (hElk1(375-404)) is sandwiched by ECFP and EYFP. Phosphorylation of hElk1(375-404) alters the FRET signal from the two fluorophores. The red part in the substrate peptide indicates the relative position of the DEF domain. B) Change in FRET efficiency of EAS-3 in the presence of activated kinases showing the specificity of EAS-3 for ERK2 (adapted from Green and Alberola-Ila, 2005).

in a change of secondary structure of the peptide, altering the FRET efficiency of the sensor protein (Fig. 1.9A). While the relatively small size of the sensor constructs makes it theoretically very interesting, the presented approach suffers serious flaws. For once, the sensor can only report ERK2 activity indirectly since a change in FRET efficiency requires binding of and phosphorylation by ppERK2, as well as the change of secondary structure of the peptide. Therefore, detecting localisation of ERK2 activity will be imprecise if not impossible due to rapid diffusion from active ERK. However, the study does not provide any *in-vivo* data. It is well known, that ERK activity increases dramatically shortly after cell stimulation (Lenormand *et al.*, 1993; Ando *et al.*, 2004; Burack and Shaw, 2005; Costa *et al.*, 2006; Cohen-Saidon *et al.*, 2009; Shankaran *et al.*, 2009). In contrast, data presented by Green and Alberola-Ila (2005) show a relatively slow continuous change of the FRET signal. While this maybe due to the specific conditions in the used *in-vitro* assay, it does not suggest a great potential for the detection of ERK2 activation dynamics in living cells. Finally, FRET efficiency changes are presented with arbitrary units (Fig. 1.9B), making it impossible to judge the dynamic range of EAS-3 (Green and Alberola-Ila, 2005).

Two other FRET-based ERK2 biosensor, named "Erkus" (Sato *et al.*, 2007) and "EKAR" (*E*xtracellular signal regulated *K*inase *A*ctivity *R*eporter, Harvey *et al.*, 2008a) have been developed, based on a generic design for FRET-based kinase activity reporters (Sato *et al.*, 2002; Zhang *et al.*, 2002). Essentially, a substrate peptide for ERK2 was fused to a phospho-peptide binding domain via a flexible peptide linker and then sandwiched by a FRET pair of fluorescent proteins (Fig. 1.10). Addition of an ERK2 docking motif is crucial for sensor specificity.

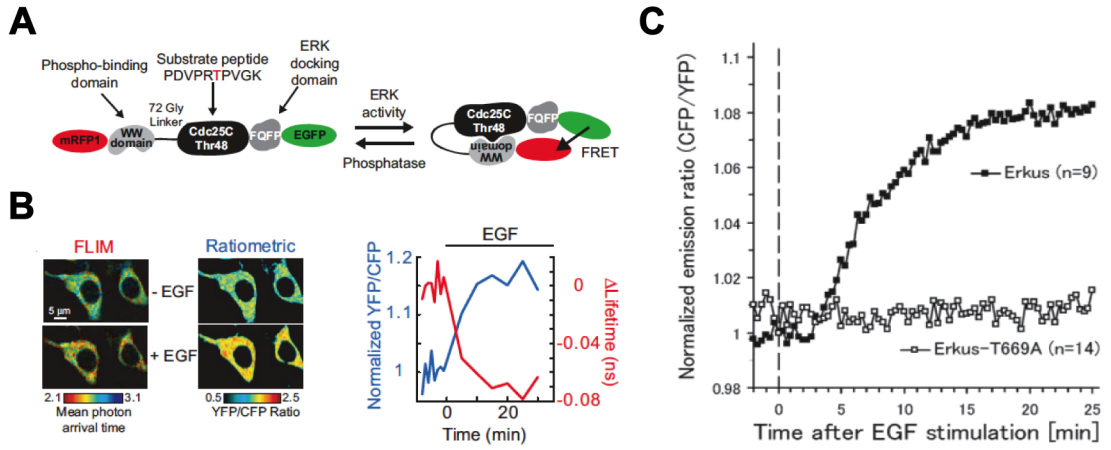

Figure 1.10: FRET-based probes for ERK2 activity based a generic design for FRET-based kinase activity reporters. A) Schematic representation of EKAR. A short substrate peptide of ERK2 and a phospho-peptide binding domain linked by a flexible peptide linker are sandwiched by a FRET pair of FPs. ERK2 phosphorylation of EKAR triggers its conformational change and the concomitant FRET signal (adapted from Harvey *et al.*, 2008a). B) and C) Dynamics of ERK2 activation as measured by Erkus and EKAR. B) (*left*): FLIM and ratio-images of HEK293 transfected with $EKAR_{cyto}$ before and after EGF treatment. (*right*): Graphs representing fluorescent lifetime (red) and FRET ratio (blue) changes from the respective images on the left (adapted from Harvey *et al.*, 2008a). C) Graphs representing the average FRET ratio change of Erkus and a dominant negative mutant expressed in MCF-7 cells upon EGF treatment (adapted from Sato *et al.*, 2007).

The dynamic range of Erkus and EKAR is not very high, as known for intramolecular FRET sensors (Li *et al.*, 2006; Aoki *et al.*, 2008). Similar to EAS-3, Erkus and EKAR also provide only indirect information about ERK2 activition and activity. Rapid diffusion of the phosphorylated sensor from active ERK will result in at best imprecise localisation of subcellular ERK2 activity. Additionally, to report dynamics of ERK2 activity rather than simple ERK2 activation kinetics, the sensor protein has to become dephosphorylated in a similar fashion as endogenous ERK2. But if the phosphatase inactivating ERK2 and dephosphorylating Erkus and/or EKAR are two different proteins, time-resolved ERK2 activity measured with those biosensors at least does not reflect true ERK2 inactivation dynamics. In fact, fusion of Erkus and EKAR to nuclear or cytoplasmic localisation sequences was necessary to discriminate at least compartmentalised ERK2 activity and resolve known ERK2 activity profiles (Sato *et al.*, 2007; Harvey *et al.*, 2008a). Taken together, the usefulness of Erkus and EKAR in detection of spatio-temporal ERK2 activity is questionable.

In addition to the general functionality of the respective sensor construct neither of the two studies introducing Erkus and EKAR has presented new findings concerning ERK signalling (Sato *et al.*, 2007; Harvey *et al.*, 2008a). Also, only one further publication

has been published until today using EKAR to investigate the effect of the A-kinase-anchoring protein AKAP-Lbc and kinase suppressor of Ras (KSR1) on MAPK signalling in HEK293 cells (Smith *et al.*, 2010).

The most direct approach to visualise spatio-temporal ERK activity would be imaging of transient enzyme-substrate interactions of ERK2. Enzymatic modification of a substrate necessarily requires its binding to the active site of the enzyme forming a transient ES complex before being released. The formation of ES complexes can be detected by measuring FRET/FLIM between a donor-tagged enzyme and an acceptor-labeled substrate peptide (Fig. 1.11) (Yudushkin *et al.*, 2007). Since the donor fluorophore is exclusively attached to the enzyme of interest, substrate-bound enzyme can be detected with almost exclusive specificity (Schultz, 2007). Using global analysis, fluorescent lifetimes can be converted into fractions of unbound and bound enzyme populations, with the latter representing the amount of ES complex (Verveer *et al.*, 2000; Lakowicz, 2006; Yudushkin *et al.*, 2007; Schultz, 2007; Grecco *et al.*, 2009). In cells, regions with high amounts of ES complexes denote regions with low enzyme activity and *vice versa* (Schultz, 2007). This technique can potentially provide information about binding affinities and kinetics of protein interactions as well as enzymatic activities both *in-vitro* and *in-vivo* (Yudushkin *et al.*, 2007; Grünberg and Serrano, 2010) and has been successfully employed to reveal spatio-temporal regulation of PTP1B upon growth factor stimulation (Yudushkin *et al.*, 2007).

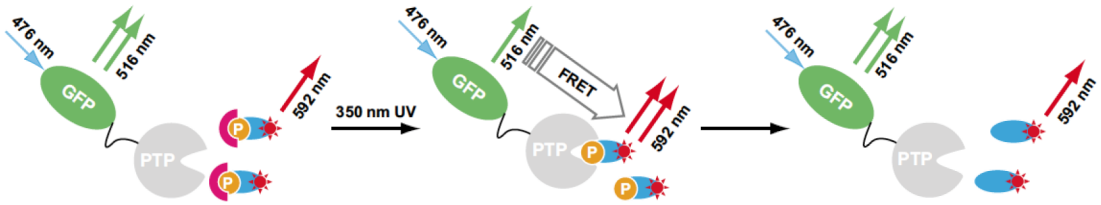

Figure 1.11: Principle of imaging enzyme-substrate interactions with FRET. Only after uncaging, the phosphorylated, synthetic substrate peptide binds to the active site of PTP1B and FRET occurs. After dephosphorylation, the substrate dissociates from the enzyme, resulting in a loss of FRET. FRET can be measured by FLIM or intensity-based methods (adapted from Yudushkin *et al.*, 2007).

No attempts to establish ES complex imaging for kinases have been published until today, though. Imaging of transient kinase-substrate and more specifically ERK2-substrate interactions follows a similar principle as visualising phosphatase-substrate interactions: the occurence and loss of FRET upon binding, phosphorylation (instead of dephosphorylation) and release of an acceptor-labeled substrate peptide to its donor-tagged kinase is recorded in spatio-temporal manner.

The ability to visualise ERK2 activity with high spatio-temporal dynamics would al-

low the investigation of a wide variety of MAPK signalling mechanisms such as growth factor signalling from endosomes (Howe and Mobley, 2004; Howe, 2005; Kholodenko, 2006), spatial gradients and travelling waves of phospho-proteins (Brown and Kholodenko, 1999; Markevich *et al.*, 2006; Kholodenko, 2006; Yudushkin *et al.*, 2007; Maeder *et al.*, 2007), oscillations in the MAPK cascade (Kholodenko, 2000, 2006), compartmental and differential MAPK signalling upon growth factor stimulation (Santos *et al.*, 2007; Nakakuki *et al.*, 2010), and the investigation of feedback loops in the MAPK module (Kholodenko, 2006; Santos *et al.*, 2007; Lin *et al.*, 2009; Smith *et al.*, 2010). However, none of the previously published FRET-based biosensor approaches developed to follow spatial and time-resolved ERK2 activity is good enough to resolve these features.

1.3 Förster Resonance Energy Transfer (FRET)

1.3.1 Principles of Förster Resonance Energy Transfer (FRET)

A molecule in an electronically excited state can relax into its ground state by emission of a photon from singlet excited states (= fluorescence) or via several non-radiative processes. One form of non-radiative relaxation into the ground state is migration of the excited state energy between the excited donor (D*) and the acceptor (A) molecule in its ground state (Fig. 1.12) (Lakowicz, 2006):

$$\mathrm{D^* + A \rightarrow D + A^*} \tag{1.1}$$

Förster resonance energy transfer (FRET), describes the non-radiative transfer of energy from an excited donor molecule to a (fluorescent) acceptor molecule located in close proximity by resonance coupling of donor and acceptor dipoles (Li *et al.*, 2006). FRET is accompanied by a decrease ("quenching") in donor quantum yield, since fewer photons are emitted directly, and excited state lifetime τ_D of the donor as the efficiency of excited state relaxation is enhanced. Simultaneously, FRET leads to enhanced (sensitised) acceptor emission because the acceptor is excited by FRET (Lakowicz, 2006; Grecco and Verveer, 2011).

The rate of energy transfer, k_T is described by (Lakowicz, 2006; Li *et al.*, 2006):

$$k_\mathrm{T} = \frac{1}{\tau_\mathrm{D}} \,\mathrm{x}\, \frac{9000 \ln k^2 \, Q_\mathrm{DA} \, J}{128 \pi^5 \, n^4 \, N_\mathrm{A}} \,\mathrm{x}\, \frac{1}{R^6} = \frac{1}{\tau_\mathrm{D}} \left(\frac{R_0}{R} \right)^6 \tag{1.2}$$

with R as the distance between the donor and acceptor. The Förster radius (R_0) is defined as the distance between the donor and acceptor where FRET efficiency is 50 % (Lakowicz, 2006; Li *et al.*, 2006):

$$R_0 = \left(\frac{9000 \ln k^2 \, Q_\mathrm{DA} \, J}{128 \pi^5 \, n^4 \, N_\mathrm{A}} \right)^{1/6} \tag{1.3}$$

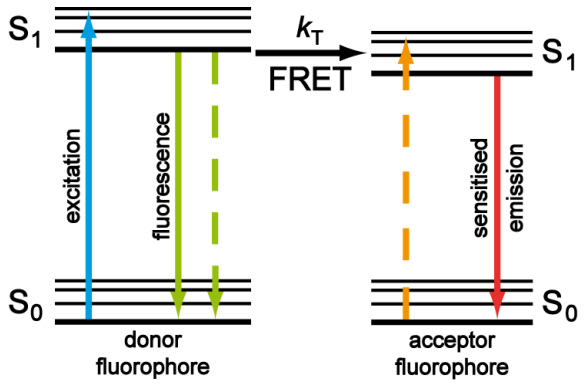

Figure 1.12: Energy transitions between electronic states during Förster Resonance Energy Transfer. Jablonski diagram illustrating the non-radiative transfer of excited state energy from the donor to the acceptor molecule. A donor molecule can be excited by the absorption of a photon from the ground state S_0 to one of the vibrational level S_1, S_2, ... (excited state of the molecule). The excited molecule returns to the ground state via several processes, e.g. the emission of photons = fluorescence. In the presence of a suitable acceptor, excited state energy can be transferred from the donor to the acceptor fluorophore without the emission of a photon. Resulting sensitised emission spectrum is similar to the acceptor emission spectrum. k_T describes the rate of energy transfer as formulated in equation 1.2.

with Q_{DA} as the quantum yield of the donor in the presence of the acceptor, n as the refractive index of the medium, N_{A} as Avogadro's number, τ_{D} as the lifetime of the donor in absence of the acceptor, k^2 as the relative orientation factor and J as the spectral overlap integral, defined by:

$$J = \int_0^\infty F_{\mathrm{D}}(\lambda)\,\epsilon_{\mathrm{A}}(\lambda)\,\lambda^4\,\mathrm{d}\lambda \tag{1.4}$$

with $F_{\mathrm{D}}(\lambda)$ as the donor emission profile and $\epsilon_{\mathrm{A}}(\lambda)$ as the acceptor's molar extinction coefficient.

The FRET efficiency (E) is defined as the probability of energy transfer per donor excitation event and can be described by (Lakowicz, 2006; Li *et al.*, 2006; Yasuda, 2006):

$$E = \frac{k_{\mathrm{T}}}{k_{\mathrm{T}} + \tau_{\mathrm{D}}^{-1}} = \frac{R_0^6}{R_0^6 + R^6} \tag{1.5}$$

The energy transfer efficiency mainly depends on three factors: the overlap of donor emission and acceptor excitation spectra (Fig. 1.13A), the orientation of donor and acceptor dipoles and the distance between the donor and acceptor fluorophore (Fig. 1.13B)(Bastiaens and Pepperkok, 2000; Chen *et al.*, 2003; Lakowicz, 2006; Li *et al.*, 2006; Grecco and Verveer, 2011).

For optimal FRET efficiencies, spectral overlap should exceed 30 % and dipole orientation of the donor acceptor pair should not be perpendicular (Chen *et al.*, 2003; Suhling

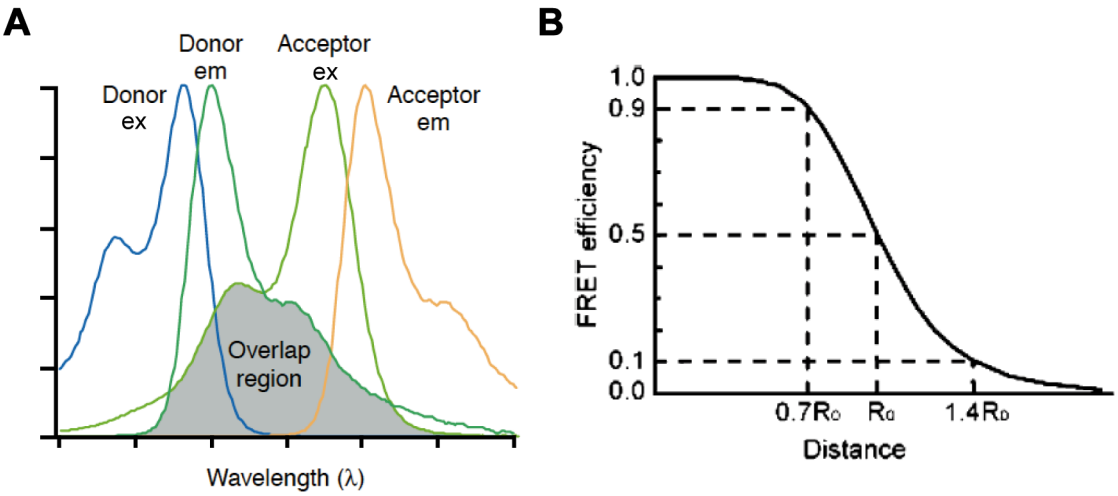

Figure 1.13: Factors influencing the FRET efficiency. A) FRET efficiency is dependent on the overlap of donor emission and acceptor excitation spectra (adapted from Bastiaens and Pepperkok, 2000). B) FRET efficiency as a function of fluorophore distance. The Förster radius (R_0) is defined as the distance between the donor and acceptor where FRET efficiency is 50 %. FRET efficiencies between 10 % and 90 % correspond to fluorophore distances of 1.4 - 0.7 R_0 (adapted from Li *et al.*, 2006).

et al., 2005). The orientation factor k^2 characterises the statistical average of relative fluorophore orientation and determines coupling of fluorophore dipoles and energy transfer efficiency. It is usually assumed to be 2/3, the value for randomised rotational diffusion of the donor and acceptor prior to FRET (Lakowicz, 2006; Li *et al.*, 2006). Preferably, the distance between the fluorophores is in a range from 0.7-1.4 R_0 (usually 4-7 nm), corresponding to 90 - 10 % FRET efficiency (Fig. 1.13B)(Li *et al.*, 2006). Since these values correspond well to the size of biomolecules or distances of protein complexes, FRET can be used as a direct proof of protein-protein interactions (Bastiaens and Pepperkok, 2000; Chen *et al.*, 2003; Lakowicz, 2006; Grecco and Verveer, 2011).

1.3.2 Intensity-Based Förster Resonance Energy Transfer (FRET) Approaches

The energy transfer efficiency is often measured using relative fluorescent intensities of the donor (and acceptor) in the prescence (I_{DA}) and absence (I_{D}) of the acceptor (Lakowicz, 2006; Yasuda, 2006):

$$E = 1 - \frac{I_{\mathrm{DA}}}{I_{\mathrm{D}}} \tag{1.6}$$

In FRET, the direct excitation of a donor molecule in close proximity to an appropriate acceptor results in sensitised emission of the acceptor fluorophore and quenching

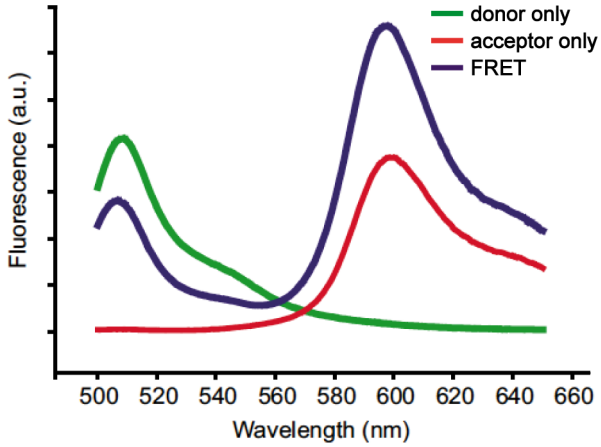

Figure 1.14: Effects of FRET on donor and acceptor fluorescence. FRET is accompanied by quenching of donor and sensitised emission of acceptor fluoroscence (adapted from Yudushkin *et al.*, 2007).

of donor fluorescence (Fig. 1.14) (Bastiaens and Pepperkok, 2000).

Several methods to assess FRET efficiency via intensity-based approaches exist, e.g. ratiometric FRET imaging, acceptor sensitised emission FRET measurements and acceptor photobleaching.

Ratiometric FRET Imaging

In ratiometric FRET imaging, the ratio of donor (I_D) and acceptor (I_A) fluorescence when excited with the donor wavelength, I_D/I_A is calculated for each pixel as a measure of relative FRET efficiencies (Yasuda, 2006). If only donor fluorophores are excited, I_D/I_A does not depend on the relative concentrations of donor and acceptor molecules. In practice, donor intensity images are divided by donor excitation/acceptor emission images, or *vice versa*. Comparison of ratio-images taken at different time points or from different conditions allows a qualitative statement about the state of FRET between two molecules. Due to the simplicity of the approach (essentially only two images are required), it can be implemented on nearly any fluorescent microscope and provides high temporal resolution limited only by the speed of the instrument. However, as relative donor and acceptor concentrations affect the FRET ratio, ratiometric imaging can only be used for fixed stoichiometries of donor and acceptor molecules (Bastiaens and Pepperkok, 2000; Zhang *et al.*, 2002; Yasuda, 2006).

Ratiometric FRET approaches are ideal to observe conformational changes of proteins and has been widely used to study signalling activities (Miyawaki *et al.*, 1997; Ting *et al.*, 2001; Itoh *et al.*, 2002; Vilardaga *et al.*, 2003; Sato and Umezawa, 2004; Fujioka *et al.*, 2006; Pertz *et al.*, 2006).

Acceptor Sensitised Emission FRET Measurements

Ratiometric FRET measurements are invalid without fixed stoichiometries of donor and acceptor molecules because fluorescent intensity is dependent on fluorophore concentration and local concentrations of donor- and acceptor-labelled proteins may vary during the course of the experiment. Alternatively, acceptor-sensitised emission can be detected as a measure of FRET. Spectral bleed through arising from the spectral overlap of the donor and acceptor molecule can contaminate the FRET signal. Several methods to avoid, minimise or correct for spectral bleed through contaminations have been developed, requiring the sequential acquisition of three (Gordon *et al.*, 1998) to seven (Elangovan *et al.*, 2003) images. Elaborate image-processing procedures are necessary to remove spectral bleedthrough and to separate direct donor and acceptor fluorescence from sensitised emission (Bastiaens and Pepperkok, 2000). Additionally, similar to ratiometric FRET imaging, the method is sensitive to differential photobleaching of donor and acceptor fluorophores.

Acceptor Photobleaching

FRET can be measured quantitatively by measuring donor fluorescence before (I_{AD}) and after acceptor (I_D) photobleaching (Bastiaens *et al.*, 1996; Kenworthy, 2001). Photobleaching of the acceptor results in an increase in donor fluorescence (dequenching). Quantitative measurements are possible when the acceptor can be bleached selectively and bleedthrough of the acceptor into the donor channel is negligible. Quantitative FRET efficiencies can be calculated by computing the ratio of donor fluorescence before and after photobleaching according to equation 1.6 (Bastiaens *et al.*, 1996; Yasuda, 2006).

Unlike sensitised emission measurements, acceptor photobleaching can be done highly specific because absorption spectra steeply drop at their red edge (Bastiaens and Pepperkok, 2000). Additionally, it requires only a single sample and FRET efficiencies can thus be directly correlated with donor and acceptor intensities. A major disadvantage of the technique is the irreversible bleaching of the acceptor fluorophore which eliminates its use for live cell and time-lapse imaging (Kenworthy, 2001).

Donor Photobleaching

Photobleaching of fluorophores occurs in electronically excited states (Lakowicz, 2006). Since FRET shortens the excited state lifetime, it protects a fluorescent molecule from photobleaching. Therefore donor photobleaching in the presence and absence of the acceptor can be used to measure FRET by comparing donor photobleaching curves. This, however, requires fitting (multi-component) time constants (Jovin and Arndt-Jovin, 1989; Kenworthy, 2001).

1.3.3 Principles of Fluorescent Lifetime Imaging Microscopy (FLIM)

One major disadvantage of intensity-based FRET approaches is their sensitivity to local fluctuations of fluorophore concentration which cannot be controlled experimentally.

Different sensitivities of donor and acceptor fluorophores to photobleaching may also lead to artifacts. Additionally, quantification of FRET efficiencies obtained by intensity-based methods often requires elaborate multiparameter calibration procedures (Elangovan *et al.*, 2003).

The fluorescence lifetime is an intrinsic property of a fluorophore that is independent of light path length and probe concentration but dependent on processes that influence the efficiency excited state relaxation such as FRET. It is also affected by the local environment, e.g. ion and/or oxygen concentration, pH, polarity, and viscosity (Suhling *et al.*, 2005; Lakowicz, 2006). Fluorescent (excited state) lifetime based FRET approaches only measure donor fluorescent lifetime and therefore do not require absolute specificity of the acceptor-labeled probe. Global analysis of FLIM data allows the quantitative estimation of FRET efficiencies as well as of fractions of interacting molecules (Verveer *et al.*, 2000; Grecco *et al.*, 2009).

The fluorescent lifetime τ is defined as the average time a fluorophore remains in the excited state following excitation and can be described by (Suhling *et al.*, 2005; Lakowicz, 2006):

$$\tau = \frac{1}{k_{\mathrm{r}}^{\mathrm{S}} + k_{\mathrm{nr}}^{\mathrm{S}}} \tag{1.7}$$

with k_{r} as the rate constant for radiative deactivation and k_{nr} as the rate constant for non-radiative deactivation, while the latter is the sum of the rate constant for internal conversion k_{ic} and the rate constant for intersystem crossing k_{isc}: $k_{\mathrm{nr}} = k_{\mathrm{ic}} + k_{\mathrm{isc}}$. It is mainly the influence of environmental factors on the non-radiative rate constant k_{nr} that is measured with FLIM (Festy *et al.*, 2007).

It is important to note that the lifetime is a statistical value, meaning the excited fluorophores emit their photons randomly after excitation into the excited state by absorption of a photon. Thus, when excited with an infinitesimal short pulse of light the excited state population and consequently the fluorescent intensity decay exponentially according to (van Munster and Gadella, 2005; Lakowicz, 2006):

$$I(t) = I_0 \exp\left(-t/\tau\right) \tag{1.8}$$

with *I(t)* as the fluorescent intensity as a function of time, I_0 as the intensity at time 0, and t as time. It should be noted that equation 1.8 is only valid for fluorophores with mono-exponential decay rates.

Fluorescent lifetime measurements are often used to measure quantitatively the occurence of FRET in biological samples. FRET leads to a decrease in donor fluorescence lifetime because it provides an additional decay process for the donor molecule by facilitating the relaxation of the donor-excited state (Breusegem *et al.*, 2006). The energy

transfer efficiency can also be calculated from the fluorescent lifetimes (τ_{DA} and τ_D) (Lakowicz, 2006):

$$E = 1 - \frac{\tau_{DA}}{\tau_D} \tag{1.9}$$

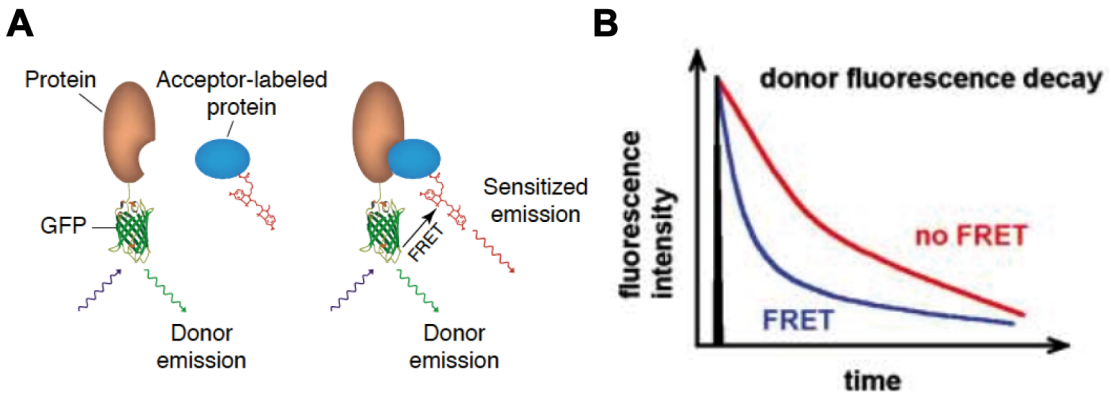

Figure 1.15: The effect of FRET on the donor fluorescence decay. A) FRET can occur when a donor (GFP)-and acceptor-tagged protein (red and blue) are within a distance of less than 10 nm. Thus, FRET can be used to show protein-protein interactions far beyond the usual resolution limit of conventional light microscopes (adapted from Wouters *et al.*, 2001). B) FRET leads to a shortened excited-state lifetime of the donor fluorophore (adapted from Suhling *et al.*, 2005).

1.3.4 Fluorescent Lifetime-Based FRET Approaches

Mainly, two different principles are used to determine fluorescent lifetimes, frequency-domain and time-domain fluorescent lifetime measurements.

Frequency-Domain Fluorescent Lifetime Measurements

For frequency-domain fluorescent lifetime measurements, the intensity of the excitation light is sinusoidally modulated with a frequency reciprocal to the fluorescent lifetime of interest. Due to the non-instant fluorescent decay (the lifetime of the fluorophore causes the emission light to be delayed in time relative to the excitation light), the fluorescence emission will be sinusoidally modulated but display a reduction in relative modulation depth and a phase shift (Fig. 1.16) (Bastiaens and Squire, 1999; van Munster and Gadella, 2005; Lakowicz, 2006). Phase shift ($\Delta\Phi$) and relative modulation depth (M) can be used to calculate phase (τ_Φ) and modulation lifetimes (τ_M) according to:

$$\tau_\Phi = \omega^{-1} \tan(\Delta\Phi) \tag{1.10}$$

$$\tau_{\mathrm{M}} = \omega^{-1} \sqrt{(\mathrm{M})^{-2} - 1} \tag{1.11}$$

with ω as the modulation frequency.

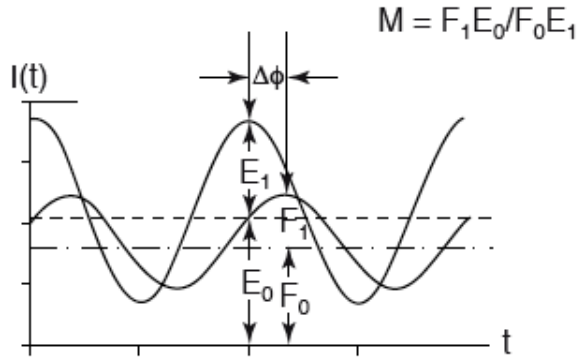

Figure 1.16: Principle of frequency-domain fluorescence lifetime measurements. In frequency-domain fluorescent lifetime measurements, the excitation light is sinusoidally modulated. From the resulting phase shift and demodulation of the emitted fluorescence, the lifetime of the fluorophore can be determined according to equations 1.10 and 1.11 with $\Delta\Phi$ as the phase shift, M the demodulation factor or modulation, E_0 as the peak-to-peak height, F_0 as the average intensity of the excitation light, and E_1 as the peak-to-peak height and F_1 as the average intensity of the emission light. The x-axis and y-axis denots time and intensity, respectively (adapted from Bastiaens and Squire, 1999).

Phase and modulation lifetimes are equal ($\tau_\Phi = \tau_{\mathrm{M}}$) in samples that contain only a single species of mono-exponentially decaying fluorophore molecules. For fluorophores with multi-exponential decay lifetimes or in samples containing more than one species of fluorophores, the phase lifetime may be smaller than the modulation lifetime ($\tau_\Phi < \tau_{\mathrm{M}}$) and the lifetime composition can be obtained by measuring phase and modulation lifetimes using multiple modulated excitation frequencies (Bastiaens and Squire, 1999; Suhling *et al.*, 2005; van Munster and Gadella, 2005).

Time-Domain Fluorescent Lifetime Measurements

In time-domain lifetime measurements, the sample is excited with a very short (relative to the lifetime to be measured) pulse of light, resulting in an exponential decrease of fluorescence emission intensity over time. The fluorescent lifetime τ can be calculated from the decay curve as the time at which the intensity decreases to $1/exp$ of the intensity at $t = 0$ (Bastiaens and Squire, 1999; van Munster and Gadella, 2005; Lakowicz, 2006).

Time correlated single photon counting (TCSPC) was used to determine fluorescent lifetimes. In TCSPC, the arrival time of the first photon after the excitation pulse is

recorded at high time resolution. These arrival times can be stored in a histogram with the x-axis denoting the arrival time and the y-axis the number of photons per time difference. Recording photon arrival time after the excitation pulse for a large number of photons yields a representation of a decay curve as exemplified in Fig. 1.17.

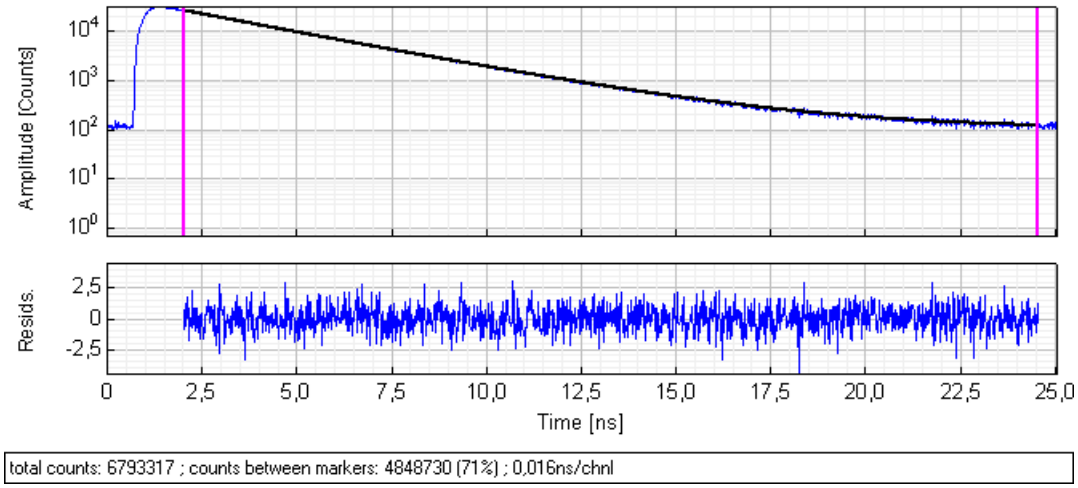

Figure 1.17: Exemplified TCSPC histogram of a fluorophore with a mono-exponential decay rate. The TCSPC histogram was recorded from living HeLa cells expressing mCitrine-ERK2 using an Olympus FluoView FV1000 laser scanning confocal microscope equipped with PicoQuant's compact lifetime and FCS upgrade kit, and displayed and analysed with PicoQuant's SymPhoTime v5.12 software. The number of photons (counts) collected for the whole 256x256 pixel image is plotted against the arrival time interval (blue lines, top). The residuals (bottom) evaluate the error in the fit. Tail-fitting (black line) for the fluorescence decay yields a lifetime of 3.04 ns and a χ^2 of 1.047.

After acquisition of the photon-counting histogram, time-domain fluorescent lifetime data are analysed by fitting fluorescence decay models to the decay curves (Fig. 1.17). For the fitting, the initial part of the decay curve including the peak is excluded as the decay curve here is influenced by the instrument response function (IRF). The corresponding analysis is called a "tailfit". When it is assumed that the decay follows a single-exponential decay model, equation 1.8 may be employed for fitting. In case more than one lifetime is to be expected in the sample, e.g. for FRET analysis, a multi-exponential fluorescence decay can be fitted according to the following model (Lakowicz, 2006):

$$I(t) = \sum_{i=1}^{n} A_i \exp(-t/\tau_i) + B \tag{1.12}$$

with B as the background, n as the number of decay times present, the pre-exponential factor A_i as the amplitudes of the components and τ_i as the fluorescent lifetimes.

The pre-exponential factors A_i have different meanings for the case of one fluorophore displaying a complex decay or a mixture of fluorophores. While for the latter A_i values depend on concentrations, absorption, quantum yield and intensities of each fluorophore,

for fluorophores with a complex decay, the A_i values yield information about the fraction of molecules in each conformation (Lakowicz, 2006). During the analysis of FRET measurements using a mono-exponentially decaying fluorophore, equation 2.1 can be used with A_2 and A_1 approximating the population of fluorophores undergoing FRET versus the population of fluorophore molecules that do not FRET, and τ_1 and τ_2 corresponding to the quenched and unquenched lifetime. The amplitudes, however, do not exactly correspond to actual fractions (= numbers of molecules) of quenched versus unquenched fluorophores as they denote intensity amplitudes and are therefore influenced by the quantum yield of the fluorophore.

2 Material and Methods

2.1 Material

2.1.1 Chemicals

Adenosin-5'-triphosphate (ATP)	Sigma-Aldrich®
Ammonium persulfate (APS)	SERVA Electrophoresis GmbH
Ampicillin sodium salt	SERVA Electrophoresis GmbH
Bromphenolblue	Sigma-Aldrich®
2'-deoxyadenosine-5'-triphosphate (dATP)	Invitrogen^{TM} Life Technologies
2'-deoxycytidine-5'-triphosphate (dCTP)	Invitrogen^{TM} Life Technologies
2'-deoxyguanosine-5'-triphosphate (dGTP)	Invitrogen^{TM} Life Technologies
2'-deoxythymidine-5'-triphosphate (dTTP)	Invitrogen^{TM} Life Technologies
Dimethyl sulfoxide (DMSO)	SERVA Electrophoresis GmbH
Disodium hydrogen phosphate (Na_2HPO_4)	Merck KG
Dithiothreitol (DTT)	Fluka® Analytical
Ethanol	J.T.Baker
Ethidium bromide (10 mg/ml)	Fisher Scientific
Ethylenediaminetetraacetic acid (EDTA)	Fluka® Analytical
Glycerol	GERBU Biotechnik GmbH
Glycine	Carl Roth GmbH
Hoechst 33342, trihydrochloride, trihydrate	Molecular Probes^{TM}
N-(2-Hydroxyethyl)Piperazine-N'-ethane-2-sulfonic acid (HEPES)	GERBU Biotechnik GmbH
Imidazole	Merck KG
Isopropanol	J.T.Baker
Isopropyl β-D-thiogalactopyranoside (IPTG)	AppliChem GmbH
Kanamycine sulfate	GERBU Biotechnik GmbH
Lissamine rhodamine B sulfonyl chloride	AnaSpec, Inc.
Magnesium chloride ($MgCl_2$)	Merck KG/J.T.Baker
Methanol	AppliChem GmbH
2-Mercapto-ethanol	SERVA Electrophoresis GmbH
Monopotassium phosphate (KH_2PO_4)	J.T. Baker
Pefabloc	Fluka® Analytical
Phosphatase Inhibitor Cocktail 1	Sigma-Aldrich®
Phosphatase Inhibitor Cocktail 2	Sigma-Aldrich®
Phorbol-12-myristat-13-acetat (PMA)	AppliChem GmbH
Potassium chloride (KCl)	J.T.Baker

Sodium acetate (NaOAc)	Merck KG
Sodium chloride (NaCl)	Fluka® Analytical
Sodium dodecyl sulfate (SDS)	SERVA Electrophoresis GmbH
Sucrose	USB Corporation
N,N,N',N'-Tetramethylene-diamine (TEMED)	Sigma-Aldrich®
Tris-base	Carl Roth GmbH
Tris-HCl	J.T. Baker
Triton X-100	SERVA Electrophoresis GmbH
Tween 20	SERVA Electrophoresis GmbH
U0126 (MEK1/2 Inhibitor)	Cell Signaling Technology®
UltraPure™ Agarose	Invitrogen™ Life Technologies
Yeast extract	Fluka® Analytical

2.1.2 Enzymes, Hormones and Antibodies

active MEK1 (250,000 U/mg)	Merck KG
*Age*I (5,000 U/ml)	New England Biolabs Inc.
alpha-Tubulin (mouse, A11126)	Invitrogen™ Life Technologies
*BamH*I (20,000 U/ml)	New England Biolabs Inc.
*BspE*I (10,000 U/ml)	New England Biolabs Inc.
*BsrG*I (10,000 U/ml)	New England Biolabs Inc.
Elk1 (I-20) (rabbit, sc-355)	Santa Cruz Biotechnology, Inc.
Epidermal Growth Factor (Human EGF)	Cell Signaling Technology®
Heregulin (HRG)	Millipore™
*Hind*III (20,000 U/ml)	New England Biolabs Inc.
Insulin from bovine pancreas	Sigma-Aldrich®
IRDye® 680 goat anti-rabbit IgG	LI-COR® Biosciences
IRDye® 800CW goat anti-mouse IgG	LI-COR® Biosciences
*Nco*I (10,000 U/ml)	New England Biolabs Inc.
p44/42 MAPK (rabbit, #9102)	Cell Signaling Technology®
PfuUltra High-Fidelity DNA polymerase AD	Stratagene
phospho-Elk1 (B-4) (mouse, sc-8406)	Santa Cruz Biotechnology, Inc.
phospho-p44/42 MAPK (Thr202/Tyr204) (E10) (monoclonal, mouse, #9106)	Cell Signaling Technology®
Platinum® Pfx DNA polymerase	Invitrogen™ Life Technologies
*Sal*I (20,000 U/ml)	New England Biolabs Inc.
shrimp alkaline phosphatase (SAP) (10,000 U/ml)	New England Biolabs Inc.
*Xho*I (20,000 U/ml)	New England Biolabs Inc.

2.1.3 Oligonucleotides

All oligonucleotides were purchased from Sigma-Aldrich Chemie GmbH in HPLC purified form. Primer sequences are detailed in S.6 .

2.1.4 Plasmids

mCherry-C1	Clontech Laboratories Inc.
mCitrine-C1	Clontech Laboratories Inc.
mCitrine-N1	Clontech Laboratories Inc.
MEK1-mCherry	kind gift by Piet Lommerse, Max-Planck-Institute of Molecular Physiology, Dortmund, Germany
pcDNA3.1(+)	Invitrogen^{TM} Life Technologies
pEGFP-C1	Clontech Laboratories Inc.
pEGFP-hElk1	kind gift by Robert A. Hipskind, Institut de Genetique Moleculaire de Montpellier, Montpellier, France
pET-ERK2	kind gift by Piet Lommerse, Max-Planck-Institute of Molecular Physiology, Dortmund, Germany
pEYFP-MEK1	kind gift by Piet Lommerse, Max-Planck-Institute of Molecular Physiology, Dortmund, Germany
pProEx HTB	kind gift by Alfred Wittinghofer, Max-Planck-Institute of Molecular Physiology, Dortmund, Germany

2.1.5 Buffers and Solutions

ERK2 elution buffer	20 mM Tris (pH 7.5), 250 mM NaCl, 200 mM imidazole, 1 mM DTT, 0.1 % Triton X-100, 0.1 mM Pefabloc, protease inhibitors
ERK2 lysis buffer	20 mM Tris (pH 7.5), 200 mM NaCl, 1 mM DTT, 0.1 % Triton X-100, 0.1 mM Pefabloc, protease inhibitors
ERK2 storage buffer	20 mM Tris (pH 7.5), 100 mM NaCl, 1 mM DTT, 0.1 % Triton X-100, 10 % glycerol, 0.1 mM Pefabloc, protease inhibitors
ERK2 wash buffer	20 mM Tris (pH 7.5), 250 mM NaCl, 5 mM imidazole, 1 mM DTT, 0.1 % Triton X-100, 0.1 mM Pefabloc, protease inhibitors
LB agar plates	add 15 g agar per litre LB medium, pour plates when the autoclaved medium has approx. 55 °C, if desired add appropriate concentration of the desired antibiotic
LB medium	10 g/l Bacto-Trypton, 5 g/l bacto-yeast extract, 10 g/l NaCl, autoclave

1x PBS (pH 7.4)	137 mM NaCl, 10 mM Na_2HPO_4, 2.6 mM KCl, 1.8 mM KH_2PO_4
5x SDS sample buffer	60 mM Tris-HCl (pH 6.8), 25 % glycerol, 2 % SDS, 14.4 mM 2-mercapto-ethanol, 0.1 % brom-phenolblue
SDS running buffer	25 mM Tris-base, 192 mM glycine, 0.1 % SDS
separating gel buffer	1.5 M Tris-HCl (pH 8.8)
SOC medium	20 g/l Bacto-Trypton, 5 g/l bacto-yeast extract, 0.5 g/l NaCl, 2.5 mM KCl, 10 mM $MgCl_2$ (SOB medium), autoclave, before use add 20 mM glucose to obtain SOC medium
stacking gel buffer	0.5 M Tris-HCl (pH 6.8)
1x TAE buffer	40 mM Tris/Acetate (pH 7.5), 20 mM NaOAc, 1 mM EDTA
1x TBST	100 mM Tris-HCl (pH 7.4), 150 mM NaCl, 0.1 % Tween 20
transfer buffer	25 mM Tris-base, 192 mM glycine, 0.1 % SDS, 20 % methanol

2.1.6 Kits and Purchased Solutions

Kits and Purchased Solutions for Working with DNA

BigDye® Terminator v3.1 cycle sequencing kit	Applied Biosystems
100x BSA	New England Biolabs Inc.
6x DNA gel loading buffer	Novagen
2-log DNA ladder	New England Biolabs Inc.
100 mM dNTP mix	Invitrogen™ Life Technologies
DyeEx® 2.0 Spin kit	QIAGEN
GelPilot loading dye, 5x	QIAGEN
50 mM Magnesium Sulfate	Invitrogen™ Life Technologies
NucleoBond® Xtra Maxi EF kit	Macherey-Nagel GmbH & Co. KG.
10x *Pfx* amplification buffer	Invitrogen™ Life Technologies
10x PCR_x Enhancer solution	Invitrogen™ Life Technologies
QIAprep® Spin Miniprep kit	QIAGEN
QIAquick® Gel Extraction kit	QIAGEN
QIAquick® PCR Purification kit	QIAGEN
Quick Ligation™ Kit	New England Biolabs Inc.
QuikChange XL Site-Directed Mutagenesis kit	Stratagene
10x Restriction Enzme Buffer 1	New England Biolabs Inc.
10x Restriction Enzme Buffer 2	New England Biolabs Inc.
10x Restriction Enzme Buffer 3	New England Biolabs Inc.
10x Restriction Enzme Buffer 4	New England Biolabs Inc.
Zero Blunt® TOPO® PCR cloning kit	Invitrogen™ Life Technologies

Kits and Purchased Solutions for Working with Proteins

30 % Acrylamide/Bis solution	Bio-Rad Laboratories, Inc.
Blocking buffer for near infra-red fluorescent western blotting	Rockland Inc.
Bradford reagent	Sigma-Aldrich®
10x Cell lysis buffer	Cell Signaling Technology®
Complete Mini EDTA-free protease inhibitor tablets	Roche Applied Science
Micro BCA™ Protein Assay reagent kit	Pierce Biotechnology Inc.
Ni-NTA His•Bind® Resins	Novagen
Odyssey Infrared Imaging System blocking buffer	Li-Cor® Biosciences
Precision Plus Protein™ standards	Bio-Rad Laboratories, Inc.
1x TBS	Sigma-Aldrich®
TC-FlAsH™ TC-ReAsH™ II In-Cell Tetracysteine Tag Detection Kit	Invitrogen™ Life Technologies

Kits and Purchased Solutions for Working with Cells

DPBS	PAN™ Biotech GmbH
Dulbecco's Modified Eagle's Medium (DMEM)	PAN™ Biotech GmbH
Fetal calf serum (FCS)	PAN™ Biotech GmbH
Fugene® 6 transfection reagent	Roche Applied Science
L-Glutamine	GIBCO®/Invitrogen™ Life Technologies
Trypsin/EDTA	PAN™ Biotech GmbH

2.1.7 Bacterial Strains

One Shot® TOP10 Competent Cells	Invitrogen™ Life Technologies
Rosetta™2(DE3) Singles™ Competent Cells	Novagen
XL10 Gold	

2.1.8 Mammalian Cell Lines

Cell line	Origin	Supplier	Reference
COS-7	african green monkey kidney fibroblast	ATCC	(Gluzman, 1981)
HeLa	human cervical adenocarcinoma	ATCC	(Gey *et al.*, 1952)
MCF-7	human mammary gland adenocarcinoma	ATCC	(Brooks *et al.*, 1973; Soule *et al.*, 1973)
MDA-MB-231	human mammary gland adenocarcinoma	ATCC	(Cailleau *et al.*, 1974)

2.1.9 Material and Equipment

Centrifuges & Rotors

Centrifuge "5415R"	Eppendorf
Centrifuge "5810R"	Eppendorf
Centrifuge "RC 26 Plus"	Sorvall®
Rotor "SH-3000"	Sorvall®
Rotor "FA-45-24-11"	Eppendorf
Rotor "FL 064-04053"	Eppendorf
Vacuum centrifuge "Concentrator 5301"	Eppendorf

Material and Equipment for Working with DNA

Gel Imaging Station	Bio-Rad Laboratories
Gene Pulser™	Bio-Rad Laboratories
PCR-Cycler "Mastercycler **ep**gradient"	Eppendorf
Power Pac™ 1000	Bio-Rad Laboratories
Pulse controller	Bio-Rad Laboratories

Material and Equipment for Working with Proteins

A-1010B™ arc lamp	PTI® - Photon Technology International
Amicon Ultra-15 centrifugal filter unit (NMWL 30K)	Millipore™
BryteBox	PTI® - Photon Technology International

1.0 mm cassettes for western blots	Invitrogen™ Life Technologies
1.0 mm 10-well combs	Invitrogen™ Life Technologies
Econo-Pac® 10 DG disposable chromatography columns	Bio-Rad Laboratories, Inc.
Fluorescence cuvettes (30 μl, 45 μl, 100 μl)	Hellma GmbH & Co. KG
Incubation box for western blots	Li-Cor® Biosciences
Incubator Shaker Series I26	New Brunswick Scientific
LPS-220B lamp power supply	PTI® - Photon Technology International
MD 5020 motor driver	PTI® - Photon Technology International
Nitrocellulose membrane	Bio-Rad Laboratories, Inc.
Odyssey Infrared Imager	Li-Cor® Biosciences
Plate reader "Multiskan Askent"	Thermo Scientific
814 photomultiplier detection system	PTI® - Photon Technology International
Power Pac™ HC	Bio-Rad Laboratories, Inc.
QuantaMaster™ fluorescent spectrometer	PTI® - Photon Technology International
Sonicator needle (MS 73)	Bandelin Electronic GmbH & Co. KG
Sonicator	
TCM-1000 control module	PTI® - Photon Technology International
Test tube rotator "34528"	Snijders
UV-Cuvettes (1 ml)	Sarstedt Aktiengesellschaft & Co.
96-well ELISA microplates	Greiner Bio-One GmbH
XCell *SureLock*™ Mini-Cell	Invitrogen™ Life Technologies
XCell II™ blot module	Invitrogen™ Life Technologies

Material and Equipment for Working with Cells

Cell scraper	BD Falcon™
Cryo vials	
Easy Grip™ tissue culture dish (60 mm)	BD Falcon™
75 mm filter unit	Nalge Nunc International
Glass pasteur pipettes (150 mm, 230 mm)	Brand GmbH & Co. KG
4-well LabTek® chambers No. 1.0	Nalge Nunc International
8-well LabTek® chambers No. 1.0	Nalge Nunc International
NALGENE® Cryo 1 °C freezing container	Nalge Nunc International
35-mm MatTek petri dishes No. 1.5	MatTek Corporation
NUAIRE™ Cellgard class II biological safety cabinet	Integra Biosciences
T75 tissue culture flask	BD Falcon™
Tissue culture plate (12 well)	BD Falcon™

Vacusafe comfort	Integra Biosciences
Vi-Cell^{TM} XR cell viability analyzer	Beckman Coulter, Inc.

General Material and Equipment

Eppendorf safe lock tubes (0.5 ml, 1.5 ml, 2.0 ml)	Eppendorf
Falcon tubes (15 ml, 50 ml)	BD Falcon^{TM}
Heatable magnetic stirrer "IKAMAG® RCT"	IKA® Labortechnik
Heating block "QBD4"	Grant Instruments
Nanodrop® ND-1000 spectrophotometer	Peqlab Biotechnologie GmbH
Parafilm®	Pechiney Plastic Packaging
PFE powder-free latex exam gloves (M)	Kimberly-Clark
Pipetboy acu	Integra Biosciences
Safegrip® nitril gloves (M)	Süd-Laborbedarf GmbH
Sarstedt serological pipettes (5 ml, 10 ml, 25 ml)	Sarstedt Aktiengesellschaft & Co.
Scale "Precisa 62 A"	Precisa Instruments AG
Scale "Precisa 620 C"	Precisa Instruments AG
Scale "type 1574"	Sartorius AG
Surgical disposable scalpel (No. 11, No. 21)	Braun Melsungen AG
Thermomixer comfort	Eppendorf
"Vortex Genie 1" touch mixer	Scientific Industries

2.1.10 Microscopes

"Axiovert 200 M" inverse fluorescence microscope	Carl Zeiss MicroImaging GmbH
"CellR"	Olympus
Compact lifetime and FCS upgrade kit for LSMs	PicoQuant GmbH
"LSM510" Confocal laser scanning system	Carl Zeiss MicroImaging GmbH
"E-665 LVPZ" controller/amplifier	Physik Instrumente GmbH & Co. KG
Fiber coupling unit	PicoQuant GmbH
"FluoView FV1000" confocal laser scanning biological microscope	Olympus
"IU-LH75XEAPO" 75 W xenon APO lamp	Olympus

"IX 81" inverse microscope	Olympus
"IX2-UCB" controlling unit	Olympus
LIFA fluorescent lifetime signal generator	Lambert Instruments
LI_2CAM MD modulated intensified camera	Lambert Instruments
"PR-IX2" motorised stage	Olympus
"PZ 116E" computer interface and command interpreter submodule for PZT controller	Physik Instrumente GmbH & Co. KG
Scan Stage	Olympus
"Sepia II" computer controlled multi-channel picosecond pulsed laser diode	PicoQuant GmbH
"U-HSTR2" hand switch	Olympus
UPLSAPO 40x/0.9 NA	Olympus
UPLSAPO 60xW/1.2 NA	Olympus
"U-RFL-T"	Olympus

2.1.11 Software

Adobe Illustrator	Adobe Systems Inc.
BibDesk 1.5.3	http://bibdesk.sourceforge.net
FeliX32	PTI® - Photon Technology International
FV10-ASW Fluoview Software	Olympus
ImageJ 1.42	http://rsbweb.nih.gov/ij/index.html
LIFA software	Lambert Instruments
Microsoft Excel 2003	Microsoft Corporation
MikTex 2.8	http://miktex.org/
MacPyMOL	http://www.pymol.org/
SymPhoTime v5.12	PicoQuant GmbH
TeX Live 2009	http://www.uoregon.edu/ koch/texshop/
Vector NTI 10	Invitrogen^{TM} Life Technologies

2.2 Methods

2.2.1 Cloning

2.2.1.1 Bacterial Cultures

E. coli cells were grown in solution (LB + appropriate antibiotic) at 37 °C and 225 rpm if not stated otherwise. Cultures of 4 ml LB medium were inoculated with a single clone (colony) grown on agar plates. After 6-10 h, the pre-culture was used to inoculate the desired volume of main culture.

2.2.1.2 Transformation of Chemically Competent *E. coli*

Transformation is defined as the non-viral introduction of foreign DNA in competent bacterial cells and is used to amplify recombinant DNA. Chemical transformation of bacteria usually has a transformation efficiency of 1 x 10^6-1 x 10^8 colonies/μg DNA.

50 μl chemically competent *E. coli* XL 10 Gold were incubated with 1.75 μl 2.25 mM DTT and 0.1 μl plasmid DNA, or 2.5 -7.5 μl ligation mix, respectively, for 20-30 min on ice. The transformation mix was heat shocked for 60 sec at 42 °C and placed back on ice for 2 min. 250 μl of SOC medium were added and bacteria were allowed to recover for 45-60 min at 37 °C, 225 rpm. 100 μl cell suspension were plated on LB agar plates containing the required antibiotics and placed at 37 °C overnight or at RT over the weekend, respectively.

2.2.1.3 Transformation of Electro-Competent *E. coli*

Electroporation is considered to be the gold standard for transformation of competent bacteria as transformation efficiencies of up to 1 x 10^{10} colonies/μg DNA can be achieved. Usually chemically competent cells were used for amplification of recombinant DNA. Especially complicated or difficult cloning experiments were instead performed using electro-competent XL10 Gold.

For electroporation 50 μl electro-competent *E. coli* XL 10 Gold were mixed with 50 μl ice-cold 10 % glycerol and 5.0 μl recombinant DNA on ice. The transformation mix was transferred to a sterile, pre-cooled electroporation cuvette and exposed to an electric field (1.3 V, 25 μF, 800 Ω) in the electroporation chamber. Time constants shown by the device were always between 4 and 6 ms. Cells were transferred to a 15 ml Falcon tube containing 950 μl SOC medium. Bacteria were allowed to recover for 45-60 min at 37 °C, 225 rpm. 100 μl of cell suspension were plated on LB agar plates containing the required antibiotics and placed at 37 °C overnight.

2.2.1.4 Plasmid Preparation Using QIAprep® Spin Miniprep Kit

The QIAprep® Spin Miniprep Kit provides a fast (less than 30 min) and simple small-scale plasmid preparation method for routine molecular biology applications. It is designed for the purification of up to 20 μg high-copy plasmid DNA in sequencing quality. The procedure is based on alkaline lysis of bacterial cells and the subsequent absorption

of the plasmid DNA onto a patented silica membrane in the presence of high salt concentrations. Plasmid DNA can then be eluted from the membrane with a low-salt buffer or ddH_2O.

Plasmid DNA was prepared according to the QIAprep® Miniprep Handbook. Bacterial cultures were grown overnight in 4 ml LB medium supplemented with the appropriate antibiotics at 37 °C, 225 rpm. Cell suspensions were transferred to 2 ml Eppendorf tubes and sequentially centrifuged for 3 min at 6,800 x *g*, RT. Plasmid DNA was eluted by adding 30 μl ddH_2O to the centre of the spin column and subsequent centrifugation for 1 min at 16,100 x *g*, RT.

2.2.1.5 Endotoxin-Free Plasmid DNA Preparation Using NucleoBond® Xtra Maxi EF Kit

For transfection of mammalian cells (see 2.2.4.3), endotoxin-free plasmid DNA was prepared on a large scale.

The outer sheet of the outer membrane that encloses the inner membrane and cell wall of Gram-negative bacteria consists of amphiphilic lipopolysaccharides, also called endotoxins. Bacterial cells release endotoxins in small amounts during cell growth and large amounts upon cell death and lysis. In mammalian cell culture, endotoxins can seriously affect transfection rates and cell viability. Due to their amphiphilic nature and negative charge, endotoxins can be co-purified with many common plasmid purification systems. The NucleoBond® Xtra Maxi EF Kit provides a fast and highly efficient method for the preparation of endotoxin-free plasmid DNA. It is designed for purification of up to 1000 μg high-copy plasmid DNA.

Endotoxin-free plasmid DNA was prepared according to the NucleoBond® Xtra Maxi EF Kit user manual. 300 ml bacterial cultures were inoculated with 4 ml pre-culture in LB medium supplemented with the appropriate antibiotics and grown overnight at 37 °C, 225 rpm. Cells were harvested by centrifugation at 4500 x *g*, 4 °C for 20 min. Endotoxin-free plasmid DNA was eluted from NucleoBond® finalizers twice with the same 500 μl buffer TE-EF. To increase yield the finalizer was washed once more with 250 μl buffer TE-EF and the eluate added to the previous one.

2.2.1.6 Agarose Gel Electrophoresis of dsDNA

Agarose gel electrophoresis is used to separate nucleic acid fragments by their size. Polymerised agarose in gels forms pores with sizes depending on the agarose concentration. Due to their negative charge, nucleic acids migrate in electric fields to the anode and the smaller the fragment, the faster it migrates.

DNA molecules were electrophoretically separated on agarose gels prepared with 1x TAE buffer supplemented with 2 μl ethidium bromide (EtBr)/50 ml gel. EtBr can be used to visualise dsDNA in agarose gels because it intercalates into double stranded DNA molecules and emits orange light of $\lambda = 590$ nm when excited with UV light at $\lambda = 312$ nm. 1x TAE buffer was used as running buffer. Electrophoresis took place at a constant voltage of 120 V for about 20 min. Samples were prepared by mixing DNA

with the appropriate amount of loading buffer and ddH_2O to a final volume as small as possible. For size estimation of dsDNA fragments, a DNA-marker with different bands of known sizes was added in one lane of the gel. The concentration of the agarose gel was chosen according to the size of the DNA molecules in question:

Agarose concentration in % (w/v)	Size of dsDNA molecules
2.5	< 100 bp
2.0	0.1 - 1.0 kb
1.8	0.2 - 2.0 kb
1.5	0.3 - 3.0 kb
1.2	0.5 - 5.0 kb
1.0	0.5 - 7.0 kb
0.8	0.8 - 12.0 kb
0.5	1.0 - 30.0 kb

2.2.1.7 Isolation of DNA from Agarose Gels Using QIAquick® Gel Extraction Kit

The QIAquick® Gel Extraction Kit is a simple and fast method to purify DNA fragments in a range of 70 bp to 10 kb from agarose gels. The procedure is based on DNA binding to a silica membrane in the presence of high salt concentrations, while contaminants are washed through the column. DNA fragments to be isolated were excised from the agarose gel, transferred to a 2 ml Eppendorf tube and purified according to the manufacturer's manual.

2.2.1.8 Purification of DNA Using QIAquick® PCR Purification Kit

The QIAquick® PCR Purification Kit is designed for the fast purification of DNA fragments in a range of 100 bp to 10 kb from PCR or enzymatic reactions. Similar to the QIAquick® Gel Extraction Kit, the purification of PCR products is based on DNA binding to a silica membrane in the presence of high salt concentrations, while contaminants are washed through the column, and was performed according to the manufacturer's manual.

2.2.1.9 Restriction Digest

Restriction endonucleases type II bind to specific DNA sequences called "restriction sites". They catalyse the hydrolysis of 3'→5'-phosphodiesterbonds in each DNA-strand and thereby the formation of a double strand break. Restriction digests were used for the control of cloning experiments as well as to linearise vector DNA and to create DNA fragments with sticky ends for ligation.

To completely digest y μg of dsDNA in 1 h at a certain restriction site, the DNA was mixed with 1/10 of an enzyme-specific 10x reaction buffer, 1/10 10x BSA if necessary and excess restriction enzyme and the reaction replenished with ddH_2O to a final volume of x μl (which was kept as small as possible). Reactions were incubated at least 1 h at 37 °C to achieve complete digestion.

2.2.1.10 Dephosphorylation of 5'-Phosphorylated DNA Fragments

To prevent self-ligation of vector DNA during the ligation of two DNA fragments, the 5'-phosphorylated ends of the digested vector DNA were dephosphorylated with alkaline phosphatase (shrimp alkaline phosphatase, CIP). The DNA fragment was mixed with 1/10 of the 10x NEB reaction buffer 3, 0.5 U CIP/μg DNA and the reaction mix was replenished with ddH_2O to a final volume of x μl. Reactions were incubated at least 1 h at 37 °C to achieve complete digestion and the DNA subsequently purified using the QIAquick® PCR Purification Kit.

2.2.1.11 Ligation of dsDNA Fragments

In DNA ligation, DNA ligase catalyses the formation of a 3'→5'-phosphodiester bond between the free 3'-hydroxyl- and the 5'-phosphate group of linear DNA fragments while consuming ATP. Usually 100 ng vector DNA were ligated with a three-fold molar excess of insert DNA ends. The required amount of insert was calculated according to the following formula:

$$\text{Amount insert [in ng]} = \frac{\text{amount vector [in ng] x insert size [in bp]}}{\text{vector size [in bp]}}$$

The appropriate amounts of vector and insert DNA were supplemented with 10 μl 2x Quick Ligation Reaction Buffer and 1 U Quick T4 DNA Ligase and replenished with ddH_2O to a final volume of 20 μl. The reaction was incubated at RT for 5-15 min and then transformed into competent *E. coli* XL 10 Gold.

2.2.1.12 TOPO®-Blunt Cloning

Zero Blunt® TOPO® PCR cloning is a highly efficient, fast, one-step cloning procedure for the insertion of blunt-end PCR products into a cloning vector. The pCR®-Blunt II-TOPO® cloning vector is a linearised plasmid vector with the Vaccinia virus DNA topoisomerase I covalently bound to the 3'-end of each DNA strand. Topoisomerase I binds to specific sites in dsDNA and cleaves its phosphodiester backbone while conserving the energy by formation of a covalent bond between the 3'-phosphate of the cleaved strand and a tyrosyl residue of topoisomerase I. As this reaction is reversible, the stored energy of the phosphodiester backbone cleavage can be used to form a new covalent bond between the 5'-hydroxyl of a blunt-end PCR product and the 3'-phosphate of the vector DNA, thereby releasing the enzyme. The Zero Blunt® TOPO® PCR cloning kit was used as a cloning vector system to save and store PCR products and to provide an efficient dsDNA basis for subcloning of defined DNA fragments.

For Zero Blunt® TOPO® PCR cloning, 4 μl blunt-end PCR product were mixed with 1μl of the included salt solution and 1 μl pCR®-Blunt II-TOPO® cloning vector, gently mixed, incubated 5-15 min, RT, and then placed on ice. Finally, 2 μl of the TOPO® cloning reaction were transformed into chemically competent *E. coli* One Shot® TOP10.

2.2.2 Polymerase Chain Reaction (PCR)

2.2.2.1 Amplification of dsDNA Fragments by PCR

The polymerase chain reaction (PCR) can be used to amplify specific DNA sequences exponentially and is based on repeated cycles of enzymatic, *in-vitro* DNA synthesis of the target sequence. Two oligonucleotide primers direct the specific amplification of target DNA sequences by DNA polymerase. The primers flank the DNA sequence of interest and can hybridise to their complementary sequence on opposite DNA single strands. Double stranded DNA molecules are separated into single strands by heat denaturation, enabling hybridisation of the primers to the single stranded DNA molecules at temperatures of 45-60 °C. Excess primer concentrations in the reaction ensure that formation of primer-template complexes is in favour of renaturation of DNA single strands. Heat-stable DNA polymerases elongate primers at an intermediary temperature as an exact copy of the original template and enabling repeated cycling of PCR without the need to add more enzyme. Since this process takes place at both DNA single strands, one cycle doubles the target DNA sequence. Cycle repetition leads to the exponential amplification of the target sequence as every dsDNA molecule synthesised in a previous cycle can serve as a template in the following cycles (Saiki *et al.*, 1988; Mülhardt, 2003).

Platinum® *Pfx* DNA polymerase was used for standard PCR. *Pfx* polymerase is a recombinant DNA polymerase isolated from *Thermococcus sp.* and provides high fidelity (approx. one mistake every 10^6 bases) because of its proofreading activity (3'→5' exonuclease activity). PCR was performed in 50 μl reaction volumes. The desired amount of template DNA was mixed with 5.0 μl 10x reaction buffer, 1.5 μl of a 2 mM dNTP mix, 1.0 μl 50 mM $MgSO_4$, 1.5 μl of 10 mM forward primer, 1.5 μl of 10 mM reverse primer and 2.5 U Platinum® *Pfx* DNA polymerase and replenished with ddH_2O to the final volume.

Platinum® *Pfx* DNA polymerase is provided in inactive form, due to specific binding of the Platinum® antibody. Polymerase activity is restored by an initial denaturation step at 94 °C for 2 min, leading to an "automatic hot start" that increases specificity, sensitivity and yield of the PCR reaction. PCR consisted of 30-32 PCR amplification cycles, formed by denaturation at 94 °C for 30 sec, primer annealing at the appropriate annealing temperature for 30 sec and elongation at 68 °C for 1 min per kb. The last PCR cycle was followed by an additional 5 min at 68 °C for elongation of unfinished PCR fragments before the reaction was cooled to 8 °C. PCR products were analysed by agarose gel electrophoresis.

For problematic and/or GC-rich templates, PCR_x Enhancer Solution was added to the reaction as recommended by the manufacturer's manual.

2.2.2.2 *In-Vitro* Site-Directed Mutagenesis

In-vitro site-directed mutagenesis is used to introduce point mutations and/or exchange, delete or insert single or a limited number of amino acids in protein sequences of interest. The procedure uses plasmid DNA and a set of two synthetic, complementary oligonucleotide primers encoding for the region to be mutated including the desired mutation.

The oligonucleotide primers bind to their complementary sequences on opposite strands of the vector and are amplified by PCR which generates a mutated plasmid containing staggered single strand breaks. Following PCR, parental vector DNA is digested by type II endonuclease *Dpn*I (target sequence: 5'-Gm^{6}ATC-3'), specific for methylated and hemimethylated DNA. DNA isolated from most *E. coli* strains is dam-methylated and therefore susceptible for *Dpn*I digestion. Digested mutated PCR products are transformed into competent *E. coli*. Bacteria repair the single strand breaks, producing a functional, mutated plasmid. Mutants can be generated with efficiencies greater than 80 %.

One set of mutagenic oligonucleotide primers contained the desired mutation and annealed to the same sequence but on opposite strands of the template DNA. The desired mutation was approximately in the middle of the primer with 15-25 nucleotides of correct sequence on both sides. Primers always ended with one or more C- or G-bases. For mutagenesis 125 ng of each primer were used. To convert nanograms to picomoles, the following formula was used:

$$\text{X pmol of oligo} = (\text{ng primer x } 1000)/(330 \text{ x number of oligo bases})$$

For mutagenesis PCR either Platinum® *Pfx* DNA polymerase of PfuUltra High-Fidelity DNA polymerase were used as suggested by the respective manufacturer. Mutation PCR was performed in 50 μl reaction volumes. 50 ng plasmid DNA was mixed with 5.0 μl of the respective 10x reaction buffer, 2.0 μl of a 2 mM dNTP mix, 1.0 μl 50 mM $MgSO_4$ (only for Platinum® *Pfx* DNA polymerase), the appropriate amounts of primer and 2.5 U DNA polymerase and replenished with ddH_2O to the final volume.

PCR reactions were started by initial denaturation of template DNA and activation of DNA polymerase as recommended by the manufacturer, followed by 25-32 PCR amplification cycles of denaturation at the enzyme's specific denaturation temperature for 30 sec, primer annealing at 55 °C for 30 sec and elongation at the appropriate temperature for 1 min per kb. Final elongation for 7 min was followed by cooling to 8 °C.

PCR products were digested with 1.0 μl *Dpn*I (10 U/μl) for 60 to 120 min at 37 °C and 2.5 μl of digested PCR product were transformed into chemically competent *E. coli* as described in 2.2.1.2. If possible, the mutated DNA sequence of the gene of interest was subcloned into the same position of the parental vector to eliminate potential mutations introduced by PCR.

2.2.2.3 Directed Mutagenesis of dsDNA by PCR

PCR can also be used to introduce, delete, exchange or insert larger numbers of amino acids into a protein sequence of interest, a technique, here referred to as directed mutagenesis of dsDNA by PCR. The method is based on amplification of plasmid DNA by PCR using a set of two synthetic mutagenic oligonucleotide primers encoding for amino acids to be inserted or exchanged. The 3'-end of each primer encodes for 15-25 nucleotides of opposite strands of the original gene directly adjacent to the desired mutation. Their 5'-end harbours one of two halves of the mutation to be introduced. Primers should always end with one or more C- or G-bases. The oligonucleotide primers bind

to their complementary sequences on opposite strands of the vector and vector DNA is then amplified by PCR. A linear, blunt end DNA molecule is generated encoding for the entire plasmid with the mutations on its 3'- and 5'-ends, each encoding for a part of the polypeptide to be introduced. The length of the introduced polypeptide stretch is limited by the length of oligonucleotide primers that can be synthesised. For deletion of any number of amino acids the respective nucleotide sequence can be excluded from the amplified plasmid regions. After generation of linear, mutated, blunt-end plasmid DNA encoding for the mutant protein of interest, parental DNA is digested by *Dpn*I. Blunt ends are then ligated and transformed into competent *E. coli*.

For mutagenesis PCR, either Platinum® *Pfx* DNA polymerase of Pfu polymerase were used as recommended by the respective manufacturer. Mutation PCR was performed in conditions as described in 2.2.2.2.

PCR products were digested with 1 μl *Dpn*I (10 U/μl) for 60 to 120 min at 37 °C and purified using the QIAquick® PCR Purification Kit. 100 ng of the digested and purified PCR product were then ligated as described in 2.2.1.11 and transformed into competent *E. coli* XL 10 Gold. If possible, the mutated DNA sequence of the gene of interest was subcloned in the same position of the parental vector to eliminate mutations introduced by PCR.

2.2.2.4 Two-Step Fusion PCR

Two step fusion PCR was used to create mutant DNA molecules that were too long to be synthesised synthetically on oligonucleotide primers. First, the two fragments to be linked were amplified separately. Here, primers for the 3'-end of the N-terminal part of the final protein were designed such that sequences at the 3'-end of the primer had a sequence overlapping with the 5'-end of the primer starting the C-terminal part of the final protein. Both PCR products from the first amplification step were then fused in a second standard PCR by amplification of both fragments in the same reaction using the 5'- and 3'- end primers for the N- and C-terminal parts of the final fusion protein, respectively. The overlapping sequence in both DNA fragments allows the annealing of the two separate fragments. Using the flanking primer set from the first PCR step, DNA polymerases can synthesise the gap from the 5'- end primer of leading and lagging strand to the annealed second DNA fragment, thereby amplifying the whole construct. For the second PCR, fragments encoding N- and C-terminal parts of the final protein were adjusted to equimolar concentrations. Fused DNA constructs were cloned into the pCR®-Blunt II-TOPO® vector and their identity confirmed by sequencing.

2.2.2.5 DNA Sequencing

Sequencing of dsDNA was performed according to the dideoxy chain terminating method (Sanger *et al.*, 1992). The used variant utilises fluorescently labelled 2',3'-dideoxy-nucleotides (ddNTPs) in addition to 2'-deoxynucleotides (dNTPs), that cannot be used to form new phosphodiester-bonds due to the missing 3'-OH group and therefore lead to the termination of the synthesised DNA strand after insertion of a ddNTP. The fluorescent

ddNTP indicating the last incorporated nucleotide can then be detected by capillary gel electrophoresis. Capillary gel electrophoresis was done by the Zentrale Einrichtung Biotechnologie at the Max-Planck-Institute for Molecular Physiology, Dortmund.

Sequencing PCRs were performed using the BigDye® Terminator v3.1 Cycle Sequencing Kit. 150-300 ng plasmid DNA, 4.0 μl ready reaction premix, 2.0 μl BigDye® sequencing buffer and 2.0 μl primer (20 pmol/μl) were replenished with ddH^2O to a final volume of 20 μl. After initial denaturation at 96 °C for 1 min, PCR cycles consisted of denaturation at 96 °C for 10 sec, 5 sec annealing at 50 °C and elongation at 60 °C for 4 min. Cycle number was 25 and finished PCR reactions were cooled to 4°C until further treatment.

Excess ddNTPs were removed from finished sequencing reactions with the DyeEx® 2.0 Spin kit according to the manufacturer's manual and transferred to new 0.5 ml Eppendorf tubes. Purified reactions were dried in a vacuum centrifuge and then sent for capillary gel electrophoresis.

2.2.3 Protein Analytics

2.2.3.1 Expression and Purification of Fluorescently Tagged MAPKs

The fluorescently tagged mammalian MAPK ERK2 and ERK2 mutants were expressed in *E. coli* and subsequently purified for *in-vitro* studies.

The expression plasmid encoding fluorescently tagged ERK2 or ERK2 mutants were transformed into Rosetta^{TM}2(DE3) Singles^{TM} competent *E. coli* as recommended by the manufacturer and plated on LB agar plates supplemented with 100 μg/ml Ampicillin (LB/Amp). Pre-cultures of 15 ml LB/Amp medium were inoculated with a single colony and incubated overnight at 37 °C, 225 rpm. Main cultures were set up by diluting the pre-culture 1:50 in LB/Amp to yield 500 ml of culture and then incubated for 2 - 4 h at 37 °C, 225 rpm until the OD reached 0.5 - 0.6. Protein expression was induced by addition of IPTG to a final concentration of 0.5 mM IPTG and cells were grown overnight at 15 °C, 225 rpm before being harvested by centrifugation at 4,500 x *g* for 20 min, 4 °C. Samples were snap-frozen in liquid nitrogen and stored at -20 °C.

2 ml of Ni-NTA His•Bind® resin were equilibrated with 5 ml ERK2 wash buffer by incubation in a 50 ml Falcon tube at RT for 5 min, gentle centrifugation and removal of the supernatant. Bacterial pellets were resuspended in 7.5 ml lysis buffer, sonicated (3x 30 sec, 40 % power) and cell suspensions were centrifuged for 20 min at 4,500 x *g*, 4 °C. Supernatants were filtered through an empty Econo-Pac® 10 DG disposable chromatography column into the 50 ml Falcon tube containing the equilibrated Ni-NTA His•Bind® resin. Protein solutions were incubated with the Ni-NTA His•Bind® resin for 1 h at 4 °C on a rotational shaker and then loaded on an Econo-Pac® 10 DG disposable chromatography column. Columns were allowed to empty by gravity flow and washed three times with one column volume ERK2 wash buffer. The protein was then eluted from the resin by repeated addition of one gel volume ERK2 elution buffer. Flow-through of wash and elution steps was collected in 1 ml fractions.

Eluted fractions containing fluorescently tagged ERK2 as observed by eye were pooled

and applied to an Amicon Ultra-15 centrifugal filter unit with a nominal molecular weight limit of 30 kDa. 2 to 5 ml ERK2 storage buffer were added and solutions centrifuged for 10 to 20 min until they were concentrated to a volume of approximately 500 μl. Storage buffer addition and centrifugation were repeated three times and purified protein transferred to a new 1.5 ml Eppendorf tube. Protein concentrations in the solution were estimated by the micro BCA assay method as described in 2.2.3.7, samples aliquoted in 100 μl fractions, snap-frozen in liquid nitrogen and stored at -80 °C.

2.2.3.2 *In-Vitro* Phosphorylation of Purified MAPKs

Purified ERK2 proteins were autophosphorylated or phosphorylated *in-vitro* by incubation with commercially available active MEK1 for further use in substrate phosphorylation experiments and *in-vitro* ES-imaging experiments.

In-vitro phosphorylation was performed in a modified version of a protocol published by (Shapiro *et al.*, 1998). Briefly, reactions contained 25 mM HEPES (pH 7.4), 10 mM $MgCl_2$, 1 mM DTT, 1 mM ATP, 0.1 μg active MEK1 if necessary and 1 μg purified ERK2 in a final volume of 50 μl and were incubated for 1 h at 30 °C. Samples were placed on ice until further use.

2.2.3.3 *In-Vitro* Phosphorylation of ERK2 Substrate Peptide

In-vitro phosphorylation of ERK2 substrate peptide was performed in a modified version of a protocol published by (Shapiro *et al.*, 1998) as described in 2.2.3.2. ERK2 substrate peptide was added to a final concentration 50 μM. Samples were incubated for 1 h at 30 °C and then placed on ice until further use.

2.2.3.4 *In-Vitro* ES-Interaction Spectroscopy

In-vitro ES-interaction spectroscopy was performed in reaction conditions as described in 2.2.3.2. ES-interactions were determined in time-based experiments with fixed excitation ($\lambda = 516$ nm) and emission wavelength ($\lambda = 529$ nm). Emission intensity was measured as a function of time. 50 μl of the ERK2 phosphorylation reaction were transferred into a fluorescent cuvette and placed into the sample chamber of the PTI fluorescent spectrometer. Spectroscopic measurements were taken for a few minutes to record a baseline. Data acquisition was paused and fluorescently labeled ERK2 substrate peptide was added in different concentrations as indicated. Data acquisition was continued as quickly as possible. Data were exported in text format and imported to Excel for further analysis.

Normalised fluorescence donor emission values were corrected for the intensity decrease generated by the dilution effect arising from substrate addition. The average difference in normalised fluorescence donor emission values of negative controls before and after substrate addition was determined. The obtained value was added to fluorescence values after substrate addition in all samples.

Alternatively, ES-interaction spectroscopy was performed as emission scan experiments with a fixed excitation wavelength of (λ = 480 nm) while the emission spectrum was measured from λ = 485 nm to λ = 700 nm. The emission intensity was measured as a function of excitation wavelength. 50 μl of ERK2 phosphorylation reaction were mixed with increasing substrate concentrations, transferred into a fluorescent cuvette and spectroscopic measurements were taken with the PTI fluorescent spectrometer. Data were exported in text format and imported to Excel for further analysis.

Recorded emission spectra were normalised according to the following formula: $nF_i = (\lambda_i F_i)/\sum(\lambda_i F_i)$, with nF_i as the normalised fluorescence intensity at each wavelength, λ_i as the wavelength measured and F_i as the fluorescence intensity at each wavelength.

2.2.3.5 *In-Vitro* Fluorescent Lifetime Spectroscopy

In-vitro fluorescent lifetime spectroscopy was performed in reaction conditions as described in 2.2.3.2 using a commercial frequency-domain fluorescent lifetime microscope (Lambert Instruments/Olympus). Reference measurements of Alexa488 and sample recordings were basically performed as suggested by the manufacturer's manual using a 40x water objective. mCitrine was excited with a 493 nm LED. Emission intensity was measured as a function of time. 50 μl of phosphorylated ERK2 (see 2.2.3.2) were placed in an 8-well LabTek chamber and the LabTek chamber mounted onto the sample holder of the Olympus IX 81 inverse microscope. The focus was adjusted to regions with maximum light intensity of the solution. Measurements were taken every 30 sec. Fluorescently labeled peptides were added in the indicated concentrations directly after a baseline recording.

2.2.3.6 Preparation of Whole Cell Lysates

Whole cell lysates for protein analysis in western blots were prepared from mammalian cells cultivated in 60-mm Easy Grip^{TM} tissue culture dishes. Cells were washed once with ice-cold PBS and harvested immediately after the addition of ice-cold 1x cell lysis buffer (1 ml 10x Cell Lysis Buffer, 1 tablet Complete Mini EDTA-free protease inhibitor and 100 μl phosphatase inhibitor cocktail 1 and 2). Lysates were transferred to 1.5 ml Eppendorf tubes, incubated for 3 min on ice and snap-frozen in liquid nitrogen. Samples were thawed on ice and centrifuged for 5 min at 16,100 x *g*, 4 °C to remove cell debris. The supernatant was transferred to new 1.5 ml Eppendorf tubes and stored at -20 °C. Cells and cell lysates were kept on ice during all steps of the procedure starting from washing with PBS to avoid degradation of proteins.

2.2.3.7 Estimation of Protein Concentrations Using the Micro BCA Assay

For determination of protein concentrations in cell extracts the BCA protein assay was used. The BCA assay is compatible with many detergents that may be present in buffers used. The assay is based on reduction of Cu^{2+}-ions by proteins in an alkaline environment forming Cu^{+}, which can then form a purple-coloured complex with bicinchonic acid (BCA) with an absorbance maximum at λ = 562 nm.

The assay was performed in 96-well plates what allows analysis of multiple protein samples and requires only small sample volumes. The micro BCA working reagent was prepared by mixing 25 parts reagent A with 24 parts reagent B and one part reagent C to yield a volume that is a product of 150 μl. Protein standards were prepared by diluting a BSA standard in the appropriate sample buffer to concentrations from 0.5 to 10 μg/μl. 5 μl of each protein standard were added to separate wells of a 96-well plate using the appropriate sample buffer as blank. Unknown protein samples were diluted to have an approximate concentration 0.5 to 10 μg/μl. All samples were set up as triplicates. Wells were complemented with 150 μl micro BCA working reagent and samples incubated for 2 h at 37 °C. 96-well plates were cooled to RT and absorbance was measured at λ = 562 nm. Obtained absorbance values were plotted against protein concentrations of each standard. Protein concentrations of the unknown samples were determined by comparing their absorbance values at λ = 562 nm against the standard curve.

2.2.3.8 Denaturing Polyacrylamide Gel Electrophoresis (SDS-PAGE)

Denaturing SDS-PAGE is used to separate proteins according to their size in a discontinuous polyacrylamide gel. SDS is an anionic detergent that binds to proteins in amounts proportional to their size (approx. one molecule SDS per two amino acid residues) and breaks physiological protein folding. Therefore proteins bound to SDS display a similar charge/size ratio. Due to this negative charge the denatured proteins migrate to the positive pole when subjected to an electric field. When this electric field applied to a discontinuous polyacrylamide gel, smaller polypeptide chains migrate faster depending on the pore size formed by polymerised acrylamide.

The acrylamide concentration of the separating gel was adjusted to the molecular weight of the protein of interest to be either 10 or 12 % (v/v), respectively. Separating gels were poured into 1.0 mm western blot cassettes according to the following recipe (volumes produced one gel):

	10 % Gel	12 % Gel
Acrylamide	2.08 ml	2.50 ml
Separating Gel Buffer	2.35 ml	2.35 ml
10 % SDS (w/v)	62.5 μl	62.5 μl
50 % Sucrose (w/v)	1.0 ml	1.0 ml
ddH_2O	0.6 ml	176 μl
TEMED	5 μl	5 μl
10 % APS (w/v)	150 μl	150 μl

Immediately after pouring, separating gels were overlaid with 1 ml ddH_2O and the acrylamide allowed to polymerise for 15 to 45 min. Stacking gels were poured on top of the separating gels, consisting of 0.835 ml acrylamide, 2.1 ml stacking gel buffer, 62.5 μl 10 % SDS, 2.82 ml ddH_2O, 6.25 μl TEMED and 0.5 ml 10 % APS. 10-well combs were inserted into the stacking gel directly after pouring to allow the formation of sample pockets. Gels could be stored overnight at 4 °C when wrapped in paper towels humidified with ddH_2O and protected from drying by a plastic bag.

Whole cell lysates were centrifuged for 1 min at 16,100 x *g*, 4 °C to remove cell debris and other aggregates. Samples were prepared by mixing the appropriate amount of whole cell lysate with 5 μl 5x SDS sample buffer and ddH_2O to a final volume of 25 μl. Samples were incubated for 5 min at 95 °C to denature proteins by heat and enable their reduction by 2-mercapto-ethanol and the association with SDS. Samples were then incubated for 2 min on ice, centrifuged briefly to remove condensed water from the lid and placed back on ice until further use.

For electrophoresis, gels were inserted into XCell SureLock^{TM} Mini-Cell gel chambers, gel chambers assembled and filled with 1x SDS running buffer according to the manufacturer's manual. Sample pockets were washed with running buffer and loaded with the prepared samples. For size determination of separated proteins, 10 μl Precision Plus Protein^{TM} Standard containing different bands of known molecular weight were loaded in one well. Electrophoresis was performed with constant voltage of 80 V until the samples reached the separating gel and 150 V for approximately 90 min.

2.2.3.9 Western Blotting

In western blotting (immuno-blotting) proteins separated during discontinuous, denaturing SDS-PAGE are electrophoretically transferred to a positively charged nitrocellulose membrane to enable immunological detection by antibody binding.

After electrophoresis blots were assembled in XCell II^{TM} blot modules according to the manufacturer's manual and placed in XCell SureLock^{TM} Mini-Cell gel chambers. Blot module were filled with 1x transfer buffer and gel chambers with approximately 600 ml ddH_2O. Proteins were blotted on nitrocellulose membrane (90 x 70 mm) for 60 min at a constant voltage of 30 V.

Before immunological detection of proteins membranes were transferred from blotting modules to Li-Cor® incubation boxes for western blotting and the remaining binding sites of the membrane blocked with Odyssey infrared imaging system blocking buffer (Li-Cor® Biosciences) for either 1 h, RT, or overnight at 4 °C. Membranes were then incubated with primary antibodies raised in different species, diluted in 5 ml Odyssey infrared imaging system blocking buffer according to the manufacturer's recommendations for either 1 h, RT, or overnight at 4 °C. Blots were washed three times, 5 min each with a 1:1 mixture of 1x TBST and blocking buffer for near infra-red fluorescent western blotting (Rockland Inc.) and incubated with secondary antibodies of different colours, diluted 1:15,000 (green labeled secondary antibodies) or 1:7,500 (red labeled secondary antibodies) in 5 ml Odyssey infrared imaging system blocking buffer for 1 h, RT. Li-Cor® incubation boxes protected the fluorescent secondary antibodies from light. Finally, blots were washed three times, 5 min each with a 1:1 mixture of 1x TBST and blocking buffer for near infrared fluorescent western blotting. Antigen-antibody complexes were detected with the Odyssey Imaging System.

2.2.3.10 *In-Vivo*-Labeling of Proteins Inside Living Cells with Biarsenical Fluorophores

Cells plated in 4-well LabTek® chambers and expressing tetracysteine-tagged proteins were incubated for 45 - 60 min with μM ReAsH in 250 μl OptiMEM. ReAsH concentration was chosen to be in the middle of the range recommended by the manufacturer. Cells were washed twice with 250 μM BAL buffer in OptiMEM for 15 min each before further treatment.

Alternatively, cells in 250 μl starvation medium were incubated with the desired concentration of ReAsH pre-diluted in 250 μl starvation medium and proceeded to imaging without washing.

2.2.4 Mammalian Cell Culture

Cos7, HeLa and MDA cells were maintained in Dulbecco's Modified Eagle's Medium (DMEM) supplemented with 10 % fetal bovine serum (FBS) and 1 % glutamine. MCF-7 cells were grown in DMEM supplemented with 10 % FBS, 1 % glutamine and 0.01 mg Insulin/ml. All cells were grown at 37 °C in a 90 % humidified incubator with 5 % CO_2. Medium was changed every two days to maintain appropriate growth conditions. Cells were starved in DMEM/0.5 % FCS/1 % glutamine.

2.2.4.1 Subculture of Mammalian Cells

When exponentially growing cells become confluent, i.e. they reach a density when all available substrate of the culture dish or flask is occupied, their growth is usually inhibited by contact inhibition (change of cell growth from log-phase to a plateau phase). Therefore cultured cells need to be split before they reach confluency.

80-90 % confluent cells were washed once with PBS and trypsinised for approximately 5 min at 37 °C. Detached cells were washed off the surface with 10 ml growth medium to inactivate trypsin and gently pipetted up and down 10-20 times to disperse cells to a single cell suspension. For maintenance of cell lines, cells were split in ratios of 1:8 to 1:15 into new cell culture flasks depending on the needs of the experiment. Alternatively, cell number per ml cell suspension was determined using the Vi-Cell^{TM} XR cell viability analyzer and the desired number of cells was seeded into cell culture dishes for further experiments.

2.2.4.2 Cryo-Conservation and Long-Term Storage of Cell Lines

Cryo-conservation is the long time storage of cells, cell lines or whole tissues to sub-zero temperatures below -80 °C. For maximal viability of stored material after cryo-preservation the use of cryo-preservatives such as DMSO or glycerin is inevitable as intracellular ice crystal formation and regional formation of high-concentration solutes could greatly reduce cell viability.

Sub-confluent cells from a T75 tissue culture flask were split as described above, counted and diluted to a concentration of 1 x 10^6 to 1.5 x 10^6 cells/ml in cryo-medium

(70 % normal growth medium, 20 % FBS, 10 % DMSO). Cells were then aliquoted into cryo-vials and transferred to a room temperature NALGENE® Cryo 1 °C freezing container. This container is filled with room temperature isopropanol and allows for a controlled freezing rate of 1 °C per minute to avoid damage of cells by the freezing process. The freezing container was placed into an -80 °C freezer overnight and individual vials were then transferred to a liquid nitrogen tank for long-term storage.

Cell thawing was done as quick as possible to avoid toxic effects of the cryo-preservative and thereby loss of cell viability. Cells were transferred from the liquid nitrogen tank to a 37 °C water bath and the cell suspension quickly diluted in 10 ml growth medium. Cells were pelleted by centrifugation at 200 x *g* for 5 min, resuspended in 10-12 ml growth medium and seeded into a new T75 flask.

2.2.4.3 Transfection with DNA

Transfection is defined as the artificial introduction of genetic material or nucleic acids into higher eukaryotic cells by non-viral means. There are numerous methods, protocols and variants as well as transfection reagents to transfect cells, ranging from classical calciumphosphate co-precipitation to electroporation. In this study, all cells were transfected with endotoxin-free plasmid DNA via lipofection, the introduction of DNA into higher eukaryotic cells by fusion of DNA loaded lipidic micells with their plasma membrane. The transfection reagent used was Fugene® 6, a multi-component reagent that forms complexes with DNA and displays high transfection efficiency in many different cell types, virtually no cytotoxicity and can be used with or without serum present in the medium.

Cells were either plated in 60-mm Easy Grip^{TM} tissue culture dishes, 35-mm MatTek petri dishes or 4-well LabTek® chambers as specified. They usually were transfected directly after passaging while plating them into the vessel chosen for a specific experiment. Fugene® 6 reagent-DNA ratios of 3:1 have been used in all experiments.

For transfection of cells in 35-mm MatTek dishes, 3.0 μl Fugene® 6 reagent were diluted in 100 μl serum-free DMEM and incubated for 5 min, RT. 1.0 μg plasmid DNA was added, the solution mixed and incubated for 15-30 min, RT. During incubation 2 x 10^5 cells per dish were plated in 2 ml full growth medium (1 x 10^5 cells/ml). 100 μl of Fugene® 6 reagent-DNA complex were added to the cells drop-wise and culture vessels swirled to ensure distribution over the entire surface. Cells were incubated at 37 °C in a 90 % humidified incubator with 5 % CO2 until further treatment. For transfection of cell culture vessels other than 35-mm MatTek dishes, amounts of Fugene® 6 reagent, DNA and DMEM were adjusted accordingly (e.g. doubled for 60-mm tissue culture dishes or divided by four for 4-well LabTek® chambers).

2.2.5 Microscopy

2.2.5.1 Laser Scanning Confocal Microscopy (LSCM)

Confocal images of live cells were obtained with an Olympus FluoView FV1000 confocal laser scanning biological microscope. Hoechst 33342 was excited with the 405 nm line

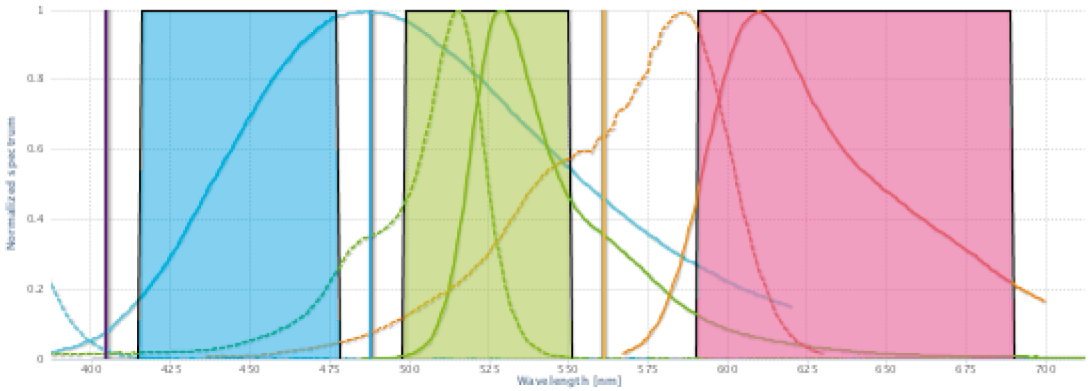

Figure 2.1: Instrumental alignment for LSCM. Lasers (vertical coloured lines) and AOTF adjustments (coloured, transparent rectangles) used for laser scanning confocal microscopy. For demonstration purposes, excitation and emission spectra of Hoechst 33528, mCitrine and mCherry are displayed as well (courtesy of Dr. Hernan E. Grecco).

and EGFP and mCitrine with the 488 nm line of an multiline Argon laser. mCherry and ReAsH were excited with the 561 nm line of a DPSS laser. Excitation light for all dyes was focused into the sample by a 40x/0.9 NA air objective or a 60x/1.2 NA water objective using a DM405/488/561/633 dichroic mirror. Fluorescence was recorded by the microscope's acousto-optic tunable filter (AOTF) and SIM scanner. Hoechst fluorescence was detected by collecting photons with a wavelength of 415-478 nm, directed to the scanner by a SDM490 emission beam splitter. Photons with wavelength of 498-551 nm were recorded to detect EGFP and mCitrine, while mCherry and ReAsH fluorescence were detected by collecting photons with a wavelength of 590-690 nm. EGFP/mCitrine and mCherry/ReAsH channels were separated by a SDM560 emission beam splitter (Fig. 2.1). Live cell imaging was performed in a temperature-controlled incubation chamber in conditions appropriate for normal cell growth.

2.2.5.2 Ratiometric FRET Imaging

Ratiometric FRET imaging was performed using a Zeiss LSM510 confocal laser scanning microscope. Images were collected with the multi-track option in the image acquisition software. Images required for ratiometric FRET analysis were recorded in the same track, while mCherry and Hoechst 33342 fluorescence were recorded on single track each to avoid bleedtrough of the Hoechst dye into the red channel. Excitation light for all dyes was focused into the sample by an Apochromat 40x/1.2 NA water objective using an HFT 405/488/561 dichroic beam splitter. The emission light passed an adjustable pinhole. To allow the maximal number of photons to be collected from the sample, the pinhole was opened completely. Donor (mCitrine) fluorescence and donor excitation/acceptor emission images were excited by a 488 nm argon laser. A NFT 565 dichroic beam splitter separated the emitted light into two different detection channels where BP 505-550 and

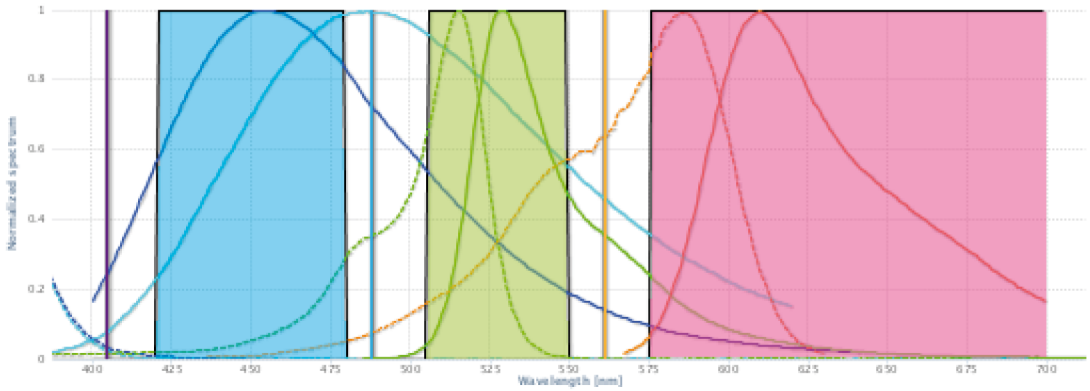

Figure 2.2: Instrumental alignment for ratiometric FRET imaging. Lasers (vertical coloured lines) and filter adjustments (coloured, transparent rectangles) used for ratiometric FRET imaging. For demonstration purposes, excitation and emission spectra of Hoechst 33528, mCitrine (donor) and mCherry (acceptor) are displayed as well (courtesy of Dr. Hernan E. Grecco).

LP 575 emission filters were used for spectral selection. Laser power of the Argon laser was set to 50 % to minimise photobleaching and phototoxicity. Hoechst 33342 was excited by the 405 nm diode laser and its emission recorded using a NFT 490 dichroic beam splitter and LP 420 or BP 420-480 emission filter, while mCherry was excited with a 561 nm diode laser and emission detected using a NFT 515 dichroic beam splitter and LP 575 emission filter. Laser lines and filter adjustments are outlined in Fig. 2.2. Transmission for all lasers was set to 1 %. Fluorescence was detected by avalanche photodiodes (APDs). Excitation light was focused into the sample by an Apochromat 40x/1.2 NA water objective. Live cell imaging was performed in a temperature-controlled incubation chamber in conditions appropriate for normal cell growth.

2.2.5.3 Fluorescence Lifetime Imaging Microscopy (FLIM)

The FLIM microscope used in this study is a commercial setup composed of a Olympus FluoView FV1000 laser scanning confocal microscope and PicoQuant's compact FLIM and FCS upgrade kit for laser scanning microscopes as an external extension. The instrumental setup is schematically outlined in Fig. 2.3. The pulsed lasers are coupled the FluoView FV1000 via the existing UV and IR ports while the continuous wave lasers for simple image acquisition enter the microscope independently. Pulsed lasers are controlled by a driver that also sends its synchronisation signal for excitation pulses to the data acquisition unit (PicoHarp 300). The laser scanner of the microscope is controlled via Olympus software but the Olympus LSM controller also connects to the PicoHarp 300 unit to provide information about the scanning process. Emission light can be directed to one or a combination of two single photon avalanche diodes (SPAD) as detectors which then transmit their signal to the PicoHarp 300 data acquisition unit.

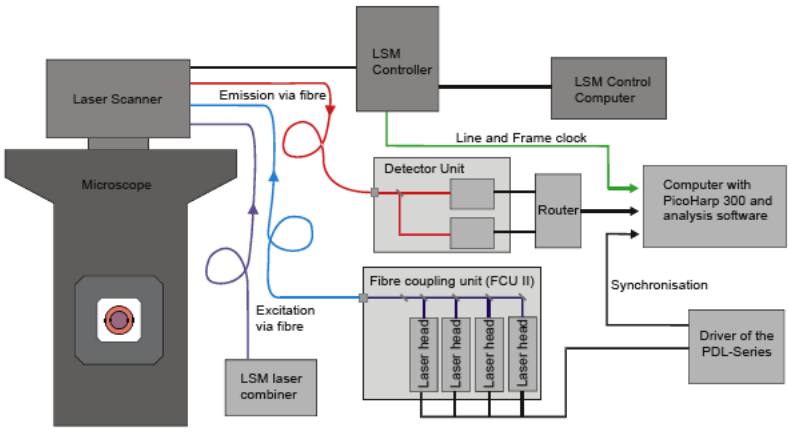

Figure 2.3: General layout of the instrumental time-domain FLIM setup. The instrumental setup for time-domain FLIM consists of an Olympus FluoView FV1000 laser scanning confocal microscope equipped with PicoQuant's compact FLIM and FCS upgrade kit for LSCMs as an external extension (adapted from http://www.picoquant.com/technotes/technote_lsm_upgrade_kit.pdf).

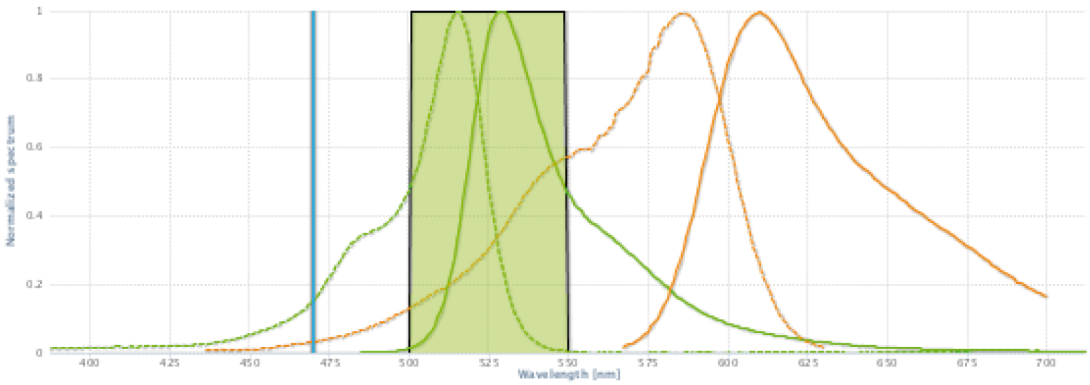

Figure 2.4: Instrumental alignment for FLIM. Laser (vertical coloured line) and filter (coloured, transparent rectangle) used for FLIM. For demonstration purposes, excitation and emission spectra of mCitrine (donor) and mCherry (acceptor) are displayed as well (courtesy of Dr. Hernan E. Grecco).

FLIM images were obtained using 40x/0.9 NA air objectives or 60x/1.2 NA water objectives (Olympus). mCitrine was excited every 25 ns with the 470 nm line of a pulsed diode laser and the excitation light directed into the sample by DM405/470 dichroic mirror. mCitrine fluorescence was detected by an APD using a 525/50 bandpass filter (Fig. 2.4). Pulsed lasers and APDs were controlled with the Sepia II software (PicoQuant GmbH). Image integration interval was approximately 30 sec (with an average total photon count of 1.0 x 10^6 to 3.0 x 10^6 per image). Confocal images to demonstrate the

presence of donor and acceptor fluorophores were recorded as described in 2.2.5.1. Live cell imaging was performed in a temperature-controlled incubation chamber in conditions appropriate for normal cell growth.

2.2.5.4 Image Manipulation and Analysis

Confocal images were converted to 32-bit images and background corrected using ImageJ. If required, brightness and contrast of images were adjusted to improve the signal-to-noise ratio.

Ratiometric FRET images were analysed with and quantified using ImageJ. Image stacks were converted to 32-bit images and each image in individual stacks was background corrected individually. Relative FRET efficiencies were calculated as the ratio of donor fluorescence (I_{D}) and donor excitation/acceptor emission intensity (I_{A}) for each pixel ($I_{\mathrm{D}}/I_{\mathrm{A}}$). $I_{\mathrm{D}}/I_{\mathrm{A}}$ images have been defined as FRET ratio images and were produced by dividing donor (mCitrine) images by donor excitation/acceptor emission images. Results were masked and used to quantify the change in FRET ratio and displayed as pseudocolour images.

FLIM data were analysed using PicoQuant's SymPhoTime v5.12 software. Donor intensity images were recalculated from the original TTTR files stored by the software during image acquisition. Images were interactively masked by selecting pixels of similar intensities to create an ROI and to exclude background intensities from the analysis. TCSPC histograms were recalculated for every ROI. Time-domain fluorescent lifetime data are best analysed by fitting fluorescence decay models to the decay curves (Fig. 1.17). Tail-fit analysis was performed on the TCPSC decay curves to alleviate the influence of the instrument response function (Lakowicz, 2006). When it was reasonable to assume that the decay follows a single-exponential decay model (i.e. for donor only images), a mono-exponential decay model according to equation 1.8 was employed. In case, more than one lifetime was to be expected in the sample (when acceptor fluorophores were present in the sample), a bi-exponential fluorescence decay model was fitted according to equation 2.1 (Lakowicz, 2006):

$$I(t) = A_1 \exp(-t/\tau_1) + A_2 \exp(-t/\tau_2) + B \tag{2.1}$$

with B as background, the pre-exponential factors A_1 and A_2 as amplitudes, and τ_1 and τ_2 as the fluorescent lifetimes. The fitted regions of the curves were kept as wide as possible excluding the onset of the decay curve but including a part representing background counts. Lifetime images were calculated by the software on a pixel-by-pixel basis. Lifetime data were presented as pseudo-coloured lifetime maps. Colours for lifetime representation were adjusted manually in the software.

Aim of the Thesis

As discussed in Chapter 1, the dynamic properties of biological systems are a result of the underlying dynamic interactions of their individual components. Thus, a complete understanding of signal transduction systems requires information about the spatio-temporal dynamics of the involved protein-protein interactions (Miyawaki, 2003; Schultz, 2007; Verveer and Bastiaens, 2008; Grecco and Verveer, 2011).

Traditional, biochemical methods to analyse signalling activities such as affinity chromatography, co-immunoprecipitation, yeast two-hybrid screens, immunoblots, and mass spectrometry are restricted to population averages and therefore provide very little or no spatio-temporal information. Immunofluorescence offers only poor temporal information about protein activities due to the fixation process. Only dynamic, live cell imaging approaches using fluorescent biosensors offer sufficient spatio-temporal resolution to probe enzyme or specifically MAPK activity (Wouters *et al.*, 2001; Miyawaki, 2003; Yasuda, 2006; Schultz, 2007; Grecco and Verveer, 2011).

Previously published FRET-based biosensors for ERK1/2 activity suffer from several serious disadvantages, including the indirect detection of ERK2 activity via substrate modification (Green and Alberola-Ila, 2005; Sato *et al.*, 2007; Harvey *et al.*, 2008a) or conformational change (Fujioka *et al.*, 2006), a low dynamic range and insufficient spatial resolution (Fujioka *et al.*, 2006; Sato *et al.*, 2007; Harvey *et al.*, 2008a).

Therefore the aim of the present thesis was to develop a new FRET-based, fluorescent biosensor that would directly report ERK2 activity with high spatio-temporal resolution and a large dynamic range.

The ERK2 biosensor would preferably be able to resolve previously inaccessible features of MAPK signalling such as spatial gradients and travelling waves of phospho-proteins (Kholodenko, 2006) or the signalling endosome hypothesis (Howe and Mobley, 2004; Kholodenko, 2006) and offer the possibility to obtain quantitative data that could be integrated into computational models of MAPK signalling. Other potential applications are the analysis of compartmental and differential MAPK signalling upon growth factor stimulation and the investigation of feedback loops in the MAPK module (Santos *et al.*, 2007; Nakakuki *et al.*, 2010).

Three different strategies were employed to achieve this goal:

In one approach a tetracysteine (4C) motif was introduced into fluorescently labeled ERK2. Specific labeling of the 4C motif with biarsenical fluorophores would allow to

measure FRET between the fluorescent (donor) protein and the biarsenical acceptor. The activation-induced conformational change of ERK2 would then change the FRET signal.

The most direct approach to measure kinase activity would be the direct observation of transient ES interactions (Yudushkin *et al.*, 2007) as the modification of a substrate by its kinase requires their physical interaction. Thus, it should be possible to detect ES complexes by measuring FRET/FLIM between donor-tagged ERK2 and an acceptor-labeled substrate peptide. However, FLIM approaches require high fractions of donor molecules undergoing FRET (i.e. high fractions of ERK2 in complex with its substrate) and K_{M}-values of known ERK2 substrates are usually in a range of 100 μM to 1 mM. It is thus difficult to get sufficient substrate concentrations inside living cells.

In an attempt to increase local substrate concentrations, the substrate peptide was fused to ERK2 via a flexible peptide linker. The chimeric sensor proteins was sandwiched by fluorescent proteins that could function as a FRET pair and thereby formed an intramolecular FRET-based biosensor for ERK2 activity. The advantage of the sensor would lie in its ability to report ERK2 activity directly, while being relatively inert to influences from endogenous proteins. It could potentially be used for FLIM as well as technically less challenging, intensity-based FRET methods.

3 Results

3.1 A Simple Assay to Assess ERK2 Activation

It is well-known, that - despite having cytosolic substrates - the main pool of phosphorylated MAPKs translocates quickly (in less than ten minutes) to the nucleus after growth factor stimulation (Chen *et al.*, 1992; Gonzalez *et al.*, 1993; Lenormand *et al.*, 1993; Volmat *et al.*, 2001; Ando *et al.*, 2004; Burack and Shaw, 2005; Costa *et al.*, 2006; Fujioka *et al.*, 2006; Cohen-Saidon *et al.*, 2009; Shankaran *et al.*, 2009). This phenomenon can be used to monitor activation of the Raf/MEK/ERK network upon growth factor stimulation by observing the translocation of fluorescently tagged ERK2.

3.1.1 Cloning of Fluorescently Tagged ERK2 Proteins

For cloning of a fluorescently tagged ERK2, the rat ERK2 coding sequence (CDS) (NCBI accession number: NM_053842) was amplified from pET-ERK2 by standard PCR as described in 2.2.2.1 and cloned into pEGFP-C1 via *BspE*I and *Sal*I. mCitrine-ERK2 was constructed by replacing EGFP in EGFP-ERK2 with mCitrine using *Age*I and *BspE*I. ERK2-mCitrine was created by subcloning the ERK2 sequence into mCitrine-N1 using *Xho*I and *BamH*I. The stop codon was removed and a Kozak sequence introduced by site-directed mutagenesis as described in 2.2.2.2 in a single PCR reaction. MEK1 was subcloned into pcDNA3.1(+) from EYFP-MEK1 using *Hind*III and *BamH*I. The identity of all constructs was confirmed by sequencing (data not shown). In EGFP-ERK2 and all resulting constructs Ala2 of ERK2 was missing.

To determine if the fluorescent protein tag still allowed phosphorylation of the ERK2 fusion proteins, mCitrine-ERK2 and ERK2-mCitrine were co-expressed with MEK1 in HeLa cells. Cells were starved overnight and stimulated with 100 ng/ml EGF for 5 min. ERK2 phosphorylation in stimulated versus non-stimulated cells was analysed in whole cell lysates (see 2.2.3.6) by western blots as described in 2.2.3.8 and 2.2.3.9.

Both mCitrine-ERK2 or ERK2-mCitrine phosphorylation was markedly increased when isolated from EGF-stimulated HeLa cells in a fashion similar to endogenous ERK2 (Fig. 3.1). This result shows that activation of N- or C-terminally tagged ERK2 is not impaired by the FP. It may be noteworthy, that phosphorylation of ERK1/2 is already apparent in imunoblots for total ERK by the band shift in stimulated samples (Fig. 3.1).

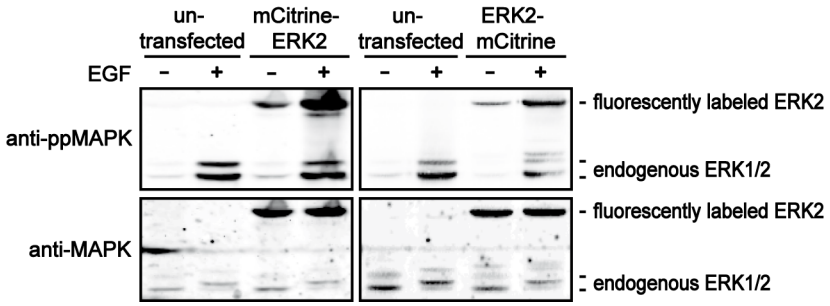

Figure 3.1: Fluorescently labeled ERK2 can be phosphorylated *in-vivo*. Western blot showing the phosphorylation of fluorescently labeled ERK2. HeLa cells were co-transfected with MEK1 and mCitrine-ERK2 or MEK1 and ERK2-mCitrine, starved overnight and stimulated with 100 ng/ml EGF for 5 min. Whole cell extracts were subjected to SDS-PAGE and western blotting.

3.1.2 ERK2 Translocation As a Read-Out of Its Activation

ERK2 translocation was observed in various cell types co-transfected with EGFP-ERK2 and MEK1-mCherry (kind gift of Dr. Piet Lommerse, MPI-Dortmund/Germany). Co-transfection of MEK1 is necessary to prevent nuclear ERK2 accumulation (Fukuda *et al.*, 1997; Rubinfeld *et al.*, 1999; Adachi *et al.*, 2000; Burack and Shaw, 2005). Cells were starved overnight and imaged every 60 sec for approx. 60 min using either an Olympus FluoView 1000 or Zeiss LSM510 confocal microscope. Cells were stimulated with 100 ng/ml EGF a few minutes after the start of an image sequence.

Upon stimulation with EGF, ERK2-EGFP translocated to the nucleus in various cell types. ERK2 translocation started on average approx. 3 min after EGF addition with a sudden rise of nuclear ERK2 levels, a peak after 8.1 ± 1.8 min and a slow exit from the nucleus, while displaying high cell to cell variability (Fig. 3.2). To measure cell to cell variability of peak timing, the coefficient of variation (CV), defined as the ratio between standard deviation and the mean (CV = SD/mean) (Cohen-Saidon *et al.*, 2009), was calculated to be 22 %. Average nuclear ERK2 levels did not return to basal levels during the time of observation, again with great cell to cell variability (CV of lowest nuclear fluorescence value after the peak = 23 %). While in some cells indeed nuclear fluorescence returned to basal levels, in others it slowly started increasing after an initial decline phase of nuclear fluorescence (Fig. 3.2). The time point of lowest fluorescence after the peak was 23.6 ± 9.3 min with a CV of 40 %.

Nuclear EGFP-ERK2 levels after EGF stimulation follow a defined fold-change (here: 1.94 ± 0.59) defined as ratio of nuclear fluorescence at maximal EGF stimulation and initial nuclear fluorescence again with high cell to cell variability (CV = 25 %). The relationship between intial and maximal nuclear ERK2 levels is approximately proportional in each cell (R^2 = 0.94), meaning that cells with higher initial nuclear ERK2 levels also show a larger absolute increase (Fig. 3.2 insert). As shown by (Cohen-Saidon

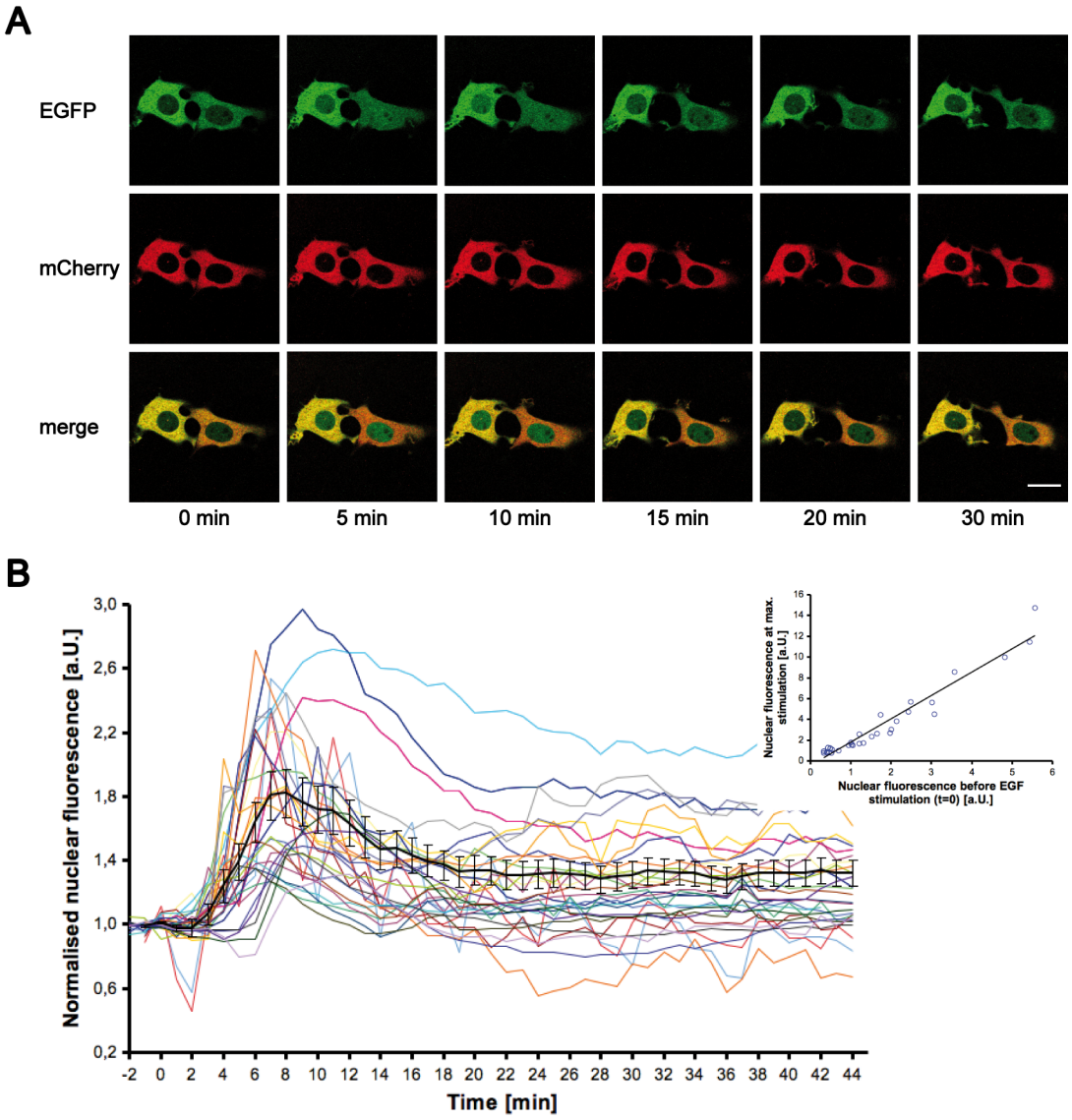

Figure 3.2: EGFP-ERK2 accumulates in the nucleus upon EGF stimulation. A) Representative pseudocolour image sequence of MCF7 cells expressing EGFP-ERK2 (upper panel) and mCherry-MEK1 (middle panel) as well as merged images of both (lower panel) showing the translocation of EGFP-ERK2 to the nucleus. Cells were starved overnight and stimulated with 100 ng/ml EGF. Scale bar = 20 μm. B) Graphs representing nuclear fluorescence. For each cell, the ratio of nuclear EGFP fluorescence and whole cell mCherry fluorescence was normalised to nuclear fluorescence before EGF addition to allow better cell to cell comparability. Coloured lines denote average nuclear fluorescence of EGFP-ERK2 in individual cells, the black line denotes average nuclear fluorescence of EGFP-ERK2 in all measured cells with S.E.M. (n=34). The insert shows the correlation of nuclear fluorescence at maximal EGF stimulation with nuclear fluorescence at t=0. Each circle represents a value from one individual cell. Black line represents the best linear fit ($R^2 = 0.94$).

et al., 2009), this behaviour can be called a "fold-change response" where the amount of ERK2 translocating to the nucleus is a constant fraction of the initial levels. However, here the ERK2 returns to a nuclear level higher than the original basal level as demonstrated by the ratio of the final and initial fluorescence level of 1.23 ± 0.29 (mean $\pm$ S.D.).

Translocation of ERK2 to the nucleus was used to assess and control successful growth factor stimulation of cells throughout this study.

3.2 An Intramolecular ReAsH-Based FRET-Biosensor for ERK2 Activation

A genetically encoded ERK2 biosensor, based on the conformational change of ERK2 upon its activation has been developed before (Fujioka *et al.*, 2006). Here, the N- and C-terminus of ERK2 were fused to cyan and yellow fluorescent protein (CFP and YFP) as a FRET pair, translating the phosphorylation-induced, conformational change of ERK2 and concurrently the positional change of the N- and C-terminus relative to each other into a change of FRET efficiency. However, the dynamic range of the sensor is rather small (Fujioka *et al.*, 2006). In an attempt to extend that approach to obtain a sensor construct with a higher dynamic range, mCitrine-tagged ERK2 was tagged with an acceptor fluorophore in regions of ERK2 that change conformation upon phosphorylation of the kinase. Unfortunately, the introduction of a large (27 kDa), second fluorescent protein (FP) may disrupt the protein's functionality (McLean *et al.*, 2001; Vilardaga *et al.*, 2003; Andresen *et al.*, 2004). Thus, short tetracysteine (4C) tags were introduced into ERK2 at the desired positions, that could be labeled with biarsenical dyes.

3.2.1 Development of an Intramolecular ReAsH-based FRET Biosensor for ERK2 Activation

By superimposing crystal structures of phosphorylated and unphosphorylated ERK2 (Zhang *et al.*, 1994; Canagarajah *et al.*, 1997), four regions of conformational sensitive regions of ERK2 were identified that would also be accessible for labeling by a chemical fluorophore (Fig. 3.3B). Especially - but not exclusively - the ERK2 activation loop undergoes a dramatic conformational change upon phosphorylation (Fig. 3.3B) (Canagarajah *et al.*, 1997). Thus, amino acids of the activation loop (Val171 to Phe181, excluding Thr183, Tyr185 and adjacent amino acids) and amino acids 9-14, 30-35 and 327-336 of rat ERK2 were chosen for replacement with either the minimal or optimised version (Martin *et al.*, 2005) of the 4C motif (Fig. 3.3B and C and Fig. S.1.1) in mCitrine-tagged ERK2. In additon, the N- or C-terminus of ERK2 were tagged with the 4C motif in ERK2-mCitrine or mCitrine-ERK2, respectively. The conformational change induced by phosphorylation of ERK2 would lead to a change of distance and/or orientation of mCitrine to ReAsH bound to the 4C motif (Fig. 3.3A and B). Since mCitrine and ReAsH form a good FRET pair, the conformational change could be detected by the resulting change in FRET signal (Fig. 3.3A).

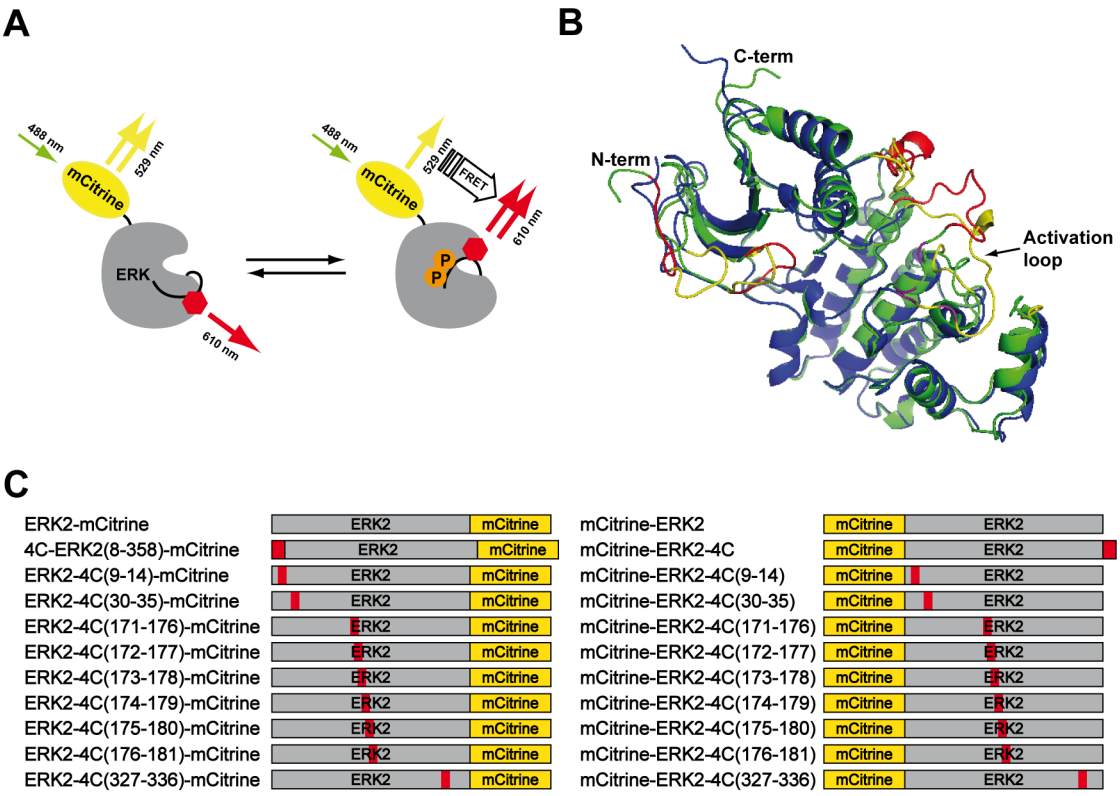

Figure 3.3: Principle and design of the ReAsH-based FRET sensor for ERK2. A) Principle of the ReAsH-based FRET sensor for ERK2. Phosphorylation of ERK2 induces a conformational change of the kinase which is translated into a change in FRET efficiency between donor and acceptor fluorophore. FRET can be measured ratiometrically or by FLIM. ReAsH is represented by the red hexagon. B) Crystal structures of phosphorylated (green and red) and unphosphorylated (blue and yellow) ERK2 were superimposed. Domains in ERK2 that change conformation upon phosphorylation are in yellow, amino acids that were replaced by the 4C motif are highlighted in red in ppERK2, phosphorylatable Thr183 and Tyr185 are marked in purple. C) Schematic representation of the ERK2 biosensor constructs cloned. All constructs were derived from rat ERK2 fused to mCitrine on the N- or C-terminus, respectively. The tetracysteine motif (red) replaced original amino acids. Amino acid sequences of wt and recombinant ERK2 proteins are detailed in Fig. S.1.1.

The 4C motif was introduced at the indicated positions (Fig. 3.3B and C) by directed mutagenesis of either ERK2-mCitrine or mCitrine-ERK2, respectively, as described in 2.2.2.3 to create nineteen different sensor constructs as listed in Table S.1.1. The identity of all constructs was confirmed by sequencing (data not shown).

To determine, whether the introduced 4C motif would hamper phosphorylation of mutant ERK2 proteins in the activation loop, sensor constructs were co-expressed

individually with MEK1 in HeLa cells. Cells were starved for 4-6 h and stimulated with 100 ng/ml EGF for 5 min. Sensor protein phosphorylation in stimulated versus non-stimulated cells was analysed in whole cell lysates by SDS-PAGE and western blotting.

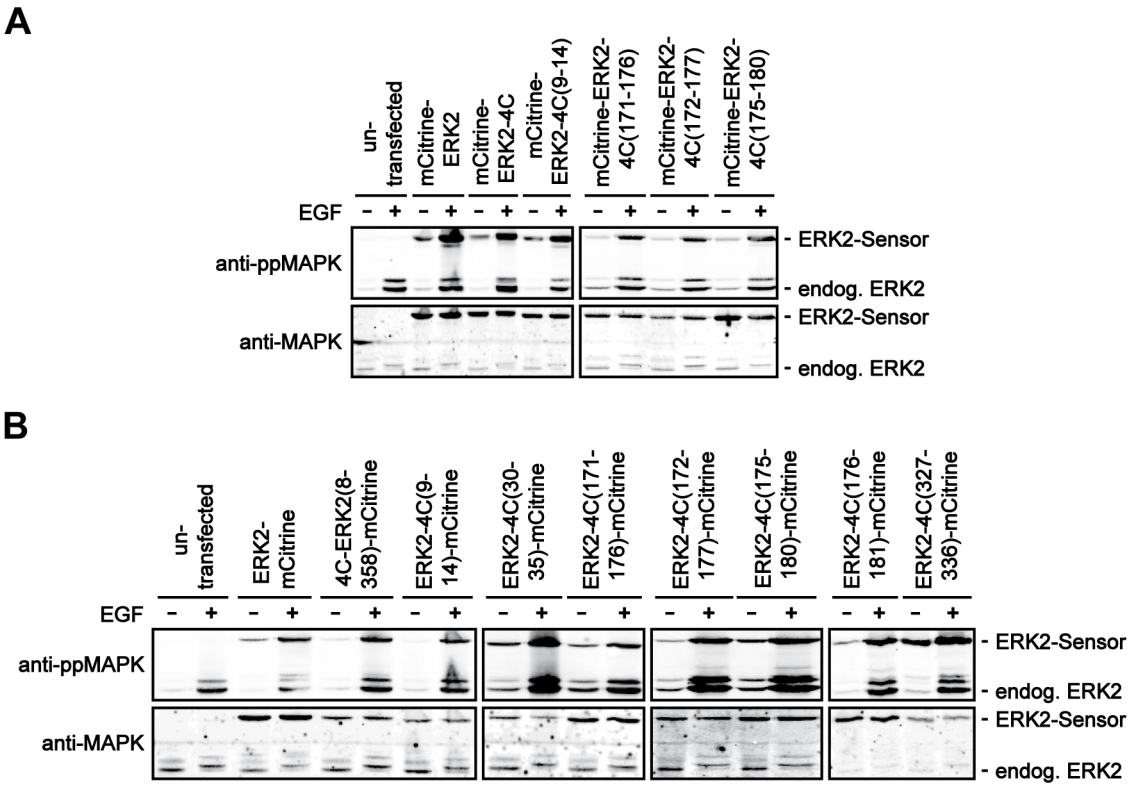

Figure 3.4: Tetracysteine motif containing ERK2 mutants can be phosphorylated *in-vivo*. Western blot showing the phosphorylation of 4C motif containing ERK2 mutants derived from mCitrine-ERK2 (A) or ERK2-mCitrine (B). HeLa cells were co-transfected with MEK1 and one of 19 ERK2 biosensor construct, starved overnight and stimulated with 100 ng/ml EGF for 5 min. Whole cell extracts were subjected to SDS-PAGE and western blotting. endog. ERK2 = endogenous ERK2

Every 4C motif containing ERK2 biosensor construct tested was strongly phosphorylated upon EGF stimulation, following closely phosphorylation of endogenuos or fluorescently labeled ERK2 (Fig. 3.4). This demonstrates that the presence of the 4C motif, especially in the activation loop, does not influence phosphorylation of the mutant ERK2 proteins. Interestingly, the phosphorylation of sensor constructs cannot be observed by a band shift with total ERK antibodies, in contrast to endogenous ERK1/2 (Fig. 3.4).

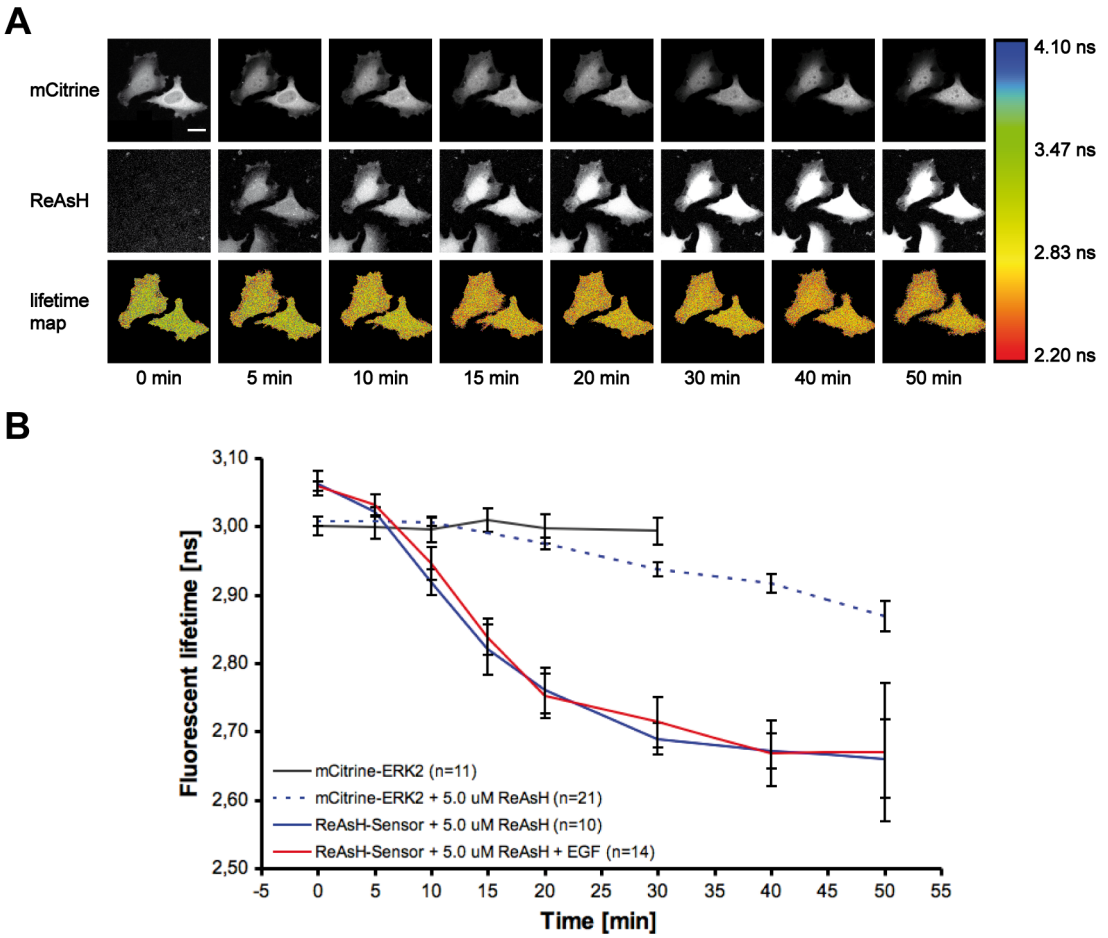

Figure 3.5: FRET between mCitrine and ReAsH in ERK2. A) Representative image sequence showing the occurence of FRET between mCitrine and ReAsH upon binding of ReAsH to the 4C motif. HeLa cells co-expressed MEK1 and mCitrine-ERK2-4C(171-176). Cells were starved for 4-6 h and incubated with 5.0 μM ReAsH. FLIM images were recorded at various time points after ReAsH addition. Confocal images of mCitrine (upper row) and ReAsH (middle row) as well as pseudocolour fluorescent donor lifetime maps (bottom row) are shown. Scale bar = 20 μm. B) ReAsH labeling kinetics. HeLa cells transiently transfected with MEK1 and either mCitrine-ERK2 or mCitrine-ERK2-4C(171-176) were incubated with 5.0 μM ReAsH. Fluorescent donor lifetimes were determined at various time points after ReAsH addition.

3.2.2 Labeling Tetracysteine-Tagged ERK2 with Biarsenical Fluorophores

To test whether it was in principle possible to specifically label 4C-tagged proteins with biarsenical fluorophores in the present experimental system, one arbitrarily chosen ReAsH-ERK2 sensor constructs (mCitrine-ERK2-4C(171-176)) was co-transfected with MEK1/pcDNA3.1(+) into HeLa cells and cells incubated with 5.0 μM ReAsH as described in 2.2.3.10. FRET between mCitrine and ReAsH was detected by measuring

mCitrine fluorescent lifetime using FLIM as described in 2.2.5.3 at various time points after ReAsH addition in the presence or absence of EGF. Background labeling of non-tagged proteins by ReAsH was assessed by measuring donor lifetime of mCitrine-ERK2 expressed in HeLa cells. Data were analysed and displayed according to 2.2.5.4.

ReAsH labeling kinetics of mCitrine-ERK2-4C(171-176) in the presence or absence of EGF were virtually identical (Fig. 3.5B). Addition of ReAsH to the cell culture medium resulted in a decrease of mCitrine lifetime of 0.41 ± 0.09 ns in the presence and 0.42 ± 0.03 ns in the absence of EGF (Fig. 3.5B), displaying the occurence of FRET between mCitrine and ReAsH. Instead, donor lifetime of mCitrine-ERK2 decreased only for 0.14 ± 0.02 ns after ReAsH addition. Labeling kinetics of mCitrine-ERK2-4C(171-176) by ReAsH could be described by a sigmoidal function. However, the time scale for full labeling until no further decrease in fluorescent lifetime could be observed was 40 - 50 min (Fig. 3.5B). Taken together, these data demonstrate that it was possible to specifically label recombinant proteins containing the 4C motif with ReAsH.

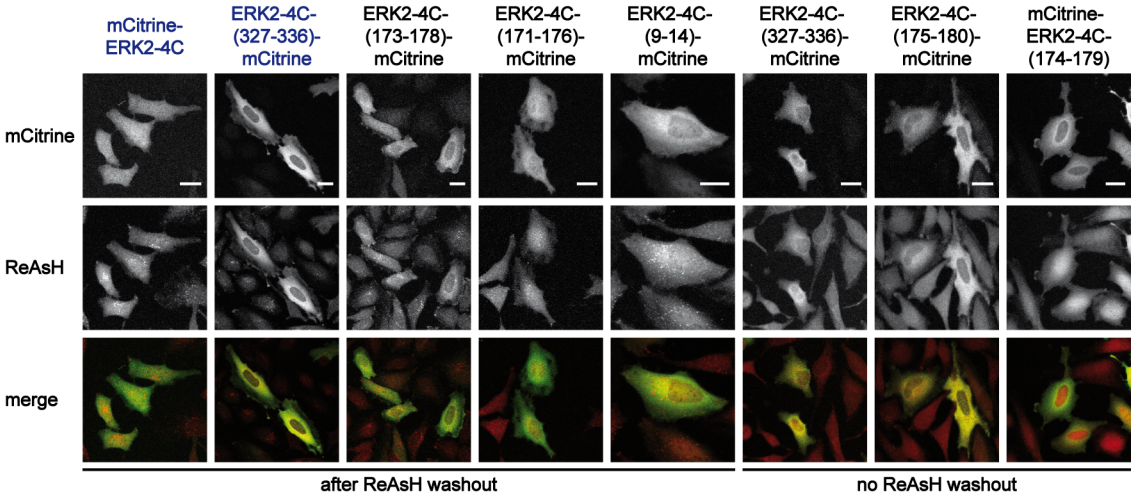

Figure 3.6: Background labeling by ReAsH can be significantly reduced by using the optimised version of the 4C motif. Representative confocal images comparing the background labeling of cells expressing mCitrine-ERK2 fusion proteins tagged with either the optimised (Martin *et al.*, 2005) or minimal version of the 4C motif (CCPGCC). HeLa cells were co-transfected with MEK1 and the desired sensor construct as indicated, starved overnight and labeled with 5.0 μM ReAsH as described in 2.2.3.10. 4C motif sequence in the first two rows (mCitrine-ERK2-4C and ERK2-4C(327-336)-mCitrine) was FLNCCPGCCMEP. mCitrine (top), ReAsH (middle) and false colour merge images (bottom) are shown. Scale bar = 25 μm.

It may be interesting to note, that while unspecific background staining by ReAsH was always observed, it could be markedly decreased by using the optimised version (Martin *et al.*, 2005) of the tetracysteine motif (Fig. 3.6). Background reduction, however, required washout of ReAsH by the washing buffer British anti-Lewisite (BAL).

Similarly high background intensity was observed with both versions of the 4C motif 60 min after incubation with ReAsH but before washout with BAL (Fig. 3.6).

3.2.3 Screening of Tetracysteine-Tagged ERK2 Biosensor Constructs Using Fluorescence Lifetime Imaging Microscopy

FLIM was used to identify a functional sensor construct with a high dynamic range. Each sensor construct was co-expressed with MEK1 in HeLa cells. Cells were starved overnight and sensor constructs labeled with 5.0 μM ReAsH as described in 2.2.3.10. Cells were stimulated with 100 ng/ml EGF and the fluorescent lifetime of donor molecules determined by FLIM before and 5, 10 and 20 min after stimulation as described in 2.2.5.3 and 2.2.5.4.

Out of the nineteen ERK2 sensor constructs, only mCitrine-ERK2-4C(174-179) showed a significant change in lifetime of 0.03 $\pm$ 0.01 ns after EGF stimulation (Fig. 3.7). In addition, none of the constructs showed a lifetime change resembling known ERK2 activation profiles. For most constructs, lifetime changes observed (usually less than 30 ps) were in a similar range as those for mCitrine-tagged ERK2 and/or - even more profoundly - lifetimes did not change consistently in only one direction (shown exemplarily for mCitrine-ERK2-4C(9-14) in Fig. 3.8, see also Table S.1.2-S.1.21). In addition to mCitrine-ERK2-4C(174-179), only ERK2-4C(175-180)-mCitrine and ERK2-4C(327-336)-mCitrine displayed a consistent change in lifetime (Tables S.1.10, S.1.12 and S.1.18).

While most of the nineteen ReAsH-ERK2 biosensor constructs failed to report ERK2 activity, mCitrine-ERK2-4C(174-179), ERK2-4C(175-180)-mCitrine and ERK2-4C(327-336)-mCitrine were tested in more detail to assess their potential. Since the observed fluorescent donor lifetime changes after labeling with ReAsH but prior to EGF stimulation were in many cases surprisingly small (Fig. 3.7), stimulation of the chosen sensor constructs with 100 ng/ml EGF was performed in the presence of 5.0 μM ReAsH without wash-out of ReAsH by BAL.

All three constructs showed markedly decreased mCitrine fluorescent lifetimes 60 min after incubation with ReAsH (Fig. 3.9). However, none showed a significant donor lifetime change upon EGF stimulation. Donor lifetimes for mCitrine-ERK2-4C(174-179) decreased as opposed to the increase seen in the first screen (compare Tables S.1.22 and S.1.18). ERK2-4C(327-336)-mCitrine displayed no consistent donor lifetime change (Table S.1.24). Thus, labeling efficiency of sensor constructs by ReAsH could be improved by omitting wash-out of ReAsH, but these tests did not reveal a functional sensor construct.

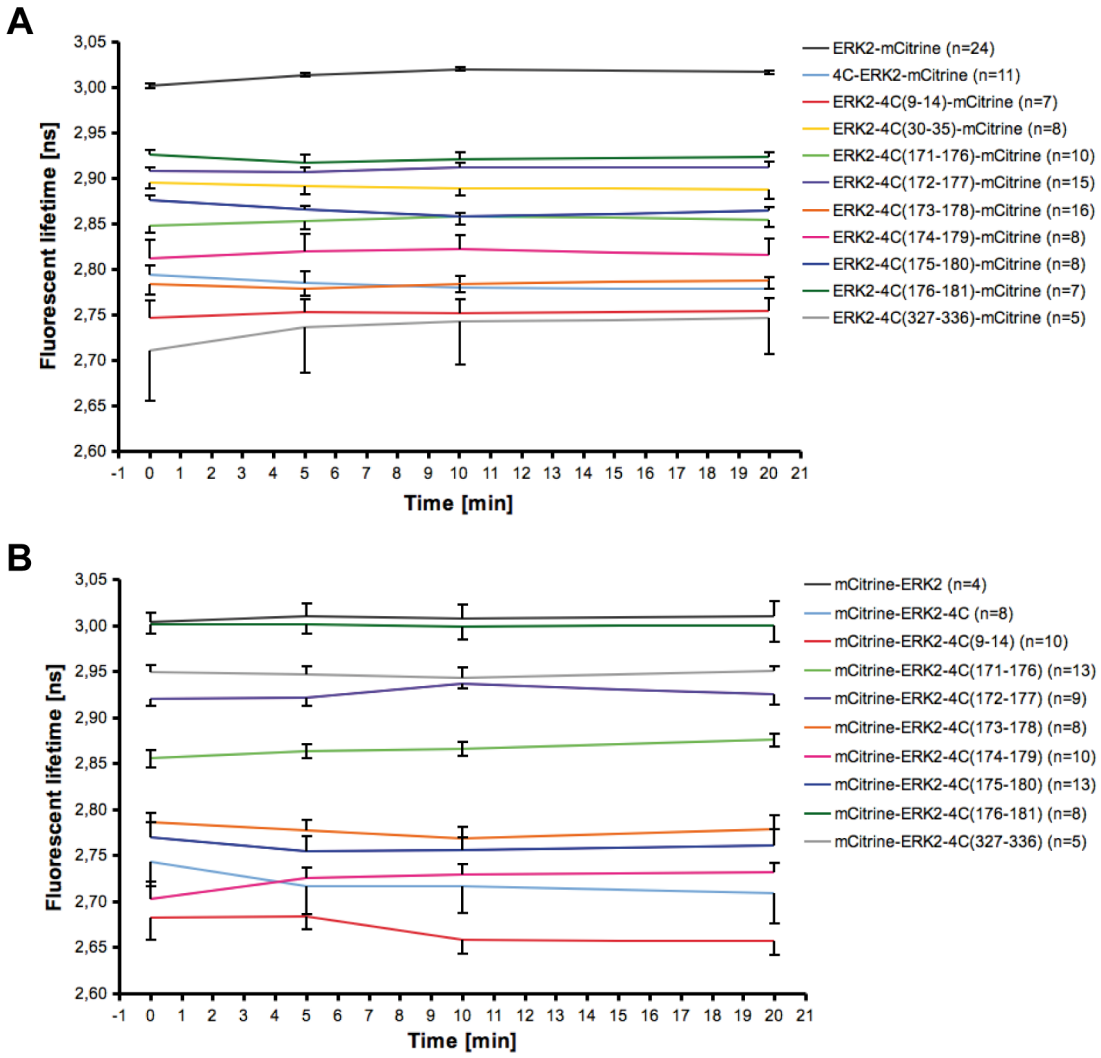

Figure 3.7: Screening of ReAsH-based FRET biosensors. Average fluorescent donor lifetimes of ReAsH-based ERK2 biosensor constructs based on ERK2-mCitrine A) or mCitrine-ERK2 (B). HeLa cells expressing MEK1 and one of nineteen sensor constructs were starved for 4-6 h, labeled with 5.0 μM ReAsH and stimulated with 100 ng/ml EGF. Fluorescent donor lifetimes were determined before and 5 min, 10 min and 20 min after stimulation.

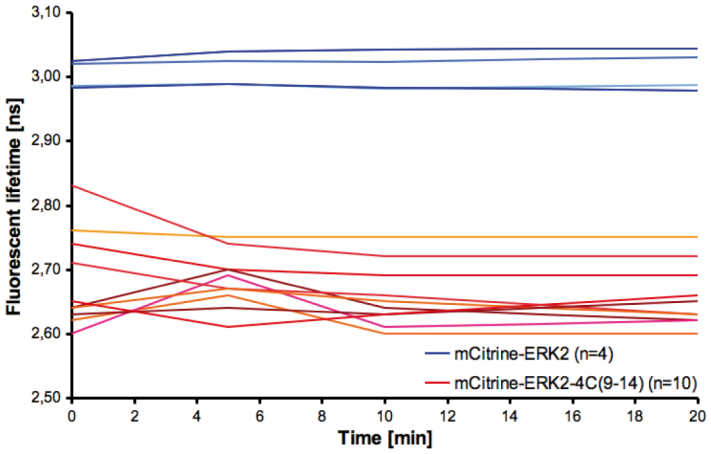

Figure 3.8: Fluorescent donor lifetimes do not change consistently in only one direction. Graphs showing representative single cell measurements of one of nineteen ReAsH-based ERK2 biosensors. HeLa cells expressing MEK1 and mCitrine-ERK2-4C(9-14) were starved for 4-6 h, labeled with 5.0 μM ReAsH and stimulated with 100 ng/ml EGF. Fluorescent donor lifetimes were determined before and 5 min, 10 min and 20 min after stimulation.

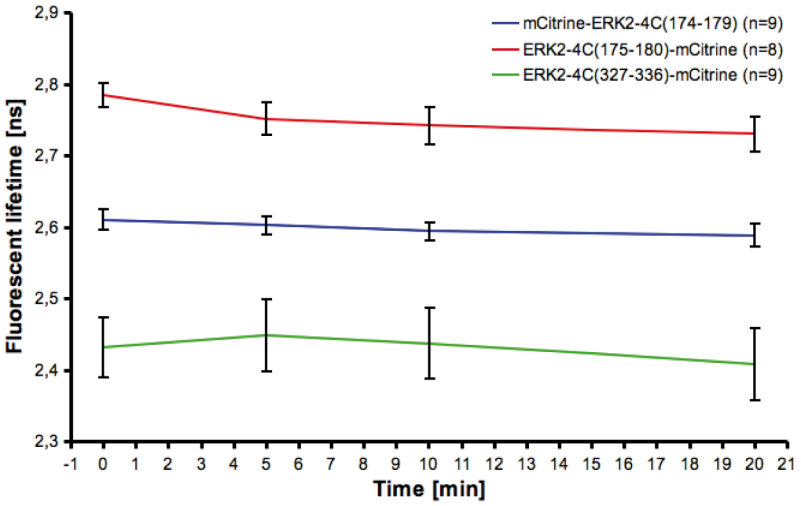

Figure 3.9: Test of ReAsH-based FRET biosensors without ReAsH wash-out. Average fluorescent donor lifetimes of mCitrine-ERK2-4C(174-179), ERK2-4C(175-180)-mCitrine and ERK2-4C(327-336)-mCitrine. HeLa cells expressing MEK1 and one of the above mentioned sensor constructs were starved for 4-6 h, incubated with 5.0 μM ReAsH for 60 min and stimulated with 100 ng/ml EGF. Fluorescent donor lifetimes were determined before and 5 min, 10 min and 20 min after stimulation.

In summary, even though it was possible to establish *in-vivo* labeling of proteins by biarsenical fluorophores, no construct could be identified as a functional fluorescent biosensor for ERK2 activity.

3.3 Visualising ERK2 Activity by Imaging Transient Enzyme-Substrate Interactions

Enzymatic modification of a substrate requires its binding to the active site of the enzyme forming a transient ES complex. Visualising ES interactions in living cells is the most direct approach to assess spatio-temporal enzyme activity and has been successfully employed to dissect spatial PTP1B regulation (Yudushkin *et al.*, 2007). Imaging of transient ERK2-substrate interactions would follow a similar principle as visualisation of PTP1B-substrate complexes: the occurence and loss of FRET upon binding and release of an acceptor-labeled substrate peptide to donor-tagged ERK2 is recorded in spatio-temporal manner (Fig. 3.10).

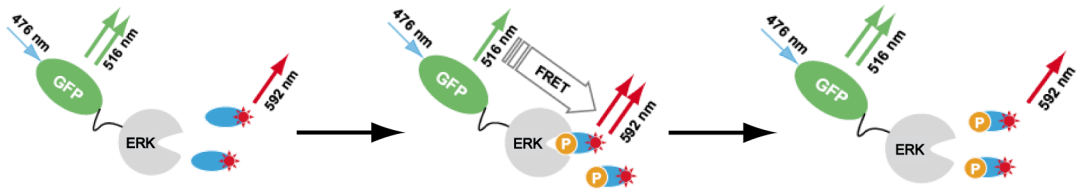

Figure 3.10: Principle of imaging ERK2-substrate interactions with FRET. The acceptor-labeled substrate peptide (blue) cannot bind to inactive, donor-tagged ERK2. Activation of the kinase induces binding of the substrate peptide to ERK2's active site and FRET, monitored by FLIM and/or emission intensity changes. After catalysis, the phosphorylated peptide dissociates from the kinase, resulting in a loss of FRET (modified from Yudushkin *et al.*, 2007).

mCitrine-ERK2 was used as donor in all attempts to establish ES complex visualisation (see Section 3.1.1). The substrate peptide corresponded to amino acids 379-403 of the human transcription factor Elk1. Elk1 is a known substrate of ERK2 including the consensus MAPK phosphorylation site (P-X-S/T-P) (Gille *et al.*, 1995; Yang *et al.*, 1998b,a) and contains a DEF-domain (F-X-F-P) (Jacobs *et al.*, 1999; Fantz *et al.*, 2001). The DEF-domain binds only to phosphorylated ERK2 as its binding pocket close to the active site of ERK2 is masked by ERK2's activation loop when in the inactive, unphosphorylated conformation (Lee *et al.*, 2004; Yoon and Seger, 2006). Substrate binding affinity to ERK2 was thus supposed to increase with incorporation of the DEF domain into the substrate peptide sequence.

3.3.1 Detection of ERK2 Enzyme-Substrate Interactions *In-Vitro*

In order to test whether formation of ES-complexes could be visualised, *in-vitro* experiments with purified components were performed as a proof of principle.

In all *in-vitro* experiments a shorter, synthetic version of the substrate peptide, corresponding to amino acids 382 to 403 of hElk1 was used. The peptide was a kind gift of Prof. Dr. Christian Becker (Dept. of Physical Biochemistry, Max-Planck-Institute of Molecular Physiology, Dortmund, Germany) and was synthesised and labeled with lissamine-rhodamine B by Sascha Gentz.

Monitoring ES-complexes *in-vitro* required purified, fluorescently labeled, active as well as inactive ERK2. An elegant protocol for the purification of active ERK2 is based on the co-expression of constitutively active MEK1 in *E.coli* (Khokhlatchev *et al.*, 1997). This, however, depends on the availability of bacterial expression vectors encoding mutant MEK1. For reasons of simplicity, mCitrine-ERK2 wt and constitutively active as well as kinase dead mutants of ERK2, mCitrine-ERK2 L73P/S151D (Emrick *et al.*, 2001) and mCitrine-ERK2 K52R (Robbins *et al.*, 1993), were expressed individually in *E. coli* and purified in non-phosphorylated form. mCitrine-labeled mutants of ERK2 were created by site-directed mutagenesis as described in 2.2.2.2 using MAPK1 K52R for and rev or MAPK1 L73P for and rev and MAPK1 S151D for and rev, respectively. mCitrine-ERK2 wt and its mutants were subcloned into the bacterial expression vector pProEx HTB using *Nco*I and *Sal*I. The identity of all constructs was confirmed by sequencing (data not shown). Purified ERK2 proteins were then activated *in-vitro* by commercially available active MEK1.

3.3.1.1 *In-Vitro* Phosphorylation of Purified ERK2 and Its Substrate

First, it was tested, whether purified, inactive, fluorescently tagged ERK2 proteins could be activated *in-vitro* by commercially available MEK1. *In-vitro* phosphorylation was performed as described in 2.2.3.2 and results subjected to SDS-PAGE and immunoblotting as described in 2.2.3.8 and 2.2.3.9. Purified His-ERK2 wt (kind gift by Piet Lommerse, Dept. of Systemic Cell Biology, Max-Planck-Institute of Molecular Physiology, Dortmund, Germany) was used as an internal control.

All ERK2 proteins and mutants showed a marked increase in phosphorylation levels upon incubation with active MEK1 (Fig. 3.11A). As expected, no phosphorylation of His-ERK2 wt, mCitrine-ERK2 wt and mCitrine-ERK2 K52R could be detected when active MEK1 was omitted from the reaction. In contrast, mCitrine-ERK2 L73P/S151D was already substantially phosphorylated before addition of MEK1, due to the increased autophosphorylation activity (Emrick *et al.*, 2001), but incubation with active MAPKK could still increase phosphorylation of ERK2 L73P/S151D (Fig. 3.11A).

Next, it was asked, whether purified ERK2 phosphorylated *in-vitro* was still active

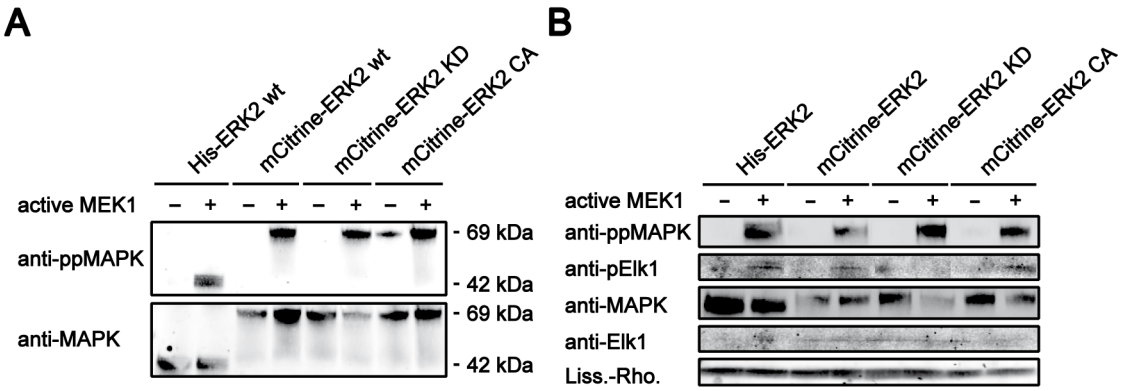

Figure 3.11: Purified ERK2 can phosphorylate a synthetic substrate peptide after activation by MEK1 *in-vitro*. A) Western blot analysis of purified ERK2 proteins after incubation with active MEK1. B) Western blot analysis of the synthetic ERK2 substrate after incubation with *in-vitro* phosphorylated ERK2 and active MEK1. The lissamine rhodamine B signal was used as loading control. 12 % SDS gel; ERK2 KD = kinase dead ERK2 (ERK2 K52R); ERK2 CA = constitutively active ERK2 (ERK2 L73P/S115D); Liss.-Rho. = lissamine-rhodamine B.

and could in turn phosphorylate the synthetic, fluorescently labeled ERK2 substrate peptide. *In-vitro* phosphorylation of ERK2 and the substrate was performed as described in 2.2.3.3 and results subjected to SDS-PAGE and immunoblotting.

ERK2 proteins and mutants could be phosphorylated *in-vitro* by active MEK1 (Fig. 3.11B). Curiously, there was only a faint band detectable for autophosphorylated mCitrine-ERK2 L73P/S151D. No phosphorylation of His-ERK2 wt, mCitrine-ERK2 wt and mCitrine-ERK2 K52R could be detected when active MEK1 was omitted from the reaction. More importantly, phosphorylated substrate peptide could be detected only in samples containing activated ERK2 (Fig. 3.11), demonstrating that at least a fraction of ERK2 was active after purification and could indeed modify its substrate *in-vitro*. As expected, no detectable phosphorylated substrate peptide could be observed in samples containing mCitrine-K52R, due to a lack of catalytic activity. Phosphorylated substrate peptide was also not observed in mCitrine-ERK2 L73P/S151D samples lacking MEK1, as expected from the low phosphorylation level.

These data show, that purified and *in-vitro* phosphorylated ERK2 is still active and able to phosphorylate a fluorescently labeled, synthetic substrate peptide *in-vitro*. Thus, detection of transient ES-complexes is theoretically possible.

3.3.1.2 *In-Vitro* ERK2 ES-Interaction Fluorescence Spectroscopy

FRET leads to a decrease in donor and an increase in acceptor intensity. It should therefore be possible to observe binding and consumption of the substrate peptide to ERK2 by measuring donor emission intensity at a fixed wavelength as a function of time. Formation of transient ES-complexes would be detected as a sudden drop in donor emission intensity upon substrate addition, displaying occurence of FRET. Donor intensity would then more or less slowly recover to initial values as the substrate peptide is modified and released from the kinase.

In-vitro ERK2 ES-interaction spectroscopy was performed as described in 2.2.3.4 using the constitutively active mutant in time-based experiments with fixed excitation (λ = 516 nm) and emission wavelength (λ = 529 nm). Substrate concentrations employed, ranged from 2.0 μM to 20.0 μM. The substrate peptide was serially diluted to allow the addition of the same volume to all samples. In negative controls, one volume of substrate dilution buffer was used.

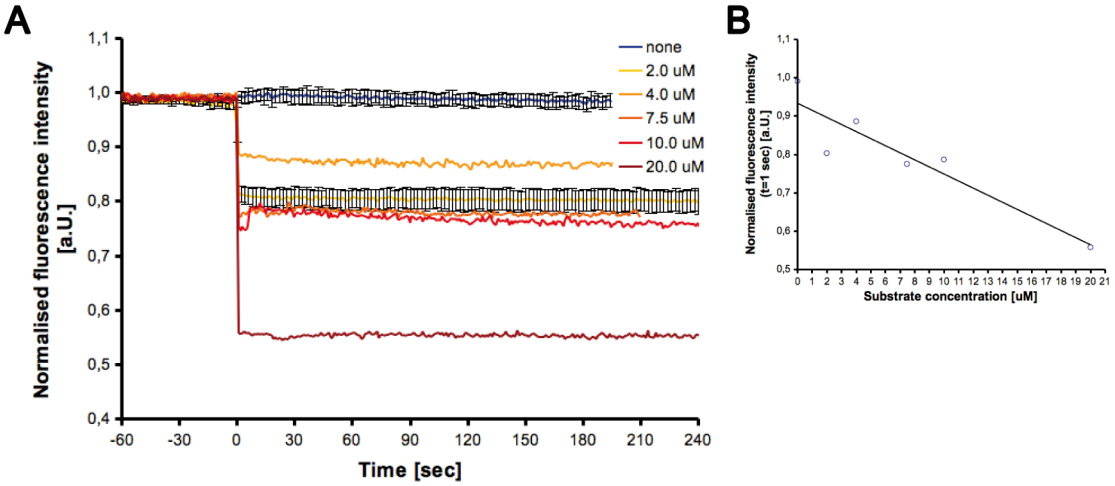

Figure 3.12: Substrate addition leads to a stable decrease in donor emission intensity in *in-vitro* ERK2 ES-interaction spectroscopy. A) Donor emission intensity was measured as a function of time at fixed excitation wavelength. Blue line represents normalised average fluorescence of mCitrine-ERK2 L73P/S151D corrected for the dilution effect of adding one volume substrate buffer with S.E.M. (n=3). Yellow to dark red lines represent the fluorescence signal of mCitrine-ERK2 L73P/S151D for increasing substrate concentrations (2.0 μM with S.E.M., n=6) and corrected for the dilution effect of adding one volume substrate buffer. B) Correlation of the fluorescence signal after substrate addition with the substrate concentration. Each circle represents fluorescence values at t = 1 sec after substrate addition from A). Black line represents the best linear fit (R^2 = 0.86).

Dilution corrected donor emission intensity values decreased upon LRh-hElk1(382-403) addition (Fig. 3.12A) in an approximately linear fashion (Fig. 3.12B), arguing

for the concentration-dependent occurence of FRET. However, no recovery of the donor emission intensity could be observed in any sample, indicating unspecific FRET independent of ERK2 activation state.

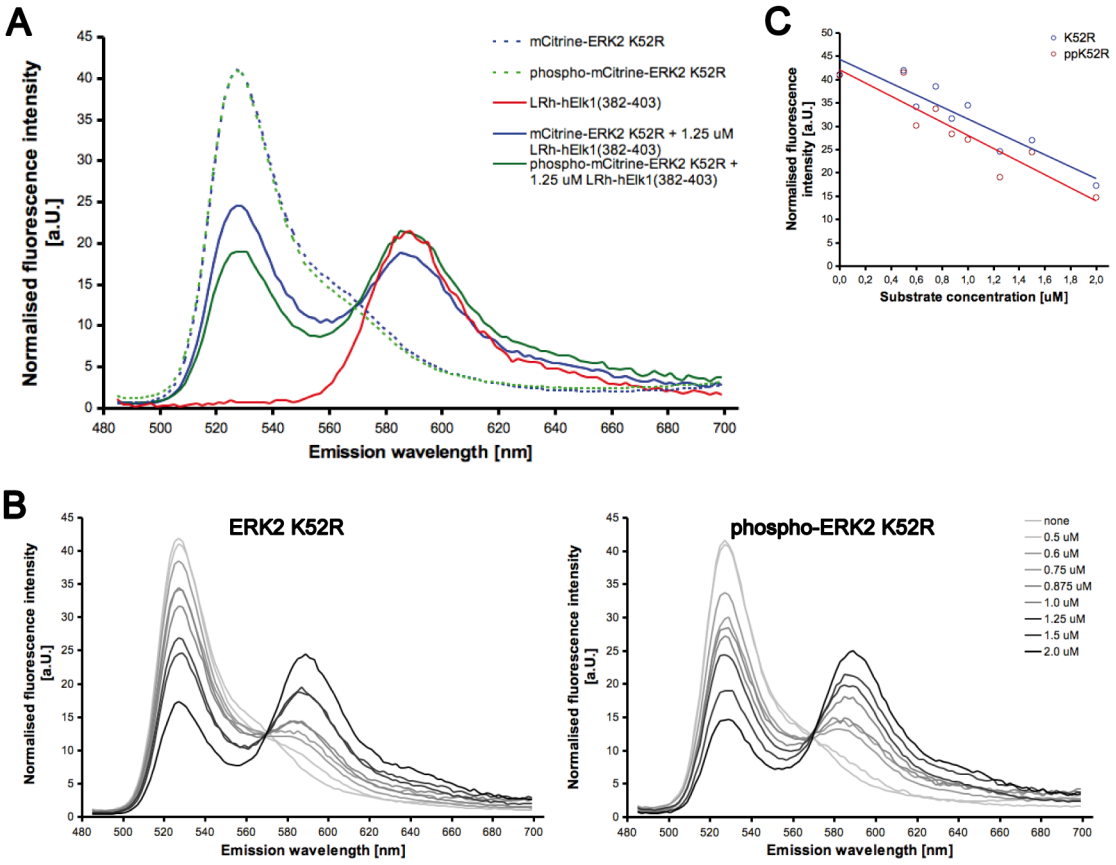

Figure 3.13: FRET can be observed between the reporter substrate peptide and mCitrine-ERK2 K52R independent of its activation state. A) Incubation of purified mCitrine-ERK2 K52R with LRh-hElk1(382-403) in the presence of ATP before and after incubation with active MEK1 resulted in FRET, observed as quenching of mCitrine fluorescence and increased emission of LRh upon excitation at 470 nm. FRET was independent of ERK2's phosphorylation state. B) Dependence of the FRET efficiency on the concentration of substrate peptide for phosphorylated and unphosphorylated mCitrine-ERK2 K52R. C) Correlation of normalised fluorescence intensity values at the donor emission maximum with substrate concentration. Blue circles represent fluorescence peak values of non-phosphorylated ERK2 K52R at increasing substrate concentrations from B); red circles represent fluorescence peak values of phosphorylated ERK2 K52R at increasing substrate concentrations from B). Blue and red lines represent the best linear fit for the respective data set ($R^2_{\mathrm{K52R}} = 0.85$; $R^2_{\mathrm{ppK52R}} = 0.84$).

Emission scan experiments allow simultaneous detection of donor emission decrease and sensitised acceptor emission increase characterising FRET. But the FRET signal

may be missed due to high specific activity of the purified kinase rapidly consuming the substrate. In case of ES-imaging with PTP1B, the problem was circumvented by using a "substrate trapping" mutant of PTP1B (Yudushkin *et al.*, 2007). Unfortunately, at least to current knowledge, there are no such mutants for ERK2 described. However, mutation of lysine 52 to arginine (ERK2 K52R) renders the kinase catalytically inactive (Robbins *et al.*, 1993) while still enabling phosphorylation of the activation loop. Since this mutant could enable substrate binding upon activation without its modification, it was suspected that ERK2 K52R might function as a "substrate trapping" mutant for ERK2. Thus, mCitrine-ERK2 K52R was employed in emission scan experiments in an attempt to stabilise transient ES intermediates and facilitate FRET detection.

Emission scan *in-vitro* ES-interaction spectroscopy was performed as described in 2.2.3.4. Substrate concentrations employed, ranged from 0.5 μM to 2.0 μM. The substrate peptide was serially diluted to allow addition of the same volume to all samples. In negative controls, one volume of substrate dilution buffer was used.

Incubation of purified mCitrine-ERK2 K52R with LRh-hElk1(382-403) resulted in FRET, observed by the approximately linear, concentration-dependent quenching of the donor (mCitrine) emission and the concurrent acceptor (lissamine) intensity increase (Fig. 3.13). However, these apparent FRET signals were largely independent of the phosphorylation state of mCitrine-ERK2 K52R (Fig. 3.13A and B), indicating that observed FRET was mainly due to unspecific interactions of substrate peptide and ERK2. Interestingly, quenching of donor fluorescence as well as acceptor emission increase after LRh-hElk1(382-403) addition were slightly stronger for phospho-mCitrine-ERK2 K52R (Fig. 3.13A and C) while the emission spectra and intensity of phosphorylated and non-phosphorylated mCitrine-ERK2 K52R in the absence of substrate peptide were identical. Although this effect was not very prominent, it was consistent throughout most substrate concentrations (Fig. 3.13C) and might therefore argue for the presence of small amounts of ES-intermediates.

In an attempt to further clarify the result obtained from emission scan experiments, purified mCitrine-ERK2 wt was activated *in-vitro* and subjected to *in-vitro* fluorescent lifetime spectroscopy as described in 2.2.3.5. Lissamine-rhodamine B-labeled hElk1(382-403) was serially diluted to allow addition of the same volume to all samples. As a further negative control, a lissamine-rhodamine B-labeled synthetic substrate peptide with the amino acid sequence DADEYL has been used (Yudushkin *et al.*, 2007). LRh-DADEYL was a kind gift of Dr. Carsten Schultz, Gene Expression Unit, EMBL Heidelberg/Germany and synthesised by Andrea Giordano.

Addition of LRh-labeled hElk1(382-403) to purified mCitrine-ERK2 wt led to an immediate and stable drop in fluorescent donor lifetime irrespective of the phosphorylation state of ERK2 (Fig. 3.14A and C) indicating the occurence of unspecific FRET between labeled substrate peptides and ERK2. This lifetime drop, however, was again more pro-

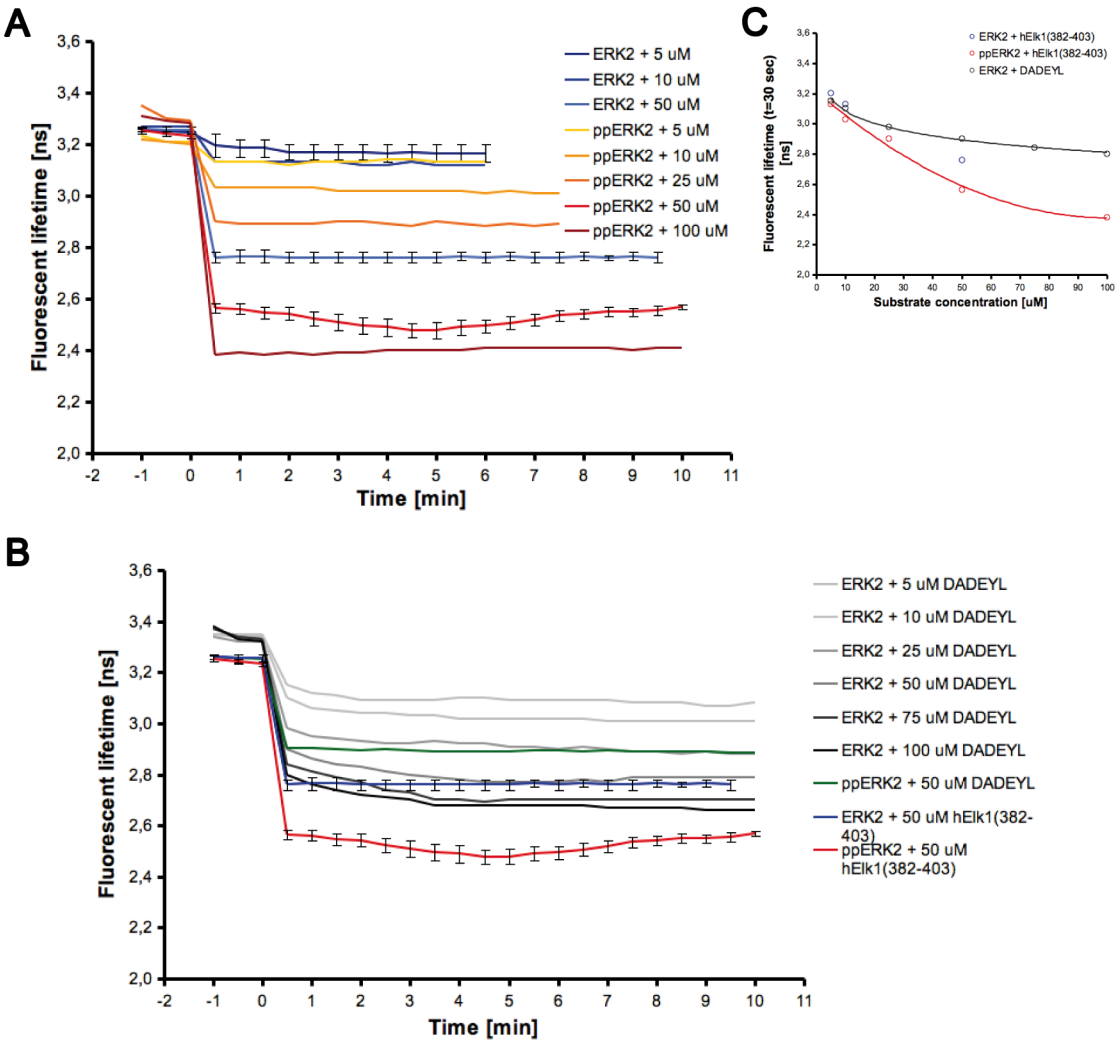

Figure 3.14: FRET occurs between mCitrine-ERK2 wt and LRh-labeled substrate peptides. A) Addition of LRh-hElk1(382-403) to purified mCitrine-ERK2 led to a stable decrease of donor fluorescent lifetime. Graphs (shown with S.E.M.) represent donor fluorescent lifetimes of unphosphorylated mCitrine-ERK2 wt (light to dark blue lines) and phosphorylated mCitrine-ERK2 wt (yellow to dark red lines) before and after the addition of increasing concentrations of ERK2 substrate peptide. Occurence of FRET was independent of ERK2's phosphorylation state but more pronounced for ppERK2. $n_{ERK2\ +\ 5\ \mu M}$=2; $n_{ERK2\ +\ 50\ \mu M}$=2; $n_{ppERK2\ +\ 50\ \mu M}$=8. B) Addition of LRh-DADEYL to purified mCitrine-ERK2 resulted in a stable decrease of donor fluorescent lifetime. Graphs (shown with S.E.M.) represent donor fluorescent lifetimes of unphosphorylated mCitrine-ERK2 wt (light grey to black lines) before and after the addition of increasing concentrations of LRh-DADEYL. Graphs representing mCitrine lifetime for ppERK2 after the addition of LRh-DADEYL (green), and ERK2 (blue, n=2) and ppERK2 (red, n=8) after the additon of LRh-hElk1(382-403) are shown for comparison. C) Correlation of the fluorescent donor lifetime at t = 30 sec with substrate concentration. Grey and red lines represent the best exponentiell fit for the respective data set($R^2_{ERK2\ +\ DADEYL}$ = 0.99; $R^2_{ppERK2\ +\ hElk1(382\text{-}403)}$ = 0.99). There were not enough data points to reliably fit data points for ERK2 + hElk1(382-403).

nounced in samples containing phosphorylated ERK2 (Fig. 3.14A and C). Although this additional drop argues for the formation of small amounts of ES-complexes, no recovery of donor lifetime neither to initial lifetime values nor to lifetime values representing complexes of substrate peptide and inactive ERK2 could be detected (Fig. 3.14A), which would have argued more conclusively for the formation of ES-intermediates.

Interestingly, when the LRh-DADEYL peptide was added to unphoshphorylated ERK2, again a concentration dependent decrease in mCitrine lifetime was observed, pointing to lissamine-rhodamine B as the cause of the unspecific FRET signals (Fig. 3.14B). It should be noted, however, that mCitrine lifetimes for both unphosphorylated and phosphorylated ERK2 were progressively lower after addition of LRh-hElk1(382-403) than after the addition of LRh-DADEYL, with an even stronger lifetime decrease for ppERK2 than for ERK2 (Fig. 3.14B).

In conclusion, the *in-vitro* experiments indicate that it might indeed be possible to detect ES-intermediates of ERK2 and a substrate peptide *in-vitro*, although the occurence of unspecific FRET signals between purified mCitrine-ERK2 and LRh-labeled peptides, probably mediated by the fluorescent dye lissamine-rhodamine B itself, prevents a clear proof.

3.3.2 *In-Vivo* Fluorescence Lifetime Imaging Microscopy of ERK2 ES-Interactions

Since the *in-vitro* experiments pointed to a possible use of the approach to detect ES interactions *in-vitro*, *in-vivo* experiments were carried out to visualise ERK2 activity in living cells.

To avoid highly manipulative techniques to introduce synthetic peptides into living cells, hElk1(379-403) was fused to the C-terminus of mCherry by amplifying the mCherry sequence from mCherry-C1 using ERK2 substrate for and rev (2.2.2.1) and subsequent cloning of the PCR product into *Age*I and *Xho*I restriction sites of mCherry-C1. The genetically encoded, fluorescently labeled substrate peptide could thus be easily transfected into cells and expressed together with donor-labeled ERK2. The short substrate peptide would be protected from degradation by the attached FP.

mCherry-hElk1(379-403) was co-transfected with MEK1/pcDNA3.1(+) and mCitrine-ERK2 wt into MDA cells. For negative controls, MDA cells were co-transfected with mCherry-C1, MEK1/pcDNA3.1(+) and mCitrine-ERK2 wt. Cells were starved overnight, stimulated with 100 ng/ml EGF and the fluorescent lifetime of donor molecules determined by FLIM before and at various time points after stimulation as described in 2.2.5.3 and 2.2.5.4.

Pseudocolour lifetime maps of donor lifetimes did not display any colour change upon EGF stimulation in MDA cells expressing MEK1, mCitrine-ERK2 wt and either

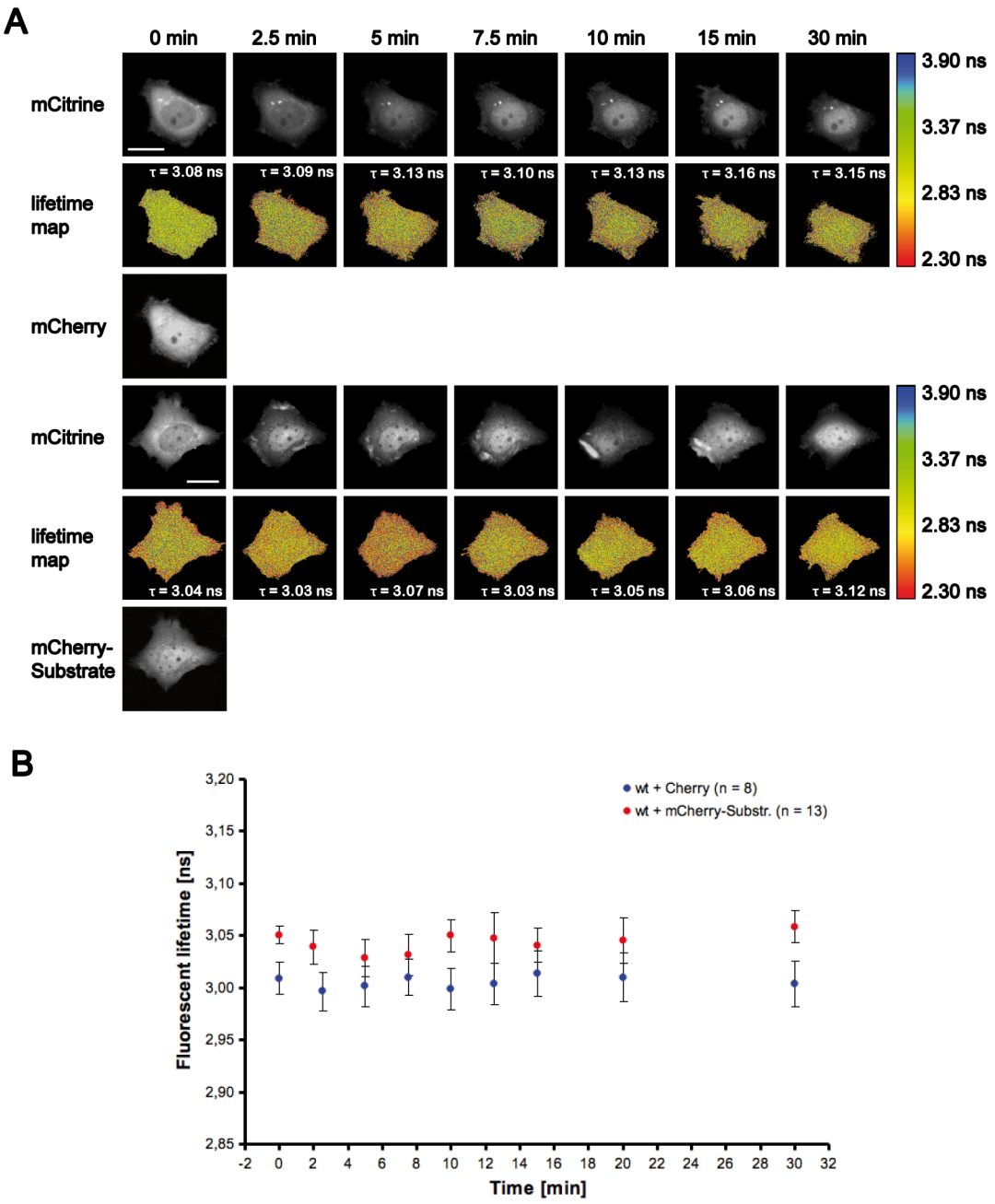

Figure 3.15: No significant formation of ES-complexes between ERK2 and hElk1(379-403) could be detected by FLIM. A) FLIM of live cells showing no visible donor fluorescent lifetime change after EGF stimulation. Representative image sequences of MDA cells co-expressing MEK1, mCitrine-ERK2 wt and either mCherry-C1 (upper panel) or mCherry-hElk1(379-403) (lower panel). Donor intensity images and pseudocolour lifetime maps with average lifetime of the whole cell are shown as indicated. Scale bar = 20 μm; τ = fluorescent lifetime. B) Graphs showing the average donor fluorescent lifetime of cells expressing mCherry-C1 (blue) or mCherry-hElk1(379-403) (red) with S.E.M.

mCherry-C1 or mCherry-hElk1(379-403) that would represent a change in fluorescent lifetime of mCitrine (Fig. 3.15A). Similarly, no significant donor lifetime change could be detected after averaging several measured cells (Fig. 3.15B). Specifically, the lifetime change observed was 20 ± 20 ps on average at 5 min EGF stimulation with a maximal change of 100 ps, 5 min after stimulation, in an individual cell (see Table S.2.1 and Table S.2.2). The shape of the curves for cells expressing mCherry or mCherry-hElk1(379-403) was nearly indistinguishable (Fig. 3.15B).

In conclusion, it has not been possible to visualise transient ES complexes of ERK2 and a genetically encoded, fluorescently tagged substrate peptide.

3.4 Development of an Intramolecular FRET-Based Biosensor for ERK2 Activity Employing Transient Enzyme-Substrate Interactions

An alternative approach to increase substrate concentrations in the immediate environment of ERK2 is to directly link the kinase to its substrate peptide. A flexible peptide linker would allow reversible formation of transient ES complexes. The approach requires a recombinant protein consisting of ERK2, the peptide linker and an ERK2 substrate peptide sequence sandwiched by a FRET pair of FPs, producing a genetically encoded, intramolecular FRET sensor. Similar to intermolecular ES-imaging, upon activation of ERK2, kinase and substrate peptide form a transient ES-complex before the phosphorylated substrate peptide dissociates from the active site (Fig. 3.16A). Since the sensor is specifically designed as an intramolecular FRET sensor, FRET between donor and acceptor fluorophores could be detected by FLIM and ratiometric FRET imaging.

3.4.1 Cloning of Intramolecular FRET-based Fluorescent Biosensor Constructs for Detection of ERK2 Activity

Four different sensor constructs were designed, named *E*RK *A*ctivity *S*ensor 1 to 4 (EAS1-4), each containing ERK2, a flexible peptide linker based on the amino acid sequence $L(GGGGS)_xAAA$ and amino acids 375-404 from human Elk1, flanked by mCitrine as donor on the N-terminus and mCherry as acceptor on the C-terminus. Constructs differed in the position of the substrate peptide in respect to the enzyme and the length of the peptide linker as shown in Fig. 3.16B.

The main parts of the ERK2 Activity Sensor constructs were cloned by a two-step fusion PCR as described in 2.2.2.4. Briefly, in a first PCR step N- and C-terminal parts of the sensor constructs (hElk1(375-404) and ERK2 for EAS1 and EAS2 or ERK2 and hElk1(375-404) for EAS3 and EAS4, respectively) were created separately with a *BspE*I site at the 5'- and the linker sequence at the 3'-end of the N-terminal part and the same linker sequence at the 5'- and a *Hind*III site at the 3'-end of the C-terminal

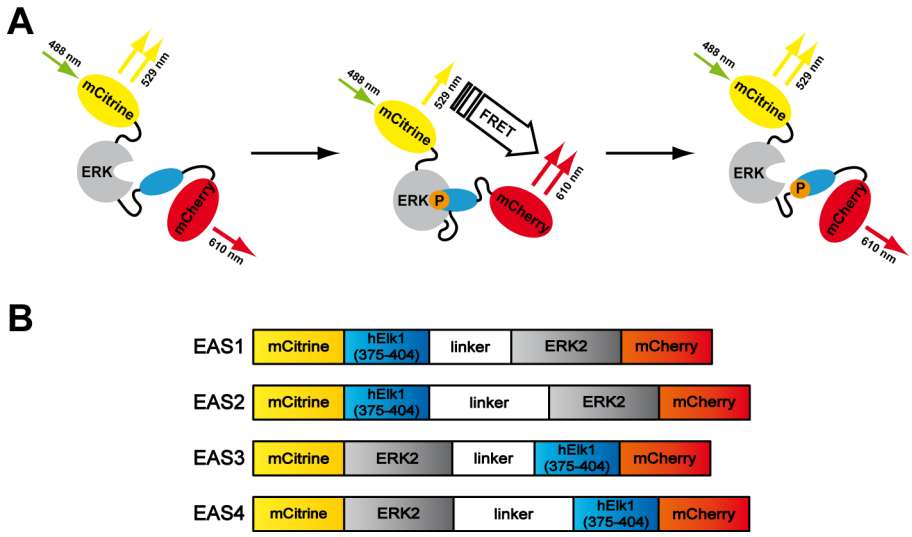

Figure 3.16: Principle and design of the intramolecular ERK2 Activity Sensor Constructs. A) Principle of the intramolecular FRET sensor. Formation of an enzyme-substrate intermediate to phosphorylate the substrate peptide (blue, phosphorylation is indicated by the orange dot) after activation of ERK2 (grey) changes the FRET signal obtained from two fluorescent proteins on the N- and C-terminus of the sensor molecule. FRET can be measured ratiometric or by FLIM (modified from Yudushkin *et al.*, 2007). B) Design of the intramolecular FRET sensor. Schematic representation of the four different constructs. Each construct consisted of mCitrine on the N- and mCherry on the C-terminus as donor and acceptor fluorophore, rat ERK2 CDS, a flexible peptide linker and amino acids 375-404 of hElk1. The constructs differed in the substrate peptide position in respect to ERK2 and peptide linker length. Short peptide linker sequence was $L(GGGGS)_2AAA$, long peptide linker sequence $L(GGGGS)_3AAA$.

part. In a second PCR step both PCR products were fused using 5'- and 3'- forward and reverse primers from the first step. mCherry CDS was amplified from mCherry-C1 by PCR as described in 2.2.2.1 using mCherry (*Hind*III) for and mCherry (*BamH*I) rev to introduce the respective restriction sites. Final sensor constructs were cloned by insertion of the main parts of each sensor construct and mCherry between the *BspE*I and *BamH*I sites of mCitrine-C1. The identity of all constructs was confirmed by sequencing (data not shown).

3.4.2 FLIM Screening of ERK2 Activity Sensor Constructs

To identify a functional sensor construct, displaying the highest dynamic range, the sensor constructs were screened using FLIM. MEK1 and one of the four sensor constructs were co-expressed in HeLa cells. Cells were starved overnight, stimulated with 100 ng/ml EGF and the fluorescent donor lifetime was determined by FLIM before and 5, 10 and 20 min after stimulation as described in 2.2.5.3 and 2.2.5.4.

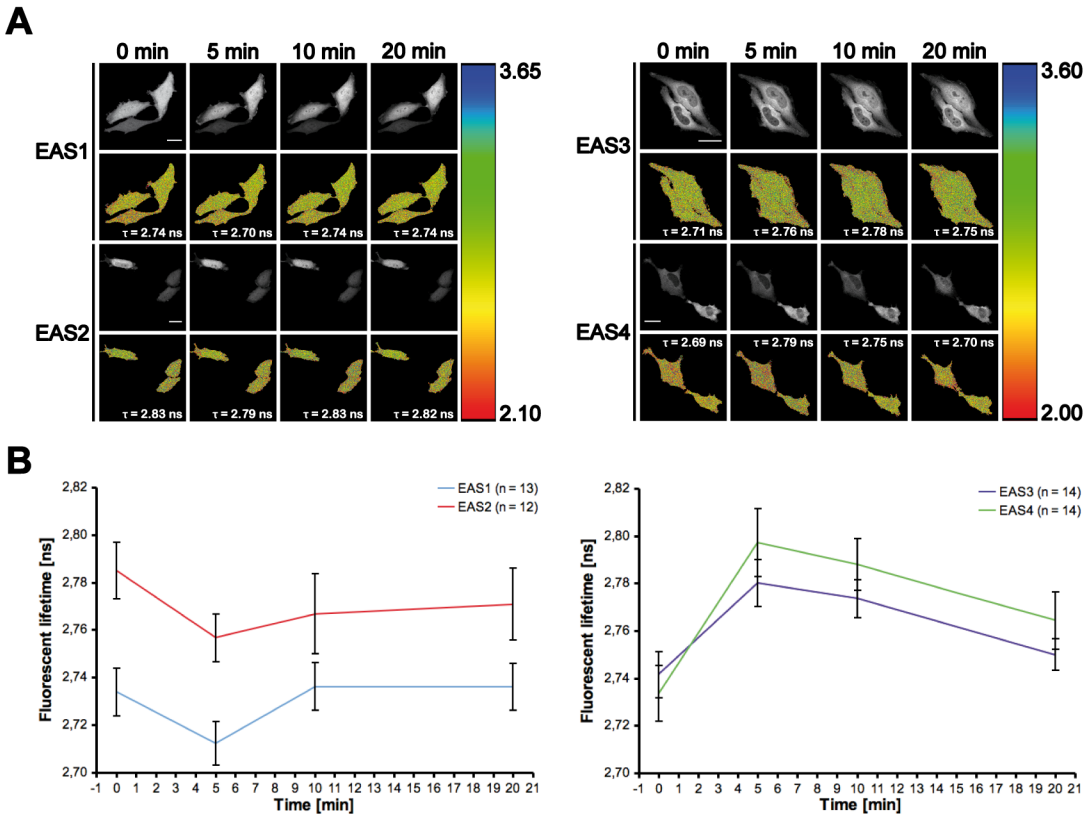

Figure 3.17: ERK Activity Sensor 4 (EAS4) exhibits the highest dynamic range of all four sensor constructs. A) FLIM of live cells expressing one of four different ERK2 activity sensor constructs showing a visible donor fluorescent lifetime change after stimulation with 100 ng/ml EGF only for EAS4. Donor intensity images (top) and pseudocolour lifetime maps (bottom) with average lifetime of the whole image for each sensor construct are shown as indicated. Scale bar = 20 μm; τ = fluorescent lifetime. B) Graphs showing the average donor fluorescent lifetime change after EGF stimulation for each sensor construct with S.E.M. as indicated. Only lifetime changes for EAS3 and EAS4 were significant ($\alpha = 0.01$)

All four sensor constructs displayed a change in fluorescent donor lifetime 5 - 10 min after stimulation with EGF returning more or less to the pre-stimulation value after 20 min (Fig. 3.17). However, this change was statistically significant only for EAS3 and EAS4 ($p_{EAS1} = 0.50$, $p_{EAS2} = 0.50$, $p_{EAS3} = 0.38 \times 10^{-8}$, $p_{EAS4} = 0.12 \times 10^{-9}$; $\alpha = 0.01$, one-tailed t-test). EAS4 was the sensor construct with the highest dynamic range of 70 $\pm$ 10 ps on average and 140 ps observed in individual cells (Fig. 3.17 and Table S.3.4). Surprisingly, the direction of observed lifetime change was not consistent among the four different constructs as expected from their design principle. In agreement with the principle of ES-imaging, EAS1 and EAS2 exhibited a decrease in lifetime after stimulation of cells with EGF, indicating an increase in FRET upon binding of the

substrate peptide to activated ERK2 (Fig. 3.16B and Fig. 3.17). In contrast, EAS3 and EAS4 displayed an increase in donor lifetime after EGF stimulation rather than the expected decrease, indicating for a loss of FRET upon sensor activation and substrate peptide binding to ERK2's active site (Fig. 3.17). The fact that the observed lifetime change was more or less reversible in all constructs indicates that the underlying ES-interactions mediating the change in FRET efficiency indeed reflect the activation state of ERK2.

3.4.3 Specificity of the ERK2 "ES-Imaging" Intramolecular FRET Sensor Construct 4

Two investigate the specificity of the observed lifetime change of the EAS4 construct to EGF stimulation three different control constructs were cloned (Fig. 3.18A). EAS4 K52R harbours the lysine 52 to arginine mutation of ERK2 rendering the kinase catalytically inactive. In EAS4 TAYA amino acids Thr183 and Tyr185 of the ERK2 sequence were mutated to alanine to prevent phosphorylation and thus activation of ERK2. In EAS4 ElkMut, amino acids corresponding to positions 383-404 of hElk1 were scrambled and reconstructed into a peptide sequence that was build from the same amino acids but lacking any structural similarity to the original hElk1 peptide sequence including the consensus phosphorylation sites and the DEF domain (Fig. 3.18A).

EAS4 K52R, EAS4 TAYA and EAS4 ElkMut were generated by *in-vitro* site-directed mutagenesis using MAPK1 K52R for and rev, MAPK1 TAYA for and rev, or MutElk1 for and rev, respectively. The identity of all constructs was confirmed by sequencing (data not shown).

Phosphorylation of EAS4 mutants in their cellular environment upon EGF stimulation was analysed by co-expressing each mutant with MEK1 in HeLa cells and comparing phosphorylation of ERK2 and hElk1(375-404) in the mutant chimeric proteins to the wt construct after EGF stimulation in western blots.

Endogenous ERK2 phosphorylation increased substantially upon stimulation with 100 ng/ml EGF in all samples. Accordingly, phosphorylation of ERK2 in EAS4 wt, EAS4 K52R and EAS4 ElkMut was also substantially elevated after EGF treatment (Fig. 3.18B). However, no phosphorylation of EAS4 TAYA, lacking the amino acid residues important for ERK2 activation, could be detected (Fig. 3.18B).

In addition, substantially more phospho-Elk1, indicating phosphorylation of the substrate peptide, could be detected after EGF stimulation in EAS4 wt, while the phospho-Elk1 antibody did not recognise the scrambled substrate peptide in EAS4 ElkMut. Unexpectedly, a minor increase in substrate peptide phosphorylation was observed for EAS4 K52R and EAS4 TAYA(Fig. 3.18B).

Next, specificity of the lifetime change of EAS4 wt to ERK2 activation was analysed by measuring donor fluorescent lifetimes of each EAS4 mutant before and 5, 10 and 20

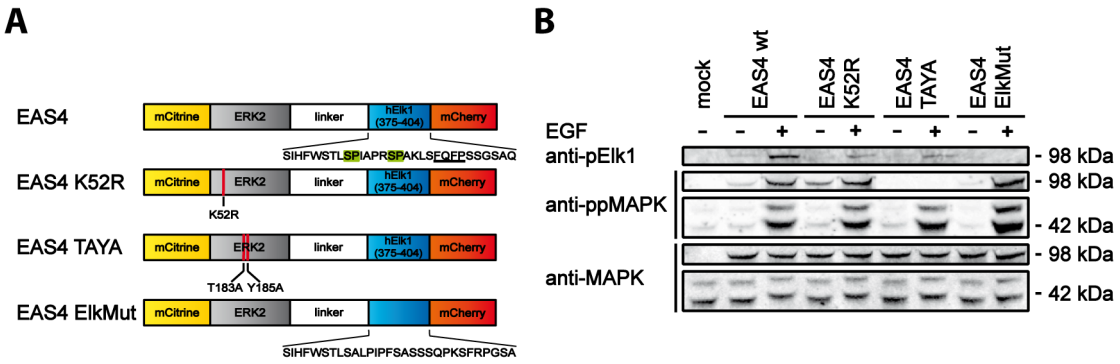

Figure 3.18: Wild-type ERK2 Activity Sensor 4 and its mutants. A) Schematic representation of wild-type EAS4 and its mutants. Primary sequence of the substrate peptide of EAS4 wt is shown with the minimal consensus phosphorylation sites (highlighted in green) and the DEF-domain (underlined). Mutated amino acid residues in EAS4 K52R and EAS4 TAYA are indicated by red lines. Primary sequence of the substrate peptide in EAS4 ElkMut (indicated in blue) is made from the same amino acids found in hElk1(375-404) but scrambled and reconstructed into a new sequence lacking any structure that can be recognised by ERK2. B) EAS4 mutants are being phosphorylated according to their mutation. Western blot analysis of whole cell lysates from cells expressing one of four EAS4 mutants in either starved or stimulated (7 min, 100 ng/ml EGF) conditions. 50 μg of protein were loaded on a 10 % polyacrylamide gel. Endogenous MAPK expression and phosphorylation was used as an internal control.

min after stimulation with 100 ng/ml EGF using FLIM.

EAS4 wt displayed a significant change in average donor lifetime of 60 $\pm$ 10 ps or 140 ps in indivual cells as described above ($p_{wt} = 0.36 \times 10^{-10}$, $\alpha = 0.01$, one-tailed t-test) as well as translocation of the sensor protein to the nucleus shortly after stimulation (Fig. 3.19 and Table S.4.1). Similarly, EAS4 K52R also showed translocation of the sensor construct to the nucleus. The observed average lifetime change 5 - 10 min after EGF stimulation was statistically significant ($p_{K52R} = 0.18 \times 10^{-8}$, $\alpha = 0.01$, one-tailed t-test) but with only 30 $\pm$ 10 ps on average smaller than for the wt construct (Fig. 3.19 and Table S.4.2). In sharp contrast to the wildtype construct, the lifetime change observed with EAS4 K52R was more or less stable for times longer than 20 min after EGF stimulation.

As expected, the non-phosphorylatable mutant of EAS4, EAS4 TAYA, did not translocate to the nucleus at any time point after EGF stimulation as ERK2 requires phosphorylation of Thr183 and Tyr185 in the activation loop for translocation. Accordingly, EAS4 TAYA did not show any change in lifetime after EGF stimulation as binding of the substrate peptide to the active site of ERK2 requires phosphorylation (Fig. 3.19 and Table S.4.3).

Since the ERK2 sequence in EAS4 ElkMut was not affected, the construct translocated to the nucleus in a fashion similar to the wt construct. But due to the inability of ERK2 to recognise the mutated substrate peptide, no lifetime change was detected

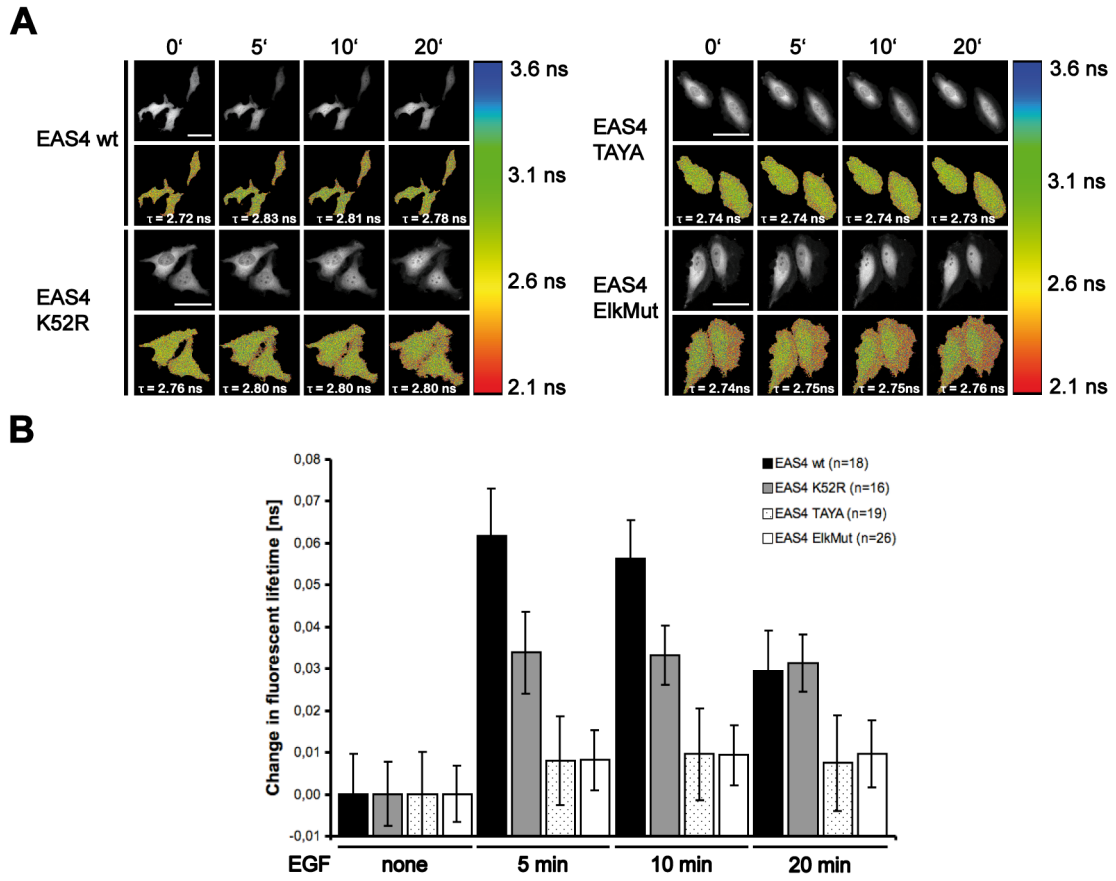

Figure 3.19: ERK Activity Sensor 4 specifically reports ERK2 activity. A)FLIM of live cells expressing one of four different EAS4 mutants showing a visible donor fluorescent lifetime change after stimulation with 100 ng/ml EGF only for EAS4 wt. Representative image sequences of cells co-expressing MEK1 and one EAS4 mutant. Fluorescent intensity images (top) and pseudocolour lifetime maps (bottom) for each EAS4 mutant are shown as indicated. Scale bar = 20 μm; τ = fluorescent lifetime. B) Graphs showing the average donor fluorescent lifetime change after EGF stimulation for each sensor construct with S.E.M. as indicated. Only lifetime changes for EAS4 wt and EAS4 K52R were significant ($\alpha = 0.05$).

after EGF stimulation (Fig. 3.19 and Table S.4.4).

These results show, that EAS4 wt specifically reports ERK2 activity in a time-dependent manner.

3.4.4 Ratiometric FRET Imaging of ERK2 Activity Sensor 4

EAS4 was designed as an intramolecular FRET sensor. Thus, FRET between donor and acceptor fluorophore could be detected by ratiometric FRET imaging, offering sig-

nificantly improved spatial and temporal resolution, greatly simplifying data acquisition and analysis and increasing the signal-to-noise ratio (Yasuda, 2006). Ratiometric FRET imaging was implemented on a confocal microscope, because the low light sensitivity of cameras installed on accessible widefield fluorescent microscopes required long exposure times, thereby compromising the photostability of the fluorophores (data not shown) To allow the maximally possible number of photons to be collected from the sample, the pinhole was opened completely, virtually transforming the confocal into a widefield microscope.

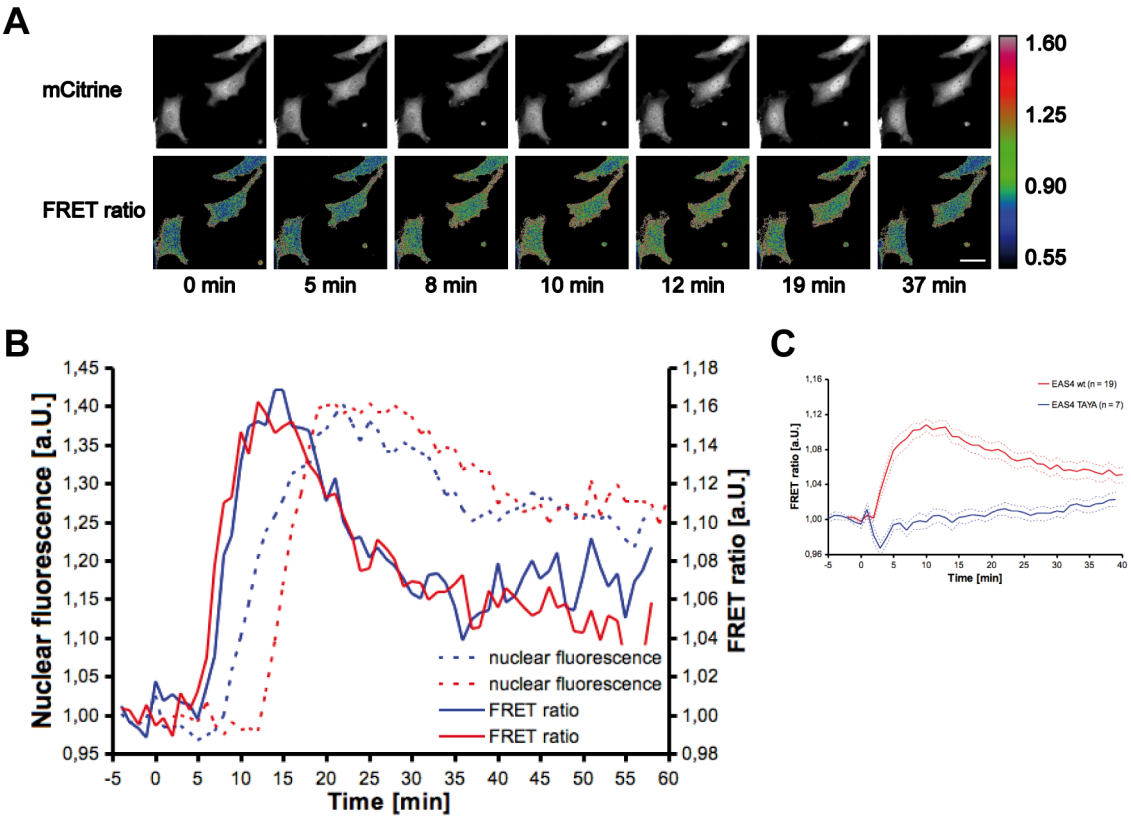

Figure 3.20: ERK2 activation precedes ERK2 translocation. Ratiometric FRET imaging can be used to analyse ERK2 activity in living cells with high spatio-temporal resolution. A) Representative image sequence of HeLa cells co-expressing MEK1 and EAS4 wt and stimulated with 100 ng/ml EGF. Fluorescent intensity (top) and pseudocolour FRET ratio images (bottom) are shown. Scale bar = 20 μm. B) Representative graphs of two cells (blue and red) depicting nuclear fluorescence (dashed lines) as a measure of ERK2 translocation and average FRET ratio per cell (continuous lines). C) Graphs depicting average whole cell FRET ratio of HeLa cells expressing EAS4 wt (red) or EAS4 TAYA (blue) after stimulation with 100 ng/ml EGF at t = 0 min. Graphs are shown with S.E.M.

To test EAS4 in ratiometric FRET imaging, EAS4 wt was co-expressed with MEK1

in HeLa cells. Cells were starved overnight and nuclei stained with Hoechst 33342 to simplify quantification. Ratiometric FRET imaging was performed as described in 2.2.5.2. Images were taken every 60 sec and cells stimulated with 100 ng/ml EGF after 3-5 min. Data were analysed as described in 2.2.5.4. FRET ratios were quantified as FRET ratios per whole individual cell.

Improved temporal resolution is demonstrated by the ability to follow translocation of EAS4 wt to the nucleus of HeLa cells after EGF stimulation (Fig. 3.20A) in a fashion similar to fluorescently labeled ERK2 (see Section 3.1.2). Whole cell FRET ratios of individual cells displayed a sudden rise 1 - 5 min after EGF addition reflecting a rapid and strong activation of the sensor construct. FRET ratios peaked between 5 - 15 min after EGF addition before slowly decreasing to approximately one third of the peak value (Fig. 3.20B). Maximal FRET ratio change observed in individual cells was 18 %. This change in FRET ratio could also be observed in pseudocolour FRET ratio images by a shift of blue to green colours at corresponding time points (Fig. 3.20A). The change in FRET ratio of the sensor generally resembles the characteristic translocation of phosphorylated ERK2 to the nucleus (see Fig. 3.2). The observed time profile for FRET ratios of EAS4 also demonstrates the reversibility of the underlying ES-interactions. More importantly, improved temporal resolution revealed that activation of EAS4 wt actually precedes ERK2 translocation (Fig. 3.20B).

In addition, FRET ratios of EAS4 TAYA did not rise significantly above pre-stimulation values for more than 40 min after EGF treatment (Fig. 3.20C).

Ratiometric FRET imaging was used for further analysis of ERK2 activation due to its superior temporal resolution and simplicity.

3.5 Resolving Spatio-Temporal Regulation of the MAPK-Module in MCF-7 (Epithelial Breast Cancer Derived) Cells

MCF-7 is a transformed mammary epithelial cell line derived from human breast epithelial adenocarcinoma (Brooks *et al.*, 1973; Soule *et al.*, 1973). In MCF-7 cells, EGF induces transient ERK1/2 activation encoding a proliferative signal, while heregulin (HRG) generates sustained ERK1/2 activation resulting in cell differentiation (Thottassery *et al.*, 2004; Nagashima *et al.*, 2007). To test the potential of EAS4 in resolving spatio-temporal ERK2 activity in breast cancer cells, EAS4 was used to analyse MAPK activation in response to EGF and HRG in MCF-7 cells.

EAS4 was co-expressed with MEK1 in MCF-7 cells. Cells were starved overnight and stimulated with 100 ng/ml EGF or 100 ng/ml HRG. Whole cell lysates were prepared, and phosphorylation of endogenous ERK1/2 and ectopically expressed EAS4 was analysed by quantitative western blotting.

Previously described transient and sustained activation (i.e. phosphorylation) in response to treatment with 100 ng/ml EGF or HRG (Fig. 3.21) was observed for endogenous ERK1/2. Overexpressed EAS4 wt showed similar phosphorylation patterns after stimulation with EGF or HRG (Fig. 3.21).

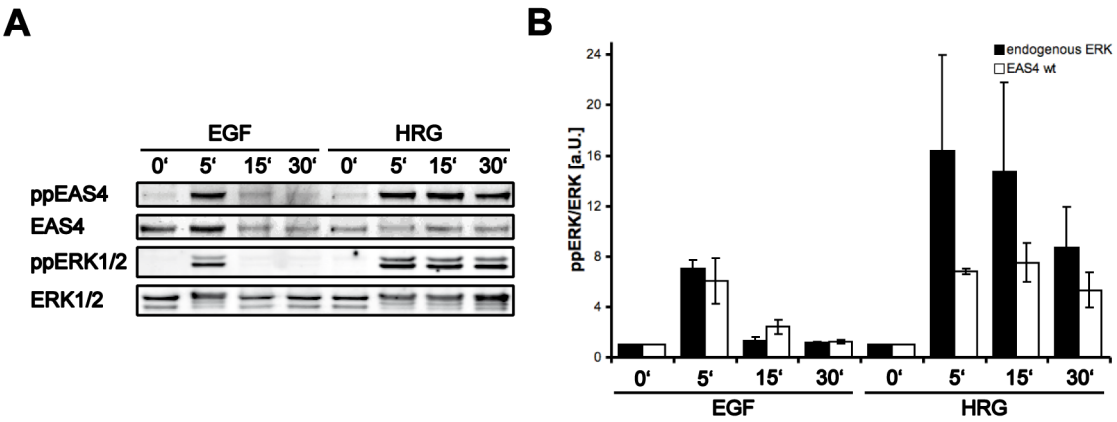

Figure 3.21: Transient vs. sustained ERK2 activity in MCF-7 cells upon stimulation with EGF vs. HRG. A) Western blot of ERK1/2 and EAS4 phosphorylation in response to EGF and HRG treatment in MCF-7 cells. Cells co-transfected with MEK1 and EAS4 wt were starved overnight and stimulated with either 100 ng/ml EGF or HRG. Whole cell lysates were prepared and subjected to SDS-PAGE and western blotting. B) Quantitative western blot data showing activity, i.e. phosphorylation state, of ERK1/2 (ppERK1/2) and EAS4 (ppEAS4) in response to EGF and HRG stimulation of MCF-7 cells as shown in A). Phospho-protein (ppERK1/2 and ppEAS4) was normalised to total protein (ERK1/2 or EAS4, respectively). For direct comparison, pre-stimulation values of EGF and HRG stimulation were normalised to 1. Data are averages from two independent experiments and shown with S.E.M.

Ratiometric FRET imaging was performed on MCF-7 cells co-expressing EAS4 and MEK1 as described in 2.2.5.2. Cells were starved overnight and stimulated with 100 ng/ml EGF or 100 ng/ml HRG. Nuclei were stained with Hoechst 33342 to simplify quantification. Images were taken every 60 sec and cells stimulated after an initial baseline recording of 3-5 min. Data were analysed as described in 2.2.5.4.

FRET ratios of EAS4 revealed the transient ERK2 response after EGF treatment, known from the literature, in both the cytosol and nucleus (Fig. 3.22B and C). Surprisingly, however, HRG-induced sustained ERK2 activity was predominantly cytosolic (Fig. 3.22C), while HRG-induced nuclear ERK2 activity was found to be transient (Fig. 3.22B).

These results show that EAS4 can indeed be used to resolve biologically meaningful characteristics of ERK2 activation that were previously unknown.

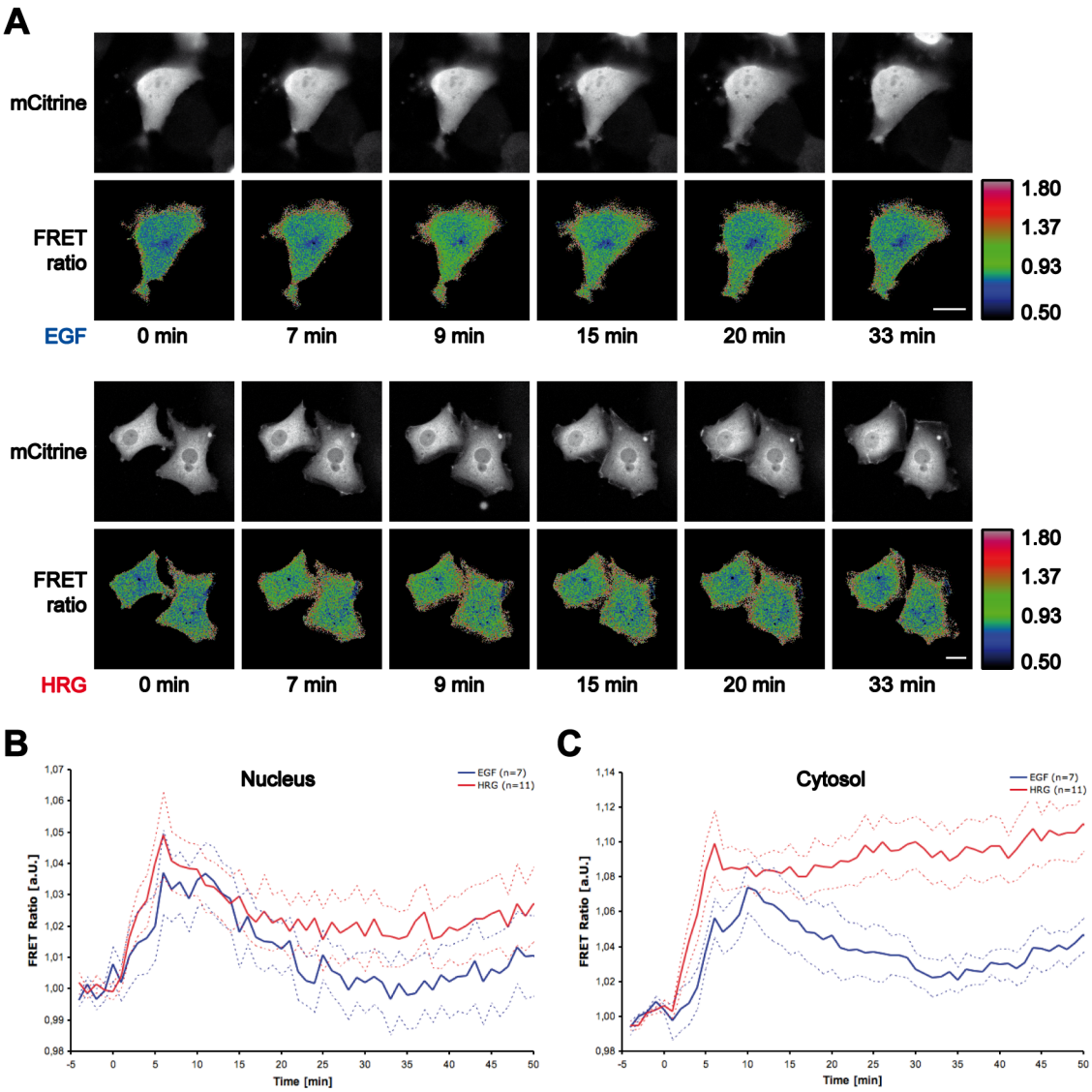

Figure 3.22: HRG-induced sustained ERK2 activity in MCF-7 cells is predominantly cytosolic. A) Ratiometric FRET imaging showing transient vs. sustained ERK2 activation upon stimulation with EGF or HRG. Representative image sequences of MCF-7 cells co-expressing MEK1 and EAS4 wt. Cells were starved overnight and stimulated with 100 ng/ml EGF or HRG. Fluorescent intensity (top) and pseudocolour FRET ratio images (bottom) for each growth factor are shown as indicated. Scale bar = 20 μm. B) and C) Average FRET ratio data showing that sustained ERK2 activity upon HRG stimulation is cytosolic. Graphs representing average normalised FRET ratios in the nucleus (B) or cytosol (C) of MCF-7 cells stimulated with EGF (blue) or HRG (red) are shown with S.E.M.

If sustained ERK2 signalling in response to HRG in MCF-7 cells is dependent on

continuous activation of ERK2, inhibition of upstream activators of ERK1/2 should abrogate the ERK signalling as well as the FRET signal obtained by EAS4. To test this hypothesis, MEK inhibitor U0126 was added to HRG-stimulated cells.

MCF-7 cells were co-transfected with EAS4 wt and MEK1, starved overnight and stimulated with 100 ng/ml HRG. 20 min after growth factor stimulation 100 μM U0126 were added. Cells were then subjected to ratiometric FRET imaging or whole cell lysates were prepared for western blotting.

Addition of U0126 to HRG-stimulated cells led to a reduction of the endogenuos ppERK1/2 below detection limits (Fig. 3.23A) in western blots. Also phosphorylation of EAS4 was markedly decreased after U0126 addition, although not as completely (Fig. 3.23A).

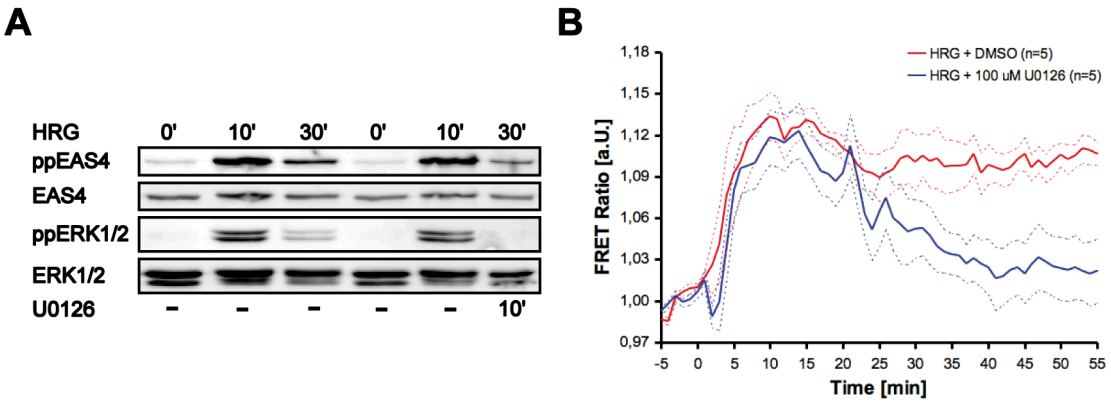

Figure 3.23: HRG-induced sustained ERK2 activation is dependent on continuous MEK1 signalling. A) Western blot of ESA4 and endogenuos ERK1/2 phosphorylation showing that addition of U0126 20 min after HRG stimulation leads to a loss of ERK activity. MCF-7 cells co-expressing MEK1 and EAS4 were starved overnight and stimulated with 100 ng/ml HRG. 100 μM U0126 were added 20 min after HRG stimulation. B) FRET ratios of MCF-7 cells expressing MEK1 and EAS4 showing decreasing ERK2 activity after U0126 treatment of HRG-stimulated cells. Graphs show average whole cell FRET ratio in cells stimulated with HRG (red) and cells where U0126 was added 20 min after stimulation (blue) with S.E.M.

In agreement with this, FRET ratios of EAS4 slowly decreased after U0126 addition over a time course of 20 min to approximately 25 % of the pre-stimulation value (Fig. 3.23B). These results indicate that continuous signalling via MEK1 is required for the HRG-induced sustained ERK2 reponse.

In PC12 cells, EGF-induced transient ERK1/2 activity can be converted into a sustained ERK1/2 response by introducing a PKC-mediated feedback loop in the MAPK module via PMA stimulation (Santos *et al.*, 2007). To test whether it might be possible to induce a similar feedback loop in MCF-7 cells and to investigate its effect

on spatio-temporal ERK signalling, MCF-7 cells were stimulated with EGF, EGF and PMA, or PMA alone. ERK2 activation was analysed by quantitative western blotting and ratiometric FRET imaging.

MCF-7 cells were starved overnight and stimulated with 100 ng/ml EGF, 100 ng/ml EGF and 100 nM PMA, or 100 nM PMA alone. Whole cell lysates were prepared for quantitative western blotting. Because they were derived from the same extract of untreated cells, pre-stimulation values of cells treated with EGF, EGF + PMA, or PMA alone were normalised to 1. In accordance with that, values for EGF treated cells from different gels were averaged as they have also been derived from the same cell extracts. Alternatively, cells co-expressing EAS4 wt and MEK1 were subjected to ratiometric FRET imaging.

Stimulation of MCF-7 cells with EGF and PMA resulted in sustained ERK1/2 phosphorylation as shown by quantitative western blotting (Fig. 3.24A and B). Stimulation with EGF or PMA alone, led to transient or sustained, but markedly lower ERK1/2 phosphorylation, respectively (Fig. 3.24A and B).

Likewise, using EAS4, sustained cytosolic ERK2 activity was detected in MCF-7 cells stimulated with EGF and PMA (Fig. 3.24D). Stimulation with PMA alone also resulted in sustained cytosolic ERK2 activity, but the amplitude of the signal was lower than in the cytosol of cells stimulated with EGF and PMA. In contrast, cytosolic ERK2 activity in cells stimulated with EGF and nuclear ERK2 activity in all cells was transient (Fig. 3.24C and D). These data hint at the existence of PKC-mediated feedback loops in the MAPK module that may be responsible for sustained ERK activation in MCF-7 cells.

These data do not only show the usefulness of EAS4 for the investigation of ERK signalling in living cells but also demonstrate its potential in uncovering previously inaccessible spatio-temporal signalling caracteristics of ERK.

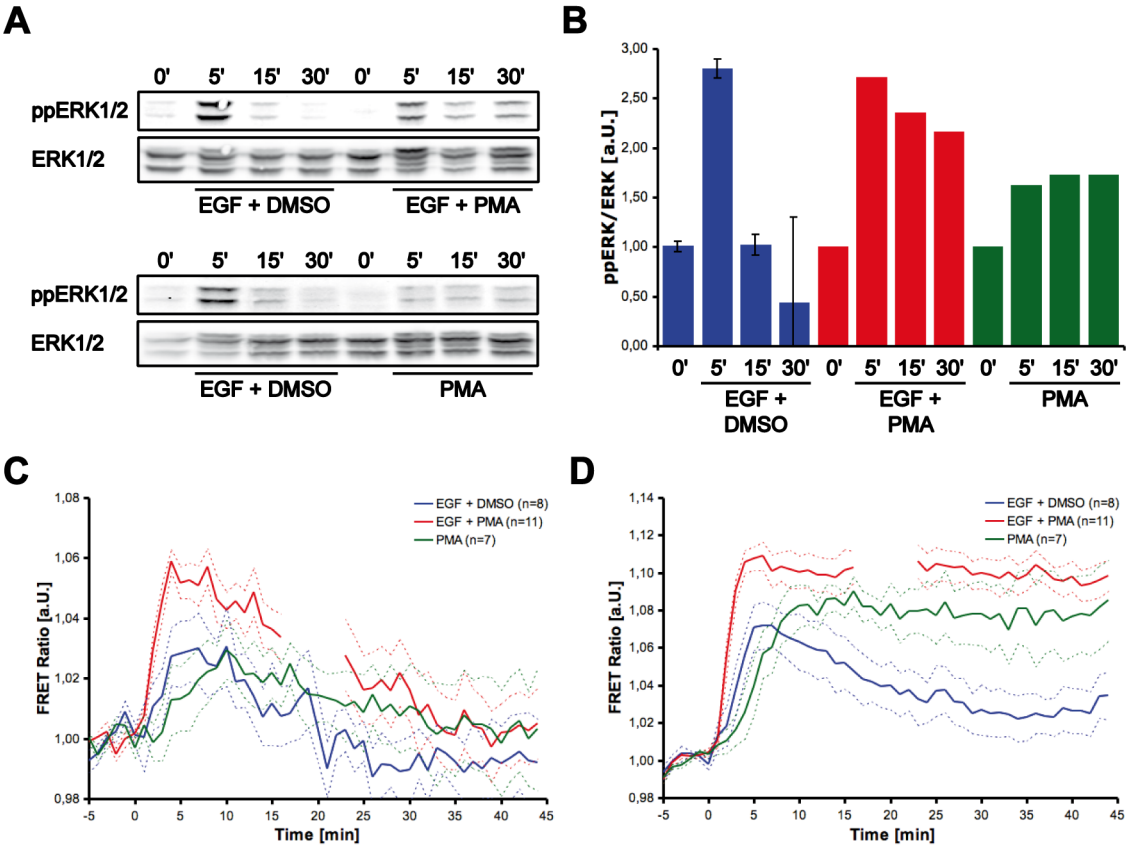

Figure 3.24: Co-activation of PKC can convert EGF-induced transient ERK2 signalling in a sustained ERK2 response in MCF-7 cells. A) Western blot of ERK1/2 in MCF-7 cells in response to treatment with EGF, EGF + PMA, or PMA alone. Cells were starved overnight and stimulated with 100 ng/ml EGF, 100 ng/ml EGF and 100 nM PMA, or 100 nM PMA alone. Whole cell lysates were prepared and subjected to SDS-PAGE and western blotting. B) Quantitative western blot data showing activity, i.e. phosphorylation state, of ERK1/2 (ppERK1/2) as shown in A). Phospho-ERK1/2 was normalised to total ERK1/2. For direct comparison, pre-stimulation values of EGF, EGF + PMA, or PMA stimulation were normalised to 1. Values for EGF treatment are the average of both gels shown in A) as they have been derived from the same cell extracts. C) and D) Average FRET ratio data showing that EGF-induced transient ERK2 activity can be converted into a sustained cytosolic ERK2 response by co-stimulation with PMA. Graphs representing average normalised FRET ratios in the nucleus (C) or cytosol (D) of MCF-7 cells stimulated with EGF (blue), EGF + PMA (red), or PMA alone (green) are shown with S.E.M. A part of the EGF + PMA curve is missing because no reliable signal could be obtained from a few of the measured cells.

4 Discussion

4.1 An Intramolecular ReAsH-Based FRET-Biosensor for ERK2 Activation

Large sized tags like GFP (27 kDa) can disrupt the functionality of fluorescently labeled proteins(McLean *et al.*, 2001; Lisenbee *et al.*, 2003; Vilardaga *et al.*, 2003; Andresen *et al.*, 2004) and can be avoided by labeling with smaller, chemical fluorophores (Andresen *et al.*, 2004; Hoffmann *et al.*, 2005; Nakanishi *et al.*, 2006; Roberti *et al.*, 2007). Usually, this requires in-vitro modification of the purified protein of interest and subsequent re-introduction of the labeled protein into the biological system in question. This process is complicated and time consuming.

By specific, *in-vivo* labeling of recombinant proteins tagged with a short tetracysteine (4C) motif by biarsenical fluorescent dyes, namely fluorescein arsenical hairpin binder (FlAsH) and resofurin arsenical hairpin binder (ReAsH) (Fig. 4.1A), the size addition can be kept to less than 2 kDa (Griffin *et al.*, 1998). FlAsH and ReAsH are able to bind to four cysteine residues in a hairpin structure (Griffin *et al.*, 1998; Martin *et al.*, 2007; Madani *et al.*, 2009). In principle, this 4C motif can be as short as six amino acids (CCPGCC), although an optimised version of the 4C motif contains 12 amino acids (FLNCCPGCCMEP) (Martin *et al.*, 2005). As FlAsH-EDT_2 and ReAsH-EDT_2 are cell-permeable, the dye can simply be added to the medium for intracellular protein labeling and will then diffuse across the cell membrane. Only when bound to the 4C motif, the virtually non-fluorescent dyes become brightly fluorescent (Fig. 4.1B) (Griffin *et al.*, 1998). To allow visualisation of specifically labeled proteins, excess, non-bound dye can be washed out with small dithiols like 2,5-dimercaptopropanol (British anti-Lewisite, BAL) or 1,2-ethandithiol (EDT), which have higher affinities for biarsenical dyes than cellular thiols (Griffin *et al.*, 1998).

FlAsH- and ReAsH-labeling of 4C-tagged proteins has been used in a variety of organisms from bacteria to mammalian cells (Andresen *et al.*, 2004; Hwang *et al.*, 2009; Copeland *et al.*, 2010) and approaches to image - among others - gap junction protein trafficking (Gaietta *et al.*, 2002), yeast microtubule association (Andresen *et al.*, 2004), amyloid formation in neurons (Roberti *et al.*, 2007; Taguchi *et al.*, 2009; Gaspersic *et al.*, 2010), virus production and trafficking (Rudner *et al.*, 2005; Turville *et al.*, 2008) and flagellar dynamics in *E.coli* (Copeland *et al.*, 2010). Additonally, biarsenical dye-based FRET approaches have been extensively used to study G protein-coupled receptor activation in living cells (Hoffmann *et al.*, 2005; Nakanishi *et al.*, 2006; Nikolaev *et al.*, 2006; Maier-Peuschel *et al.*, 2010). However, no FRET-based approach to assess kinase activity using biarsenical fluorophores has been found in the literature until today.

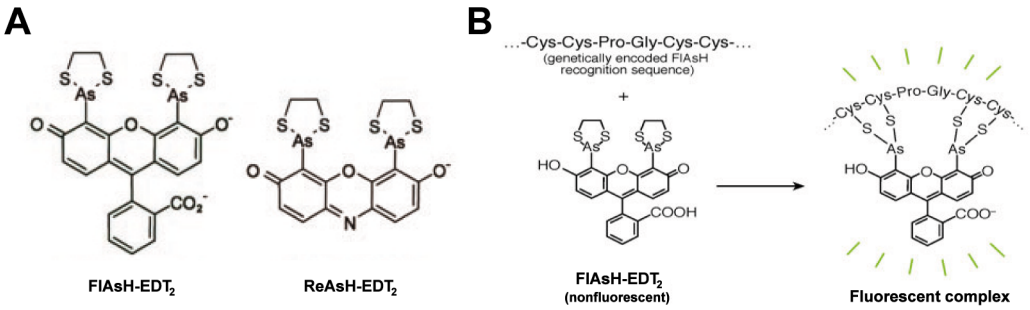

Figure 4.1: Structure and principle of biarsenical fluorophores. A) Chemical structure of FlAsH-EDT$_2$ and ReAsH-EDT$_2$ ligands (adapted from Gaietta *et al.*, 2002). B) Binding of nonfluorescent biarsenical dyes to a recombinantly expressed 4C motif results in a highly fluorescent complex (adapted from www.invitrogen.com/site/us/en/home/Products-and-Services/Applications/Cell-and-Tissue-Analysis/Cellular-Imaging/High-Content-Screening/FlAsH-and-ReAsH.html).

In an attempt to identify regions in ERK2 that change conformation upon activation of the kinase and are accessible for labeling by an external chemical fluorophore, crystal structures of phosphorylated and unphosphorylated ERK2 (Zhang *et al.*, 1994; Canagarajah *et al.*, 1997) were superimposed. Four suitable regions were identified (Fig. 3.3B and Canagarajah *et al.*, 1997). Of those regions, especially the activation loop of ERK2 undergoes a dramatic conformational change upon phosphorylation of the kinase (Canagarajah *et al.*, 1997). The original amino acid sequence of ERK2 in the identified regions were chosen for replacement with either the minimal or optimised 4C motif (Fig. 3.3B and C and Fig. S.1.1) similar to the approach of Nakanishi *et al.*, 2006. In addition, the N- or C-terminus of ERK2 were tagged with the 4C motif in ERK2-mCitrine or mCitrine-ERK2, respectively. A FRET pair of FPs were fused to ERK2 at the N- and C-terminus to form a functional, intramolecular, conformational FRET-sensor for ERK2 (Sato *et al.*, 2007). Therefore, labeling of mCitrine-tagged ERK2 with ReAsH at the N- or C-terminus was supposed to build a functional sensor construct, theoretically offering an increased dynamic range due to a possible smaller distance between the two fluorophores.

The conformational change of ERK2 induced by its phosphorylation would concurrently lead to a change of distance and/or orientation of mCitrine to ReAsH, bound to the 4C motif (Fig. 3.3A and B). Since mCitrine and ReAsH form a good FRET pair, the conformational change could be detected by the resulting change in FRET signal (Fig. 3.3A). FRET could theoretically be measured ratiometrically or by FLIM. It should be kept in mind that although the sensor design and principle is based on intramolecular FRET, labeling efficiency by ReAsH may not reach 100 %. Correct ratiometric FRET analysis, however, relies on equimolar stoichiometries of donor and acceptor fluorophores (Miyawaki, 2003; Yasuda, 2006). Indeed, although the fluorescent lifetime decay of mCitrine is reported to be mono-exponential (Walther *et al.*, 2011)

and fitted well to a single exponential when expressed as an ERK2 fusion protein alone (data not shown), fluorescent lifetime decays in the presence of ReAsH could never be described by a mono-exponential decay model (data not shown), indicating labeling efficiencies of less than 100 %. Therefore, FLIM or other FRET approaches appropriate for intermolecular FRET should be used to determine FRET.

Specific binding of ReAsH to the 4C motif introduced into fluorescently labeled ERK2 could be shown by a marked decrease in fluorescent donor (mCitrine) lifetime (Fig. 3.5B), due to the occurence of FRET between mCitrine and the biarsenical dye. Addition of ReAsH to the medium of cells that did not express 4C motif-tagged proteins led to a markedly smaller decrease in mCitrine lifetime. It is interesting to note that the observed changes in lifetime as a measure of the FRET efficiency were highly dependent on the positions of the donor fluorophore and the 4C motif (Fig. 3.9). For example, positions of the 4C-motif in mCitrine-ERK2-4C(174-179) and ERK2-4C(175-180)-mCitrine differ only in one amino acid, but still they display remarkably different fluorescent donor lifetimes after 60 min of incubation with ReAsH. This exemplifies the importance of the donor fluorophore position for FRET in general.

Kinetics of binding of ReAsH to the 4C motif could be described by a sigmoidal function, in contrast to previous reports (compare Fig. 3.5B and Griffin *et al.*, 1998; Hoffmann *et al.*, 2005). There is no good explanation for that discrepancy as those data were also measured in living mammalian cells. Slow diffusion of the DMSO-dissolved ReAsH cannot be considered as the cause, because ReAsH was pre-diluted in 250 μl medium before being added to cells covered by 250 μl medium. However, the time scale for full labeling until no further decrease in fluorescent lifetime could be observed was similar to previously published results (compare Fig. 3.5B and Griffin *et al.*, 1998; Hoffmann *et al.*, 2005).

Taken together, these data demonstrate that it is possible to specifically label recombinant proteins containing the 4C motif with ReAsH in agreement with previously published data. It may be interesting to note that unspecific background staining by ReAsH was always present, but could be markedly decreased by using the optimised version (Martin *et al.*, 2005) of the tetracysteine motif (Fig. 3.6). Background reduction, however, required washout of ReAsH by BAL. Similarly high background intensity was observed with both versions of the 4C motif 60 min after incubation with ReAsH but before washout with BAL (Fig. 3.6). Since ReAsH (acceptor) background fluorescence may influence results of intensity-based fluorescent imaging techniques, the use of biarsenical dyes for protein labeling can only be recommended for fluorescence lifetime approaches or *in-vitro* studies with purified proteins (researchers should make sure there are no other cysteine residues that could bind to the biarsenical dyes).

Interestingly, the ReAsH-ERK2 biosensor construct used for the labeling experiments accumulated slowly in the nucleus of HeLa cells over the time course of ReAsH incubation (Fig. 3.5A). Two scenarios are conceivable: The conformational state of the activation loop in ERK2 represents a dynamic equilibrium. In phosphorylated ERK2, the activation loop primarily adopts the active, “open” conformation, while in non-phosphorylated

ERK2, the equilibrium is shifted to the "closed", inactive conformation. Biarsenical dyes may preferably label the 4C motif in the activation loop when in the "open" conformation. Binding of ReAsH to the 4C motif in the small fraction of non-phosphorylated ERK2 with the activation loop in the "open" conformation may then "lock" the activation loop in the active conformation, mimicking full activation of ERK2 and subsequent translocation. In addition, basal levels of active ERK2 exists even in resting cells (Ando *et al.*, 2004; Fujioka *et al.*, 2006; Santos *et al.*, 2007 and Fig. 3.24). ReAsH labeling of basally active ERK2 would also add to the pool of ReAsH bound ERK, slowly accumulating in the nucleus. As a consequence, ReAsH labeling kinetics of active 4C-ERK2 (e.g. in the presence of EGF) should be faster than those of inactive ERK2 and could already be used as a sensor of active ERK2 by itself. Alternatively, sensor construct translocation could be an artifact of the imaging process, e.g. ERK2 activation via a light-induced stress response.

However, the first scenario is rather unlikely because of a number of reasons:

First and most importantly, labeling kinetics of the tested ReAsH-ERK2 biosensor construct in the presence or absence of EGF were virtually identical (Fig. 3.5B). Second, slow nuclear accumulation of other chimeric proteins containing ERK2 in starving cells has also been observed after imaging for more than 20-30 min or high laser powers (Fig. S.5.1). Third, ERK2 activity as measured by a newly developed FRET-based biosensor for ERK2 (see Sections 3.4 and 4.3) slowly increases in starving cells when imaged for more than 20-30 min, coinciding with slow nuclear accumulation (Fig. S.5.1). Fourth, membrane translocation of fluorescently labeled RafRBD as a measure of Ras activation (Rocks *et al.*, 2005) can be observed without growth factor stimulation at late time points during imaging (Dr. Ali Kinkhabwala, personal communication). Taken together, these results strongly hint at a light-induced artifact for the cause of the observed slow nuclear accumulation of ReAsH-ERK2 biosensor constructs. Indeed, light-induced ERK1/2 activation as well as both the light-induced production of reactive oxygen species (ROS) and activation of ERK1/2 by ROS are known in the literature (Chen *et al.*, 1995; Obrietan *et al.*, 1998; Rittié and Fisher, 2002).

Cloned ReAsH-ERK2 sensors were screened for a functional sensor construct by FLIM. From the nineteen constructs, only one showed a significant change in lifetime after EGF stimulation (Fig. 3.7). With no construct, lifetime changes resembling known ERK2 activation profiles could be observed. For most constructs, lifetime changes were in a similar range as those observed for donor only samples and/or did not change consistently in only one direction. Three constructs were tested further in an experiment omitting the washing step with BAL. FLIM measures only the donor fluorescent lifetime while acceptor fluorescence is not detected, allowing the presence of saturating amounts of acceptor or acceptor-labeled molecules (Bastiaens and Pepperkok, 2000). Thus, removal of ReAsH from the medium is in principle not required. Omitting the washing step with BAL led to significantly lower fluorescent lifetimes of mCitrine in the ReAsH-ERK2 sensor constructs (Fig. 3.9). On the other hand, unspecific FRET signals as measured by a decrease in fluorescent lifetime also increased due to background labeling in cells without 4C motif-tagged cells (Fig. 3.5). Also, without ReAsH washout

no labeling difference between the minimal and optimised 4C motif could be detected anymore (Fig. 3.6).

As a result, it has not been possible to identify a functional sensor construct. Potentially, the attempted design simply does not yield a functional ERK2 sensor. Conformational changes in the aa 9-14 and aa 30-35 regions have been estimated to be in the range of less than 1 nm and might therefore be too small to result in a significant change in FRET efficiency, as protein conformational changes optimal for FRET are in a range of 4-7 nm (Li *et al.*, 2006). On the other hand, changes in FRET efficiencies are thought to result most often from reorientation of the fluorophore rather than distance changes (Giepmans *et al.*, 2006). Thus, it is possible that a conformational change that could change the FRET efficiency is counteracted by a concurrent opposite change in dipole orientation.

Structural studies of phosphorylated ERK2 show that amino acids between Asp173 and His176 are important for the coordination of the phosphorylated activation loop to the so-called L16 lip essential for ERK2 activation (Canagarajah *et al.*, 1997). In all mutant ERK2 proteins containing the 4C motif in the activation loop, at least one of these amino acids is replaced by amino acids of the 4C motif. It is thus very likely that these mutant ERK2 proteins simply cannot undergo the normal conformational change induced by phosphorylation.

Although, C- or N-terminal fusions of mCitrine-tagged ERK2 with the 4C motif, did not yield a functional ERK2 sensor, ERK2 sandwiched by a FRET-pair of FPs did (Fujioka *et al.*, 2006). This, in contrast, might be an indication that other reasons play a role for the inability to identify at least those ReAsH-ERK2 sensor constructs as a functional sensor.

In summary, it was possible to establish *in-vivo* labeling of tetracysteine-tagged proteins with biarsenical fluorophores. Important points to consider, when planning to use biarsenical fluorophores are: a) use of the optimised 4C motif provides reduced background labeling after the washout of the biarsenical fluorophores. b) ReAsH is known to be less photo-stable than FlAsH, therefore, FlAsH is the biarsenical dye recommended for labeling 4C motifs, if possible, in the given experimental setup (TC-FlAsH^{TM} TC-ReAsH^{TM} II In-Cell Tetracysteine Tag Detection Kit manual, Invitrogen^{TM}). c) ReAsH can induce transient morphological changes (TC-FlAsH TC-ReAsH II In-Cell Tetracysteine Tag Detection Kit manual, Invitrogen), possibly due to generation of ROS when ReAsH is exposed to light (Adams *et al.*, 2002). d) Relatively long incubation times (more than 60 min) for full labeling may be required. It may be reasonable to label cells before starvation, if starvation is required for the planned experiment.

However, the technique could not be successfully employed to create a ReAsH-based, intramolecular FRET biosensor for ERK2 activity. The sensor design followed principles previously used to create biosensors for GPCR activity (Nakanishi *et al.*, 2006) or conformational ERK2 FRET-sensors (Fujioka *et al.*, 2006) and would have been the first kinase sensor based on biarsenical dyes.

Nevertheless, the presented data do not rule out the possibility that a conformational

ERK2 sensor based on labeling with biarsenical fluorophores can function in principle. Introduction of the 4C motif as an additonal loop between adjacent amino acids in the activation loop rather than replacing a number of amino acids might conserve the activation loop properties required for normal protein function. Relatively slow image acquisition times of the time-domain FLIM microscope may compromise the dynamic range of the approach as discussed in detail in Section 4.2.2. Faster FLIM equipment (Yasuda, 2006; Harvey *et al.*, 2008b) or a fast intensity-based FRET method circumventing the problem of ReAsH background labeling might help to detect significant fluorescent donor lifetime changes. Improvements may also result from the use of mTFP as a donor fluorophore for FLIM (Padilla-Parra *et al.*, 2009; Walther *et al.*, 2011) and FlAsH with its higher photostability and lack of potential to induce morphological changes.

4.2 Visualising Spatio-Temporal ERK2 Activity by Imaging Transient Enzyme-Substrate Interactions

Traditional, biochemical methods to analyse MAPK signaling using immunoblots and radioactive labeling are restricted to population averages and therefore provide very little or no spatio-temporal information. Immunofluorescence also only provides poor temporal information about protein activities, due to the fixation process. According to present knowledge, only dynamic, live-cell imaging approaches using fluorescent biosensors are able to resolve protein activity in spatio-temporal manner (Miyawaki, 2003; Yasuda, 2006; Schultz, 2007).

An approach to detect and potentially even measure enzyme activity directly with high spatio-temporal resolution is the visualisation of transient enzyme-substrate (ES) complexes. As shown in Fig. 3.10, the binding of a substrate peptide to the active site of the enzyme required for modification and thus the formation of the ES complexes can be detected by measuring FRET/FLIM between a donor-tagged enzyme and an acceptor-labeled substrate peptide (Yudushkin *et al.*, 2007). Exclusive specificity is achieved by attaching the donor fluorophore specifically to the enzyme of interest (Schultz, 2007). Fluorescent lifetimes can be converted into fractions of unbound and bound enzyme populations, with the latter representing the amount of ES complex, by global analysis (Verveer *et al.*, 2000; Lakowicz, 2006; Yudushkin *et al.*, 2007; Schultz, 2007; Grecco *et al.*, 2009). High amounts of ES complexes denote low enzyme activity and *vice versa* (Schultz, 2007). This technique can potentially provide information about binding affinities and kinetics of protein interactions as well as enzymatic activities both *in-vitro* and *in-vivo* (Yudushkin *et al.*, 2007; Grünberg and Serrano, 2010) and has been successfully employed to reveal spatio-temporal regulation of PTP1B upon growth factor stimulation (Yudushkin *et al.*, 2007).

In an attempt to visualise MAPK activity by imaging transient ES intermediates of ERK2 and a short substrate peptide, both *in-vitro* and *in-vivo* experiments were

performed (see Section 3.3).

4.2.1 *In-Vitro* Detection of Transient ERK2 Enzyme-Substrate Interactions

In the proof-of-principle *in-vitro* experiments, bacterially expressed and purified wt and mutant mCitrine-ERK2 proteins and a lissamine-rhodamine B-labeled, synthetic ERK2 substrate peptide representing amino acids 382-403 of the human transcription factor Elk1 were employed. Elk1 is a known substrate of ERK2 including the consensus MAPK phosphorylation site (P-X-S/T-P) (Gille *et al.*, 1995; Yang *et al.*, 1998b,a) and contains a DEF-domain (F-X-F-P) (Jacobs *et al.*, 1999; Fantz *et al.*, 2001). The DEF-domain binds only to phosphorylated ERK2 as it cannot access its binding pocket when the unphosphorylated activation loop of ERK2 is in the inactive conformation (Lee *et al.*, 2004; Yoon and Seger, 2006).

Elegant protocols for the purification of active ERK2 have been described in the literature. One is based on the co-expression of constitutively active MEK1 in *E. coli* (Khokhlatchev *et al.*, 1997). This, however, depends on the availability of bacterial expression vectors encoding for constitutively active MEK1. Also, one has to express and purify ERK2 proteins without the presence of mutant MEK1 for control experiments, significantly exentending the number of samples with all the associated disadvantages. Other protocols uses immunoprecipitation of HA-tagged ERK2 proteins from resting and growth factor-stimulated mammalian cells (Brunet *et al.*, 1994). While immunoprecipitation is a highly laborious technique by itself, again ERK2 and ppERK2 have to be purified from different samples and in addition for full activation of ERK2, also the time point of purifcation is crucial, causing even more potential errors. For reasons of simplicity, mCitrine-ERK2 wt and mutants were expressed in *E. coli*, purified in non-phosphorylated form and phosphorylated *in-vitro* by commercially available MEK1.

MEK1 requires ERK1/2 to adopt their native conformation to become phosphorylated (Seger *et al.*, 1992) and to exert its activity, a protein has to be correctly folded. Bacterially expressed and purified ERK2 proteins acquired their native conformation and were active after purification, as demonstrated by their ability to become well phosphorylated by MEK1 and to phosphorylate the synthetic substrate peptide *in-vitro* (Fig. 3.11). Although a high degree of specific activity of purified ERK2 is crucial for the implementation of *in-vitro* observations of ES complexes, because a change in FRET efficiency might be obscured by measuring a majority of non-interacting enzyme, a detailed kinase activity assay was not performed. This may explain, why phospho-Elk1 staining was not very prominent (Fig. 3.11B) as it cannot be excluded that purified ERK2 only exhibits low specific activity. However, all phospho-Elk1 antibodies used in this study recognised Ser383 of hElk1 rather than Ser389, which was used as the major phospho-acceptor site of the ERK2 substrate here. Thus, although the ERK2 substrate did include Ser383, it is likely, that the phosphorylated ERK2 substrate peptide epitope simply was no optimal recognition.

Using purified and *in-vitro* phosphorylated mCitrine-ERK2, a concentration-dependent occurence of FRET could be observed consistently, irrespective of the phospho-

rylation state of ERK2 by timebased experiments with fixed excitation and emission wavelength, fluorescent emission scan experiments and *in-vitro* fluorescent lifetime spectroscopy (see Section 3.3.1). The occurence of unspecific FRET was further confirmed by using a lissamine-rhodamine B-labeled substrate peptide (LRh-DADEYL) that could not be phosphorylated by ERK2 (Yudushkin *et al.*, 2007) (Fig. 3.14). This strongly indicates that the fluorescent dye LRh mediates the binding of substrate peptides to mCitrine-ERK2. Indeed, rhodamine dyes are known to be highly lipophilic and tend to associate to intracellular membranes (Dittrich *et al.*, 2001). It thus seems very likely, that rhodamine dyes may also associate with hydrophobic protein surfaces, especially in aqueous solutions, further explaining the observed results.

It should be noted, though, that binding of LRh-hElk1(382-403) to ppERK2 usually led to a higher FRET efficiency in fluorescent emission scan and *in-vitro* fluorescent lifetime spectroscopy experiments (Fig. 3.13 and Fig. 3.14). In addition, fluorescent donor lifetime values for ERK2 and LRh-hElk1(382-403), ERK2 and LRh-DADEYL, and ppERK2 and LRh-DADEYL exhibited more or less the same value during the course of the experiment (Fig. 3.14). While this difference on one hand does argue for an activity-dependent occurence of FRET on top of unspecific, LRh-mediated substrate binding to ERK2, the time course of LRh-hElk1(382-403) binding to ppERK2 complicates the matter. If LRh-hElk1(382-403) binding to ppERK2 was activity dependent, a recovery of donor fluorescent lifetime to at least fluorescent lifetime values of unphoshporylated ERK bound to LRh-hElk1(382-403) should have been observed, which was not the case. Instead, donor fluorescent lifetime remained more or less stable after substrate addition for the time of the experiment (Fig. 3.14).

In summary, the *in-vitro* experiments maintain the possibility that direct detection of ERK2 interactions with a substrate peptide using FRET is possible, although the formation and consumption of ERK2 ES intermediates could not be conclusively detected *in-vitro*. However, establishing the technique would require a careful and detailed analysis of the specific activity of purified ERK2 proteins and well designed, detailed *in-vitro* experiments in combination with the exchange of the chemical fluorophore on the synthetic substrate peptides.

4.2.2 *In-Vivo* Visualisation of Spatio-Temporal ERK2 Activity by Imaging Transient Enzyme-Substrate Interactions

As the *in-vitro* experiments did not definitely exclude the potential detection of ERK2 ES complexes and thereby the visualisation of ERK2 activity, it was attempted to establish the approach *in-vivo* (see Section 3.3.2). To avoid highly manipulative techniques like microinjection or protein transfection methods to introduce the synthetic substrate peptides into living cells, hElk1(379-403) was fused to the C-terminus of a fluorescent protein that could serve as an acceptor fluorophore for mCitrine. The genetically encoded, fluorescently labeled substrate peptide could thus be easily expressed together with donor-labeled ERK2 in the experimental system. In addition, the short substrate peptide would be protected from degradation by the attached FP (Wharton and

Hipkiss, 1984; Corish and Tyler-Smith, 1999).

It has not been possible to detect a significant fluorescent donor lifetime change upon stimulation of MDA (Fig. 3.15) or COS-7 (data not shown) cells with 100 ng/ml EGF. The lifetime change observed was 20 ± 20 ps on average at 5 min EGF stimulation with a maximal change of 100 ps 5 min after stimulation in an individual cell (see Table S.2.2). The shape of the curves for cells expressing mCherry or mCherry-hElk1(379-403) was nearly indistinguishable. Also, no spatial aspects of ERK2 signaling could be revealed. This, however, cannot necessarily be interpreted as a failure of the approach in general. Several scenarios are conceivable:

First, it is possible that the observed small change in donor lifetime represents true formation of ERK2 ES complexes and therefore activation of ERK2 but the relatively low number of measured cells does not allow to determine a significant result. A low number of ERK2 molecules activated upon growth factor stimulation or a low FRET efficiency even when substrate is bound to ERK2 (e.g. because of a too large Förster radius or unfavorable orientation of donor and acceptor fluorophore) could be an explanation. Measuring a large number of cells (as many as possible) may allow more meaningful statement, but this would be very laborious and time consuming without a guarantee of success. Also, careful quantitative western blot analysis in combination with calibration of the number of ERK1/2 molecules used could determine the fraction of active ERK2. However, this possibility is rather unlikely, as fluorescent lifetimes for 5 min EGF stimulation (which should be maximal activation of ERK2 and therefore should show maximum FRET efficiency) did not consistently decrease in cells expressing the ERK2 substrate (see Table S.2.2).

Second, formation of ERK2 ES complexes is detected with the low dynamic range observed in Fig. 3.15 due to the inherent fundamental principles of time-domain FLIM and the setup of the used FLIM microscope. Time-domain FLIM using TCSPC is an inherently relatively slow technique because it requires large numbers of photons to be collected for an exact estimation of fluorescent decay kinetics (Gratton *et al.*, 2003; Peter and Ameer-Beg, 2004; Thaler *et al.*, 2005; Lakowicz, 2006; Pelet *et al.*, 2006; Yasuda, 2006). To complicate the matter even further, ERK2 activation is a rather rapid process (Ando *et al.*, 2004; Burack and Shaw, 2005; Costa *et al.*, 2006; Fujioka *et al.*, 2006), at least compared to the relatively long integration times for image acquisition. As a consequence, the dynamic range of the method as well as spatial resolution may be compromised due to an averaging effect. This effect would be based on merging different fluorescent lifetimes occurring in each pixel during image acquisition, due to formation of ES intermediates, into a single value (see Fig. 4.2). Different lifetimes could arise from the short-lived formation of ES complexes that would persist for only a fraction of the image acquisition period, or from the "migration" of active ERK2 proteins through a pixel. This single value then represents the average lifetime value per integration time per pixel, which is naturally in between maximum values. This explains the low signal-to-noise ratio in the fluorescent lifetime maps (Fig. 3.15A), as image acquisition times

were reduced to maximal 30 sec as a trade-off between spatial resolution and the signal-to-noise ratio. Technical advances in form of faster imaging equipment could aid in this issue. Image acquisition with the available frequency-domain FLIM instrument (Squire *et al.*, 2000), however, was only marginally faster than with the time-domain FLIM microscope (data not shown).

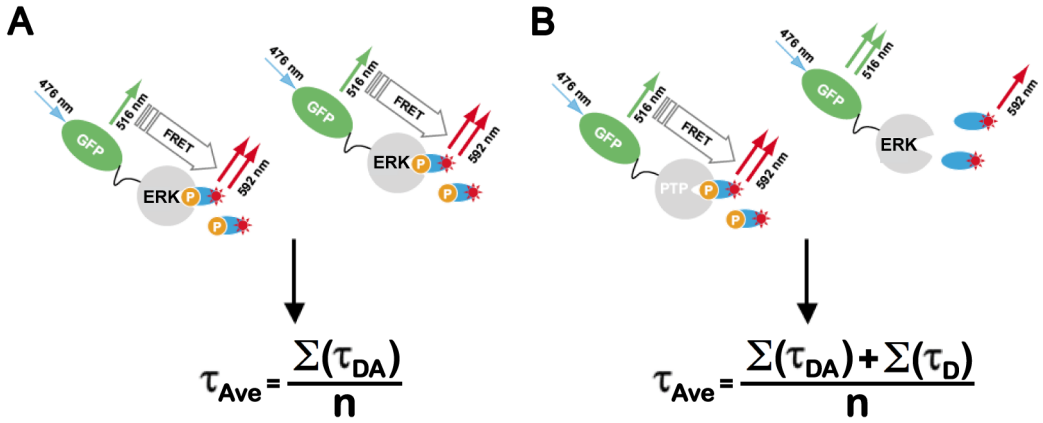

Figure 4.2: In ES-imaging the fraction of (donor-labeled) enzyme bound to (acceptor-labeled) substrate should be high. Schematic representation of the influence of enzyme saturation on the measured lifetime and dynamic range of an ES-imaging assay. A) The average fluorescent lifetime in a region of interest is equal to the qhenched lifetime of the donor when the enzyme is saturated with substrate. In the special case of τ_{DA} = constant, τ_{Ave} = τ_{DA}. B) The average fluorescent lifetime in a region of interest is a mixture of quenched and unquenched lifetimes when the enzyme is not saturated with substrate. τ_{Ave} = average fluorescent lifetime in the region of interest; τ_{DA} = fluorescent lifetime of donor in complex with acceptor (quenched lifetime); τ_{D} = fluorescent lifetime of non-bound donor (donor lifetime); n = number of donor molecules.

Third, the substrate concentration in living cells is not sufficiently high to take advantage of the full, theoretically possible dynamic range of the ES complex visualisation/imaging approach. For any FRET assay, the fraction of donor molecules undergoing FRET (i.e. the fraction mCitrine-ERK2 in complex with its fluorescently labeled substrate peptide) should be as high as possible, preferably 100 %, as illustrated in Fig. 4.2. It should be kept in mind that a high fraction of donor molecules undergoing FRET and a high FRET efficiency are two separate things. The former is simply the amount of donor in sufficient proximity to the acceptor for FRET to occur. In contrast, the FRET efficiency characterises the fraction of energy transfer per donor excitation event and is dependent on the distance between donor and acceptor, the spectral overlap between donor emission and acceptor excitation spectrum and the relative orientation of donor emission and acceptor excitation dipoles (Lakowicz, 2006). For FLIM, the FRET efficiency should not be 100 %, because if all energy is transferred to the acceptor, no photons could be emitted from the donor fluorophore preventing the determination of its fluorescent lifetime.

If ERK2 is saturated with substrate peptide, i.e. the fraction of donor molecules undergoing FRET is 1, the average fluorescent lifetime (τ_{Ave}) of the region of interest (e.g. the whole image, a cell or pixel) can be calculated according to the equation in Fig. 4.2A, or in a more simplified version, τ_{Ave} is equal to the quenched lifetime (fluorescent lifetime of the donor in complex with the acceptor, τ_{DA}). In this case, the difference between donor fluorescent lifetimes for inactive (no substrate bound and therefore no FRET) and active ERK2 is maximal and thus the dynamic range of the assay as well. In contrast, if only a fraction of ERK2 molecules would be in complex with substrate peptide (Fig. 4.2B), the sample would contain a mixture of quenched and unquenched lifetimes. Average fluorescent lifetime of the region of interest would then be calculated according to the equation in Fig. 4.2B and would adopt a value in between maximal (no FRET) and minimal lifetime.

Thus, substrate concentrations sufficiently high to saturate ERK2 are crucial for the visualisation of ES complexes. According to Michealis-Menten kinetics, saturated enzymes operate at their maximum reaction velocity (V_{max}). Since it is difficult to determine the substrate concentration of V_{max} ($[S]_{(V_{\mathrm{max}})}$), the Michaelis constant K_{M} can be used to at least get an idea about the order of magnitudes in substrate concentrations that would have to be used. The K_{M}-value is defined as the substrate concentration at which the reaction velocity is $V_{\mathrm{max}}/2$ (Nelson and Cox, 2004) and is sometimes (inappropriately) used to characterise the affinity of an enzyme to its substrate. Michealis-Menten kinetics implicate that $[S]_{(V_{\mathrm{max}})}$ is considerably higher than K_{M} (Fig. 4.3.

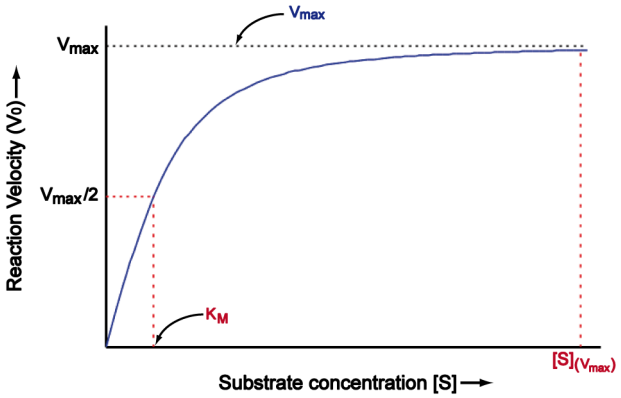

Figure 4.3: Saturating substrate concentrations for an enzyme can be estimated from its K_{M}-value. Saturated enzymes operate at their maximum reaction velocity (V_{max}). According to Michealis-Menten kinetics $[S]_{(V_{\mathrm{max}})}$ may have to be orders of magnitudes higher than K_{M}, defined as $V_{\mathrm{max}}/2$.

However, K_{M}-values of ERK2 for short peptides reported in the literature are usually in the range of 0.1 - 1 mM (Table 4.1). K_{M}-values for Elk1 were determined either using a 121 aa petide (Jacobs *et al.*, 1999; Fantz *et al.*, 2001; Matsuura *et al.*, 2005) or a synthetic peptide based on hElk1(387-399) with two additional Arg residues at the N-terminus (Jacobs *et al.*, 1999; Fantz *et al.*, 2001). Both peptides include the consensus

phosphorylation site of the substrate peptide used in this study and resulted in K_M-values from 0.8 - 1.8 μM or 51 - 130 μM, respectively (Table 4.1). It is therefore reasonable to assume, that the K_M-value of ERK2 for hElk1(379-403) is situated in a similar range, although the exact K_M-values for hElk1(379-403) or mCherry-hElk1(379-403) have not been determined experimentally.

Table 4.1: K_M-values of ERK2 for different proteins or peptides.

Protein/Peptide		K_M (in μM)	Reference
Aop(480-732)		0.7 ± 0.3	(Jacobs *et al.*, 1999)
DAPK	- Serum	35.8	(Chen *et al.*, 2005)
DAPK	+ Serum	17.4	(Chen *et al.*, 2005)
EGFR(661-668)		470 ± 90	(Jacobs *et al.*, 1999)
Elk1(307-428)		1.5 ± 0.5	(Jacobs *et al.*, 1999)
		0.8 ± 0.3	(Fantz *et al.*, 2001)
		1.8 ± 0.3	(Matsuura *et al.*, 2005)
Elk1(387-399)		130 ± 30	(Jacobs *et al.*, 1999)
		51 ± 6	(Fantz *et al.*, 2001)
ERK1(182-199)		> 5000	(Gonzalez *et al.*, 1991)
Ets1		5.1 ± 1.2	(Seidel and Graves, 2002)
Ets1(1-138)		19	(Waas and Dalby, 2001)
		6.8 ± 1.8	(Seidel and Graves, 2002)
Ets1(1-52)		190 ± 35	(Seidel and Graves, 2002)
Ets2(1-172)		2.8 ± 0.4	(Seidel and Graves, 2002)
Jun(230-255)		520 ± 30	(Gonzalez *et al.*, 1991)
KSR1(281-479)		3.4 ± 0.9	(Jacobs *et al.*, 1999)
		1.2 ± 0.1	(Fantz *et al.*, 2001)
LIFR(856-1097)		3.9 ± 1.7	(Schiemann *et al.*, 1995)
LIN(281-441)		0.8 ± 0.5	(Jacobs *et al.*, 1999)
MBP		5.1 ± 1.0	(Matsuura *et al.*, 2005)
MBP(89-107)		280 ± 20	(Gonzalez *et al.*, 1991)
Myc(51-66)		640 ± 50	(Gonzalez *et al.*, 1991)
Raf1		0.1	(Lee *et al.*, 1992)
Smad3		11.8 ± 2.3	(Matsuura *et al.*, 2005)

As a general rule inferred from Table 4.1, the shorter a substrate peptide for ERK2, the higher are obtained K_M-values. This can be easily understood for certain circumstances (two step reactions with the rate constant for substrate formation from the ES complex (k_2) as the rate limting step) when K_M indeed represents a measure of the affinity of the enzyme to its substrate (Nelson and Cox, 2004). Here, the affinity of the enzyme for its substrate decreases (and thus the K_M-value increases) with truncation of the substrate protein as it looses domains and/or structures important for the interaction with the enzyme.

In principle, this may explain the high K_M-values obtained for short substrate peptides, e.g. taken from EGFR, ERK1, Ets1, Jun, MBP or Myc (Table 4.1). Strikingly, the K_M-values especially for Elk1(387-399) are considerably lower than those for comparably short peptides (Table 4.1), most probably due to the DEF-domain of Elk1 (Jacobs *et al.*, 1999; Fantz *et al.*, 2001) which is lacking in EGFR, ERK1, Ets1, Jun, MBP and Myc.

Still, with an assumed K_M-value of 10 - 100 μM and the notion that $[S]_{(V_{max})}$ has to be considerably, probably orders of magnitudes, higher than K_M, sufficiently high substrate concentrations for the visualisation of ES complexes would probably have to be in a range of at least 10 - 100 mM. Further adding to the problem is the sequestration of substrate peptide by endogenous (unlabeled) ERK1/2 and potentially other proteins able to bind hElk1(379-403) which require even higher substrate concentrations to compensate the sequestration effect (Blüthgen *et al.*, 2006). It is impossible to achieve mM-expression levels of plasmid encoded proteins in mammalian cells. While protein transfection methods and microinjection may perform better, they are still not able to provide sufficiently high substrate concentrations in living cells that would allow the visualisation of transient ERK2 ES interactions.

K_M-values for longer peptides of Elk1 are in the range of 1 μM (Jacobs *et al.*, 1999; Fantz *et al.*, 2001; Matsuura *et al.*, 2005) and thus K_M-values for the whole protein might be even lower. The detection of FRET between donor-labeled ERK2 and acceptor-labeled, overexpressed Elk1 with FLIM might be more likely. Additionally, while Elk1 is primarily a nuclear protein (Janknecht *et al.*, 1994; Pingoud *et al.*, 1994), it can also be found in the cytoplasm of cells (Sgambato *et al.*, 1998; Salinas *et al.*, 2004). Therefore, probing spatio-temporal ERK2-Elk1 interactions in living cells would be a variant of the visualisation of transient ERK2 ES-interactions with acceptor-labeled Elk1 as the substrate for ERK. However, it was not possible to show the interaction of mCherry-Elk1 and mCitrine-ERK2 with FRET (data not shown), unlike MEK1-ERK2 interactions (Burack and Shaw, 2005). In addition to reasons discussed for the substrate peptide-based ES-imaging approach (such as too low substrate = Elk1 concentrations inside cells), the distance between the donor and acceptor fluorophores simply might have been too far. It might be interesting to see whether intermolecular FRET can be observed between donor-labeled ERK2 and two acceptor-labeled, high affinity substrate proteins of ERK2, one with a cytosolic and the other with a primarily nuclear localisation. Since a potential lifetime change of the donor fluorophore would be sufficient to probe ERK2 activity, substrate proteins could be labeled with the same acceptor molecule. Alternatively, three-chromophore FRET (Galperin *et al.*, 2004) could be applied.

In summary, it has not been possible to visualise transient ERK2 ES interactions *in-vivo*, most likely because low binding affinities of the used substrate peptide to ERK2 and insufficient substrate concentrations prevented the detection of FRET between donor-labeled ERK2 and acceptor-labeled substrate.

Many protein kinases display low affinities to peptide substrates and higher affinities

are only provided by additional docking or binding domains (Adams, 2001). This is an essential requirement, given the number of existing bona fide phosphorylation sites in the background of up to 10^6 potentially phosphorylatable residues (Ubersax and Ferrell, 2007), further demonstrated by the fact that highly specific protein kinases (e.g. MEK1) can display low K_M-values (Ferrell, 1996). However, it greatly complicates the visualisation of transient kinase-substrate interactions.

Recently, short, modular substrate peptides for ERK were designed using docking peptides that increase binding affinities 200-fold (Fernandes *et al.*, 2007). It may be worth testing these peptides for their potential in visualising ERK2 ES-interactions. Fluorescence cross correlation spectroscopy may help to circumvent the issue of low binding affinities of substrate peptides to ERK2 as it does not rely on averaging different fluorescent lifetimes displaying different activity states of the kinase but is rather able to detect ES complexes and kinase-substrate interactions on a single molecule level (Kettling *et al.*, 1998; Haustein and Schwille, 2003).

Alternative approaches are conceivable to evade the problem that detection of enzyme-substrate intermediates using FRET is prohibited by low binding affinities of substrate peptides to their kinase. For example, in case of a kinase with a specific subcellular localisation, e.g. the plasma membrane, substrate peptides could be enriched in that particular intracellular compartment, e.g. by tethering it to the plasma membrane, so that its local concentration on the plasma membrane is elevated and the pool of enzyme molecules can be more readily saturated. This approach, however, is not available for ERK2 as it is (in the inactive state) primarily a cytosolic protein. One could also try to increase local substrate concentrations by linking the substrate peptide to a matrix (Zhang *et al.*, 2002; Niethammer *et al.*, 2007), e.g. silicon beads, for *in-vitro* experiments (Grecco *et al.*, 2010) or microinjection into living cells.

4.3 An Intramolecular FRET-Based Biosensor for ERK2 Activity Employing Transient Enzyme-Substrate Interactions

As another promising alternative to increase substrate concentrations in the immediate environment of ERK2, it was suggested to directly link the substrate peptide to ERK2 via a flexible peptide linker. The peptide linker would allow the reversible binding of the substrate peptide to the active site of ERK2 and keep the substrate peptide in close proximity to ERK2, to increase the probability of binding. The approach required a recombinant sensor construct including ERK2, the flexible peptide linker and an ERK2 substrate peptide sequence flanked by two fluorescent proteins suitable for FRET. The resulting genetically encoded, intramolecular FRET-based biosensor reports the formation of transient ES-complexes between ERK2 and the substrate peptide upon activation of the kinase, before the phosphorylated substrate peptide dissociates from the active site. Similar to intermolecular ES-imaging, binding of the substrate to the enzyme changes the FRET signal obtained from the donor-acceptor pair (Fig. 3.16A). But in contrast to intermolecular ES-imaging, this approach with its

fixed stoichiometry of donor and acceptor fluorophores is designed as an intramolecular FRET-based biosensor. Therefore, in addition to FLIM, changes in FRET efficiency can also be detected by ratiometric FRET imaging, greatly simplifying data acquisition and analysis and increasing the signal to noise ratio (Miyawaki, 2003; Yasuda, 2006).

Screening for a functional sensor construct identified *E*RK *A*ctivity *S*ensor 4 (EAS4), consisting of mCitrine, a spacer (SGLRSRA), rat ERK2, the long version of the flexible linker (L(GGGGS)$_3$AAA), amino acids 375-404 of hElk1, a spacer (ASL) and mCherry (Fig. 3.16B), as the sensor construct with the highest dynamic range (Fig. 3.17).

Interestingly, the fluorescent donor lifetimes observed for EAS4 increased upon stimulation with EGF, indicating a loss of FRET when ERK2 was activated, rather than an increase in FRET (Fig. 3.17B). Intuitively, considering the sensor design and principles of ES-imaging (Fig. 3.10 and 3.16), activation of ERK2 allows binding of the substrate peptide, bringing the donor-acceptor pair within a distance sufficient for FRET (Yudushkin *et al.*, 2007). Thus, stimulation and activation of ERK2 was expected to result in decreasing donor lifetimes indicating an increased FRET efficiency. This is in sharp contrast to the time profile obtained from EAS4. Nevertheless, the conformational change of the sensor protein may lead to a reorientation of the fluorophores that is unfavorable for FRET. Indeed, the change in FRET signals from intramolecular FRET sensors is believed to often result from reorientation of the fluorophores instead of a significant change in distance (Giepmans *et al.*, 2006). The true nature of the unexpected FRET change has not been explored further. Despite that, the basic principle of EAS4 can be formulated as such: binding of the substrate peptide to the active site of ERK2 results in a decreased FRET efficiency (Fig. 4.4).

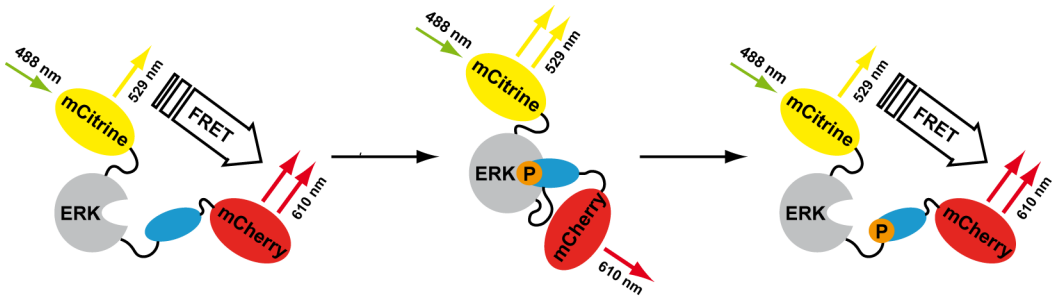

Figure 4.4: Principle of ERK2 Activity Sensor 4. Binding of the substrate peptide (blue, phosphorylation is indicated by the orange dot) to the active site in phosphorylated ERK2 (grey) results in a decrease of FRET from the donor to the acceptor fluorophore.

Due to the inherent characteristics of time-domain FLIM and the setup of the FLIM microscope, it was only possible to take a few "snap-shots" of events following MAPK activation in living cells. In consequence, the resulting low temporal resolution was comparable to western blots. Furthermore, as the observed process is relatively fast, relatively long intergration times for image acquisition compromise the dynamic range of the sensor as well as spatial resolution due to an averaging effect as discussed in

Section 4.2.2. On the other hand, sensor design predestines it to be used in ratiometric FRET imaging. Due to its simplicity and speed (essentially only two images are required to calculate a FRET ratio image, see Section 1.3.2), ratiometric FRET imaging can be implemented on nearly any fluorescent microscope and provides a high temporal resolution limited only by the speed of the instrument. The possibility to gather much more photons per time interval than with time-domain FLIM, also offers improved spatial resolution and signal-to-noise ratio.

Improved temporal resolution of ratiometric FRET is demonstrated by the ability to follow translocation of EAS4 wt to the nucleus of HeLa cells after EGF stimulation (Fig. 3.20A) in a fashion similar to fluorescently labeled ERK2 (Ando *et al.*, 2004; Costa *et al.*, 2006; Cohen-Saidon *et al.*, 2009). Whole cell FRET ratios of individual cells reveal a sudden rise in ERK2 activity 1 - 5 min after EGF addition, with a peak after 5 - 15 min, before slowly decreasing to approximately one third of the peak value at approximately 35 min for at least another 30 min (Fig. 3.20B). The observed dynamics of ERK2 activity revealed by EAS4 generally resembles the characteristic translocation of phosphorylated and thus activated ERK2 to the nucleus upon EGF treatment with a sudden onset and a quick rise to a maximal value, followed by a slow decline (see Fig. 3.2 and Ando *et al.*, 2004; Burack and Shaw, 2005; Costa *et al.*, 2006; Fujioka *et al.*, 2006; Cohen-Saidon *et al.*, 2009). These characteristics of ERK2 activation in response to EGF stimulation are widely known in the literature as assessed by the phosphorylation state of ERK2 (Lenormand *et al.*, 1993; Fujioka *et al.*, 2006; Santos *et al.*, 2007; Nakakuki *et al.*, 2010). Interestingly, it has been suggested, that the well described and aforementioned, short-lived translocation of ERK1/2 to the nucleus may be an artifact of overexpression, since ERK1/2 expressed on endogenous levels reside in the nucleus for hours after stimulation while being quickly dephosphorylated (Volmat *et al.*, 2001; Lidke *et al.*, 2010). One should therefore be careful to draw conclusions about physiological ERK signalling simply by observing its nuclear translocation.

The observed time profile of fluorescent donor lifetime and FRET ratio changes obtained with EAS4 wt after EGF stimulation demonstrate the reversibility of the underlying ES-interactions. It is therefore justified to conclude, that the change in FRET efficiency detected from EAS4 wt indeed reflects the activation state of ERK2.

However, it should be kept in mind, that the mechanism by which EAS4 functions is not entirely clear. For example, the substrate peptide could bind to the active site of phosphorylated ERK2 in EAS4, rapidly being phosphorylated and released. To allow the observed detection of increasing donor lifetimes or FRET ratios, the respective phosphatase would have to rapidly dephosphorylate the substrate peptide as well, so that a new cycle of binding, phosphorylation, release and dephosphorylation could begin. In this scenario, the measured changes in FRET efficiency represent the fraction of active ERK2 in the region of interest.

Alternatively, opening of the activation loop in phosphorylated ERK2 allows the substrate peptide to bind in ERK2's active site. Phosphorylated and unphosphorylated

substrate peptide may reside in the active site independent of modification, e.g. due to circumstances controlled by the sensor design with the close proximity of ERK2 and the substrate peptide. Dephosphorylation of the ERK2 activation loop in EAS4 and the subsequent conformational change of ERK2 may force the substrate peptide from the active site and its binding pocket. In the second scenario, the observed change in FRET efficiency upon ERK activation rather represents phosphorylation of ERK2 than actual activity. As the binding of substrates to their enzyme is supposed to dynamic equilibrium with a shift in the total amount substrate bound while maintaining its binding and release, the second scenario is less likely.

Improved temporal resolution of ratiometric FRET imaging revealed that activation of EAS4 wt actually precedes ERK2 translocation (Fig. 3.20B and Fujioka *et al.*, 2006). While this is expected, as the activating phosphorylation of ERK1/2 is a prerequisite for the subsequent translocation (Fukuda *et al.*, 1997; Adachi *et al.*, 1999), only since the development of fluorescent biosensors for ERK2 it has been shown in such a detail (Fujioka *et al.*, 2006).

Even more interestingly, EAS4 wt was able to distinguish different levels of ERK2 activation. It has been shown, that stimulation of PC-12 cells with EGF, EGF and PMA or PMA alone results in sustained ERK activation when treated with EGF and PMA or PMA alone as opposed to stimulation with EGF alone. However, PMA-induced sustained ERK1/2 phosphorylation was much less strong than EGF + PMA-induced ERK response (Santos *et al.*, 2007). A similar effect was observed in MCF-7 cells (Fig. 3.24) and resolved by EAS4 wt, further demonstrating the potential of the sensor construct.

The specificity of the signal obtained by EAS4 was demonstrated using dominant negative mutants of the sensor construct (see Section 3.4.3). Neither with a non-phosphorylatable mutant of EAS4 (EAS4-TAYA) nor with an EAS4 construct including a mutated substrate peptide (EAS4-ElkMut) exhibited significant donor lifetime changes. In EAS4-ElkMut, the mutated substrate cannot bind to the active site. EAS4-TAYA lacks Thr183 and Tyr185, the amino acid residues that have to be phosphorylated for the activation loop to open and expose the active site of ERK2. Therefore, the substrate cannot bind to ERK. In a third mutant, EAS4-K52R, ERK2's catalytic activity was lost (Robbins *et al.*, 1993). Since in ERK2 K52R, Thr183 and Tyr185 can still be phosphorylated (Fig. 3.11 and 3.18B), the activation loop can adopt the "open" or "active" conformation and the substrate peptide bind in the active site. However, kinase dead ERK2 cannot modify the substrate. Therefore it was suspected that ERK2 K52R incorporated into EAS4 might function as a "trapping mutant" for the substrate peptide and result in a stable donor lifetime change (see Section 3.3.1.2). Indeed, in sharp contrast to the wildtype construct, the lifetime change observed with EAS4 K52R was stable for times longer than 20 min after EGF stimulation, indicating prolonged enzyme substrate interactions. These results support the hypothesis that the kinase dead mutant of ERK2 might function as a "substrate trapping" mutant.

Ratiometric FRET imaging of EAS4 TAYA further confirmed the specificity of the signal obtained by EAS4 wt as demonstrated by the observation, that FRET ratios

of EAS4 TAYA did not rise significantly above pre-stimulation values during the time frame of the experiment (Fig. 3.20C).

These data show that EAS4 wt specifically reports ERK2 activity in a time-dependent manner.

The average change in FRET ratio of EAS4 was found to be about 11 ± 1 % in HeLa cells (Fig. 3.20C) and 13 ± 2 % in MCF-7 cells (Fig. 3.23) with changes of up to 20 % observed in individual MCF-7 cells (data not shown). The dynamic range of EAS4 in individual cells is therefore 3 - 4 times bigger than that of Miu2 (Fujioka *et al.*, 2006).

It is difficult to compare the dynamic range of EAS4 with those of Erkus and EKAR. Average FRET ratios presented for Erkus exhibit a dynamic range of 8-9 % (Sato *et al.*, 2007). This is an average over a number of cells and thus does not include information about the maximally possible FRET ratio change in single cells. However, the average FRET ratio change of EAS4 is still about 40 % bigger than that of Erkus. In contrast, FRET ratios of EKAR show 20 % changes before and after EGF stimulation as observed with EAS4.

Interestingly, donor fluorescent lifetimes of EKAR decreased by 70 - 80 ps in individual cells by and 20 - 30 ps on average (Harvey *et al.*, 2008a). In comparison, donor lifetimes of EAS4 in single cells increased by 60 - 70 ps on average upon stimulation of cells with EGF. The maximal lifetime change observed in indivdual cells was up to 140 ps (Fig. 3.19 and Table S.4.1). There is clearly a discrepancy between the dynamic ranges of EKAR obtained by FLIM or ratiometric FRET imaging. However, none of the published values for EKAR exceeds the dynamic range measured with EAS4. In fact, while ratiometric FRET imaging of EKAR yields a similar dynamic range, FLIM measurements report a dynamic range of EAS4 that is about a factor of two better than that of EKAR.

This demonstrates that the dynamic range of EAS4 exceeds those of previously published FRET-based biosensors for ERK2 activity. The dynamic range of the sensor may be improved by the use of a more optimal FRET pair as mTFP in combination with a yellow acceptor fluorophore such as EYFP, mCitrine or Venus (Padilla-Parra *et al.*, 2009) or the FRET optimised FP pair CyPET and YPET (Nguyen and Daugherty, 2005). In addition, the spacer between mCitrine and ERK2 as well as hElk1(375-404) and mCherry are potential targets for sensor optimisation.

The signal-to-noise ratio (as judged by the calibration bars and colour differences in the pseudocolour images representing FRET ratios or fluorescent donor lifetimes before and after cell stimulation) of Miu2, Erkus and EKAR seems to be better than that of EAS4 (compare e.g. Fig. 3.19 and 3.22 with Fujioka *et al.*, 2006; Sato *et al.*, 2007; Harvey *et al.*, 2008a). The better the signal-to-noise ratio, the smaller is the range of different FRET or lifetime values, that distribute around an average value. In other words, the signal-to-noise ratio determines how well two states (e.g. high and low FRET efficiencies displayed as high and low FRET ratios or fluorescent lifetimes) can be distinguished when displayed as pseudocolour images. One should keep in mind though, that the signal-to-noise ratio depends in large parts on the imaging system and is higher the

more photons can be acquired (Pelet *et al.*, 2006; Yasuda, 2006).

It is noteworthy that Miu2, Erkus and EKAR have been imaged using widefield fluorescent microscopes (Fujioka *et al.*, 2006; Sato *et al.*, 2007; Harvey *et al.*, 2008a), that acquire more photons in a given period of time compared to confocal microscopes. In contrast, imaging of EAS4 was performed with confocal microscopes. Ratiometric FRET imaging was implemented on a Zeiss LSM 510 confocal laser scanning microscope because the low light sensitivity of cameras installed on accessible widefield fluorescent microscopes required long exposure times and thereby compromised photostability of the fluorophores (data not shown). While the pinhole of the microscope was opened completely (to 10 μm) to allow the maximally possible number of photons to be collected from the sample, the obtained image was still a (thick) section through the cell to be imaged (data not shown). Using a true widefield microscope might therefore further improve the signal-to-noise ratio of FRET ratio images.

The rate-limiting factor in the acquisition of time-domian FLIM images was the sensitivity of the detector. Simply, photon counts were not allowed to exceed a certain value per time unit for two reasons: the highly sensitive APDs could be burned with too high light intensities and the photon-counting histogram will be biased to shorter donor lifetimes, if the chance of photon detection after each excitation pulse is higher than 1 % (van Munster and Gadella, 2005; Lakowicz, 2006). Thus, opening the pinhole to acquire more photons during FLIM images acquisition is of limited use. Interestingly, Harvey *et al.* (2008a) achieved high sampling rates during image acquisition using a custom-build time-domain FLIM setup (Yasuda, 2006; Harvey *et al.*, 2008b). It would be highly interesting to see the performance of EAS4 in their microscope and directly compare results.

Erkus and EKAR required specific targeting to the nucleus or cytoplasm by the respective nuclear or cytosolic localisation sequences to differentiate ERK2 activity on the level of subcellular compartments. In addition, both sensor constructs required subcellular targeting to resolve the known ERK2 activity profile. Sensor proteins freely diffusing throughout the cell only reported ERK2 activation but not inactivation (or rather substrate phosphorylation kinetics but not substrate dephosphorylation) (Sato *et al.*, 2007; Harvey *et al.*, 2008a). EAS4 wt, in contrast, includes the full ERK2 protein and therefore behaves more or less as fluorescently labeled ERK2. In that respect, ERK-like translocation was observed with EAS4 wt. But most importantly EAS4 wt is able to resolve compartmentalised ERK2 signalling without specific localisation signals (Fig. 3.5 and Fig. 3.24).

To test the potential of EAS4 in resolving spatio-temporal ERK2 activity in a real biological context, EAS4 was used to analyse MAPK activation in response to EGF and HRG in MCF-7 breast cancer cells.

MCF-7 is a transformed mammary epithelial cell line derived from human breast epithelial adenocarcinoma (Brooks *et al.*, 1973; Soule *et al.*, 1973). In MCF-7 cells, EGF induces transient ERK1/2 activation encoding a proliferative signal, while heregulin

(HRG) generates sustained ERK1/2 activation resulting in cell differentiation (Thottassery *et al.*, 2004; Nagashima *et al.*, 2007).

EAS wt is indeed able to capture transient versus sustained ERK signalling in MCF-7 cells when treated with EGF or HRG, respectively (see Section 3.5). Immunoblotting of ectopically expressed EAS4 wt in whole cell lysates (Fig. 3.21) and averaging FRET ratios over whole cells (data not shown) purely displayed these known features of EGF and HRG signal transduction. Surprisingly, quantification of ERK2 activity in the cytosol versus the nucleus revealed that HRG-induced sustained ERK2 activity was predominantly cytosolic (Fig. 3.22C), while HRG-induced nuclear ERK2 activity was found to be transient (Fig. 3.22B). In contrast, the transient ERK2 response after EGF treatment known from the literature in both the cytosol and nucleus (Fig. 3.22B and C). This in agreement with a recent publication, analysing the role of dynamics of the MAPK module on c-Fos expression in reponse to EGF and HRG stimulation in MCF-7 cells (Nakakuki *et al.*, 2010). However, those experiments were performed by immunoflourescence with antibodies for phosphorylated ERK and thus a) do not report true ERK activity and b) only offer poor temporal resolution.

As EGF versus HRG stimulation shows ERK responses in MCF-7 cells similar to EGF and neural growth factor (NGF) stimulation in PC12 cells, it was hypothesised that the underlying feedback mechanism observed in PC12 cells also exist in MCF-7 cells. To approach that idea, preliminary experiments with EAS4 wt were performed.

The role of signalling upstream of ERK in the sustained ERK response to HRG was investigated by treatment of HRG-stimulated cells with high concentrations of the MEK inhibitor U0126. Indeed, quickly after U0126 addition, ERK2 was inactivated showing that continuous signalling from upstream of ERK is necessary for sustained ERK activity (Fig. 3.23).

In PC12 cells, EGF-induced transient ERK1/2 activity can be converted into a sustained ERK1/2 response by introducing a PKC-mediated feedback loop in the MAPK module via PMA stimulation (Santos *et al.*, 2007). To test whether it is possible to induce a similar feedback loop in MCF-7 cells and to investigate its effect on spatio-temporal ERK signalling, MCF-7 cells were stimulated with EGF, EGF and PMA, or PMA alone. ERK2 activation was analysed by quantitative western blotting and ratiometric FRET imaging.

Stimulation of MCF-7 cells with EGF and PMA resulted in sustained cytosolic ERK2 activity as shown by quantitative western blotting and ratiometric FRET imaging (Fig. 3.24). Stimulation with PMA alone also resulted in sustained cytosolic ERK2 activity, but with a markedly lower amplitude of the signal than in the cytosol of cells stimulated with EGF and PMA. In contrast, cytosolic ERK2 activity in cells stimulated with EGF and nuclear ERK2 activity in all cells was transient. These data hint at the existence of PKC-mediated feedback loops in the MAPK module that may be responsible for sustained ERK activation in MCF-7 cells.

These results show that EAS4 can indeed be used to resolve biologically meaningful

characteristics of ERK2 activation.

In summary, a new intramolecular FRET-based fluorescent biosensor for the visualisation of ERK2 activity has been developed. The sensor design principle is generic and thus should in principle be applicable to all kinases. It is based on the reversible binding and phosphorylation of a short substrate peptide by the kinase of interest. The peptide is directly linked to the kinase via a flexible peptide linker. Binding of the substrate peptide to the active site of the enzyme induces a global conformational change of the sensor protein. Attaching a FRET pair of FPs to the sensor allows detection of an activation-induced change in FRET signal. Therefore, it is the first FRET-based fluorescent biosensor approach, that directly reports spatio-temporal kinase activity by visualising transient enzyme-substrate interactions rather than the conformational change of a kinase or binding of a phospho-protein binding domain to a phosphorylated substrate peptide of the kinase in question.

In addition, EAS4 displays high temporal resolution, virtually only limited by the speed of the used microscope. It also exhibits a dynamic range and spatial resolution superior to that of previously published ERK2 biosensors. EAS4 can be used with various techniques to assess its FRET signal, including ratiometric FRET and FLIM.

EAS4 is able to resolve actual and biological meaningful differences in ERK2 activity upon stimulation with various growth factors.

5 Future Perspectives and Directions

5.1 General Characteristics of MAPK Signalling

In principle, EAS4 is a useful tool to obtain information about spatio-temporal activity of ERK2.

Using EAS4, dynamics of ERK2 activation in most experimental systems are now accessible with precise information about the time and location of ERK activity on single cell level (rather than population averages). Plus, EAS4 offers the possibility to obtain these information in form of direct activity rather than phophorylation state. Besides these advantages, it should be kept in mind, that the short-lived nuclear translocation of ERK1/2 may be an artifact of overexpression, since ERK1/2 expressed on endogenous levels reside in the nucleus for hours after stimulation (Volmat *et al.*, 2001; Lidke *et al.*, 2010). Thus, it should be considered, whether creation of cell lines stably expressing EAS4 on levels of or close to endogenous expression levels of ERK1/2 may help to obtain data that reflect the physiological situation in more detail.

EAS4 offers the opportunity to track features of ERK signalling in living cells that have yet only been theoretically investigated, such as the impact of spatial gradients of phospho-proteins on signal propagation (Brown and Kholodenko, 1999; Kholodenko, 2006; Maeder *et al.*, 2007; Yudushkin *et al.*, 2007). Other features of MAPK signalling that await experimental proof include travelling waves of phospho-proteins (Markevich *et al.*, 2006; Kholodenko, 2006), compartmental and differential MAPK signalling upon growth factor stimulation (Santos *et al.*, 2007; Nakakuki *et al.*, 2010), and the investigation of feedback loops in the MAPK module (Kholodenko, 2006; Santos *et al.*, 2007; Lin *et al.*, 2009; Smith *et al.*, 2010). Before the development of EAS4, none of the previously published FRET-based biosensor approaches to follow spatial and time-resolved ERK2 activity was good enough to resolve these features. EAS4 may also provide new insights into the relationship of endocytosis and MAPK signalling (Di Guglielmo *et al.*, 1994; Vieira *et al.*, 1996; Kranenburg *et al.*, 1999; Pierce *et al.*, 2000; Jiang and Sorkin, 2002; Taub *et al.*, 2007; Uhles *et al.*, 2007).

5.2 Differential ERK Activation in Response to Stimulation with Different Growth Factors

Spatio-temporal signalling of the MAPK module with its core components Raf, MEK and ERK is critically regulated via positive or negative feedback loops (Avraham and Yarden, 2011) by the use of additional kinases (Santos *et al.*, 2007) phosphatases and scaffold proteins (Pouysségur *et al.*, 2002; O'Neill and Kolch, 2004; Torii *et al.*, 2004; Ebisuya *et al.*, 2005).

Transient versus sustained activation of ERK1/2 in response to different stimuli is a well-known feature of the MAPK module (Gotoh *et al.*, 1990; Kahan *et al.*, 1992; Traverse *et al.*, 1992; Costa *et al.*, 2006; Santos *et al.*, 2007).

In PC12 cells, cell fates are determined by the duration of ERK1/2 activation. The response of PC12 cells to receptor tyrosine kinase (RTK) stimulation has been extensively studied as a model system to analyse how signal transduction specificity is achieved by different RTK that use the same downstream signalling module (Marshall, 1995). NGF stimulation of PC12 cells results in neurite outgrowth and cell differentiation (Greene and Tischler, 1976). In contrast, EGF treatment enhances proliferation of PC12 cells (Huff *et al.*, 1981). The observation, that NGF stimulation results in prolonged ERK activation (for several hours after stimulation) while EGF-induced ERK activation is very short, has led to the idea, that is is this transient versus sustained ERK activation profile that determines cell fate (Fig. 5.1) (Gotoh *et al.*, 1990; Traverse *et al.*, 1992; Marshall, 1995).

Cell fate decisions determined by the duration of ERK activity can be controlled on various levels (Fig. 5.1) (Avraham and Yarden, 2011). Rapid internalisation and degradation of one receptor, but not the other, eliminates its potential for prolonged signalling and affects the duration of its signal. Indeed, the EGFR is downregulated through phosphorylation (Countaway *et al.*, 1992). In additon, feedback loops in the MAPK module have been found to control ERK activation. A negative feedback loop from ERK to Raf inhibits further activation of ERK activators and results in transient ERK signalling. In contrast, NGF stimulation induces a positive feedback loop in the MAPK module and its continuous activation of ERK activators results, in combination with PKC activation (Corbit *et al.*, 2003; Santos *et al.*, 2007), in sustained ERK activation.

The duration of ERK activation is sensed by a network of immediate early genes (IEG), including the transcription factor c-Fos (Murphy *et al.*, 2002, 2004). HRG-mediated sustained ERK1/2 and its downstream target p90 ribosomal S6 kinase (RSK) stimulate c-Fos transcription and stabilise the protein by multiple phosphorylation (Chen *et al.*, 1992; Murphy *et al.*, 2002). Phosphorylation of c-Fos also enhances its transcriptional activity (Pellegrino and Stork, 2006) and a differentiation-specific gene expression program is induced. In contrast, transient ERK1/2 activation fails to stabilise c-Fos, resulting in the induction of a different, proliferation-specific gene expression programm. Therefore, c-Fos or its phosphorylated version may be definded

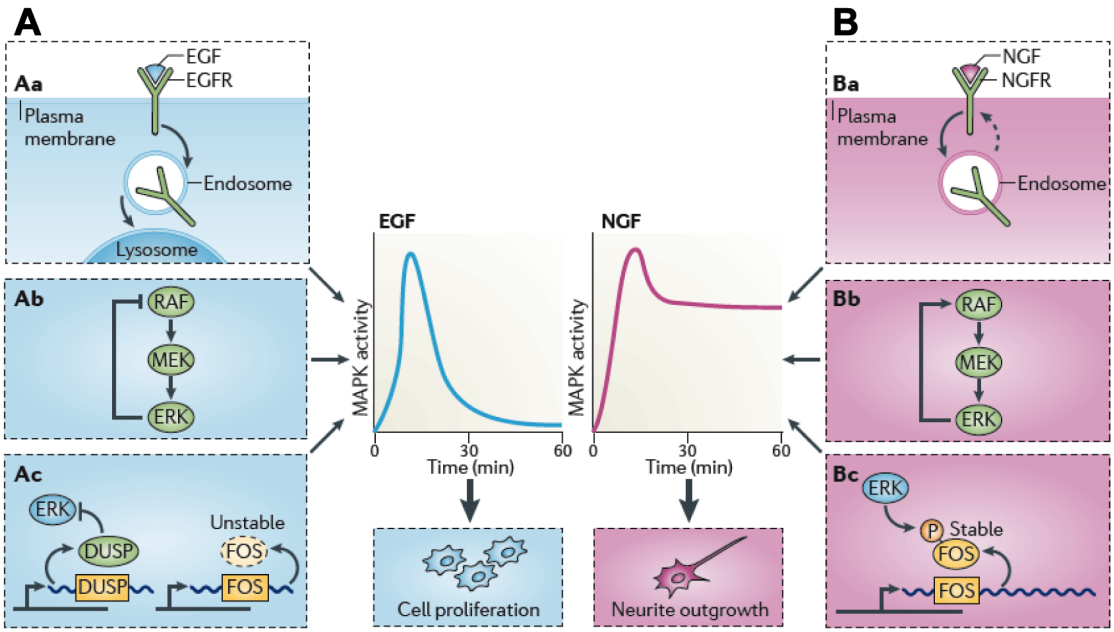

Figure 5.1: Decision making in PC12 cells. Temporal activation profiles of ERK determine cell fate decisions in PC12 cells stimulated with EGF or NGF (cell proliferation versus cell differentiation). Transient (A) versus sustained (B) ERK activation profiles in response to EGF or NGF stimulation, respectively, are shown alongside the underlying signalling mechanisms. Aa) EGF-induced transient ERK activation is determined by rapid degradation of the EGFR. Ab) A negative feedback loop from ERK to Raf ensures rapid signal termination. Ac) ERK mediated induction of MKP transcription finally terminates ERK activity. Resulting transient ERK activity leads to short-lived expression of Fos protein and culminates in a proliferation-specific gene expression programm. Ba) NGF-induced sustained ERK activity is accompanied by receptor recycling. Bb) A positive feedback loop from ERK to Raf results in continuous upstream activation. Bc) Sustained Fos activity (as a result of phosphorylation-mediated stabilisation of the Fos protein) leads to the induction of a differentiation-specific gene expression programm (adapted from Avraham and Yarden, 2011).

as the functional ouput of the system (Murphy *et al.*, 2002, 2004).

The duration of spatio-temporal MAPK signalling also determines cell fate in the ErbB network as - similar to PC12 cells - different stimuli induce different activation kinetics which result in different cell fate decisions. In MCF-7 cells, derived from human breast cancer epithelial adenocarcinoma (Brooks *et al.*, 1973; Soule *et al.*, 1973), stimulation with EGF induces transient ERK1/2 activation encoding for a proliferative signal, while heregulin (HRG) treatment generates sustained ERK1/2 activation resulting in cell differentiation (Thottassery *et al.*, 2004; Nagashima *et al.*, 2007). Indeed, HRG-induced sustained ERK activity also results in sustained RSK activation and subsequently in ERK- and RSK-dependent c-Fos transcription and stabilisation (Fig. 5.2) (Nagashima *et al.*, 2007; Nakakuki *et al.*, 2010).

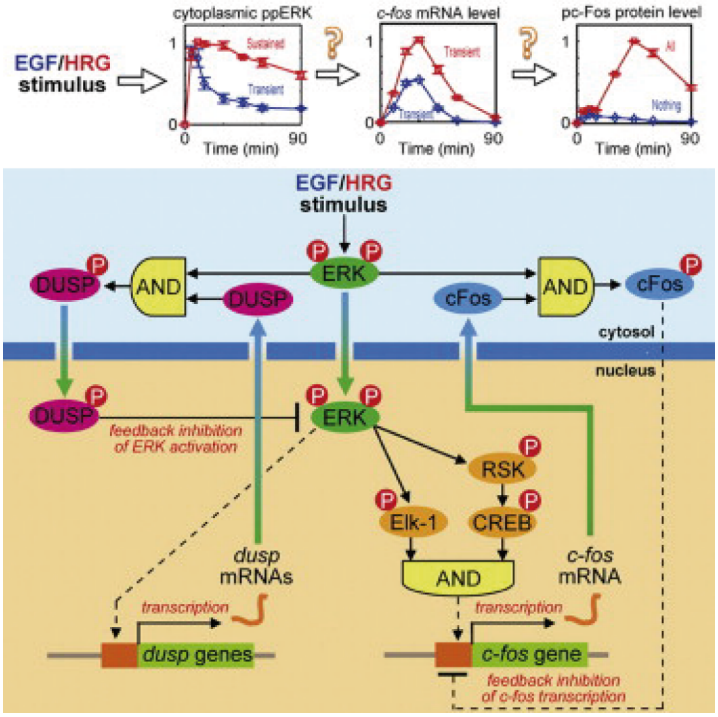

Figure 5.2: Sustained ERK activity results in increased phospho-c-Fos protein levels. EGF and HRG stimulation in MCF-7 cells induce transient versus sustained cytosolic ERK activity. HRG stimulation also leads to increased c-*fos* mRNA and phospho-c-Fos protein levels. (adapted from Nakakuki *et al.*, 2010).

Stabilisation of the IEG product c-Fos by phosphorylation is a hallmark for the activation of differentiation-specific gene expression in PC-12 cells. Based on the finding that HRG stimulation results sustained ERK activation and in a similar type of c-Fos response, it was hypothesised, that the same feedback mechanisms underlying cell fate decisions in PC12 cells also control the MAPK module in MCF-7 cells.

A thorough analysis of the feedback mechanisms incorporated into the MAPK module of MCF-7 cells will be performed using modular response analysis (MRA) (Kholodenko *et al.*, 2002; Santos *et al.*, 2007) and is in progress (data not shown). On the basis of the feedback structure it should be possible to suggest experiments that would rewire the MAPK module in MCF-7 cells in a way that would revert sustained ERK signalling into a transient ERK response and *vice-versa*. While the MRA analysis can be performed without EAS4, the new ERK2 biosensor has already proven to be an invaluable tool to uncover previously inaccessible features of spatial ERK signalling (Fig. 3.22). Analysing the rewiring of feedback loops in the MAPK module by EAS4 would not only be a fast and convient appraoch, but also provide information about the spatio-temporal

dynamics of ERK activation.

Similar to PC12 cells (Corbit *et al.*, 2003; Santos *et al.*, 2007), PKC activity may be required for sustained ERK activation in response to HRG treatment in MCF-7 cells. Preliminary experiments reverting the negative feedback loop in response to EGF stimulation into a positive one by co-activating PKC with PMA, thereby inducing a sustained ERK response (Fig. 3.24), indicate that indeed PKC activity may be involved in sustained ERK signalling in MCF-7 cells. Other experiments will involve the inhibition of PKC by selective chemical inhibitors and knock-down of Raf kinase inhibitory protein (RKIP).

5.3 The role of scaffold proteins in ERK regulation

A different but equally interesting question concerns the mechanism leading to the purely cytosolic nature of HRG-induced sustained ERK activation. Scaffold proteins of the Raf/MEK/ERK module offer likely candidates.

Theoretically, scaffold proteins play two - in part related - functional roles: First, cells use scaffold proteins to maintain a high degree of specificity in signalling pathways. This is achieved by assembling proteins of the same signalling pathway on the scaffold so that interaction and signal propagation is facilitated. Second, scaffolds may catalyse the activation of the pathway components, functioning as an allosteric regulator of catalysis. Here scaffolds may present the kinases towards each other in a manner, that directly enhances their mutual interaction. This could enhance the phosphorylation of the downstream partner (Burack and Shaw, 2000).

One interesting candidate is the scaffold protein kinase suppressor of Ras (KSR). KSR1 was first identified in genetic screens in *Drosophila melanogaster* and *Caenorhabditis elegans* as an modulator of Ras signalling (Kornfeld *et al.*, 1995; Sundaram and Han, 1995; Therrien *et al.*, 1995). KSR displays high structural similarity to proteins of the Raf family (as reviewed in Morrison, 2001) but lacks the key residues essential for catalytic activity of serine/threonine kinases. KSR is able to bind to all members of the Raf/MEK/ERK module, but while a fraction of MEK is constitutively bound, ERK seems to be recruited in a stimulus-dependent manner (Müller *et al.*, 2000; Casar *et al.*, 2008). The interaction of Raf seems to require additional proteins, such as MEK, and seems to be cell-type specific (Therrien *et al.*, 1996; Xing *et al.*, 1997; Nguyen *et al.*, 2002).

Overexpression of KSR has led to the confusing result, that KSR can both enhance and impair Raf/MEK/ERK signalling. This is explained by the nature of scaffold proteins outlined above. Initially, increasing scaffold concentrations enhance the activation of ERK by increasing the number signalling-competent complexes. However, at too high concentrations of scaffold protein, every component of the MAPK module would be bound to a separate KSR molecule and this sequestration would effectively

abrogate activation of ERK by MEK (Burack and Shaw, 2000; Kortum and Lewis, 2004).

Based on the observation that cytosolic substrates of ERK bind in large quantities to KSR upon EGF stimulation, but the binding sites of ERK for these substrates and KSR are vitually identical, Casar *et al.* (2008) proposed that KSR serves as "dimerisation platforms". Upon activation, phosphorylated ERK would dimerise with ERK pre-bound to KSR and would then bind its cytosolic substrate (Fig. 5.3). It has been further reported that the formation of ERK2 dimers and their association with cytosolic scaffold proteins is required for the activation of cytosolic targets of ERK2. At the same time, scaffold proteins and ERK2 dimer formation were not required for activation of nuclear ERK2 substrates (Casar *et al.*, 2008).

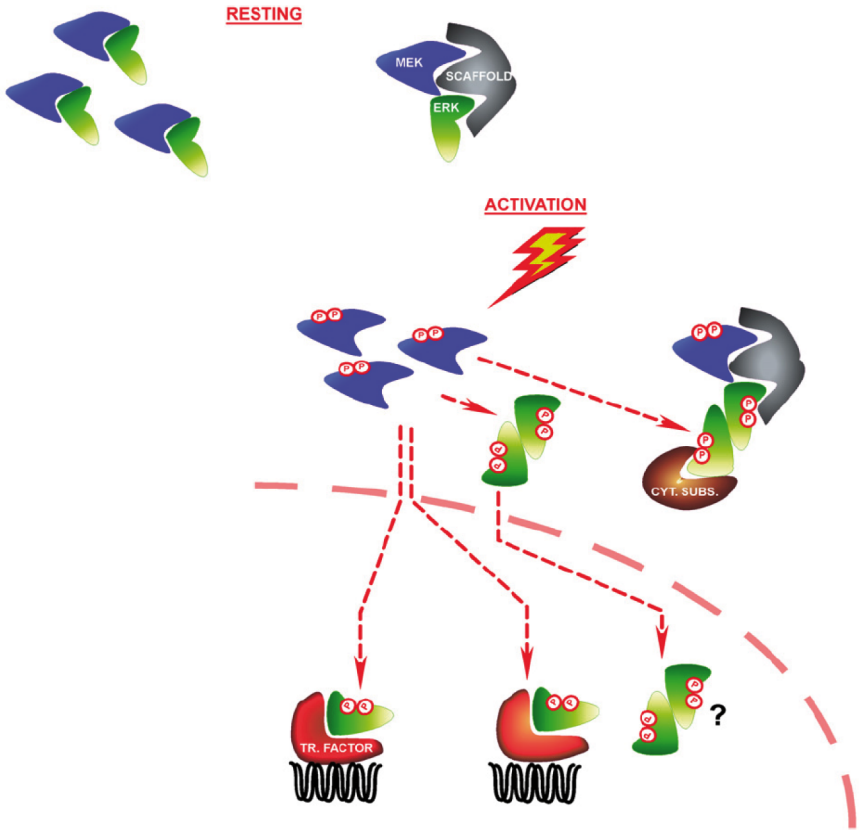

Figure 5.3: A model for the role of KSR in ERK signalling. Under resting coniditons, ERK exists in complex with MEK of KSR. Phosphorylated ERK dissociates from these complexes and monomers may follow three different destinies: (1) ppERK could translocate to the nucleus as a monomer to activate transcription factors. (2) ppERK may dimerise in the cytoplasm. Free dimers could be transported to the nucleus (Khokhlatchev *et al.*, 1998) or remain in the cytosol. The function of free dimers is still unclear. (3) ppERK monomers could associate with ERK monomers in complex with KSR to form a ppERK dimer. The ERK-KSR complex can then interact with cytosolic substrates (adapted from Casar *et al.*, 2008).

In addition, cytosolic ERK2 signalling is essential/required for cellular proliferation and transformation processes as its blocking is sufficient to abrogate proliferative signals, foci formation and tumor growth (Casar *et al.*, 2008). This only seems to contradict earlier reports, that nuclear ERK2 activation is sufficient for cellular transformation (Robinson *et al.*, 1998), but it is possible that the nuclear ERK signal constitutes the main proliferation-driving signal, while the cytosol component of ERK signalling is required as well.

It was therefore proposed that cytosolic ERK2 scaffold proteins, namely KSR, is the main molecular mechanism mediating HRG-induced sustained ERK2 activity in the cytosol. Future research exploring the role of KSR in growth factor-induced sustained ERK signalling would include to analyse the effect of KSR knock-down and/or overexpression on ERK activity (as determined by EAS4).

Interestingly, ERK signalling in T-cells isolated from KSR knock-out mice did not show a change in its digital or graded nature in response to superantigen-loaded antigen-presenting cells or the chemokine SDF-1, when compared to wt mice. In agreement with general scaffold function, only the activation threshold was increased (Lin *et al.*, 2009).

Another interesting candidate to mediate HRG-induced cytosolic signaling may be phosphoprotein enriched in astrocytes (PEA15). PEA15, first isolated from astrocytes (Araujo *et al.*, 1993), binds ERK1/2 and prevents nuclear accumulation of ERK as well as phosphorylation of nuclear ERK substrates. PEA15, however, does not inhibit activation of ERK1/2, nor phosphorylation of cytosolic ERK substrates. As a result, PEA15 blocks ERK-dependent transcription and cell proliferation (Formstecher *et al.*, 2001; Gaumont-Leclerc *et al.*, 2004).

As with KSR, EAS4 would be used to analyse the effect of PEA15 knock-down and/or overexpression on sustained cytosolic ERK activity.

References

Adachi M., Fukuda M., and Nishida E. (1999). Two Co-Existing Mechanisms for Nuclear Import of MAP Kinase: Passive Diffusion of a Monomer and Active Transport of a Dimer. *EMBO J*, **18** (19), 5347–58.

Adachi M., Fukuda M., and Nishida E. (2000). Nuclear Export of MAP Kinase (ERK) Involves a MAP Kinase Kinase (MEK)-Dependent Active Transport Mechanism. *J Cell Biol*, **148** (5), 849–56.

Adams J.A. (2001). Kinetic and catalytic mechanisms of protein kinases. *Chem Rev*, **101** (8), 2271–90.

Adams S.R., Campbell R.E., Gross L.A., Martin B.R., Walkup G.K., Yao Y., Llopis J., and Tsien R.Y. (2002). New Biarsenical Ligands and Tetracysteine Motifs for Protein Labeling in Vitro and in Vivo: Synthesis and Biological Applications. *J Am Chem Soc*, **124** (21), 6063–76.

Ahn N.G., Seger R., Bratlien R.L., Diltz C.D., Tonks N.K., and Krebs E.G. (1991). Multiple Components in an Epidermal Growth Factor-Stimulated Protein Kinase Cascade. In Vitro Activation of a Myelin Basic Protein/Microtubule-Associated Protein 2 Kinase. *J Biol Chem*, **266** (7), 4220–7.

Ando R., Mizuno H., and Miyawaki A. (2004). Regulated Fast Nucleocytoplasmic Shuttling Observed by Reversible Protein Highlighting. *Science*, **306** (5700), 1370–3.

Andresen M., Schmitz-Salue R., and Jakobs S. (2004). Short Tetracysteine Tags to beta-Tubulin Demonstrate the Significance of Small Labels for Live Cell Imaging. *Mol Biol Cell*, **15** (12), 5616–22.

Aoki K., Kiyokawa E., Nakamura T., and Matsuda M. (2008). Visualization of Growth Signal Transduction Cascades in Living Cells With Genetically Encoded Probes Based on Förster Resonance Energy Transfer. *Philos Trans R Soc Lond B Biola Sci*, **363** (1500), 2143–51.

Araujo H., Danziger N., Cordier J., Glowinski J., and Chneiweiss H. (1993). Characterization of PEA-15, a Major Substrate for Protein Kinase C in Astrocytes. *J Biol Chem*, **268** (8), 5911–20.

Avraham R. and Yarden Y. (2011). Feedback Regulation of EGFR Signalling: Decision Making by Early and Delayed Loops. *Nat Rev Mol Cell Biol*, **12** (2), 104–17.

Bastiaens P.I., Majoul I.V., Verveer P.J., Söling H.D., and Jovin T.M. (1996). Imaging the Intracellular Trafficking and State of the AB5 Quaternary Structure of Cholera Toxin. *EMBO J*, **15** (16), 4246–53.

Bastiaens P.I. and Pepperkok R. (2000). Observing Proteins in Their Natural Habitat: the Living Cell. *Trends Biochem Sci*, **25** (12), 631–7.

Bastiaens P.I. and Squire A. (1999). Fluorescence Lifetime Imaging Microscopy: Spatial Resolution of Biochemical Processes in the Cell. *Trends Cell Biol*, **9** (2), 48–52.

Blanco-Aparicio C., Torres J., and Pulido R. (1999). A Novel Regulatory Mechanism of MAP Kinases Activation and Nuclear Translocation Mediated by PKA and the PTP-SL Tyrosine Phosphatase. *J Cell Biol*, **147** (6), 1129–36.

Blüthgen N., Bruggeman F.J., Legewie S., Herzel H., Westerhoff H.V., and Kholodenko B.N. (2006). Effects of Sequestration on Signal Transduction Cascades. *FEBS J*, **273** (5), 895–906.

Breusegem S.Y., Levi M., and Barry N.P. (2006). Fluorescence Correlation Spectroscopy and Fluorescence Lifetime Imaging Microscopy. *Nephron Exp Nephrol*, **103** (2), e41–9.

Brooks S.C., Locke E.R., and Soule H.D. (1973). Estrogen Receptor in a Human Cell Line (MCF-7) from Breast Carcinoma. *J Biol Chem*, **248** (17), 6251–3.

Brown G.C. and Kholodenko B.N. (1999). Spatial Gradients of Cellular Phospho-Proteins. *FEBS Lett*, **457** (3), 452–4.

Brunet A., Pagès G., and Pouysségur J. (1994). Growth Factor-Stimulated MAP Kinase Induces Rapid Retrophosphorylation and Inhibition of MAP Kinase Kinase (MEK1). *FEBS Lett*, **346** (2-3), 299–303.

Burack W.R. and Shaw A.S. (2000). Signal Transduction: Hanging on a Scaffold. *Curr Opin Cell Biol*, **12** (2), 211–6.

Burack W.R. and Shaw A.S. (2005). Live Cell Imaging of ERK and MEK: Simple Binding Equilibrium Explains the Regulated Nucleocytoplasmic Distribution of ERK. *J Biol Chem*, **280** (5), 3832–7.

Cailleau R., Young R., Olivé M., and Reeves Jr W.J. (1974). Breast Tumor Cell Lines from Pleural Effusions. *J Natl Cancer Inst*, **53** (3), 661–74.

Camps M., Nichols A., and Arkinstall S. (2000). Dual Specificity Phosphatases: a Gene Family for Control of MAP Kinase Function. *FASEB J*, **14** (1), 6–16.

Canagarajah B.J., Khokhlatchev A., Cobb M.H., and Goldsmith E.J. (1997). Activation Mechanism of the MAP Kinase ERK2 by Dual Phosphorylation. *Cell*, **90** (5), 859–69.

Casar B., Pinto A., and Crespo P. (2008). Essential Role of ERK Dimers in the Activation of Cytoplasmic But Not Nuclear Substrates by ERK-Scaffold Complexes. *Mol Cell*, **31** (5), 708–21.

Casar B., Pinto A., and Crespo P. (2009). ERK Dimers and Scaffold Proteins: Unexpected Partners for a Forgotten (Cytoplasmic) Task. *Cell Cycle*, **8** (7), 1007–13.

Chang L. and Karin M. (2001). Mammalian MAP Kinase Signalling Cascades. *Nature*, **410** (6824), 37–40.

Chen C.H., Wang W.J., Kuo J.C., Tsai H.C., Lin J.R., Chang Z.F., and Chen R.H. (2005). Bidirectional Signals Transduced by DAPK-ERK Interaction Promote the Apoptotic Effect of DAPK. *EMBO J*, **24** (2), 294–304.

Chen Q., Olashaw N., and Wu J. (1995). Participation of Reactive Oxygen Species in the Lysophosphatidic Acid-Stimulated Mitogen-Activated Protein Kinase Kinase Activation Pathway. *J Biol Chem*, **270** (48), 28499–502.

Chen R.H., Sarnecki C., and Blenis J. (1992). Nuclear Localization and Regulation of ERK- and RSK-Encoded Protein Kinases. *Mol Cell Biol*, **12** (3), 915–27.

Chen Y., Mills J.D., and Periasamy A. (2003). Protein Localization in Living Cells and Tissues Using FRET and FLIM. *Differentiation*, **71** (9-10), 528–41.

Chen Z., Gibson T.B., Robinson F., Silvestro L., Pearson G., Xu B., Wright A., Vanderbilt C., and Cobb M.H. (2001). MAP Kinases. *Chem Rev*, **101** (8), 2449–76.

Chuderland D., Konson A., and Seger R. (2008). Identification and Characterization of a General Nuclear Translocation Signal in Signaling Proteins. *Mol Cell*, **31** (6), 850–61.

Cohen-Saidon C., Cohen A.A., Sigal A., Liron Y., and Alon U. (2009). Dynamics and Variability of ERK2 Response to EGF in Individual Living Cells. *Mol Cell*, **36** (5), 885–93.

Copeland M.F., Flickinger S.T., Tuson H.H., and Weibel D.B. (2010). Studying the Dynamics of Flagella in Multicellular Communities of Escherichia Coli by Using Biarsenical Dyes. *Appl Environ Microbiol*, **76** (4), 1241–50.

Corbit K.C., Trakul N., Eves E.M., Diaz B., Marshall M., and Rosner M.R. (2003). Activation of Raf-1 Signaling by Protein Kinase C Through a Mechanism Involving Raf Kinase Inhibitory Protein. *J Biol Chem*, **278** (15), 13061–8.

Corish P. and Tyler-Smith C. (1999). Attenuation of Green Fluorescent Protein Half-Life in Mammalian Cells. *Protein Eng*, **12** (12), 1035–40.

Costa M., Marchi M., Cardarelli F., Roy A., Beltram F., Maffei L., and Ratto G.M. (2006). Dynamic Regulation of ERK2 Nuclear Translocation and Mobility in Living Cells. *J Cell Sci*, **119** (Pt 23), 4952–63.

Countaway J.L., Nairn A.C., and Davis R.J. (1992). Mechanism of Desensitization of the Epidermal Growth Factor Receptor Protein-Tyrosine Kinase. *J Biol Chem*, **267** (2), 1129–40.

Debata P.R., Ranasinghe B., Berliner A., Curcio G.M., Tantry S.J., Ponimaskin E., and Banerjee P. (2010). Erk1/2-Dependent Phosphorylation of PKCalpha at Threonine 638 in Hippocampal 5-HT(1A) Receptor-Mediated Signaling. *Biochem Biophys Res Commun*, **397** (3), 401–6.

Dehmelt L. and Bastiaens P.I.H. (2010). Spatial Organization of Intracellular Communication: Insights from Imaging. *Nat Rev Mol Cell Biol*, **11** (6), 440–52.

Dhillon A.S., Hagan S., Rath O., and Kolch W. (2007). MAP Kinase Signalling Pathways in Cancer. *Oncogene*, **26** (22), 3279–90.

Di Guglielmo G.M., Baass P.C., Ou W.J., Posner B.I., and Bergeron J.J. (1994). Compartmentalization of SHC, GRB2 and mSOS, and Hyperphosphorylation of Raf-1 by EGF But Not Insulin in Liver Parenchyma. *EMBO J*, **13** (18), 4269–77.

Dittrich P., Malvezzi-Campeggi F., Jahnz M., and Schwille P. (2001). Accessing Molecular Dynamics in Cells by Fluorescence Correlation Spectroscopy. *Biol Chem*, **382** (3), 491–4.

Ebisuya M., Kondoh K., and Nishida E. (2005). The Duration, Mmagnitude and Compartmentalization of ERK MAP Kinase Activity: Mechanisms for Providing Signaling Specificity. *J Cell Sci*, **118** (Pt 14), 2997–3002.

Elangovan M., Wallrabe H., Chen Y., Day R.N., Barroso M., and Periasamy A. (2003). Characterization of One- and Two-Photon Excitation Fluorescence Resonance Energy Transfer Microscopy. *Methods*, **29** (1), 58–73.

Emrick M.A., Hoofnagle A.N., Miller A.S., Ten Eyck L.F., and Ahn N.G. (2001). Constitutive Activation of Extracellular Signal-Regulated Kinase 2 by Synergistic Point Mutations. *J Biol Chem*, **276** (49), 46469–79.

Fantz D.A., Jacobs D., Glossip D., and Kornfeld K. (2001). Docking Sites on Substrate Proteins Direct Extracellular Signal-Regulated Kinase to Phosphorylate Specific Residues. *J Biol Chem*, **276** (29), 27256–65.

Fernandes N., Bailey D.E., Vanvranken D.L., and Allbritton N.L. (2007). Use of Docking Peptides to Design Modular Substrates With High Efficiency for Mitogen-Activated Protein Kinase Extracellular Signal-Regulated Kinase. *ACS Chem Biol*, **2** (10), 665–73.

Ferrell Jr J.E. (1996). Tripping the Switch Fantastic: How a Protein Kinase Cascade Can Convert Graded Inputs Into Switch-Like Outputs. *Trends Biochem Sci*, **21** (12), 460–6.

Ferrell Jr J.E. and Bhatt R.R. (1997). Mechanistic Studies of the Dual Phosphorylation of Mitogen-Activated Protein Kinase. *J Biol Chem*, **272** (30), 19008–16.

Festy F., Ameer-Beg S.M., Ng T., and Suhling K. (2007). Imaging Proteins in Vivo Using Fluorescence Lifetime Microscopy. *Mol Biosyst*, **3** (6), 381–91.

Formstecher E., Ramos J.W., Fauquet M., Calderwood D.A., Hsieh J.C., Canton B., Nguyen X.T., Barnier J.V., Camonis J., Ginsberg M.H., and Chneiweiss H. (2001). PEA-15 Mediates Cytoplasmic Sequestration of ERK MAP Kinase. *Dev Cell*, **1** (2), 239–50.

Fujioka A., Terai K., Itoh R.E., Aoki K., Nakamura T., Kuroda S., Nishida E., and Matsuda M. (2006). Dynamics of the Ras/ERK MAPK Cascade as Monitored by Fluorescent Probes. *J Biol Chem*, **281** (13), 8917–26.

Fukuda M., Gotoh Y., and Nishida E. (1997). Interaction of MAP Kinase With MAP Kinase Kinase: Its Possible Role in the Control of Nucleocytoplasmic Transport of MAP Kinase. *EMBO J*, **16** (8), 1901–8.

Gaietta G., Deerinck T.J., Adams S.R., Bouwer J., Tour O., Laird D.W., Sosinsky G.E., Tsien R.Y., and Ellisman M.H. (2002). Multicolor and Electron Microscopic Imaging of Connexin Trafficking. *Science*, **296** (5567), 503–7.

Galperin E., Verkhusha V.V., and Sorkin A. (2004). Three-Chromophore FRET Microscopy to Analyze Multiprotein Interactions in Living Cells. *Nat Methods*, **1** (3), 209–17.

Gaspersic J., Hafner-Bratkovic I., Stephan M., Veranic P., Bencina M., Vorberg I., and Jerala R. (2010). Tetracysteine-Tagged Prion Protein Allows Discrimination Between the Native and Converted Forms. *FEBS J*, **277** (9), 2038–50.

Gaumont-Leclerc M.F., Mukhopadhyay U.K., Goumard S., and Ferbeyre G. (2004). PEA-15 Is Inhibited by Adenovirus E1A and Plays a Role in ERK Nuclear Export and Ras-Induced Senescence. *J Biol Chem*, **279** (45), 46802–9.

Gey G.O., Coffman W.D., and Kubicek M.T. (1952). Tissue Culture Studies of the Proliferative Capacity of Cervical Carcinoma and Normal Epithelium. *Cancer Research*, **12**, 264–265.

Giepmans B.N.G., Adams S.R., Ellisman M.H., and Tsien R.Y. (2006). The Fluorescent Toolbox for Assessing Protein Location and Function. *Science*, **312** (5771), 217–24.

Gille H., Kortenjann M., Thomae O., Moomaw C., Slaughter C., Cobb M.H., and Shaw P.E. (1995). ERK Phosphorylation Potentiates Elk-1-Mediated Ternary Complex Formation and Transactivation. *EMBO J*, **14** (5), 951–62.

Gluzman Y. (1981). SV40-Ttransformed Simian Cells Support the Replication of Early SV40 Mutants. *Cell*, **23** (1), 175–82.

Gonzalez F.A., Raden D.L., and Davis R.J. (1991). Identification of Substrate Recognition Determinants for Human ERK1 and ERK2 Protein Kinases. *J Biol Chem*, **266** (33), 22159–63.

Gonzalez F.A., Seth A., Raden D.L., Bowman D.S., Fay F.S., and Davis R.J. (1993). Serum-Induced Translocation of Mitogen-Activated Protein Kinase to the Cell Surface Ruffling Membrane and the Nucleus. *J Cell Biol*, **122** (5), 1089–101.

Gordon G.W., Berry G., Liang X.H., Levine B., and Herman B. (1998). Quantitative Fluorescence Resonance Energy Transfer Measurements Using Fluorescence Microscopy. *Biophys J*, **74** (5), 2702–13.

Gotoh Y., Nishida E., Yamashita T., Hoshi M., Kawakami M., and Sakai H. (1990). Microtubule-Associated-Protein (MAP) Kinase Activated by Nerve Growth Factor and Epidermal Growth Factor in PC12 Cells. Identity With the Mitogen-Activated MAP Kinase of Fibroblastic Cells. *Eur J Biochem*, **193** (3), 661–9.

Gratton E., Breusegem S., Sutin J., Ruan Q., and Barry N. (2003). Fluorescence Lifetime Imaging for the Two-Photon Microscope: Time-Domain and Frequency-Domain Methods. *J Biomed Opt*, **8** (3), 381–90.

Grecco H.E., Roda-Navarro P., Girod A., Hou J., Frahm T., Truxius D.C., Pepperkok R., Squire A., and Bastiaens P.I.H. (2010). In Situ Analysis of Tyrosine Phosphorylation Networks by FLIM on Cell Arrays. *Nat Methods*, **7** (6), 467–72.

Grecco H.E., Roda-Navarro P., and Verveer P.J. (2009). Global Analysis of Time Correlated Single Photon Counting FRET-FLIM Data. *Opt Express*, **17** (8), 6493–508.

Grecco H.E. and Verveer P.J. (2011). FRET in Cell Biology: Still Shining in the Age of Super-Resolution? *Chemphyschem*, **12** (3), 484–90.

Green H.M. and Alberola-Ila J. (2005). Development of ERK Activity Sensor, an in Vitro, FRET-Based Sensor of Extracellular Regulated Kinase Activity. *BMC Chem Biol*, **5**, 1.

Greene L.A. and Tischler A.S. (1976). Establishment of a Noradrenergic Clonal Line of Rat Adrenal Pheochromocytoma Cells Which Respond to Nerve Growth Factor. *Proc Natl Acad Sci USA*, **73** (7), 2424–8.

Griffin B.A., Adams S.R., and Tsien R.Y. (1998). Specific Covalent Labeling of Recombinant Protein Molecules Inside Live Cells. *Science*, **281** (5374), 269–72.

Grünberg R. and Serrano L. (2010). Strategies for Protein Synthetic Biology. *Nucleic Acids Res*, **38** (8), 2663–75.

Harvey C.D., Ehrhardt A.G., Cellurale C., Zhong H., Yasuda R., Davis R.J., and Svoboda K. (2008a). A Genetically Encoded Fluorescent Sensor of ERK Activity. *Proc Natl Acad Sci USA*, **105** (49), 19264–9.

Harvey C.D., Yasuda R., Zhong H., and Svoboda K. (2008b). The Spread of Ras Activity Triggered by Activation of a Single Dendritic Spine. *Science*, **321** (5885), 136–40.

Haustein E. and Schwille P. (2003). Ultrasensitive Investigations of Biological Systems by Fluorescence Correlation Spectroscopy. *Methods*, **29** (2), 153–66.

Hoffmann C., Gaietta G., Bünemann M., Adams S.R., Oberdorff-Maass S., Behr B., Vilardaga J.P., Tsien R.Y., Ellisman M.H., and Lohse M.J. (2005). A FlAsH-Based FRET Approach to Determine G Protein-Coupled Receptor Activation in Living Cells. *Nat Methods*, **2** (3), 171–6.

Howe C.L. (2005). Modeling the Signaling Endosome Hypothesis: Why a Drive to the Nucleus Is Better Than a (Random) Walk. *Theor Biol Med Model*, **2**, 43.

Howe C.L. and Mobley W.C. (2004). Signaling Endosome Hypothesis: A Cellular Mechanism for Long Distance Communication. *J Neurobiol*, **58** (2), 207–16.

Huff K., End D., and Guroff G. (1981). Nerve Growth Factor-Induced Alteration in the Response of PC12 Pheochromocytoma Cells to Epidermal Growth Factor. *J Cell Biol*, **88** (1), 189–98.

Hwang R.D., Chen C.C., and Knecht D.A. (2009). ReAsH: Another Viable Option for in Vivo Protein Labelling in Dictyostelium. *J Microsc*, **234** (1), 9–15.

Itoh R.E., Kurokawa K., Ohba Y., Yoshizaki H., Mochizuki N., and Matsuda M. (2002). Activation of Rac and Cdc42 Video Imaged by Fluorescent Resonance Energy Transfer-Based Single-Molecule Probes in the Membrane of Living cells. *Mol Cell Biol*, **22** (18), 6582–91.

Jacobs D., Glossip D., Xing H., Muslin A.J., and Kornfeld K. (1999). Multiple Docking Sites on Substrate Proteins Form a Modular System That Mediates Recognition by ERK MAP Kinase. *Genes Dev*, **13** (2), 163–75.

Janknecht R., Zinck R., Ernst W.H., and Nordheim A. (1994). Functional Dissection of the Transcription Factor Elk-1. *Oncogene*, **9** (4), 1273–8.

Jiang X. and Sorkin A. (2002). Coordinated Traffic of Grb2 and Ras During Epidermal Growth Factor Receptor Endocytosis Visualized in Living Cells. *Mol Biol Cell*, **13** (5), 1522–35.

Jovin T.M. and Arndt-Jovin D.J. (1989). Luminescence Digital Imaging Microscopy. *Annu Rev Biophys Biophys Chem*, **18**, 271–308.

Kahan C., Seuwen K., Meloche S., and Pouysségur J. (1992). Coordinate, Biphasic Activation of p44 Mitogen-Activated Protein Kinase and S6 Kinase by Growth Factors in Hamster Fibroblasts. Evidence for Thrombin-Induced Signals Different from Phosphoinositide Turnover and Adenylylcyclase Inhibition. *J Biol Chem*, **267** (19), 13369–75.

Kenworthy A.K. (2001). Imaging Protein-Protein Interactions Using Fluorescence Resonance Energy Transfer Microscopy. *Methods*, **24** (3), 289–96.

Kettling U., Koltermann A., Schwille P., and Eigen M. (1998). Real-Time Enzyme Kinetics Monitored by Dual-Color Fluorescence Cross-Correlation Spectroscopy. *Proc Natl Acad Sci USA*, **95** (4), 1416–20.

Khokhlatchev A., Xu S., English J., Wu P., Schaefer E., and Cobb M.H. (1997). Reconstitution of Mitogen-Activated Protein Kinase Phosphorylation Cascades in Bacteria. Efficient Synthesis of Active Protein Kinases. *J Biol Chem*, **272** (17), 11057–62.

Khokhlatchev A.V., Canagarajah B., Wilsbacher J., Robinson M., Atkinson M., Goldsmith E., and Cobb M.H. (1998). Phosphorylation of the MAP Kinase ERK2 Promotes Its Homodimerization and Nuclear Translocation. *Cell*, **93** (4), 605–15.

Kholodenko B.N. (2000). Negative Feedback and Ultrasensitivity Can Bring About Oscillations in the Mitogen-Activated Protein Kinase Cascades. *Eur J Biochem*, **267** (6), 1583–8.

Kholodenko B.N. (2006). Cell-Signalling Dynamics in Time and Space. *Nat Rev Mol Cell Biol*, **7** (3), 165–76.

Kholodenko B.N., Kiyatkin A., Bruggeman F.J., Sontag E., Westerhoff H.V., and Hoek J.B. (2002). Untangling the Wires: a Strategy to Trace Functional Interactions in Signaling and Gene Networks. *Proc Natl Acad Sci USA*, **99** (20), 12841–6.

Kolch W. (2005). Coordinating ERK/MAPK Signalling Through Scaffolds and Inhibitors. *Nat Rev Mol Cell Biol*, **6** (11), 827–37.

Kornfeld K., Hom D.B., and Horvitz H.R. (1995). The KSR-1 Gene Encodes a Novel Protein Kinase Involved in Ras-Mediated Signaling in C. Elegans. *Cell*, **83** (6), 903–13.

Kortum R.L. and Lewis R.E. (2004). The Molecular Scaffold KSR1 Regulates the Proliferative and Oncogenic Potential of Cells. *Mol Cell Biol*, **24** (10), 4407–16.

Kranenburg O., Verlaan I., and Moolenaar W.H. (1999). Dynamin Is Required for the Activation of Mitogen-Activated Protein (MAP) Kinase by MAP Kinase Kinase. *J Biol Chem*, **274** (50), 35301–4.

Lakowicz J.R. (2006). *Principles of Fluorescence Spectroscopy*, Chapter 4. Time-Domain Lifetime Measurements. Springer Science+Business Media, LLC, New York, USA, 3rd Edition.

Lee R.M., Cobb M.H., and Blackshear P.J. (1992). Evidence that Extracellular Signal-Regulated Kinases are the Insulin-Activated Raf-1 Kinase Kinases. *J Biol Chem*, **267** (2), 1088–92.

Lee T., Hoofnagle A.N., Kabuyama Y., Stroud J., Min X., Goldsmith E.J., Chen L., Resing K.A., and Ahn N.G. (2004). Docking Motif Interactions in MAP Kinases Revealed by Hydrogen Exchange Mass Spectrometry. *Mol Cell*, **14** (1), 43–55.

Lenormand P., Brondello J.M., Brunet A., and Pouysségur J. (1998). Growth Factor-Induced p42/p44 MAPK Nuclear Translocation and Retention Requires Both MAPK Activation and Neosynthesis of Nuclear Anchoring Proteins. *J Cell Biol*, **142** (3), 625–33.

Lenormand P., Sardet C., Pagès G., L'Allemain G., Brunet A., and Pouysségur J. (1993). Growth Factors Induce Nuclear Translocation of MAP Kinases (p42MAPK and p44MAPK) But Not of Their Activator MAP Kinase Kinase (p45MAPKK) in Fibroblasts. *J Cell Biol*, **122** (5), 1079–88.

Li I.T., Pham E., and Truong K. (2006). Protein Biosensors Based on the Principle of Fluorescence Resonance Energy Transfer for Monitoring Cellular Dynamics. *Biotechnol Lett*, **28** (24), 1971–82.

Lidke D.S., Huang F., Post J.N., Rieger B., Wilsbacher J., Thomas J.L., Pouysségur J., Jovin T.M., and Lenormand P. (2010). ERK Nuclear Translocation Is Dimerization-Independent But Controlled by the Rate of Phosphorylation. *J Biol Chem*, **285** (5), 3092–102.

Lin J., Harding A., Giurisato E., and Shaw A.S. (2009). KSR1 Modulates the Sensitivity of Mitogen-Activated Protein Kinase Pathway Activation in T Cells Without Altering Fundamental System Outputs. *Mol Cell Biol*, **29** (8), 2082–91.

Lisenbee C.S., Karnik S.K., and Trelease R.N. (2003). Overexpression and Mislocalization of a Tail-Anchored GFP Redefines the Identity of Peroxisomal ER. *Traffic*, **4** (7), 491–501.

Madani F., Lind J., Damberg P., Adams S.R., Tsien R.Y., and Gräslund A.O. (2009). Hairpin Structure of a Biarsenical-Tetracysteine Motif Determined by NMR Spectroscopy. *J Am Chem Soc*, **131** (13), 4613–5.

Maeder C.I., Hink M.A., Kinkhabwala A., Mayr R., Bastiaens P.I.H., and Knop M. (2007). Spatial Regulation of Fus3 MAP Kinase Activity Through a Reaction-Diffusion Mechanism in Yeast Pheromone Signalling. *Nat Cell Biol*, **9** (11), 1319–26.

Maier-Peuschel M., Frölich N., Dees C., Hommers L.G., Hoffmann C., Nikolaev V.O., and Lohse M.J. (2010). A Fluorescence Resonance Energy Transfer-Based M2 Muscarinic Receptor Sensor Reveals Rapid Kinetics of Allosteric Modulation. *J Biol Chem*, **285** (12), 8793–800.

Markevich N.I., Tsyganov M.A., Hoek J.B., and Kholodenko B.N. (2006). Long-Range Signaling by Phosphoprotein Waves Arising from Bistability in Protein Kinase Cascades. *Mol Syst Biol*, **2**, 61.

Marshall C.J. (1995). Specificity of Receptor Tyrosine Kinase Signaling: Transient Versus Sustained Extracellular Signal-Regulated Kinase Activation. *Cell*, **80** (2), 179–85.

Martin B.R., Deerinck T.J., Ellisman M.H., Taylor S.S., and Tsien R.Y. (2007). Isoform-Specific PKA Dynamics Revealed by Dye-Triggered Aggregation and DAKAP1alpha-Mediated Localization in Living Cells. *Chem Biol*, **14** (9), 1031–42.

Martin B.R., Giepmans B.N.G., Adams S.R., and Tsien R.Y. (2005). Mammalian Cell-Based Optimization of the Biarsenical-Binding Tetracysteine Motif for Improved Fluorescence and Affinity. *Nat Biotechnol*, **23** (10), 1308–14.

Matsuura I., Wang G., He D., and Liu F. (2005). Identification and Characterization of ERK MAP Kinase Phosphorylation Sites in Smad3. *Biochemistry*, **44** (37), 12546–53.

McLean P.J., Kawamata H., and Hyman B.T. (2001). Alpha-Synuclein-Enhanced Green Fluorescent Protein Fusion Proteins Form Proteasome Sensitive Inclusions in Primary Neurons. *Neuroscience*, **104** (3), 901–12.

Miyawaki A. (2003). Visualization of the Spatial and Temporal Dynamics of Intracellular Signaling. *Dev Cell*, **4** (3), 295–305.

Miyawaki A., Llopis J., Heim R., McCaffery J.M., Adams J.A., Ikura M., and Tsien R.Y. (1997). Fluorescent Indicators for Ca2+ Based on Green Fluorescent Proteins and Calmodulin. *Nature*, **388** (6645), 882–7.

Morrison D.K. (2001). KSR: a MAPK Scaffold of the Ras Pathway? *J Cell Sci*, **114** (Pt 9), 1609–12.

Mülhardt C. (2003). *Der Experimentator: Molekularbiologie/Genomics*, Chapter 4. Die Polymerase-Kettenreaktion (PCR). Elsevier, Spektrum Akademischer Verlag, Heidelberg/Berlin, 4th Edition.

Müller J., Cacace A.M., Lyons W.E., McGill C.B., and Morrison D.K. (2000). Identification of B-KSR1, a Novel Brain-Specific Isoform of KSR1 That Functions in Neuronal Signaling. *Mol Cell Biol*, **20** (15), 5529–39.

Murphy L.O., MacKeigan J.P., and Blenis J. (2004). A Network of Immediate Early Gene Products Propagates Subtle Differences in Mitogen-Activated Protein Kinase Signal Amplitude and Duration. *Mol Cell Biol*, **24** (1), 144–53.

Murphy L.O., Smith S., Chen R.H., Fingar D.C., and Blenis J. (2002). Molecular Interpretation of ERK Signal Duration by Immediate Early Gene Products. *Nat Cell Biol*, **4** (8), 556–64.

Nagashima T., Shimodaira H., Ide K., Nakakuki T., Tani Y., Takahashi K., Yumoto N., and Hatakeyama M. (2007). Quantitative Transcriptional Control of ErbB Receptor Signaling Undergoes Graded to Biphasic Response for Cell Differentiation. *J Biol Chem*, **282** (6), 4045–56.

Nakakuki T., Birtwistle M.R., Saeki Y., Yumoto N., Ide K., Nagashima T., Brusch L., Ogunnaike B.A., Okada-Hatakeyama M., and Kholodenko B.N. (2010). Ligand-Specific c-Fos Expression Emerges from the Spatiotemporal Control of ErbB Network Dynamics. *Cell*, **141** (5), 884–96.

Nakanishi J., Takarada T., Yunoki S., Kikuchi Y., and Maeda M. (2006). FRET-Based Monitoring of Conformational Change of the beta2 Adrenergic Receptor in Living Cells. *Biochem Biophys Res Commun*, **343** (4), 1191–6.

Nelson D.L. and Cox M.M. (2004). *Lehninger - Principles of Biochemistry*, Chapter 6. Enzymes. Springer-Verlag, Berlin, Heidelberg, New York, 4th Edition.

Nguyen A., Burack W.R., Stock J.L., Kortum R., Chaika O.V., Afkarian M., Muller W.J., Murphy K.M., Morrison D.K., Lewis R.E., McNeish J., and Shaw A.S. (2002). Kinase Suppressor of Ras (KSR) Is a Scaffold Which Facilitates Mitogen-Activated Protein Kinase Activation in Vivo. *Mol Cell Biol*, **22** (9), 3035–45.

Nguyen A.W. and Daugherty P.S. (2005). Evolutionary Optimization of Fluorescent Proteins for Intracellular FRET. *Nat Biotechnol*, **23** (3), 355–60.

Niethammer P., Bastiaens P., and Karsenti E. (2004). Stathmin-Tubulin Interaction Gradients in Motile and Mitotic Cells. *Science*, **303** (5665), 1862–6.

Niethammer P., Kronja I., Kandels-Lewis S., Rybina S., Bastiaens P., and Karsenti E. (2007). Discrete states of a protein interaction network govern interphase and mitotic microtubule dynamics. *PLoS Biol*, **5** (2), e29.

Nikolaev V.O., Hoffmann C., Bünemann M., Lohse M.J., and Vilardaga J.P. (2006). Molecular Basis of Partial Agonism at the Neurotransmitter alpha2A-Adrenergic Receptor and Gi-Protein Heterotrimer. *J Biol Chem*, **281** (34), 24506–11.

Obrietan K., Impey S., and Storm D.R. (1998). Light and Circadian Rhythmicity Regulate MAP Kinase Activation in the Suprachiasmatic Nuclei. *Nat Neurosci*, **1** (8), 693–700.

O'Neill E. and Kolch W. (2004). Conferring Specificity on the Ubiquitous Raf/MEK Signalling Pathway. *Br J Cancer*, **90** (2), 283–8.

Padilla-Parra S., Audugé N., Lalucque H., Mevel J.C., Coppey-Moisan M., and Tramier M. (2009). Quantitative Comparison of Different Fluorescent Protein Couples for Fast FRET-FLIM Acquisition. *Biophys J*, **97** (8), 2368–76.

Pagès G., Brunet A., L'Allemain G., and Pouysségur J. (1994). Constitutive Mutant and Putative Regulatory Serine Phosphorylation Site of Mammalian MAP Kinase Kinase (MEK1). *EMBO J*, **13** (13), 3003–10.

Payne D.M., Rossomando A.J., Martino P., Erickson A.K., Her J.H., Shabanowitz J., Hunt D.F., Weber M.J., and Sturgill T.W. (1991). Identification of the Regulatory Phosphorylation Sites in p42/Mitogen-Activated Protein Kinase (MAP Kinase). *EMBO J*, **10** (4), 885–92.

Pelet S., Previte M.J.R., and So P.T.C. (2006). Comparing the Quantification of Forster Resonance Energy Transfer Measurement Accuracies Based on Intensity, Spectral, and Lifetime Imaging. *J Biomed Opt*, **11** (3), 34017.

Pellegrino M.J. and Stork P.J.S. (2006). Sustained Activation of Extracellular Signal-Regulated Kinase by Nerve Growth Factor Regulates c-Fos Protein Stabilization and Transactivation in PC12 Cells. *J Neurochem*, **99** (6), 1480–93.

Pertz O. (2010). Spatio-Temporal Rho GTPase Signaling - Where Are We Now? *J Cell Sci*, **123** (Pt 11), 1841–50.

Pertz O., Hodgson L., Klemke R.L., and Hahn K.M. (2006). Spatiotemporal Dynamics of RhoA Activity in Migrating Cells. *Nature*, **440** (7087), 1069–72.

Peter M. and Ameer-Beg S.M. (2004). Imaging Molecular Interactions by Multiphoton FLIM. *Biol Cell*, **96** (3), 231–6.

Pierce K.L., Maudsley S., Daaka Y., Luttrell L.M., and Lefkowitz R.J. (2000). Role of Endocytosis in the Activation of the Extracellular Signal-Regulated Kinase Cascade by Sequestering and Nonsequestering G Protein-Coupled Receptors. *Proc Natl Acad Sci USA*, **97** (4), 1489–94.

Pingoud V., Zinck R., Hipskind R.A., Janknecht R., and Nordheim A. (1994). Heterogeneity of Ternary Complex Factors in HeLa Cell Nuclear Extracts. *J Biol Chem*, **269** (37), 23310–7.

Pouysségur J., Volmat V., and Lenormand P. (2002). Fidelity and Spatio-Temporal Control in MAP Kinase (ERKs) Signalling. *Biochem Pharmacol*, **64** (5-6), 755–63.

Reszka A.A., Seger R., Diltz C.D., Krebs E.G., and Fischer E.H. (1995). Association of Mitogen-Activated Protein Kinase With the Microtubule Cytoskeleton. *Proc Natl Acad Sci USA*, **92** (19), 8881–5.

Rittié L. and Fisher G.J. (2002). UV-Light-Induced Signal Cascades and Skin Aging. *Ageing Res Rev*, **1** (4), 705–20.

Robbins D.J., Zhen E., Owaki H., Vanderbilt C.A., Ebert D., Geppert T.D., and Cobb M.H. (1993). Regulation and Properties of Extracellular Signal-Regulated Protein Kinases 1 and 2 in Vitro. *J Biol Chem*, **268** (7), 5097–106.

Roberti M.J., Bertoncini C.W., Klement R., Jares-Erijman E.A., and Jovin T.M. (2007). Fluorescence Imaging of Amyloid Formation in Living Cells by a Functional, Tetracysteine-Tagged alpha-Synuclein. *Nat Methods*, **4** (4), 345–51.

Robinson M.J., Stippec S.A., Goldsmith E., White M.A., and Cobb M.H. (1998). A Constitutively Active and Nuclear Form of the MAP Kinase ERK2 Is Sufficient for Neurite Outgrowth and Cell Transformation. *Curr Biol*, **8** (21), 1141–50.

Rocks O., Peyker A., Kahms M., Verveer P.J., Koerner C., Lumbierres M., Kuhlmann J., Waldmann H., Wittinghofer A., and Bastiaens P.I.H. (2005). An Acylation Cycle Regulates Localization and Activity of Palmitoylated Ras Isoforms. *Science*, **307** (5716), 1746–52.

Rubinfeld H., Hanoch T., and Seger R. (1999). Identification of a Cytoplasmic-Retention Sequence in ERK2. *J Biol Chem*, **274** (43), 30349–52.

Rudner L., Nydegger S., Coren L.V., Nagashima K., Thali M., and Ott D.E. (2005). Dynamic Fluorescent Imaging of Human Immunodeficiency Virus Type 1 gag in Live Cells by Biarsenical Labeling. *J Virol*, **79** (7), 4055–65.

Saiki R.K., Gelfand D.H., Stoffel S., Scharf S.J., Higuchi R., Horn G.T., Mullis K.B., and Erlich H.A. (1988). Primer-Directed Enzymatic Amplification of DNA With a Thermostable DNA Polymerase. *Science*, **239** (4839), 487–91.

Salinas S., Briançon-Marjollet A., Bossis G., Lopez M.A., Piechaczyk M., Jariel-Encontre I., Debant A., and Hipskind R.A. (2004). SUMOylation Regulates Nucleo-Cytoplasmic Shuttling of Elk-1. *J Cell Biol*, **165** (6), 767–73.

Sanger F., Nicklen S., and Coulson A.R. (1992). DNA Sequencing With Chain-Terminating Inhibitors. 1977. *Biotechnology*, **24**, 104–8.

Santos S.D.M., Verveer P.J., and Bastiaens P.I.H. (2007). Growth Factor-Induced MAPK Network Topology Shapes Erk Response Determining PC-12 Cell Fate. *Nat Cell Biol*, **9** (3), 324–30.

Sato M., Kawai Y., and Umezawa Y. (2007). Genetically Encoded Fluorescent Indicators to Visualize Protein Phosphorylation by Extracellular Signal-Regulated Kinase in Single Living Cells. *Anal Chem*, **79** (6), 2570–5.

Sato M., Ozawa T., Inukai K., Asano T., and Umezawa Y. (2002). Fluorescent Indicators for Imaging Protein Phosphorylation in Single Living Cells. *Nat Biotechnol*, **20** (3), 287–94.

Sato M. and Umezawa Y. (2004). Imaging Protein Phosphorylation by Fluorescence in Single Living Cells. *Methods*, **32** (4), 451–5.

Schiemann W.P., Graves L.M., Baumann H., Morella K.K., Gearing D.P., Nielsen M.D., Krebs E.G., and Nathanson N.M. (1995). Phosphorylation of the Human Leukemia Inhibitory Factor (LIF) Receptor by Mitogen-Activated Protein Kinase and the Regulation of LIF Receptor Function by Heterologous Receptor Activation. *Proc Natl Acad Sci USA*, **92** (12), 5361–5.

Schoeberl B., Eichler-Jonsson C., Gilles E.D., and Müller G. (2002). Computational Modeling of the Dynamics of the MAP Kinase Cascade Activated by Surface and Internalized EGF Receptors. *Nat Biotechnol*, **20** (4), 370–5.

Schultz C. (2007). Molecular Tools for Cell and Systems Biology. *HFSP J*, **1** (4), 230–48.

Seger R., Ahn N.G., Posada J., Munar E.S., Jensen A.M., Cooper J.A., Cobb M.H., and Krebs E.G. (1992). Purification and Characterization of Mitogen-Activated Protein Kinase Activator(s) from Epidermal Growth Factor-Stimulated A431 Cells. *J Biol Chem*, **267** (20), 14373–81.

Seger R. and Krebs E.G. (1995). The MAPK Signaling Cascade. *FASEB J*, **9** (9), 726–35.

Seidel J.J. and Graves B.J. (2002). An ERK2 Docking Site in the Pointed Domain Distinguishes a Subset of ETS Transcription Factors. *Genes Dev*, **16** (1), 127–37.

Sgambato V., Vanhoutte P., Pagès C., Rogard M., Hipskind R., Besson M.J., and Caboche J. (1998). In Vivo Expression and Regulation of Elk-1, a Target of the Extracellular-Regulated Kinase Signaling Pathway, in the Adult Rat Brain. *J Neurosci*, **18** (1), 214–26.

Shankaran H., Ippolito D.L., Chrisler W.B., Resat H., Bollinger N., Opresko L.K., and Wiley H.S. (2009). Rapid and Sustained Nuclear-Cytoplasmic ERK Oscillations Induced by Epidermal Growth Factor. *Mol Syst Biol*, **5**, 332.

Shapiro P.S., Vaisberg E., Hunt A.J., Tolwinski N.S., Whalen A.M., McIntosh J.R., and Ahn N.G. (1998). Activation of the MKK/ERK Pathway During Somatic Cell Mitosis: Direct Interactions of Active ERK With Kinetochores and Regulation of the Mitotic 3F3/2 Phosphoantigen. *J Cell Biol*, **142** (6), 1533–45.

Smith F.D., Langeberg L.K., Cellurale C., Pawson T., Morrison D.K., Davis R.J., and Scott J.D. (2010). AKAP-Lbc Enhances Cyclic AMP Control of the ERK1/2 Cascade. *Nat Cell Biol*, **12** (12), 1242–9.

Soule H.D., Vazguez J., Long A., Albert S., and Brennan M. (1973). A Human Cell Line from a Pleural Effusion Derived from a Breast Carcinoma. *J Natl Cancer Inst*, **51** (5), 1409–16.

Squire A., Verveer P.J., and Bastiaens P.I. (2000). Multiple Frequency Fluorescence Lifetime Imaging Microscopy. *J Microsc*, **197** (Pt 2), 136–49.

Suhling K., French P.M.W., and Phillips D. (2005). Time-Resolved Fluorescence Microscopy. *Photochem Photobiol Sci*, **4** (1), 13–22.

Sundaram M. and Han M. (1995). The C. Elegans KSR-1 Gene Encodes a Novel Raf-Related Kinase Involved in Ras-Mediated Signal Transduction. *Cell*, **83** (6), 889–901.

Taguchi Y., Shi Z.D., Ruddy B., Dorward D.W., Greene L., and Baron G.S. (2009). Specific Biarsenical Labeling of Cell Surface Proteins Allows Fluorescent- and Biotin-Tagging of Amyloid Precursor Protein and Prion Proteins. *Mol Biol Cell*, **20** (1), 233–44.

Tanoue T., Adachi M., Moriguchi T., and Nishida E. (2000). A Conserved Docking Motif in MAP Kinases Common to Substrates, Activators and Regulators. *Nat Cell Biol*, **2** (2), 110–6.

Taub N., Teis D., Ebner H.L., Hess M.W., and Huber L.A. (2007). Late Endosomal Traffic of the Epidermal Growth Factor Receptor Ensures Spatial and Temporal Fidelity of Mitogen-Activated Protein Kinase Signaling. *Mol Biol Cell*, **18** (12), 4698–710.

Thaler C., Koushik S.V., Blank P.S., and Vogel S.S. (2005). Quantitative Multiphoton Spectral Imaging and its Use for Measuring Resonance Energy Transfer. *Biophys J*, **89** (4), 2736–49.

Therrien M., Chang H.C., Solomon N.M., Karim F.D., Wassarman D.A., and Rubin G.M. (1995). KSR, a Novel Protein Kinase Required for RAS Signal Transduction. *Cell*, **83** (6), 879–88.

Therrien M., Michaud N.R., Rubin G.M., and Morrison D.K. (1996). KSR Modulates Signal Propagation Within the MAPK Cascade. *Genes Dev*, **10** (21), 2684–95.

Thottassery J.V., Sun Y., Westbrook L., Rentz S.S., Manuvakhova M., Qu Z., Samuel S., Upshaw R., Cunningham A., and Kern F.G. (2004). Prolonged Extracellular Signal-Regulated Kinase 1/2 Activation During Fibroblast Growth Factor 1- or Heregulin beta1-Induced Antiestrogen-Resistant Growth of Breast Cancer Cells is Resistant to Mitogen-Activated Protein/Extracellular Regulated Kinase Kinase Inhibitors. *Cancer Res*, **64** (13), 4637–47.

Ting A.Y., Kain K.H., Klemke R.L., and Tsien R.Y. (2001). Genetically Encoded Fluorescent Reporters of Protein Tyrosine Kinase Activities in Living Cells. *Proc Natl Acad Sci USA*, **98** (26), 15003–8.

Torii S., Nakayama K., Yamamoto T., and Nishida E. (2004). Regulatory Mechanisms and Function of ERK MAP Kinases. *J Biochem*, **136** (5), 557–61.

Traverse S., Gomez N., Paterson H., Marshall C., and Cohen P. (1992). Sustained Activation of the Mitogen-Activated Protein (MAP) Kinase Cascade May Be Required for Differentiation of PC12 Cells. Comparison of the Effects of Nerve Growth Factor and Epidermal Growth Factor. *Biochem J*, **288 (Pt 2)**, 351–5.

Turville S.G., Aravantinou M., Stössel H., Romani N., and Robbiani M. (2008). Resolution of De Novo HIV Production and Trafficking in Immature Dendritic Cells. *Nat Methods*, **5** (1), 75–85.

Ubersax J.A. and Ferrell Jr J.E. (2007). Mechanisms of Specificity in Protein Phosphorylation. *Nat Rev Mol Cell Biol*, **8** (7), 530–41.

Uhles S., Moede T., Leibiger B., Berggren P.O., and Leibiger I.B. (2007). Selective Gene Activation by Spatial Segregation of Insulin Receptor B Signaling. *FASEB J*, **21** (7), 1609–21.

van Munster E.B. and Gadella T.W.J. (2005). Fluorescence Lifetime Imaging Microscopy (FLIM). *Adv Biochem Eng Biotechnol*, **95**, 143–75.

Verveer P.J. and Bastiaens P.I.H. (2008). Quantitative Microscopy and Systems Biology: Seeing the Whole Picture. *Histochem Cell Biol*, **130** (5), 833–43.

Verveer P.J., Squire A., and Bastiaens P.I. (2000). Global Analysis of Fluorescence Lifetime Imaging Microscopy Data. *Biophys J*, **78** (4), 2127–37.

Vieira A.V., Lamaze C., and Schmid S.L. (1996). Control of EGF Receptor Signaling by Clathrin-Mediated Endocytosis. *Science*, **274** (5295), 2086–9.

Vilardaga J.P., Bünemann M., Krasel C., Castro M., and Lohse M.J. (2003). Measurement of the Millisecond Activation Switch of G Protein-Coupled Receptors in Living Cells. *Nat Biotechnol*, **21** (7), 807–12.

Volmat V., Camps M., Arkinstall S., Pouysségur J., and Lenormand P. (2001). The Nucleus, a Site for Signal Termination by Sequestration and Inactivation of p42/p44 MAP Kinases. *J Cell Sci*, **114** (Pt 19), 3433–43.

Waas W.F. and Dalby K.N. (2001). Purification of a Model Substrate for Transcription Factor Phosphorylation by ERK2. *Protein Expr Purif*, **23** (1), 191–7.

Walther K.A., Papke B., Sinn M.B., Michel K., and Kinkhabwala A. (2011). Precise Measurement of Protein Interacting Fractions With Fluorescence Lifetime Imaging Microscopy. *Mol Biosyst*, **7** (2), 322–36.

Wharton S.A. and Hipkiss A.R. (1984). Abnormal Proteins of Shortened Length Are Preferentially Degraded in the Cytosol of Cultured MRC5 Fibroblasts. *FEBS Lett*, **168** (1), 134–8.

Wolf I. and Seger R. (2002). The Mitogen-Activated Protein Kinase Signaling Cascade: from Bench to Bedside. *Isr Med Assoc J*, **4** (8), 641–7.

Wouters F.S., Verveer P.J., and Bastiaens P.I. (2001). Imaging Biochemistry Inside Cells. *Trends Cell Biol*, **11** (5), 203–11.

Xing H., Kornfeld K., and Muslin A.J. (1997). The Protein Kinase KSR Interacts With 14-3-3 Protein and Raf. *Curr Biol*, **7** (5), 294–300.

Yang S.H., Whitmarsh A.J., Davis R.J., and Sharrocks A.D. (1998a). Differential Targeting of MAP Kinases to the ETS-Domain Transcription Factor Elk-1. *EMBO J*, **17** (6), 1740–9.

Yang S.H., Yates P.R., Whitmarsh A.J., Davis R.J., and Sharrocks A.D. (1998b). The Elk-1 ETS-Domain Transcription Factor Contains a Mitogen-Activated Protein Kinase Targeting Motif. *Mol Cell Biol*, **18** (2), 710–20.

Yao Z. and Seger R. (2009). The ERK Signaling Cascade - Views from Different Subcellular Compartments. *Biofactors*, **35** (5), 407–16.

Yasuda R. (2006). Imaging Spatiotemporal Dynamics of Neuronal Signaling Using Fluorescence Resonance Energy Transfer and Fluorescence Lifetime Imaging Microscopy. *Curr Opin Neurobiol*, **16** (5), 551–61.

Yoon S. and Seger R. (2006). The Extracellular Signal-Regulated Kinase: Multiple Substrates Regulate Diverse Cellular Functions. *Growth Factors*, **24** (1), 21–44.

Yudushkin I.A., Schleifenbaum A., Kinkhabwala A., Neel B.G., Schultz C., and Bastiaens P.I.H. (2007). Live-Cell Imaging of Enzyme-Substrate Interaction Reveals Spatial Regulation of PTP1B. *Science*, **315** (5808), 115–9.

Zhang F., Strand A., Robbins D., Cobb M.H., and Goldsmith E.J. (1994). Atomic Structure of the MAP Kinase ERK2 at 2.3 A Resolution. *Nature*, **367** (6465), 704–11.

Zhang J., Campbell R.E., Ting A.Y., and Tsien R.Y. (2002). Creating New Fluorescent Probes for Cell Biology. *Nat Rev Mol Cell Biol*, **3** (12), 906–18.

Abbreviations

aa	amino acid
bp	base pair
BSA	bovine serum albumine
CDS	coding sequence
C-terminal	carboxy-terminal
Da	Dalton
DMEM	Dulbecco's modified Eagle's medium
DNA	deoxyribonucleic acid
dNTP	deoxynucleotide-5'-triphosphate
ddH_2O	double distilled water
ddNTP	dideoxynucleotide-5'-triphosphate
DMSO	dimethyl-sulphoxide
dsDNA	double stranded DNA
E. coli	*Escherichia coli*
EGF	epidermal growth factor
(E)GFP	(enhanced) green fluorescent protein
Fig.	figure
for	forward
g	acceleration of gravity
g	gram
h	hour
k	kilo
l	litre
LB	Luria Bertani
MAPKK	MAPK kinase
m	milli
M	mol/l
min	minute
mol	mole
μ	micro
n	nano
NA	numerical aperture
NES	nuclear export sequence
ns	nanosecond
N-terminal	amino-terminal
PAGE	polyacrylamide gel electrophoresis
PBS	phosphate buffered saline

PCR	polymerase chain record
PKC	protein kinase C
ps	picosecond
ROI	region of interest
rev	reverse
RT	room temperature
sec	second
S.E.M.	standard error of the mean
SDS	sodium dodecyl sulfate
TBS	Tris buffered saline
TBST	TBS + 0.5 % Tween-20
Tris	*tris*-(hydroxylmethyl)aminomethane
U	unit
V	voltage
wt	wild-type
w/v	weight/volume
Ω	Ohm

Supplementary Material

S.1 A FRET-Based ERK2 Biosensor Employing ReAsH Labeling

Table S.1.1: Template and primers used to create ERK2-ReAsH sensor constructs.

Final construct	Template	Forward primer	Reverse primer
4C-ERK2-mCitrine	ERK2-mCitrine	4C-ERK2 for	4C-ERK2 rev
ERK2-4C(9-14)-mCitrine	ERK2-mCitrine	4C(9-14) for	4C(9-14) rev
ERK2-4C(30-35)-mCitrine	ERK2-mCitrine	4C(30-35) for	4C(30-35) rev
ERK2-4C(171-176)-mCitrine	ERK2-mCitrine	4C(171-176) for	4C(171-176) rev
ERK2-4C(172-177)-mCitrine	ERK2-mCitrine	4C(172-177) for	4C(172-177) rev
ERK2-4C(173-178)-mCitrine	ERK2-mCitrine	4C(173-178) for	4C(173-178) rev
ERK2-4C(174-179)-mCitrine	ERK2-mCitrine	4C(174-179) for	4C(174-179) rev
ERK2-4C(175-180)-mCitrine	ERK2-mCitrine	4C(175-180) for	4C(175-180) rev
ERK2-4C(176-181)-mCitrine	ERK2-mCitrine	4C(176-181) for	4C(176-181) rev
ERK2-4C(327-336)-mCitrine	ERK2-mCitrine	4C(327-336) for	4C(327-336) rev
mCitrine-ERK2-4C	mCitrine-ERK2	ERK2-4C for	ERK2-4C rev
mCitrine-ERK2-4C(9-14)	mCitrine-ERK2	4C(9-14) for	4C(9-14) rev
mCitrine-ERK2-4C(171-176)	mCitrine-ERK2	4C(171-176) for	4C(171-176) rev
mCitrine-ERK2-4C(172-177)	mCitrine-ERK2	4C(172-177) for	4C(172-177) rev
mCitrine-ERK2-4C(173-178)	mCitrine-ERK2	4C(173-178) for	4C(173-178) rev
mCitrine-ERK2-4C(174-179)	mCitrine-ERK2	4C(174-179) for	4C(174-179) rev
mCitrine-ERK2-4C(175-180)	mCitrine-ERK2	4C(175-180) for	4C(175-180) rev
mCitrine-ERK2-4C(176-181)	mCitrine-ERK2	4C(176-181) for	4C(176-181) rev
mCitrine-ERK2-4C(327-336)	mCitrine-ERK2	4C(327-336) for	4C(327-336) rev

```
ERK2 wt                 MAAAAAAGPEMVRGQVFDVGPRYTNLSYIGEGAYGMVCSAYDNLNKVRVAIKKISPFEHQT
4C-ERK2(8-358)      MFLNCCPGCCMEPEMVRGQVFDVGPRYTNLSYIGEGAYGMVCSAYDNLNKVRVAIKKISPFEHQT
ERK2-4C(9-14)           M AAAAAGCCPGCCQVFDVGPRYTNLSYIGEGAYGMVCSAYDNLNKVRVAIKKISPFEHQT
ERK2-4C(30-35)          M AAAAAGPEMVRGQVFDVGPRYTNLSYICCPGCCMVCSAYDNLNKVRVAIKKISPFEHQT
ERK2-4C(171-176)        M AAAAAGPEMVRGQVFDVGPRYTNLSYIGEGAYGMVCSAYDNLNKVRVAIKKISPFEHQT
ERK2-4C(172-177)        M AAAAAGPEMVRGQVFDVGPRYTNLSYIGEGAYGMVCSAYDNLNKVRVAIKKISPFEHQT
ERK2-4C(173-178)        M AAAAAGPEMVRGQVFDVGPRYTNLSYIGEGAYGMVCSAYDNLNKVRVAIKKISPFEHQT
ERK2-4C(174-179)        M AAAAAGPEMVRGQVFDVGPRYTNLSYIGEGAYGMVCSAYDNLNKVRVAIKKISPFEHQT
ERK2-4C(175-180)        M AAAAAGPEMVRGQVFDVGPRYTNLSYIGEGAYGMVCSAYDNLNKVRVAIKKISPFEHQT
ERK2-4C(176-181)        M AAAAAGPEMVRGQVFDVGPRYTNLSYIGEGAYGMVCSAYDNLNKVRVAIKKISPFEHQT
ERK2-4C(327-336)        M AAAAAGPEMVRGQVFDVGPRYTNLSYIGEGAYGMVCSAYDNLNKVRVAIKKISPFEHQT
ERK2-4C                 M AAAAAGPEMVRGQVFDVGPRYTNLSYIGEGAYGMVCSAYDNLNKVRVAIKKISPFEHQT

ERK2 wt             YCQRTLREIKILLRFRHENIIGINDIIRAPTIEQMKDVYIVQDLMETDLYKLLKTQHLSNDHICY
4C-ERK2(8-358)      YCQRTLREIKILLRFRHENIIGINDIIRAPTIEQMKDVYIVQDLMETDLYKLLKTQHLSNDHICY
ERK2-4C(9-14)       YCQRTLREIKILLRFRHENIIGINDIIRAPTIEQMKDVYIVQDLMETDLYKLLKTQHLSNDHICY
ERK2-4C(30-35)      YCQRTLREIKILLRFRHENIIGINDIIRAPTIEQMKDVYIVQDLMETDLYKLLKTQHLSNDHICY
ERK2-4C(171-176)    YCQRTLREIKILLRFRHENIIGINDIIRAPTIEQMKDVYIVQDLMETDLYKLLKTQHLSNDHICY
ERK2-4C(172-177)    YCQRTLREIKILLRFRHENIIGINDIIRAPTIEQMKDVYIVQDLMETDLYKLLKTQHLSNDHICY
ERK2-4C(173-178)    YCQRTLREIKILLRFRHENIIGINDIIRAPTIEQMKDVYIVQDLMETDLYKLLKTQHLSNDHICY
ERK2-4C(174-179)    YCQRTLREIKILLRFRHENIIGINDIIRAPTIEQMKDVYIVQDLMETDLYKLLKTQHLSNDHICY
ERK2-4C(175-180)    YCQRTLREIKILLRFRHENIIGINDIIRAPTIEQMKDVYIVQDLMETDLYKLLKTQHLSNDHICY
ERK2-4C(176-181)    YCQRTLREIKILLRFRHENIIGINDIIRAPTIEQMKDVYIVQDLMETDLYKLLKTQHLSNDHICY
ERK2-4C(327-336)    YCQRTLREIKILLRFRHENIIGINDIIRAPTIEQMKDVYIVQDLMETDLYKLLKTQHLSNDHICY
ERK2-4C             YCQRTLREIKILLRFRHENIIGINDIIRAPTIEQMKDVYIVQDLMETDLYKLLKTQHLSNDHICY

ERK2 wt             FLYQILRGLKYIHSANVLHRDLKPSNLLLNTTCDLKICDFGLARVADPDHDHTGFLTEYVATRWY
4C-ERK2(8-358)      FLYQILRGLKYIHSANVLHRDLKPSNLLLNTTCDLKICDFGLARVADPDHDHTGFLTEYVATRWY
ERK2-4C(9-14)       FLYQILRGLKYIHSANVLHRDLKPSNLLLNTTCDLKICDFGLARVADPDHDHTGFLTEYVATRWY
ERK2-4C(30-35)      FLYQILRGLKYIHSANVLHRDLKPSNLLLNTTCDLKICDFGLARVADPDHDHTGFLTEYVATRWY
ERK2-4C(171-176)    FLYQILRGLKYIHSANVLHRDLKPSNLLLNTTCDLKICDFGLARCCPGCCDHTGFLTEYVATRWY
ERK2-4C(172-177)    FLYQILRGLKYIHSANVLHRDLKPSNLLLNTTCDLKICDFGLARVCCPGCCHTGFLTEYVATRWY
ERK2-4C(173-178)    FLYQILRGLKYIHSANVLHRDLKPSNLLLNTTCDLKICDFGLARVACCPGCCTGFLTEYVATRWY
ERK2-4C(174-179)    FLYQILRGLKYIHSANVLHRDLKPSNLLLNTTCDLKICDFGLARVADCCPGCCGFLTEYVATRWY
ERK2-4C(175-180)    FLYQILRGLKYIHSANVLHRDLKPSNLLLNTTCDLKICDFGLARVADPCCPGCCFLTEYVATRWY
ERK2-4C(176-181)    FLYQILRGLKYIHSANVLHRDLKPSNLLLNTTCDLKICDFGLARVADPDCCPGCCLTEYVATRWY
ERK2-4C(327-336)    FLYQILRGLKYIHSANVLHRDLKPSNLLLNTTCDLKICDFGLARVADPDHDHTGFLTEYVATRWY
ERK2-4C             FLYQILRGLKYIHSANVLHRDLKPSNLLLNTTCDLKICDFGLARVADPDHDHTGFLTEYVATRWY

ERK2 wt             RAPEIMLNSKGYTKSIDIWSVGCILAEMLSNRPIFPGKHYLDQLNHILGILGSPSQEDLNCIINL
4C-ERK2(8-358)      RAPEIMLNSKGYTKSIDIWSVGCILAEMLSNRPIFPGKHYLDQLNHILGILGSPSQEDLNCIINL
ERK2-4C(9-14)       RAPEIMLNSKGYTKSIDIWSVGCILAEMLSNRPIFPGKHYLDQLNHILGILGSPSQEDLNCIINL
ERK2-4C(30-35)      RAPEIMLNSKGYTKSIDIWSVGCILAEMLSNRPIFPGKHYLDQLNHILGILGSPSQEDLNCIINL
ERK2-4C(171-176)    RAPEIMLNSKGYTKSIDIWSVGCILAEMLSNRPIFPGKHYLDQLNHILGILGSPSQEDLNCIINL
ERK2-4C(172-177)    RAPEIMLNSKGYTKSIDIWSVGCILAEMLSNRPIFPGKHYLDQLNHILGILGSPSQEDLNCIINL
ERK2-4C(173-178)    RAPEIMLNSKGYTKSIDIWSVGCILAEMLSNRPIFPGKHYLDQLNHILGILGSPSQEDLNCIINL
ERK2-4C(174-179)    RAPEIMLNSKGYTKSIDIWSVGCILAEMLSNRPIFPGKHYLDQLNHILGILGSPSQEDLNCIINL
ERK2-4C(175-180)    RAPEIMLNSKGYTKSIDIWSVGCILAEMLSNRPIFPGKHYLDQLNHILGILGSPSQEDLNCIINL
ERK2-4C(176-181)    RAPEIMLNSKGYTKSIDIWSVGCILAEMLSNRPIFPGKHYLDQLNHILGILGSPSQEDLNCIINL
ERK2-4C(327-336)    RAPEIMLNSKGYTKSIDIWSVGCILAEMLSNRPIFPGKHYLDQLNHILGILGSPSQEDLNCIINL
ERK2-4C             RAPEIMLNSKGYTKSIDIWSVGCILAEMLSNRPIFPGKHYLDQLNHILGILGSPSQEDLNCIINL

ERK2                KARNYLLSLPHKNKVPWNRLFPNADSKALDLLDKMLTFNPHKRIEVEQALAHPYLEQYYDPSDEP
4C-ERK2(8-358)      KARNYLLSLPHKNKVPWNRLFPNADSKALDLLDKMLTFNPHKRIEVEQALAHPYLEQYYDPSDEP
ERK2-4C(9-14)       KARNYLLSLPHKNKVPWNRLFPNADSKALDLLDKMLTFNPHKRIEVEQALAHPYLEQYYDPSDEP
ERK2-4C(30-35)      KARNYLLSLPHKNKVPWNRLFPNADSKALDLLDKMLTFNPHKRIEVEQALAHPYLEQYYDPSDEP
ERK2-4C(171-176)    KARNYLLSLPHKNKVPWNRLFPNADSKALDLLDKMLTFNPHKRIEVEQALAHPYLEQYYDPSDEP
ERK2-4C(172-177)    KARNYLLSLPHKNKVPWNRLFPNADSKALDLLDKMLTFNPHKRIEVEQALAHPYLEQYYDPSDEP
ERK2-4C(173-178)    KARNYLLSLPHKNKVPWNRLFPNADSKALDLLDKMLTFNPHKRIEVEQALAHPYLEQYYDPSDEP
ERK2-4C(174-179)    KARNYLLSLPHKNKVPWNRLFPNADSKALDLLDKMLTFNPHKRIEVEQALAHPYLEQYYDPSDEP
ERK2-4C(175-180)    KARNYLLSLPHKNKVPWNRLFPNADSKALDLLDKMLTFNPHKRIEVEQALAHPYLEQYYDPSDEP
ERK2-4C(176-181)    KARNYLLSLPHKNKVPWNRLFPNADSKALDLLDKMLTFNPHKRIEVEQALAHPYLEQYYDPSDEP
ERK2-4C(327-336)    KARNYLLSLPHKNKVPWNRLFPNADSKALDLLDKMLTFNPHKRIEVEQALAHPYLEQYYDPSDEP
ERK2-4C             KARNYLLSLPHKNKVPWNRLFPNADSKALDLLDKMLTFNPHKRIEVEQALAHPYLEQYYDPSDEP

ERK2 wt             IAEAPFKFDMELDDLP KEKLKELIFEETARFQPGYRS*
4C-ERK2(8-358)      IAEAPFKFDMELDDLP KEKLKELIFEETARFQPGYRS*
ERK2-4C(9-14)       IAEAPFKFDMELDDLP KEKLKELIFEETARFQPGYRS*
ERK2-4C(30-35)      IAEAPFKFDMELDDLP KEKLKELIFEETARFQPGYRS*
ERK2-4C(171-176)    IAEAPFKFDMELDDLP KEKLKELIFEETARFQPGYRS*
ERK2-4C(172-177)    IAEAPFKFDMELDDLP KEKLKELIFEETARFQPGYRS*
ERK2-4C(173-178)    IAEAPFKFDMELDDLP KEKLKELIFEETARFQPGYRS*
ERK2-4C(174-179)    IAEAPFKFDMELDDLP KEKLKELIFEETARFQPGYRS*
ERK2-4C(175-180)    IAEAPFKFDMELDDLP KEKLKELIFEETARFQPGYRS*
ERK2-4C(176-181)    IAEAPFKFDMELDDLP KEKLKELIFEETARFQPGYRS*
ERK2-4C(327-336)    IAEAPFLNCCPGCCMEPKEKLKELIFEETARFQPGYRS*
ERK2-4C             IAEAPFKFDMELDDLP KEKLKELIFEETARFQPGYRSMFLNCCPGCCMEP*
```

Figure S.1.1: Amino acid sequences of wt and recombinant rat ERK2 proteins. Domains that change conformation upon activation of ERK2 are labeled in green, phosphorylatable Thr183 and Tyr185 are highlighted in purple. The 4C motif in the ERK2 mutants is highlighted in red.

Table S.1.2: Single cell FLIM measurements of ERK2-mCitrine. HeLa cells co-expressing MEK1 and ERK2-mCitrine were starved overnight and stimulated with 100 ng/ml EGF. Fluorescent lifetimes were measured prior to and 5, 10 and 20 min after EGF stimulation and are displayed as average of whole individual cells in ns (average with S.E.M.). Cells measured were from different days and dishes.

Cell	Time after EGF addition			
	0 min	5 min	10 min	20 min
1	3.07	3.08	3.08	3.08
2	3.05	3.05	3.05	3.07
3	3.03	3.05	3.04	3.05
4	3.01	3.02	3.02	3.02
5	3.00	3.01	3.03	3.03
6	3.00	3.00	3.00	3.01
7	3.00	3.01	3.01	3.00
8	3.00	3.01	3.02	3.00
9	3.01	3.03	3.02	3.01
10	3.02	3.02	3.02	3.03
11	2.97	3.00	3.01	3.02
12	2.98	3.02	3.04	3.04
13	3.00	3.02	3.02	3.01
14	3.01	3.02	3.03	3.00
15	2.99	3.04	3.02	3.02
16	3.01	3.01	3.03	3.01
17	3.01	3.02	3.02	3.01
18	3.02	3.01	3.03	3.02
19	3.00	3.02	3.01	3.01
20	3.01	3.01	3.02	3.03
21	3.01	3.00	3.02	3.03
22	3.00	3.00	3.03	3.02
23	2.99	3.01	3.01	3.01
24	2.99	3.01	3.02	3.02
Average	3.00 ± 0.01	3.01 ± 0.01	3.02 ± 0.01	3.02 ± 0.01

Table S.1.3: Single cell FLIM measurements of 4C(8-358)-ERK2-mCitrine. HeLa cells co-expressing MEK1 and 4C(8-358)-ERK2-mCitrine were starved overnight and stimulated with 100 ng/ml EGF. Fluorescent lifetimes were measured prior to and 5, 10 and 20 min after EGF stimulation and are displayed as average of whole individual cells in ns (average with S.E.M.). Cells measured were from different days and dishes.

Cell	Time after EGF addition			
	0 min	5 min	10 min	20 min
1	2.80	2.79	2.79	2.79
2	2.80	2.80	2.80	2.80
3	2.86	2.87	2.86	2.86
4	2.82	2.83	2.80	2.80
5	2.83	2.83	2.82	2.82
6	2.79	2.77	2.77	2.76
7	2.78	2.75	2.75	2.76
8	2.78	2.77	2.77	2.77
9	2.78	2.76	2.77	2.75
10	2.75	2.74	2.73	2.74
11	2.74	2.72	2.71	2.71
Average	2.79 ± 0.03	2.79 ± 0.05	2.78 ± 0.04	2.78 ± 0.04

Table S.1.4: Single cell FLIM measurements of ERK2-4C(9-14)-mCitrine. HeLa cells co-expressing MEK1 and ERK2-4C(9-14)-mCitrine were starved overnight and stimulated with 100 ng/ml EGF. Fluorescent lifetimes were measured prior to and 5, 10 and 20 min after EGF stimulation and are displayed as average of whole individual cells in ns (average with S.E.M.).

Cell	Time after EGF addition			
	0 min	5 min	10 min	20 min
1	2.82	2.81	2.81	2.81
2	2.77	2.78	2.79	2.78
3	2.80	2.78	2.77	2.78
4	2.71	2.73	2.71	2.74
5	2.69	2.72	2.70	2.71
6	2.71	2.72	2.73	2.74
7	2.72	2.73	2.75	2.72
Average	2.75 ± 0.05	2.75 ± 0.04	2.75 ± 0.04	2.75 ± 0.04

Table S.1.5: Single cell FLIM measurements of ERK2-4C(30-35)-mCitrine. HeLa cells co-expressing MEK1 and ERK2-4C(30-35)-mCitrine were starved overnight and stimulated with 100 ng/ml EGF. Fluorescent lifetimes were measured prior to and 5, 10 and 20 min after EGF stimulation and are displayed as average of whole individual cells in ns (average with S.E.M.).

Cell	Time after EGF addition			
	0 min	5 min	10 min	20 min
1	2.89	2.89	2.90	2.91
2	2.89	2.89	2.88	2.87
3	2.88	2.87	2.87	2.87
4	2.88	2.86	2.86	2.84
5	2.87	2.86	2.86	2.86
6	2.91	2.92	2.91	2.91
7	2.93	2.92	2.91	2.92
8	2.91	2.92	2.92	2.92
Average	2.90 ± 0.02	2.89 ± 0.03	2.89 ± 0.02	2.89 ± 0.03

Table S.1.6: Single cell FLIM measurements of ERK2-4C(171-176)-mCitrine. HeLa cells co-expressing MEK1 and ERK2-4C(171-176)-mCitrine were starved overnight and stimulated with 100 ng/ml EGF. Fluorescent lifetimes were measured prior to and 5, 10 and 20 min after EGF stimulation and are displayed as average of whole individual cells in ns (average with S.E.M.).

Cell	Time after EGF addition			
	0 min	5 min	10 min	20 min
1	2.87	2.84	2.85	2.85
2	2.85	2.83	2.83	2.84
3	2.88	2.88	2.89	2.88
4	2.87	2.87	2.89	2.88
5	2.80	2.81	2.81	2.80
6	2.84	2.85	2.87	2.86
7	2.83	2.85	2.86	2.86
8	2.87	2.91	2.89	2.88
9	2.83	2.84	2.84	2.84
10	2.84	2.85	2.85	2.85
Average	2.85 ± 0.03	2.85 ± 0.03	2.86 ± 0.03	2.85 ± 0.03

Table S.1.7: Single cell FLIM measurements of ERK2-4C(172-177)-mCitrine. HeLa cells co-expressing MEK1 and ERK2-4C(172-177)-mCitrine were starved overnight and stimulated with 100 ng/ml EGF. Fluorescent lifetimes were measured prior to and 5, 10 and 20 min after EGF stimulation and are displayed as average of whole individual cells in ns (average with S.E.M.).

Cell	Time after EGF addition			
	0 min	5 min	10 min	20 min
1	2.90	2.92	2.92	2.93
2	2.91	2.91	2.91	2.91
3	2.91	2.92	2.91	2.91
4	2.92	2.93	2.93	2.93
5	2.89	2.88	2.89	2.88
6	2.88	2.88	2.89	2.89
7	2.94	2.93	2.94	2.95
8	2.89	2.88	2.88	2.88
9	2.91	2.90	2.92	2.91
10	2.89	2.89	2.90	2.89
11	2.91	2.90	2.91	2.91
12	2.93	2.93	2.93	2.94
13	2.92	2.93	2.94	2.92
14	2.90	2.89	2.90	2.90
15	2.91	2.91	2.91	2.92
Average	2.91 ± 0.02	2.91 ± 0.02	2.91 ± 0.02	2.91 ± 0.02

Table S.1.8: Single cell FLIM measurements of ERK2-4C(173-178)-mCitrine. HeLa cells co-expressing MEK1 and ERK2-4C(173-178)-mCitrine were starved overnight and stimulated with 100 ng/ml EGF. Fluorescent lifetimes were measured prior to and 5, 10 and 20 min after EGF stimulation and are displayed as average of whole individual cells in ns (average with S.E.M.).

Cell	Time after EGF addition			
	0 min	5 min	10 min	20 min
1	2.80	2.84	2.83	2.83
2	2.81	2.81	2.82	2.82
3	2.80	2.80	2.82	2.79
4	2.81	2.79	2.80	2.80
5	2.82	2.81	2.80	2.83
6	2.78	2.79	2.79	2.79
7	2.80	2.79	2.78	2.79
8	2.83	2.81	2.82	2.80
9	2.82	2.780	2.77	2.77
10	2.82	2.78	2.78	2.82
11	2.70	2.71	2.70	2.71
12	2.76	2.77	2.78	2.78
13	2.67	2.72	2.73	2.74
14	2.74	2.73	2.73	2.72
15	2.79	2.77	2.80	2.79
16	2.79	2.76	2.79	2.81
Average	2.78 ± 0.05	2.78 ± 0.04	2.78 ± 0.04	2.79 ± 0.04

Table S.1.9: Single cell FLIM measurements of ERK2-4C(174-179)-mCitrine. HeLa cells co-expressing MEK1 and ERK2-4C(174-179)-mCitrine were starved overnight and stimulated with 100 ng/ml EGF. Fluorescent lifetimes were measured prior to and 5, 10 and 20 min after EGF stimulation and are displayed as average of whole individual cells in ns (average with S.E.M.).

Cell	Time after EGF addition			
	0 min	5 min	10 min	20 min
1	2.75	2.79	2.78	2.79
2	2.74	2.76	2.78	2.76
3	2.83	2.82	2.83	2.82
4	2.87	2.88	2.87	2.86
5	2.82	2.83	2.82	2.82
6	2.85	2.86	2.85	2.84
7	2.89	2.88	2.88	2.89
8	2.74	2.73	2.76	2.74
Average	2.81 ± 0.06	2.82 ± 0.06	2.82 ± 0.05	2.82 ± 0.05

Table S.1.10: Single cell FLIM measurements of ERK2-4C(175-180)-mCitrine. HeLa cells co-expressing MEK1 and ERK2-4C(175-180)-mCitrine were starved overnight and stimulated with 100 ng/ml EGF. Fluorescent lifetimes were measured prior to and 5, 10 and 20 min after EGF stimulation and are displayed as average of whole individual cells in ns (average with S.E.M.).

Cell	Time after EGF addition			
	0 min	5 min	10 min	20 min
1	2.87	2.87	2.86	2.87
2	2.89	2.87	2.85	2.86
3	2.87	2.85	2.83	2.86
4	2.86	2.85	2.84	2.88
5	2.86	2.85	2.86	2.85
6	2.88	2.88	2.88	2.86
7	2.90	2.88	2.87	2.88
8	2.88	2.87	2.85	2.85
Average	2.88 ± 0.01	2.87 ± 0.01	2.86 ± 0.01	2.86 ± 0.01

Table S.1.11: Single cell FLIM measurements of ERK2-4C(176-181)-mCitrine. HeLa cells co-expressing MEK1 and ERK2-4C(176-181)-mCitrine were starved overnight and stimulated with 100 ng/ml EGF. Fluorescent lifetimes were measured prior to and 5, 10 and 20 min after EGF stimulation and are displayed as average of whole individual cells in ns (average with S.E.M.). Cells measured were from different days and dishes.

Cell	Time after EGF addition			
	0 min	5 min	10 min	20 min
1	2.94	2.95	2.94	2.94
2	2.93	2.92	2.93	2.93
3	2.94	2.94	2.95	2.95
4	2.93	2.90	2.92	2.92
5	2.90	2.89	2.89	2.91
6	2.92	2.91	2.90	2.91
7	2.92	2.91	2.91	2.91
Average	2.93 ± 0.01	2.92 ± 0.02	2.92 ± 0.02	2.92 ± 0.02

Table S.1.12: Single cell FLIM measurements of ERK2-4C(327-336)-mCitrine. HeLa cells co-expressing MEK1 and ERK2-4C(327-336)-mCitrine were starved overnight and stimulated with 100 ng/ml EGF. Fluorescent lifetimes were measured prior to and 5, 10 and 20 min after EGF stimulation and are displayed as average of whole individual cells in ns (average with S.E.M.).

Cell	Time after EGF addition			
	0 min	5 min	10 min	20 min
1	2.81	2.82	2.82	2.82
2	2.84	2.86	2.86	2.84
3	2.60	2.64	2.66	2.68
4	2.57	2.60	2.61	2.63
5	2.73	2.76	2.76	2.76
Average	2.71 ± 0.12	2.74 ± 0.11	2.74 ± 0.1	2.75 ± 0.90

Table S.1.13: Single cell FLIM measurements of mCitrine-ERK2-4C. HeLa cells co-expressing MEK1 and mCitrine-ERK2-4C were starved overnight and stimulated with 100 ng/ml EGF. Fluorescent lifetimes were measured prior to and 5, 10 and 20 min after EGF stimulation and are displayed as average of whole individual cells in ns (average with S.E.M.).

Cell	Time after EGF addition			
	0 min	5 min	10 min	20 min
1	2.83	2.82	2.82	2.83
2	2.83	2.82	2.81	2.81
3	2.76	2.75	2.77	2.76
4	2.77	2.76	2.75	2.76
5	2.74	2.69	2.67	2.67
6	2.73	2.69	2.69	2.65
7	2.63	2.60	2.61	2.59
8	2.65	2.60	2.61	2.60
Average	2.74 ± 0.07	2.72 ± 0.09	2.72 ± 0.08	2.71 ± 0.09

Table S.1.14: Single cell FLIM measurements of mCitrine-ERK2-4C(9-14). HeLa cells co-expressing MEK1 and mCitrine-ERK2-4C(9-14) were starved overnight and stimulated with 100 ng/ml EGF. Fluorescent lifetimes were measured prior to and 5, 10 and 20 min after EGF stimulation and are displayed as average of whole individual cells in ns (average with S.E.M.).

Cell	Time after EGF addition			
	0 min	5 min	10 min	20 min
1	2.76	2.75	2.75	2.75
2	2.83	2.74	2.72	2.72
3	2.74	2.70	2.69	2.69
4	2.64	2.70	2.64	2.62
5	2.62	2.66	2.60	2.60
6	2.60	2.69	2.61	2.62
7	2.71	2.67	2.66	2.63
8	2.64	2.67	2.65	2.63
9	2.63	2.64	2.63	2.65
10	2.65	2.61	2.63	2.66
Average	2.68 ± 0.07	2.68 ± 0.04	2.66 ± 0.05	2.66 ± 0.05

Table S.1.15: Single cell FLIM measurements of mCitrine-ERK2-4C(171-176). HeLa cells co-expressing MEK1 and mCitrine-ERK2-4C(171-176) were starved overnight and stimulated with 100 ng/ml EGF. Fluorescent lifetimes were measured prior to and 5, 10 and 20 min after EGF stimulation and are displayed as average of whole individual cells in ns (average with S.E.M.).

Cell	Time after EGF addition			
	0 min	5 min	10 min	20 min
1	2.76	2.82	2.80	2.81
2	2.85	2.87	2.86	2.88
3	2.85	2.89	2.89	2.89
4	2.84	2.88	2.87	2.89
5	2.86	2.90	2.86	2.85
6	2.84	2.83	2.86	2.87
7	2.88	2.87	2.87	2.90
8	2.89	2.89	2.90	2.90
9	2.88	2.85	2.88	2.90
10	2.88	2.87	2.91	2.89
11	2.87	2.86	2.87	2.89
12	2.85	2.83	2.84	2.85
13	2.85	2.85	2.85	2.86
Average	2.85 ± 0.03	2.86 ± 0.03	2.87 ± 0.03	2.88 ± 0.03

Table S.1.16: Single cell FLIM measurements of mCitrine-ERK2-4C(172-177). HeLa cells co-expressing MEK1 and mCitrine-ERK2-4C(172-177) were starved overnight and stimulated with 100 ng/ml EGF. Fluorescent lifetimes were measured prior to and 5, 10 and 20 min after EGF stimulation and are displayed as average of whole individual cells in ns (average with S.E.M.).

Cell	Time after EGF addition			
	0 min	5 min	10 min	20 min
1	2.91	2.91	2.92	2.91
2	2.93	2.95	2.94	2.95
3	2.95	2.94	2.96	2.95
4	2.94	2.93	2.95	2.94
5	2.92	2.93	2.92	2.96
6	2.93	2.94	2.92	2.94
7	2.87	2.90	2.92	2.85
8	2.90	2.88	2.94	2.91
9	2.92	2.89	2.94	2.91
Average	2.92 ± 0.02	2.92 ± 0.03	2.94 ± 0.01	2.93 ± 0.04

Table S.1.17: Single cell FLIM measurements of mCitrine-ERK2-4C(173-178). HeLa cells co-expressing MEK1 and mCitrine-ERK2-4C(173-178) were starved overnight and stimulated with 100 ng/ml EGF. Fluorescent lifetimes were measured prior to and 5, 10 and 20 min after EGF stimulation and are displayed as average of whole individual cells in ns (average with S.E.M.).

Cell	Time after EGF addition			
	0 min	5 min	10 min	20 min
1	2.81	2.78	2.80	2.83
2	2.82	2.82	2.82	2.85
3	2.77	2.78	2.76	2.75
4	2.76	2.79	2.76	2.77
5	2.80	2.78	2.77	2.78
6	2.80	2.79	2.79	2.77
7	2.74	2.72	2.72	2.73
8	2.79	2.76	2.73	2.75
Average	2.79 ± 0.03	2.78 ± 0.03	2.77 ± 0.03	2.78 ± 0.04

Table S.1.18: Single cell FLIM measurements of mCitrine-ERK2-4C(174-179). HeLa cells co-expressing MEK1 and mCitrine-ERK2-4C(174-179) were starved overnight and stimulated with 100 ng/ml EGF. Fluorescent lifetimes were measured prior to and 5, 10 and 20 min after EGF stimulation and are displayed as average of whole individual cells in ns (average with S.E.M.).

Cell	Time after EGF addition			
	0 min	5 min	10 min	20 min
1	2.66	2.71	2.71	2.71
2	2.65	2.71	2.70	2.71
3	2.63	2.70	2.71	2.74
4	2.68	2.73	2.73	2.74
5	2.64	2.69	2.69	2.71
6	2.78	2.78	2.78	2.77
7	2.78	2.79	2.79	2.78
8	2.79	2.75	2.77	2.76
9	2.70	2.70	2.72	2.70
10	2.69	2.69	2.70	2.69
Average	2.70 ± 0.06	2.72 ± 0.04	2.73 ± 0.04	2.73 ± 0.03

Table S.1.19: Single cell FLIM measurements of mCitrine-ERK2-4C(175-180). HeLa cells co-expressing MEK1 and mCitrine-ERK2-4C(175-180) were starved overnight and stimulated with 100 ng/ml EGF. Fluorescent lifetimes were measured prior to and 5, 10 and 20 min after EGF stimulation and are displayed as average of whole individual cells in ns (average with S.E.M.).

Cell	Time after EGF addition			
	0 min	5 min	10 min	20 min
1	2.74	2.73	2.74	2.73
2	2.75	2.76	2.75	2.76
3	2.78	2.78	2.77	2.78
4	2.77	2.76	2.75	2.75
5	2.76	2.76	2.76	2.77
6	2.78	2.75	2.79	2.77
7	2.78	2.72	2.75	2.73
8	2.72	2.69	2.72	2.69
9	2.71	2.70	2.69	2.71
10	2.75	2.70	2.71	2.75
11	2.89	2.87	2.86	2.88
12	2.87	2.88	2.85	2.89
13	2.71	2.70	2.68	2.69
Average	2.77 ± 0.06	2.75 ± 0.06	2.76 ± 0.05	2.76 ± 0.06

Table S.1.20: Single cell FLIM measurements of mCitrine-ERK2-4C(176-181). HeLa cells co-expressing MEK1 and mCitrine-ERK2-4C(176-181) were starved overnight and stimulated with 100 ng/ml EGF. Fluorescent lifetimes were measured prior to and 5, 10 and 20 min after EGF stimulation and are displayed as average of whole individual cells in ns (average with S.E.M.).

Cell	Time after EGF addition			
	0 min	5 min	10 min	20 min
1	3.03	3.07	3.03	3.05
2	3.01	3.03	3.03	3.05
3	3.01	3.06	3.04	3.05
4	3.00	3.04	3.02	3.04
5	3.01	3.00	2.99	2.99
6	3.03	2.98	3.00	2.97
7	2.96	2.95	2.95	2.94
8	2.95	2.94	2.93	2.92
Average	3.00 ± 0.03	3.00 ± 0.03	3.00 ± 0.04	3.00 ± 0.05

Table S.1.21: Single cell FLIM measurements of mCitrine-ERK2-4C(327-336). HeLa cells co-expressing MEK1 and mCitrine-ERK2-4C(327-336) were starved overnight and stimulated with 100 ng/ml EGF. Fluorescent lifetimes were measured prior to and 5, 10 and 20 min after EGF stimulation and are displayed as average of whole individual cells in ns (average with S.E.M.).

Cell	Time after EGF addition			
	0 min	5 min	10 min	20 min
1	2.96	2.97	2.95	2.95
2	2.97	2.96	2.97	2.96
3	2.94	2.95	2.91	2.95
4	2.95	2.94	2.97	2.93
5	2.93	2.92	2.93	2.95
Average	2.95 ± 0.02	2.95 ± 0.02	2.94 ± 0.03	2.95 ± 0.1

Table S.1.22: Single cell FLIM measurements of mCitrine-ERK2-4C(174-179) without wash-out of ReAsH. HeLa cells co-expressing MEK1 and mCitrine-ERK2-4C(174-179) were starved overnight, incubated with 5.0 μM ReAsH for 60 min and stimulated with 100 ng/ml EGF. Fluorescent lifetimes were measured prior to and 5, 10 and 20 min after EGF stimulation and are displayed as average of whole individual cells in ns (average with S.E.M.).

Cell	Time after EGF addition			
	0 min	5 min	10 min	20 min
1	2.58	2.58	2.58	2.54
2	2.57	2.55	2.55	2.52
3	2.63	2.63	2.63	2.64
4	2.62	2.61	2.62	2.62
5	2.65	2.65	2.65	2.66
6	2.55	2.54	2.54	2.55
7	2.58	2.61	2.55	2.55
8	2.66	2.63	2.61	2.60
9	2.65	2.62	2.61	2.61
Average	2.61 ± 0.01	2.60 ± 0.01	2.59 ± 0.01	2.59 ± 0.02

Table S.1.23: Single cell FLIM measurements of ERK2-4C(175-180)-mCitrine) without wash-out of ReAsH. HeLa cells co-expressing MEK1 and ERK2-4C(175-180)-mCitrine were starved overnight, incubated with 5.0 μM ReAsH for 60 min and stimulated with 100 ng/ml EGF. Fluorescent lifetimes were measured prior to and 5, 10 and 20 min after EGF stimulation and are displayed as average of whole individual cells in ns (average with S.E.M.).

Cell	Time after EGF addition			
	0 min	5 min	10 min	20 min
1	2.79	2.75	2.75	2.74
2	2.84	2.81	2.80	2.80
3	2.77	2.76	2.75	2.73
4	2.72	2.67	2.65	2.62
5	2.71	2.65	2.62	2.65
6	2.84	2.83	2.83	2.83
7	2.79	2.76	2.75	2.73
8	2.81	2.78	2.78	2.75
Average	2.78 ± 0.02	2.75 ± 0.02	2.74 ± 0.03	2.73 ± 0.02

Table S.1.24: Single cell FLIM measurements of ERK2-4C(327-336)-mCitrine without wash-out of ReAsH. HeLa cells co-expressing MEK1 and ERK2-4C(327-336)-mCitrine were starved overnight, incubated with 5.0 μM ReAsH for 60 min and stimulated with 100 ng/ml EGF. Fluorescent lifetimes were measured prior to and 5, 10 and 20 min after EGF stimulation and are displayed as average of whole individual cells in ns (average with S.E.M.).

Cell	Time after EGF addition			
	0 min	5 min	10 min	20 min
1	2.29	2.27	2.25	2.21
2	2.27	2.23	2.21	2.18
3	2.49	2.54	2.55	2.52
4	2.57	2.64	2.61	2.58
5	2.59	2.65	2.61	2.57
6	2.42	2.38	2.38	2.33
7	2.37	2.35	2.35	2.32
8	2.45	2.49	2.50	2.48
9	2.43	2.58	2.47	2.48
Average	2.43 ± 0.04	2.45 ± 0.05	2.44 ± 0.05	2.41 ± 0.05

S.2 Visualisation of ERK2 ES-Complexes - Single Cell Measurements

Table S.2.1: Single cell FLIM measurements of control cells. MDA cells co-expressed MEK1, mCitrine-ERK2 and mCherry-C. Cells were starved overnight and stimulated with 100 ng/ml EGF. Fluorescent lifetimes were measured prior to and at different time points after EGF stimulation and is displayed as average of whole individual cells in ns. Cells measured were from different days and dishes.

Sample	0 min	2.5 min	5 min	7.5 min	10 min	12.5 min	15 min	20 min	30 min
Cell 1	3.00	2.97	2.98	2.98	2.97	3.01	3.00	2.96	2.99
Cell 2	3.06	2.97	2.97	3.02	2.99	3.04	3.02	3.00	3.00
Cell 3	3.02	3.06	3.00	3.05	2.99	2.99	3.00	3.03	2.98
Cell 4	2.97	2.97	3.00	2.97	2.98	2.97	2.98	3.03	2.98
Cell 5	3.01	2.97	2.99	2.99	3.00	2.99	3.00	2.98	3.00
Cell 6	2.97	2.91	2.95	2.96	2.95	2.94	2.95	3.01	2.95
Cell 7	2.96	2.97	2.99	2.96	2.98	2.97	2.98	2.96	2.98
Cell 8	3.08	3.10	3.13	3.11	3.13	3.12	3.16	3.16	3.15
Average	3.01	3.00	3.00	3.01	3.00	3.00	3.01	3.01	3.00

Table S.2.2: Single cell FLIM measurements of cells expressing mCherry-hElk1(379-403). MDA cells co-expressed MEK1, mCitrine-ERK2 and the mCherry-labeled ERK2 substrate. Cells were starved overnight and stimulated with 100 ng/ml EGF. Fluorescence lifetimes of whole individual cells was measured prior to and at different time points after EGF stimulation. Cells measured were from different days and dishes.

Sample	0 min	2 min	5 min	7.5 min	10 min	12.5 min	15 min	20 min	30 min
Cell 1	2.98	2.89	2.88	2.85	2.91	2.81	2.89	2.87	2.89
Cell 2	3.01	2.99	2.94	2.94	2.99	2.97	2.99	2.97	2.98
Cell 3	3.09	3.08	3.03	3.05	3.05	3.07	3.04	3.03	3.04
Cell 4	3.07	3.02	3.01	3.02	3.04	3.04	3.03	3.02	3.03
Cell 5	3.08	3.07	3.04	3.09	3.08	3.09	3.02	3.03	3.02
Cell 6	3.02	2.97	2.96	2.98	3.03	3.00	3.02	2.98	3.01
Cell 7	3.07	3.06	3.08	3.07	3.08	3.08	3.06	3.12	3.17
Cell 8	3.08	3.08	3.08	3.08	3.06	3.09	3.06	3.13	3.14
Cell 9	3.04	3.03	3.07	3.03	3.05	3.08	3.06	3.08	3.12
Cell 10	3.06	3.08	3.08	3.09	3.11	3.13	3.12	3.15	3.12
Cell 11	3.05	3.06	3.11	3.10	3.14	3.16	3.13	3.12	3.17
Cell 12	3.06	3.09	3.04	3.05	3.06	3.05	3.06	3.04	3.04
Cell 13	3.05	3.09	3.05	3.06	3.05	3.05	3.05	3.05	3.04
Average	3.05	3.04	3.03	3.03	3.05	3.05	3.04	3.05	3.06

S.3 EAS Screening - Single Cell Measurements

Table S.3.1: Single cell FLIM measurements of EAS1. HeLa cells co-expressing MEK1 and EAS1 were starved overnight and stimulated with 100 ng/ml EGF. Fluorescent lifetimes were measured prior to and 5, 10 and 20 min after EGF stimulation and are displayed as average of whole individual cells in ns (average with S.E.M.). Cells measured were from different days and dishes.

Cell	Time after EGF addition			
	0 min	5 min	10 min	20 min
1	2.74	2.71	2.73	2.73
2	2.74	2.69	2.74	2.74
3	2.78	2.73	2.76	2.75
4	2.75	2.74	2.75	2.75
5	2.72	2.69	2.74	2.75
6	2.78	2.76	2.77	2.78
7	2.78	2.76	2.80	2.79
8	2.77	2.76	2.77	2.78
9	2.69	2.68	2.72	2.72
10	2.71	2.69	2.74	2.69
11	2.70	2.68	2.68	2.72
12	2.69	2.68	2.69	2.69
13	2.69	2.69	2.68	2.68
Average	2.73 ± 0.01	2.71 ± 0.01	2.74 ± 0.01	2.74 ± 0.01

Table S.3.2: Single cell FLIM measurements of EAS2. HeLa cells co-expressing MEK1 and EAS2 were starved overnight and stimulated with 100 ng/ml EGF. Fluorescent lifetimes were measured prior to and 5, 10 and 20 min after EGF stimulation and are displayed as average of whole individual cells in ns (average with S.E.M.). Cells measured were from different days and dishes.

Cell	Time after EGF addition			
	0 min	5 min	10 min	20 min
1	2.82	2.78	2.83	2.81
2	2.83	2.79	2.84	2.82
3	2.85	2.81	2.82	2.82
4	2.75	2.71	2.74	2.71
5	2.75	2.75	2.74	2.71
6	2.85	2.81	2.85	2.87
7	2.77	2.71	2.69	2.76
8	2.78	2.76	2.73	2.74
9	2.77	2.75	2.67	2.70
10	2.75	2.73	2.76	2.75
11	2.76	2.75	2.77	2.77
12	2.74	2.73	2.76	2.79
Average	2.79 ± 0.01	2.76 ± 0.01	2.77 ± 0.02	2.77 ± 0.02

Table S.3.3: Single cell FLIM measurements of EAS3. HeLa cells co-expressing MEK1 and EAS3 were starved overnight and stimulated with 100 ng/ml EGF. Fluorescent lifetimes were measured prior to and 5, 10 and 20 min after EGF stimulation and are displayed as average of whole individual cells in ns (average with S.E.M.). Cells measured were from different days and dishes.

Cell	Time after EGF addition			
	0 min	5 min	10 min	20 min
1	2.76	2.79	2.80	2.78
2	2.74	2.78	2.75	2.74
3	2.75	2.78	2.76	2.76
4	2.75	2.80	2.76	2.75
5	2.78	2.86	2.81	2.77
6	2.71	2.77	2.76	2.72
7	2.73	2.73	2.74	2.77
8	2.73	2.77	2.78	2.74
9	2.69	2.75	2.77	2.75
10	2.71	2.73	2.74	2.70
11	2.70	2.74	2.75	2.73
12	2.72	2.78	2.76	2.73
13	2.80	2.82	2.83	2.79
14	2.81	2.82	2.82	2.77
Average	2.74 ± 0.01	2.78 ± 0.01	2.77 ± 0.01	2.75 ± 0.01

Table S.3.4: Single cell FLIM measurements of EAS4. HeLa cells co-expressing MEK1 and EAS4 were starved overnight and stimulated with 100 ng/ml EGF. Fluorescent lifetimes were measured prior to and 5, 10 and 20 min after EGF stimulation and are displayed as average of whole individual cells in ns (average with S.E.M.). Cells measured were from different days and dishes.

Cell	Time after EGF addition			
	0 min	5 min	10 min	20 min
1	2.70	2.81	2.78	2.73
2	2.73	2.85	2.82	2.80
3	2.73	2.84	2.83	2.81
4	2.76	2.78	2.79	2.78
5	2.74	2.78	2.80	2.78
6	2.70	2.74	2.75	2.73
7	2.70	2.75	2.71	2.72
8	2.72	2.86	2.78	2.69
9	2.66	2.72	2.72	2.70
10	2.82	2.85	2.82	2.82
11	2.77	2.86	2.79	2.83
12	2.81	2.85	2.86	2.79
13	2.72	2.74	2.79	2.77
14	2.71	2.73	2.79	2.75
Average	2.73 ± 0.01	2.80 ± 0.01	2.79 ± 0.01	2.76 ± 0.01

S.4 FLIM of EAS4 Mutants - Single Cell Measurements

Table S.4.1: Single cell FLIM measurements of EAS4 wt. HeLa cells co-expressing MEK1 and EAS4 wt were starved overnight and stimulated with 100 ng/ml EGF. Fluorescent lifetimes were measured prior to and 5, 10 and 20 min after EGF stimulation and are displayed as average of whole individual cells in ns (average with S.E.M.). Cells measured were from different days and dishes.

Cell	Time after EGF addition			
	0 min	5 min	10 min	20 min
1	2.70	2.81	2.78	2.73
2	2.73	2.85	2.82	2.80
3	2.73	2.84	2.83	2.81
4	2.76	2.78	2.79	2.78
5	2.74	2.78	2.80	2.78
6	2.70	2.74	2.75	2.73
7	2.70	2.75	2.71	2.72
8	2.72	2.86	2.78	2.69
9	2.66	2.72	2.72	2.70
10	2.82	2.85	2.82	2.82
11	2.77	2.86	2.79	2.83
12	2.81	2.85	2.86	2.79
13	2.72	2.74	2.79	2.77
14	2.71	2.73	2.79	2.75
15	2.77	2.82	2.85	2.80
16	2.77	2.82	2.82	2.78
17	2.74	2.80	2.79	2.77
18	2.74	2.80	2.81	2.77
Average	2.74 ± 0.01	2.80 ± 0.01	2.79 ± 0.01	2.77 ± 0.01

Table S.4.2: Single cell FLIM measurements of EAS4 K52R. HeLa cells co-expressing MEK1 and EAS4 K52R were starved overnight and stimulated with 100 ng/ml EGF. Fluorescent lifetimes were measured prior to and 5, 10 and 20 min after EGF stimulation and are displayed as average of whole individual cells in ns (average with S.E.M.). Cells measured were from different days and dishes.

Cell	Time after EGF addition			
	0 min	5 min	10 min	20 min
1	2.75	2.77	2.78	2.78
2	2.76	2.79	2.77	2.79
3	2.81	2.85	2.85	2.83
4	2.79	2.82	2.81	2.84
5	2.82	2.84	2.84	2.84
6	2.81	2.84	2.85	2.84
7	2.78	2.82	2.82	2.83
8	2.78	2.81	2.81	2.81
9	2.83	2.84	2.85	2.84
10	2.80	2.84	2.83	2.84
11	2.78	2.83	2.83	2.80
12	2.78	2.88	2.81	2.80
13	2.76	2.79	2.79	2.79
14	2.75	2.80	2.80	2.80
15	2.74	2.74	2.78	2.77
16	2.72	2.74	2.77	2.76
Average	2.78 ± 0.01	2.81 ± 0.01	2.81 ± 0.01	2.81 ± 0.01

Table S.4.3: Single cell FLIM measurements of EAS4 TAYA. HeLa cells co-expressing MEK1 and EAS4 TAYA were starved overnight and stimulated with 100 ng/ml EGF. Fluorescent lifetimes were measured prior to and 5, 10 and 20 min after EGF stimulation and are displayed as average of whole individual cells in ns (average with S.E.M.). Cells measured were from different days and dishes.

Cell	Time after EGF addition			
	0 min	5 min	10 min	20 min
1	2.75	2.79	2.78	2.76
2	2.80	2.78	2.83	2.79
3	2.80	2.82	2.82	2.82
4	2.79	2.80	2.79	2.80
5	2.78	2.79	2.78	2.80
6	2.78	2.80	2.80	2.82
7	2.79	2.80	2.80	2.82
8	2.78	2.81	2.80	2.80
9	2.78	2.81	2.81	2.80
10	2.73	2.73	2.73	2.73
11	2.74	2.74	2.75	2.74
12	2.68	2.69	2.69	2.68
13	2.73	2.74	2.74	2.74
14	2.73	2.73	2.73	2.72
15	2.73	2.73	2.72	2.72
16	2.86	2.89	2.89	2.88
17	2.86	2.83	2.84	2.85
18	2.78	2.77	2.77	2.78
19	2.78	2.77	2.78	2.78
Average	2.77 ± 0.01	2.78 ± 0.01	2.78 ± 0.01	2.78 ± 0.01

Table S.4.4: Single cell FLIM measurements of EAS4 ElkMut. HeLa cells co-expressing MEK1 and EAS4 TAYA were starved overnight and stimulated with 100 ng/ml EGF. Fluorescent lifetimes were measured prior to and 5, 10 and 20 min after EGF stimulation and are displayed as average of whole individual cells in ns (average with S.E.M.). Cells measured were from different days and dishes.

Cell	Time after EGF addition			
	0 min	5 min	10 min	20 min
1	2.77	2.77	2.79	2.76
2	2.73	2.74	2.73	2.73
3	2.66	2.66	2.65	2.64
4	2.75	2.75	2.75	2.74
5	2.77	2.78	2.80	2.78
6	2.77	2.79	2.78	2.82
7	2.79	2.81	2.79	2.80
8	2.74	2.74	2.75	2.74
9	2.74	2.76	2.75	2.77
10	2.80	2.80	2.80	2.78
11	2.78	2.78	2.79	2.85
12	2.78	2.79	2.79	2.80
13	2.77	2.78	2.80	2.80
14	2.76	2.78	2.77	2.77
15	2.74	2.75	2.74	2.76
16	2.81	2.81	2.81	2.81
17	2.78	2.80	2.80	2.79
18	2.78	2.79	2.81	2.82
19	2.83	2.82	2.83	2.82
20	2.76	2.78	2.78	2.77
21	2.78	2.77	2.78	2.79
22	2.80	2.81	2.80	2.80
23	2.79	2.79	2.81	2.79
24	2.79	2.79	2.79	2.79
25	2.83	2.87	2.83	2.83
26	2.77	2.77	2.78	2.77
Average	2.77 ± 0.01	2.78 ± 0.01	2.78 ± 0.01	2.78 ± 0.01

S.5 Light-Induced Activation of ERK2

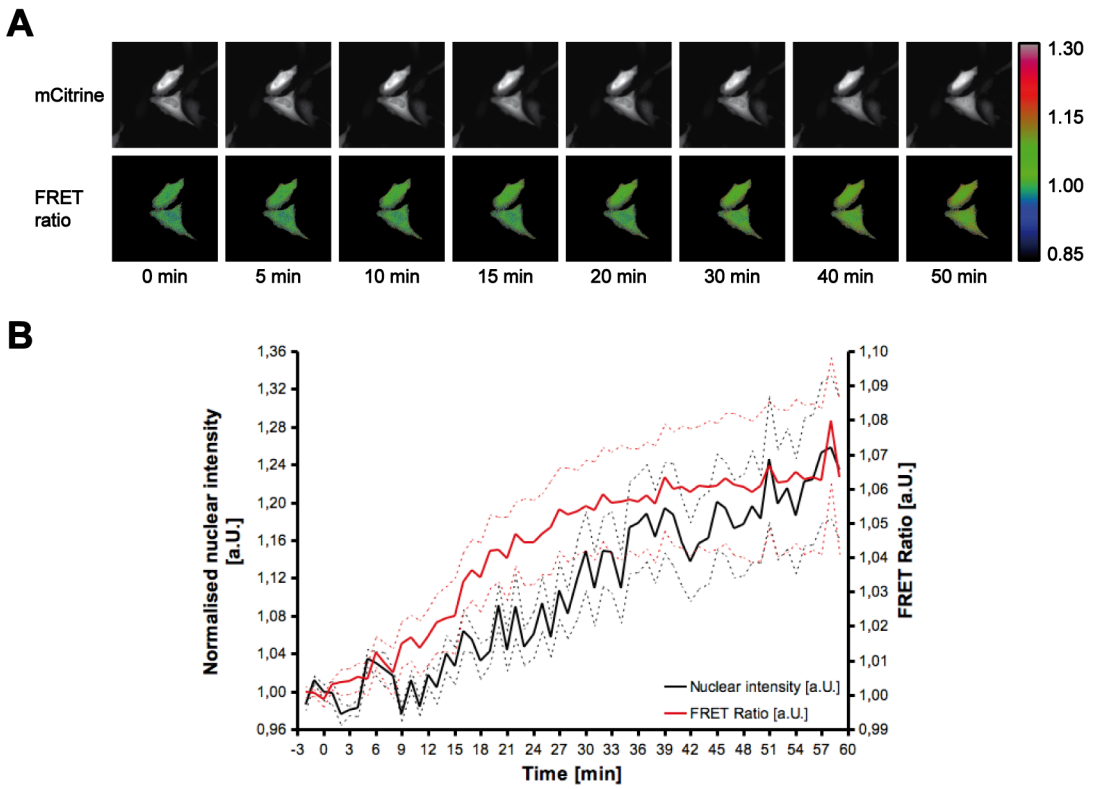

Figure S.5.1: Light-induced activation of ERK2. A) Representative confocal image sequence showing slow nuclear accumulation (top) following slowly increasing activity (bottom) of ERK2 in starving cells. HeLa cells co-expressing EAS4 wt and MEK1 were starved overnight and imaged every 60 sec without growth factor addition. Scale bar = μm. B) Average nuclear fluorescence intensity (broken lines) and average whole cell FRET ratios obtained from HeLa cells expressing EAS4 wt, showing slow nuclear accumulation of ERK2 and concurrent slow increase in ERK2 activity in resting cells. Cells were treated as in A).

S.6 Primer Sequences

4C(9-14) for	5'- GGC TGC TGC CAG GTG TTC GAC GTG GGG -3'
4C(9-14) rev	5'- CGG GCA GCA GCC CGC CGC CGC CGC CGC -3'
4C(30-35) for	5'- GGC TGC TGC ATG GTT TGT TCT GCT TAT GAT AAT CTC -3'
4C(30-35) rev	5'- CGG GCA GCA GAT GTA CGA GAG ATT AGT GTA GC -3'

4C(171-176) for	5'- GGC TGC TGC GAT CAT ACA GGG TTC TTG ACA GAG -3'
4C(171-176) rev	5'- CGG GCA GCA ACG GGC AAG GCC AAA GTC ACA G -3'
4C(172-177) for	5'- GGC TGC TGC CAT ACA GGG TTC TTG ACA GAG -3'
4C(172-177) rev	5'- CGG GCA GCA AAC ACG GGC AAG GCC AAA GTC AC -3'
4C(173-178) for	5'- GGC TGC TGC ACA GGG TTC TTG ACA GAG TAT GTA GC -3'
4C(173-178) rev	5'- CGG GCA GCA TGC AAC ACG GGC AAG GCC -3'
4C(174-179) for	5'- GGC TGC TGC GGG TTC TTG ACA GAG TAT GTA GC -3'
4C(174-179) rev	5'- CGG GCA GCA ATC TGC AAC ACG GGC AAG G -3'
4C(175-180) for	5'- GGC TGC TGC TTC TTG ACA GAG TAT GTA GC -3'
4C(175-180) rev	5'- CGG GCA GCA TGG ATC TGC AAC ACG GGC -3'
4C(176-181) for	5'- GGC TGC TGC TTG ACA GAG TAT GTA GCC ACG -3'
4C(176-181) rev	5'- CGG GCA GCA GTC TGG ATC TGC AAC ACG GGC -3'
4C(327-336) for	5'- GGC TGC TGC ATG GAA CCT AAG GAG AAG C -3'
4C(327-336) rev	5'- CGG GCA GCA GTT CAG AAA TGG TGC TTC AGC -3'
4C-ERK2 for	5'- GGG CTG CTG CAT GGA ACC GGA GAT GGT CCG CGG GCA GG -3'
4C-ERK2 rev	5'- GGG CAG CAG TTC AGA AAC ATG GTG GAG CTC GAG ATC TGA GTC C -3'
ERK2-4C for	5'- GGG CTG CTG CAT GGA ACC GTA AGT CGA CGG TAC CGC GG -3'
ERK2-4C rev	5'- GGG CAG CAG TTC AGA AAC ATA GAT CTG TAT CCT GGC TGG -3'
ERK2 Stop for	5'- CCA GCC AGG ATA CAG ATC TTC GAC GGT ACC GCG GGC CC -3'
ERK2 Stop rev	5'- GGG CCC GCG GTA CCG TCG AAG ATC TGT ATC CTG GCT GG -3'
ERK2 substrate for	5'- GCT ACC GGT CGC CAC CAT GGT GAG C -3'
ERK2 substrate rev	5'- CTC GAG TTA GGC GCT GCC ACT GGA TGG AAA CTG GAA GGA GAG CTT GGC CGG GCT ACG GGG CGC AAT GGG ACT CAG GGT GCT CCA GGA TGA GTC CGG ACT TGT ACA GCT C -3'
ERK2 +Kozak for	5'- GGA CTC AGA TCT CGA GCT CCA CCA TGG CGG CGG CGG CGG CGG G -3'
ERK2 +Kozak rev	5'- GCC GCC GCC GCC GCC ATG GTG GAG CTC GAG ATC TGA GTC CGG -3'
hElk1 (BspEI) for	5'- GCT CCG GAC TCA GAT CTC GAG CTA GCA TTC ACT TCT GGA GCA CCC TG -3'

hElk1 (HindIII) rev	5'- CGA AGC TTG CCT GGG CGC TGC CAC TGG ATG GAA A -3'
hElk1-linker(long) rev	5'- GGC AGC GGC GCT TCC TCC ACC GCC GCT TCC TCC ACC GCC GCT TCC TCC ACC GCC CAG CTG GGC GCT GCC ACT GGA TCC AAA -3'
hElk1-linker(long) rev	5'- GGC AGC GGC GCT TCC TCC ACC GCC GCT TCC TCC ACC GCC CAG CTG GGC GCT GCC ACT GGA TCC AAA -3'
linker-hElk1(long) for	5'- CTG GGC GGT GGA GGA AGC GGC GGT GGA GGA AGC GGC GGT GGA GGA AGC GCC GCT GCC AGC ATT CAC TTC TGG AGC ACC -3'
linker-hElk1(short) for	5'- CTG GGC GGT GGA GGA AGC GGC GGT GGA GGA AGC GCC GCT GCC AGC ATT CAC TTC TGG AGC ACC -3'
linker-MAPK1(long) for	5'- TCG GGC GGT GGA GGA AGC GGC GGT GGA GGA AGC GGC GGT GGA GGA AGC GCC GCT GCC ATG GCG GCG GCG GCG GCG GGC CCG -3'
linker-MAPK1(short) for	5'- TCG GGC GGT GGA GGA AGC GGC GGT GGA GGA AGC GCC GCT GCC ATG GCG GCG GCG GCG GCG GGC CCG -3'
M13 for	5'- GTA AAA CGA CGG CCA G -3'
M13 rev	5'- CAG GAA ACA GCT ATG A -3'
MAPK1 (BspEI) for	5'- GCT CCG GAC TCA GAT CTC GAG CTA TGG CGG CGG CGG CGG CGG CGG GCC CG -3'
MAPK1 (HindIII) rev	5'- CGA AGC TTG CAG ATC TGT ATC CTG GCT GGA ATC G -3'
MAPK1 K52R for	5'- CAA AGT TCG AGT TGC TAT CAG AAA AAT CAG TCC TTT TGA GC -3'
MAPK1 K52R rev	5'- GCT CAA AAG GAC TGA TTT TTC TGA TAG CAA CTC GAA CTT TG -3'
MAPK1 L73P for	5'- GAG AGA GAT AAA AAT CCC ACT GCG CTT CAG ACA TG -3'
MAPK1 L73P rev	5'- CAT GTC TGA AGC GCA GTG GGA TTT TTA TCT CTC TC -3'
MAPK1-linker(long) rev	5'- GGC AGC GGC GCT TCC TCC ACC GCC GCT TCC TCC ACC GCC GCT TCC TCC ACC GCC CAG AGA TCT GTA TCC TGG CTG GAA TCG -3'
MAPK1-linker(short) rev	5'- GGC AGC GGC GCT TCC TCC ACC GCC GCT TCC TCC ACC GCC CAG AGA TCT GTA TCC TGG CTG GAA TCG -3'
MAPK1 S151D for	5'- CGT GAC CTC AAG CCT GAC AAC CTC CTG CTG AAC -3'
MAPK1 S151D rev	5'- GTT CAG CAG GAG GTT GTC AGG CTT GAG GTC ACG -3'
MAPK1 Stop rev	5'- CGG TCG ACT TA GAT CTG TAT CCT GGC TGG AAT CG -3'

MAPK1 TAYA for	5'- CCA TGA TCA TAC AGG GTT CTT GGC AGA GGC TGT AGC CAC GCG TTG GTA CGA AGC -3'
MAPK1 TAYA rev	5'- GCT CTG TAC CAA CGC GTG GCT ACA GCC TCT GCC AAG AAC CCT GTA TGA TCA TGG -3'
mCherry (BamHI) rev	5'- CGG GAT CCT TAC TTG TAC AGC TCG TCC ATG CC -3'
mCherry (HindIII) for	5'- GCA AGC TTG GTC GCC ACC ATG GTG AGC AAG GGC -3'
MutElk1 for	5'- CAG CAT TCA CTT CTG GAG CAC CCT GAG TGC GCT CCC CAT TCC CTT CAG CGC CTC CTC CTC CCA GCC AAA GAG TTT TCG TCC GGG CAG CGC -3'
MutElk1 rev	5'- CCA TGG TGG CGA CCA AGC TTG CGG CGC TGC CCG GAC GAA AAC TCT TTG GCT GGG AGG AGG AGG CGC TGA AGG GAA TGG GGA GCG C -3'
sensor seq for1	5'- CGA GTT GCT ATC AAG AAA ATC AGT C -3'
sensor seq for2	5'- CCA TCA CAG GAA GAT CTG AAT TG -3'
sensor seq rev	5'- CAT CTT TCA TCT GCT CAA TGG TT -3'

Acknowledgments

I would like to express my appreciation of the efforts that Frank Domhardt, Friedhelm Horn and Ralf Anders made for my social and intellectual progression. I am also very thankful to Dr. Rolf Grempler for teaching me the basics of scientific work, both on theoretical and practical levels. I am especially and deeply grateful to Prof. Dr. Berthe Marie Willumsen for so many things, amongst them teaching me how science should really be done and for believing in me!

I would like to thank Prof. Dr. Philippe I.H. Bastiaens for accepting me in his lab, for the interesting and challenging project, and for the creative freedom. In addition, I am very grateful to Prof. Dr. Frank Wehner for taking over the job as second reviewer.

I would like to thank present and previous members of the Bastiaens lab for help, discussions and support, and - most importantly - being the Bastiaens lab to me, amongst those namely Dr. Oliver Rocks, Dr. Christiana Stute, Dr. Mark Hink, Dr. Anna Peyker a.k.a. Lorentzen, Dr. Thomas Keith Stackhouse, Eva Nievergal, Eulashini Chuntharpursat, Anchal Chandra, Maja Sinn, Michael Sulc, Franziska Thorwirth and Jens Christmann.

Additionally, there have been a number of individuals whose knowledge, sharing of ideas, continuous fruitful discussion, technical assistance, proof-reading, help and undivided support, scientifically as well as emotionally, encouragment and so much more certainly had its share in the completion of this piece of work and to whom I would like to pay all my deepest respect. These individuals are - without any specific order - Piet Lommerse, Thomas Frahm, Hernan Grecco, Christina Hecker, Pedro Roda-Navarro, Malte Schmick, Sven Fengler, Johann Jarzombek, Rahul Ravindran, Martin Bierbaum, Jian Hou, Hendrike Schütz, Kirsten Michel, Jutta Luig, Sven Müller, Ola Sabet and Lisa Karajannis. You made a difference and became close friends! I am so much looking forward to not working with you anymore and will truely and deeply miss all of you! See you in the north!

I would like to thank the people of the LC Rapid Dortmund for the distraction.

Special thanks go to Kaizers Orchestra, Tom Waits, Daniel Kahn (& the Painted Birds), Johnny Cash, the Clash, Travis, Muse, Amanda Jenssen, John Lennon, Emiliano Zapata, Mahatma Gandhi, John Harris from tpuc.org, Danny Shine from "Everything is OK", Volker Pispers, Georg Schramm, Hagen Rether, the unknown war veteran and all the others that fight for a better world. May it be a brighter place one day!

I am deeply thankful to my family, both on a wider and narrower sense of the word, for all the emotional support. I know it wasn't easy. Thank you, Andrea, Olaf and Tim,

for Anne and the patience.

Thank you, Sönke, for being there and especially for the music that keeps me running. Thank you Wiebke, Andy and Erik, for being there and believing in me.

Danke, Papa, für die Liebe, für die Geduld, für's an mich glauben und für einfach Alles! Danke, Mama, ebenfalls für Alles und dafür, dass Du immer noch jeden Tag bei mir bist! Ich liebe Euch beide!

Finally, Terje, thank you for joining my life, little Kaizer! Thank you for being there and for being what you are! And then I would like to express my deepest respect and my deepest love to you, Anne! Thank you for joining me in bad and in even worse times! Without you, this would not have been possible! Thank you for all your support! Thank you for Terje! Thank you for staying! Thank you for everything! I love you!

Eidestattliche Erklärung

Ich versichere hiermit an Eides Statt, dass ich die vorliegende Dissertationsarbeit selbständig verfasst und ohne unzulässige fremde Hilfe erarbeitet habe. Ich habe keine anderen als die hier angegebenen Quellen und Hilfsmittel benutzt, sowie wörtliche und sinngemäße Zitate durch Angabe der Quelle als Entlehnung kenntlich gemacht. Diese Arbeit ist bisher weder in Teilen noch als Ganzes für die Erlangung eines Promotionstitels eingereicht worden.

Ort, Datum (Thies Klüßendorf)